# ICCESEN-2025

## 12th International Conference on Computational and Experimental Science and ENgineering

Antalya-TURKEY

17-20 October 2025

# Proceedings

## of

# ICCESEN-2025

EDITORS

## Prof.Dr. İskender AKKURT

### Dr. Sabiha Anas BOUSSAA

iccesen2025@gmail.com

www.iccesen.org

**Antalya-TURKEY**
**17-20 October 2025**

# Proceedings

# of

# ICCESEN-2025

**Editors:**
**Prof.Dr. İskender AKKURT**
**Dr. Sabiha ANAS BOUSSAA**

**ISBN: 978-605-68728-9-1**

i

**Proceedings of ICCESEN-2025 ,**

12th International Conference on Computational and Eperimental Science and Engineering (**ICCESEN-2025**)

17-20 October 2025, Antalya-TURKEY

**Editors:**
Prof. Dr. İskender AKKURT
Dr. Sabiha ANAS BOUSSAA

**Published :** 31 October 2025
**ISBN:** 978-605-68728-9-1

i

# TABLE OF CONTENTS

# FOREWORD



Dear Colleagues,

It is a great honor for me to host you all in **"12<sup>th</sup> International Conference on Computational and Experimental Science and Engineering (ICCESEN-2025)"** was taken place in Antalya-TURKEY in the period of 17-20 October 2025.

We are also happy to publish the proceeding of ICCESEN-2025. All papers have been reviewed by two reviewers.

Prof. Dr. İskender AKKURT

Chair for ICCESEN-2025
Editor for Proceedings of ICCESEN-2025

# ORGANISATION COMMITTEE

| | |
|---|---|
| **Prof.Dr. Iskender AKKURT (Chair)** | Suleyman Demirel University, Isparta -Turkey |
| Dr. Sabiha Anas BOUSSAA (Secretary) | CRTSE-Algeria |
| Dr. Hakan AKYILDIRIM | Suleyman Demirel University, Isparta -Turkey |
| Dr. Nurdan KARPUZ | Amasya University, Amasya -Turkey |
| Dr. Feride KULALI | Üsküdar University, Istanbul-Turkey |
| Dr. Osman GÜNAY | Yıldız Technical University, Istanbul -Turkiye |
| Dr. Feride KULALI | Üsküdar University, Istanbul-Turkey |
| Dr. Mucize SARIHAN | Okan University, Istanbul-Turkey |
| Dr. Seher POLAT | Sakarya University, Sakarya-Turkey |
| Dr. Cemal ÇARBOĞA | Nevşehir Hacı Bektaş Veli University, Nevşehir-Turkey |
| Dr. Aycan ŞENGÜL | Akdeniz University, Antalya-Turkey |
| Lect. Berra Seda SARIHAN | Okan University, Istanbul-Turkey |

iv

# SCIENTIFIC COMMITTEE

| | |
|---|---|
| **Prof.Dr. Iskender AKKURT (Chair)** | Suleyman Demirel University, Isparta –Turkey |
| Prof.Dr. Majid ABBASPOUR | Sharif University of Technology-Iran |
| Prof.Dr. Zahid Hussain ABRA | Quadi-E-Awam University, Sindh-Pakistan |
| Prof.Dr. Abdullah ALAMRI | King Saud University, Saudi Arabia |
| Prof.Dr. Nezam Mahdavi-AMIRI | Sharif University Iran |
| Dr.Sabiha Anas Boussaa | CRTSE,Algeria. |
| Dr. John R.M.ANNAND | Glasgow University, Glasgow-Scotland (UK) |
| Dr. Majda AOUITITEN | Abdelmalek Essaadi University-Morocco |
| Prof.Dr. Mohamed Kheireddine AROUA | University of Malaya-Malaysia |
| Dr. Rachid BELKADA | CRSTSE -Algeria |
| Dr. Radhey S BENIWAL | CSIR-NISCAIR, New Delhi 110012, India |
| Dr. Mahmoud Abdullah BENNASER | Kuwait University-Kuwait |
| Dr. Djoudi BOUHAFS | Centre de Recherche en Technologie -Algeria |
| Prof. Oleg BURDAKOV | Linköping University Linköping, Sweden |
| Dr. Yusuf CEYLAN | Selcuk University, Konya-Turkey |
| Prof.Dr. Lotfi CHOUCHANE | Weill Cornell MEdical College-Qatar |
| Dr. Manju D CHOUDHARY | Niscair-India |
| Dr. Nermin DEMİRKOL | Kocaeli University, Kocaeli –Turkey |
| Prof.Dr. İbrahim DİNÇER | University of Ontario Institue of Technology (UOIT)-Canada |
| Prof. Dr. Mitra DJAMAL | Institute Teknologi Bandung-Indonesia |
| Prof.Dr. Mahmut DOĞRU | Bitlis Eren University, Bitlis-Turkey |
| Prof.Dr. Mohammed Mostafa EL TOKHI | United Arab Emirates University-UAE |
| Dr. Zuhal ER | Istanbul Technical University, Istanbul-Turkey |
| Prof.Dr. Mustafa EROL | Dokuz Eylul University, İzmir-Turkey |
| Prof.Dr. Madjid FATHI | Dept. of EECS University of Siegen- Germany |
| Prof.Dr. Jan FELBA | Wroclaw University of Technology-Poland |
| Prof.Dr. S. Mostafa GHIAASIAAN | Mechanical/Nuclear   Engineering, Georgia Tech USA |
| Prof.Dr. Mustafa GÜNAL | Gaziantep University, Gaziantep-Turkey |
| Prof. Dr. Amir HUSSAIN | University of Stirling- Scotland(UK) |
| Dr. Nabi IBADOV | Warsaw University of Technology-Poland |
| Prof.Dr. Fatma KARİPCİN | Nevşehir Hacı Bektaşi Veli University-Turkey |
| Prof.Dr. Hamdi Ş. KILIÇ | Selcuk University, Konya-Turkey |

v

| | |
|---|---|
| Dr. Menekşe V. KILIÇARSLAN | İstanbul Aydın University, Istanbul-Turkey |
| Prof.Dr. Ziya Erdem KOÇ | Selcuk University, Konya-Turkey |
| Prof. Dr. İsmail KOYUNCU | Istanbul Technical University, Istanbul-Turkey |
| Dr. Irida MARKJA | Polytechnic University,Tirana-Albania |
| Dr. F.Zümrüt Biber MÜFTÜLER | Ege University, Izmir-Turkey |
| Dr. Susan Shukur NOORI | Kirkuk University, Kirkuk-lraq |
| Prof.Dr. Ravindra NUGGEHALLI | New Jersey Institute of Technology-USA |
| Prof.Dr. İbrahim ÖRÜN | Aksaray University, Aksaray-Turkey |
| Prof.Dr. Necati ÖZDEMİR | Balıkesir University, Balıkesir-Turkey |
| Dr. Zeynep PARLAR | Istanbul Technical University, Istanbul-Turkey |
| Prof.Dr. Ioana G. Petrisor | ToxStrategies, Inc., Mission Viejo, CA |
| Dr. Tomasz PIOTROWSKI | Warsaw University of Technology, Warsaw-Poland |
| Prof.Dr. Javad RAHIGHI | AEOI, Tehran-Iran. |
| Dr. Abdelmadjid RECIOUI | University of Boumerdes-Algeria |
| Prof.Dr. Osman SAGDIÇ | Yıldız Technical University, Istanbul-Turkey |
| Prof.Dr. Miljko SATARIC | Faculty of Technical Sciences Novi Sad-Serbia |
| Prof.Dr. Saleh SULTANSOY | TOBB University, Ankara-Turkey |
| Dr. Naim SYLA | University of Prishtina-Kosova |
| Prof. Dr. Mustafa TAVASLI | Uludag University, Bursa-Turkey |
| Dr. Huseyin TOROS | Istanbul Technical University, Istanbul-Turkey |
| Prof.Dr. Ahmad UMAR | Najran University-Saudi Arabia |
| Prof.Dr. Gerhard-Wilhelm WEBER | Middle East Technical University Ankara-Turkey |
| Prof.Dr. Erol YAŞAR | Mersin University, Mersin-Turkey |

# INVITED SPEAKERS

| | |
|---|---|
|  | **Prof. Dr.  Amir HUSSEIN**<br><br>*Edinburgh Napier University, UK*<br><br>**Title:**  Trustworthy AI-enabled Sustainable Technologies |
|  | **Prof.Dr. Madjid FATHI**<br><br>*Dept. of EECS University of Siegen, GERMANY*<br><br>**Title:**  Artificial Intelligent as a Concept or as a System: utilizing and conceptualizing AI in Industrial and health care |
|  | **Dr. Hayat ARBOUZ**<br><br>*University Saad Dahlab Blida1, Algeria*<br><br>**Title:** Investigation of the potential of the double perovskite materials Cs2BX6 and Cs2BB'X6 as absorbers in single and tandem solar cells for high-efficiency photovoltaic conversion |
|  | **Prof.Dr. Mansour Almatarneh**<br><br>*University of Jordan-Jordan*<br><br>**Title:** Sustainable Development in the Global Rankings |
|  | **Prof.Dr. Gerhard-Wilhelm WEBER**<br><br>*Poznan University of Technology-POLAND*<br><br>**Title:**  Regime-switching models via stochastic optimal control & robust control theory, with applications in finance and insurance |

# Integrating Computational Modeling with Experimental Methods in Bending Behavior Analysis of Round Rods

## Rilindë RAÇI[1], Latif HASI[2*]

[1] *University of Prishtina/Faculty of Mathematics and Natural Sciences/Department of Phsyics, Prishtina, Kosova*

[2*] *University of Prishtina/Faculty of Mechanical Engineering, Prishtina, Kosova*

*[*latif.hasi@uni-pr.edu](mailto:latif.hasi@uni-pr.edu)*

## ABSTRACT

The integration of modeling software into scientific research has gained significant traction as a reliable complement to traditional experimental methods. This study examines the mechanical behavior of three different round rods under three-point bending tests, combining experimental procedures with computational simulations. Using ANSYS software, the bending tests are modelled to analyze stress distribution, deflection, and overall material performance. A comparative analysis between experimental results and simulations evaluates the accuracy and reliability of computational modeling in replicating physical behavior. By highlighting the potential of modeling software in predicting material responses under loading conditions, this study underscores its growing significance in both engineering research and educational applications.

**KEYWORDS** - Three-point bending test, Finite element analysis (FEA), ANSYS simulation.

## 1. INTRODUCTION

A Three-Point Bend test is performed on a round rod as shown in Figure 1. As a downward force (F) is applied in the middle of the rod, the flex ($\Delta x$) is recorded. The ratio ($F/\Delta x$) is the effective stiffness of the length of rod being tested. The distance between the anvils (see inset) is varied, and the resulting effect on the stiffness of the beam is measured. A graph of the resulting data yields the Flexural Elastic Modulus for the material. (PASCO)
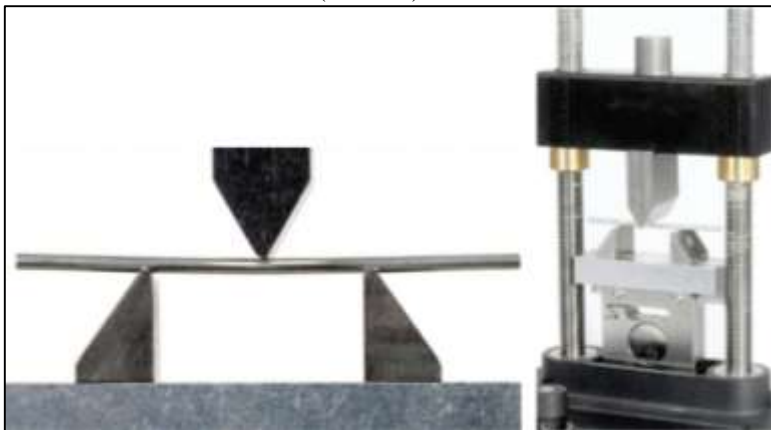


*Figure 1. Three-point bending (PASCO)*

1

After completing the experimental measurements, we continue by modelling the same problem with the same parameters in the ANSYS modelling software. This is a computer program that enables the modelling of various physical and engineering problems and simulating them to generate results as if by experiment. A great advantage of this program is that in its database there is data for many different materials. Also, if we use a material that is not recognized by ANSYS, we can determine the parameters of that material (Young's Modulus, Flexural Modulus, Poisson's ratio, etc.) experimentally and then use that data to model more complex structures and simulate them for testing, thus saving us a lot of time and materials.

## 2. EXPERIMENTAL METHODS

A sample is supported by two anvils placed at a distance, L, as shown in Figure 2. A force $F$ of $100N$ is applied in the middle, at an equal distance from each anvil, and the deflection $\Delta x$ is measured. The force is applied by moving the upper anvil, namely by rotating its upper part which causes the vertical displacement of the anvil. The distance between the two anvils is changed several times and in each case $F/\Delta x$ is measured, which we read in the PASCO Capstone program.
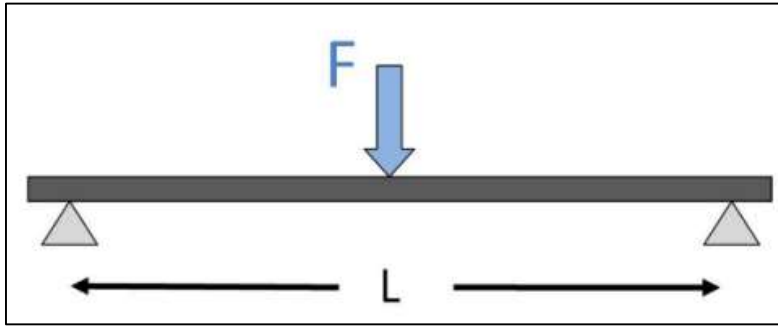


*Figure 2. 3-Point Bending Test (PASCO)*

The ratio $F/\Delta x$ is the stiffness of the sample, and depends on the length, $L$. It also depends on the shape and cross-sectional area of the sample, as well as the material. If $E$ is the flexural modulus for the material, and $I$ is the surface moment of inertia for the sample, then:

$$\frac{F}{\Delta x} = \frac{48IE}{L^3}$$

The Area Moment of Inertia depends on the shape of the cross section of the sample. For a round rod of radius, r,

$$I_{rod} = \frac{1}{4}\pi r^4$$

Thus, we see from Eqn. (1) that the stiffness (F/Δx) is inversely proportional to the cube of the anvil separation, L, and a graph F/Δx vs. 1/L³, yields a straight line with a slope = 48IE. Finally, solving for E yields

$$E = \frac{gradient}{48I}$$

(PASCO)

Flexural modulus is technically not the same as Young's modulus. Flexural testing involves tensile and compressive stresses, and for some materials these moduli are different. For isotropic and homogeneous materials, these two moduli have the same values, but for some materials, such as

2

composites and polymers, the flexural modulus is greater than Young's modulus due to the nonlinearity of the material in bending.

The measurements were performed using PASCO Capstone. There we generate a table $F/\Delta x$ *vs L*. Its graph will highlight the fact that the hardness is inversely proportional to the cube of the distance between the two anvils.

The same procedure was repeated for three different materials: aluminum, steel, and brass.

## 3.EXPERIMENTAL RESULTS

These are experimental measurements carried out in the laboratory.

*Table 1. Experimental results for Aluminum*

| L (m) | F/Δx (N/m) |
|-------|------------|
| 0.079 | 33900 |
| 0.0645 | 59900 |
| 0.045 | 184000 |
| 0.031 | 577000 |

*Table 2. Experimental results for Steel*

| L (m) | F/Δx (N/m) |
|-------|------------|
| 0.050 | 347000 |
| 0.077 | 89400 |
| 0.033 | 1240000 |
| 0.027 | 2540000 |

*Table 3. Experimental results for Brass*

| L (m) | F/Δx (N/m) |
|-------|------------|
| 0.078 | 50700 |
| 0.057 | 125000 |
| 0.038 | 445000 |
| 0.027 | 1250000 |

### 3.1Analysis of experimental results

From the experimental measurements, we are first generating the graph $F/(N/m)$ versus $L(m)$ for each material.
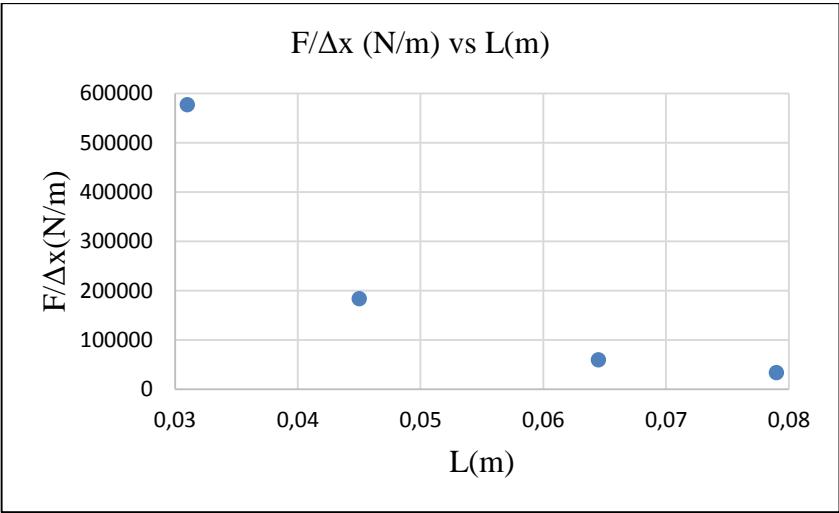
**Figure 3.** *Graph of stiffness F/Δx versus distance L for aluminum*
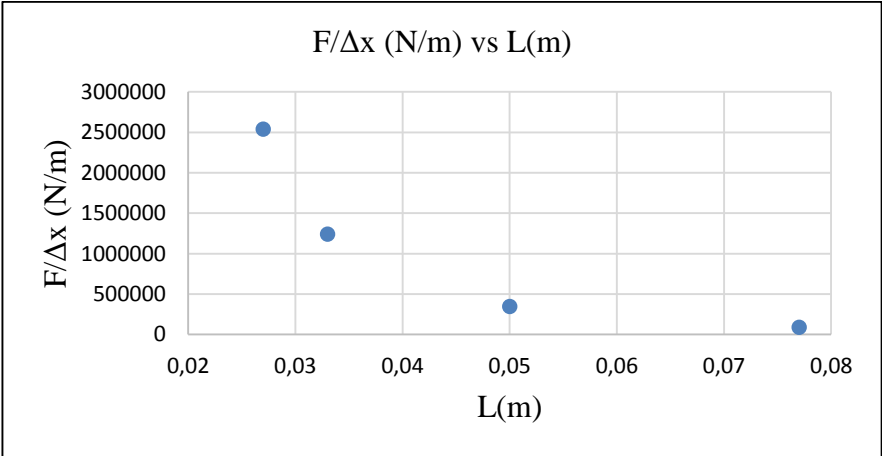


**Figure 4.** *Graph of stiffness F/Δx versus distance L for steel*

4
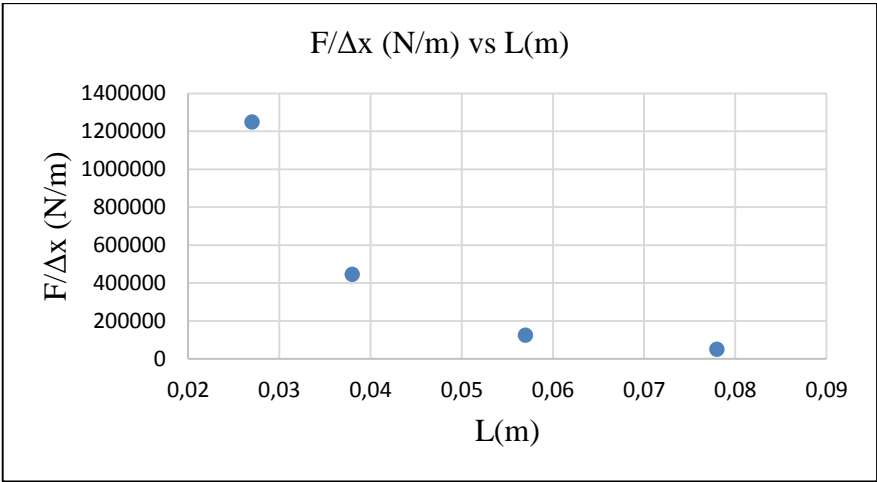
**Figure 5.** *Graph of stiffness F/Δx versus distance L for brass*

From the graphs above (figures 3,4, and 5) it is clear that the strength of the material is inversely proportional to the cube of the distance between the holding anvils. If we generate the graph of $F/\Delta x$ against $1/L^3$, we will obtain a linear graph.

### 3.1.1 Material 1 (aluminium)

Below I am presenting the graph of the material's hardness $F/\Delta x$ against $L^{-3}$. This is expected to give us a linear graph based on equation (1), where the gradient of this line will be equal to $48IE$.
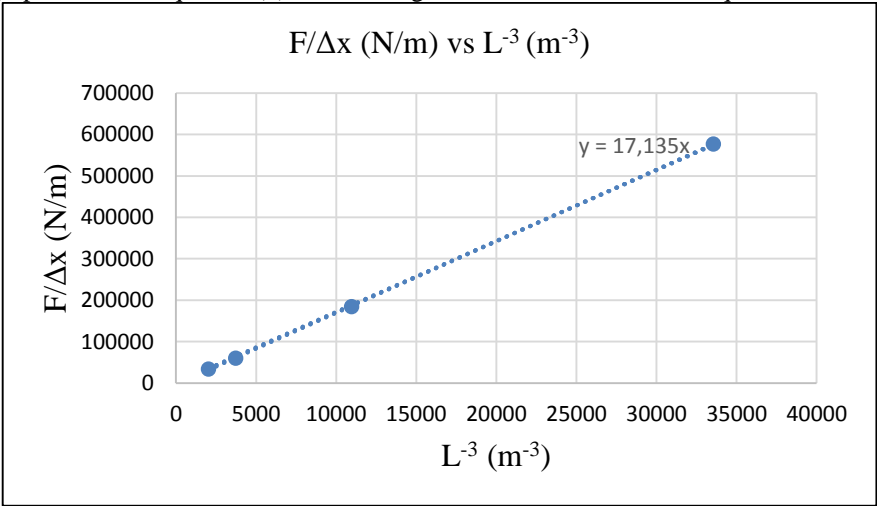


**Figure 6.** *Graph of F/Δx versus L-3 for aluminum*

As expected, this graph is a straight line. The next step is to determine the gradient of this line. Then, using equation (3), we can calculate the flexural modulus, after calculating the moment of inertia using equation (2). I will calculate the gradient of the line in the above graph using the method of least squares. This can also be done in Excel, which is able to generate the best-fit line. It generates the line and the equation of this line. An important step here is to select the Set intercept option and

5

make the intercept zero. This is because equation (3), through which we will calculate the value of the modulus $E$, does not have an intercept.

   For this material, Excel has provided this equation:

$$y = 17.235x$$

Here the variable $y$ represents the stiffness $F/\Delta x$, while $x$ represents $L{-}3$. We see that the gradient of this line is 17.135. From equation (3) we find:

$$E = (89.79 \pm 0.51)GPa$$

We calculate the uncertainty using the LINEST function, which finds the uncertainty in the gradient, through which we then find the uncertainty in E.

According to the method of least squares we have these two formulae:

$$m = \frac{n\sum xy - \sum x \sum y}{n\sum x^2 - (\sum x)^2} \tag{5}$$

$$c = \frac{\sum y - m\sum x}{n} \tag{6}$$

Replacing $x$ with $L^{-3}$, and $y$ with $F/\Delta x$, we get:

$$m = \frac{n\sum (L^{-3})(F/\Delta x) - \sum(L^{-3})(\sum F/\Delta x)}{n\sum(L^{-3})^2 - (\sum L^{-3})^2} \tag{7}$$

$$c = \frac{\sum(F/\Delta x) - m\sum(L^{-3})}{n} \tag{8}$$

I entered these formulas in Excel and obtained these values:

$$m = 17.27535 \approx 17.3, c = -3520.41 \approx -3520.4 \tag{9}$$

We obtain the same values in Excel if we do not make the intercept zero. From the gradient value we obtain the value of the flexural modulus: $9.05 \cdot 10^{10}\frac{N}{m^2} = 90.5GPa$. The least squares method described above does not make the intercept zero so it gives us another result, which is not so reliable. The value stated above fits the expected value for aluminium alloys which is expected to be in the range 70-90GPa.

### 3.1.2 Material 2 (steel)

We are continuing the same procedure for the second material. First, I am presenting the graph of $F/\Delta x$ against $L^{-3}$.
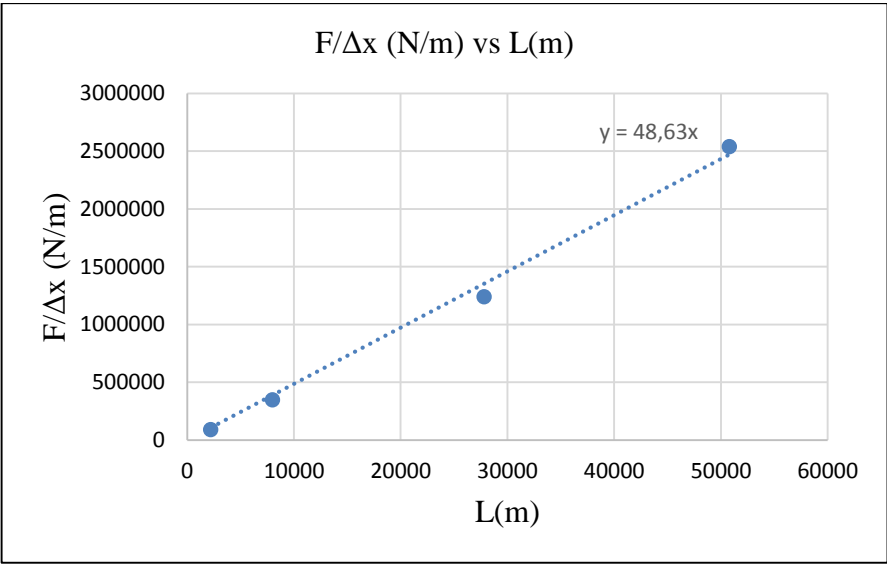
*Figure 7. Graph of F/Δx versus L⁻³ for steel*

It can be seen that the gradient of the best-fit line is equal to 48.63. Using the method of least squares, I obtained the value 50.30239 (without forcing the line to pass through the point (0,0)).
Using the same equations as for the first material, we obtain a value of the flexural modulus of

$$E = (254.81 \pm 7.23)GPa$$

This value is significantly higher than the common value of steel alloys, which have flexural moduli of around $200 GPa$.

### 3.1.3 Material 3 (brass)

Below I present the F/Δx vs. L⁻³ graph for the third material.
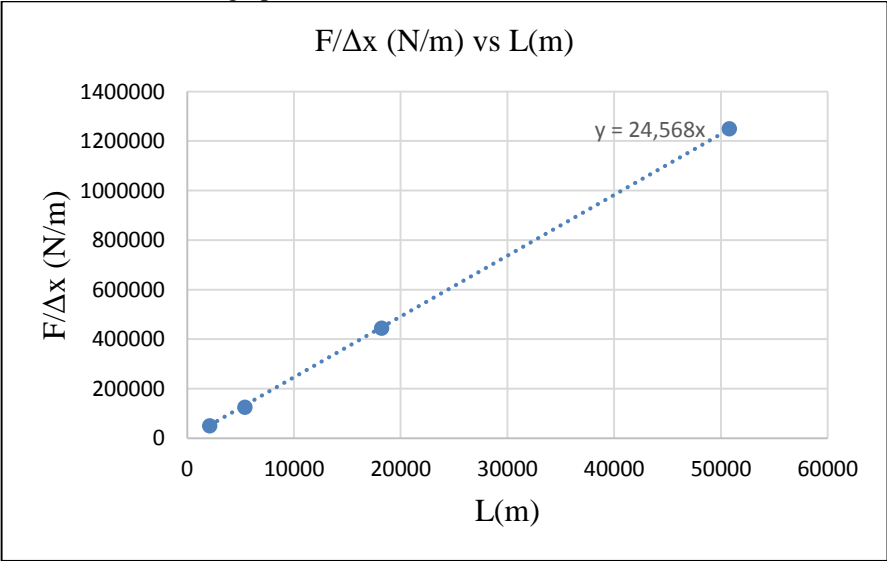


*Figure 8. Graph of F/Δx versus L⁻³ for brass*

7

We can see that the gradient of the best-fit line is equal to 24.568. Using the method of least squares, I obtained the value 24.69176. Using the same equations as for the first material, we obtain a value of the flexural modulus of $E = (128.73 \pm 0.47)GPa$.

For brass, which is a copper-nickel alloy, a value of the flexural modulus in the range $90 - 110GPa$ is expected. It is seen that our sample has a significantly higher value of this modulus.

## 4.MODELING IN ANSYS

In the ANSYS program, I have modeled a thin metal rod with a cylindrical shape with a radius of $1.5mm$ and a length of $100mm = 10cm$ which is supported at two points. I will generate the supporting rods by adding the condition that these rods are stationary (static). Then, right in the middle of the rod, I will place a force of $100N$ with a vertically downward direction. To make the problem as realistic as possible, I can also add the gravitational force, in which case the bending contribution due to the weight of the rod itself is also added. For the dimensions of our rods, we do not expect a large force, so this contribution is not expected to be very large, but this practice can be very useful in other modeling cases, e.g. if the rod represents a part of the structure of a building or house, where this rod can have the function of supporting the floor, there, due to the larger dimensions of the rod, we would be dealing with a greater weight of the rod that could significantly affect its strength and bending, as well as the safety of the residents.

I will note all lengths in mm, so I must choose the mm unit before starting to model this problem. I made the geometry of the experiment using Design Modeler and Space Claim that ANSYS Workbench enables.

First, I generated a cylinder with a radius of 1.5mm (diameter 3mm) and a length of 100mm (10cm) that fits the length of the sample used in the laboratory. As for the supporting anvils, it is not necessary to draw them. It is enough to know the coordinates of the meeting points between the anvils and the rod. Then, at those points, we set the movement constraints. We limit the movement in the vertical direction (the $y$ axis), because these points should not move in this direction since they represent the support points. However, we should leave them free to move in the $x$ and $y$ directions, as well as rotations. I set these support points at distances $L$=60$mm$, 70$mm$, 80$mm$, and 90$mm$; and I generated the results for these distances. I did this for the Structural Steel, Aluminum Alloy, and BRASS materials, which are in the ANSYS material database.
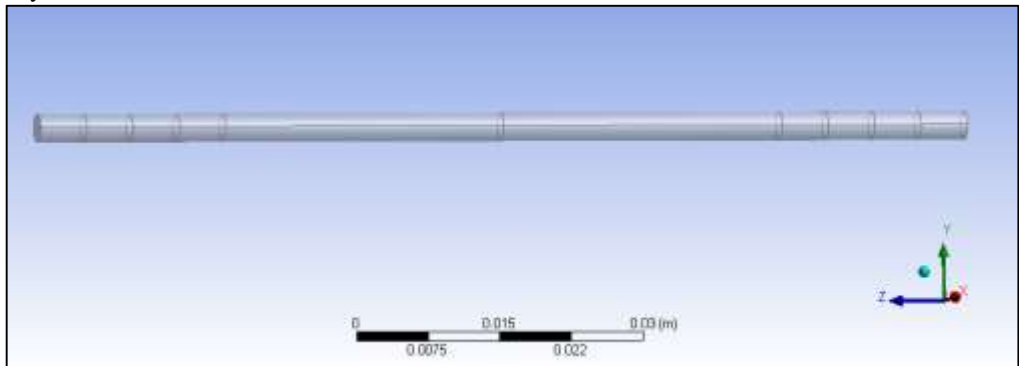


***Figure 9.*** *Model geometry in ANSYS Workbench (Design Modeler)*
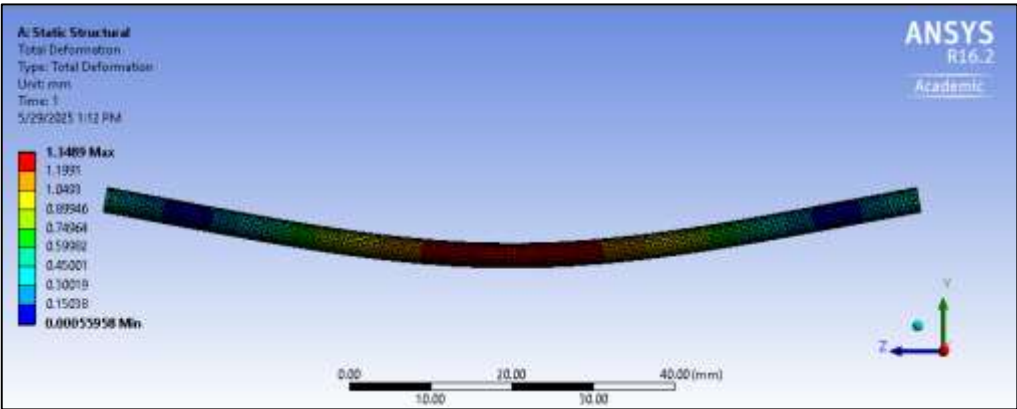
**Figure 10.** *Curvature generated in ANSYS Workbench*

## 4.1 ANSYS results

These are the results generated in ANSYS.

**Table 4.** *ANSYS Results for Structural Steel*

| L (m) | F/Δx (N/m) |
|-------|------------|
| 0.06  | 174972.0045 |
| 0.07  | 110717.4491 |
| 0.08  | 74134.47995 |
| 0.09  | 51639.5559 |

**Table 5.** *ANSYS Results for Aluminum Alloy*

| L (m) | F/Δx (N/m) |
|-------|------------|
| 0.06  | 62262.62375 |
| 0.07  | 39277.29772 |
| 0.08  | 26143.79085 |
| 0.09  | 18248.17518 |

**Table 6.** *ANSYS Results for BRASS*

| L (m) | F/Δx (N/m) |
|-------|------------|
| 0.06  | 104128.7031 |
| 0.07  | 65932.61687 |
| 0.08  | 44016.02183 |
| 0.09  | 30726.68613 |

## 4.2 Analysis of ANSYS results

Based on the ANSYS Workbench results, we first generate the $F/(N/m)$ versus $L(m)$ graph for each material.

9
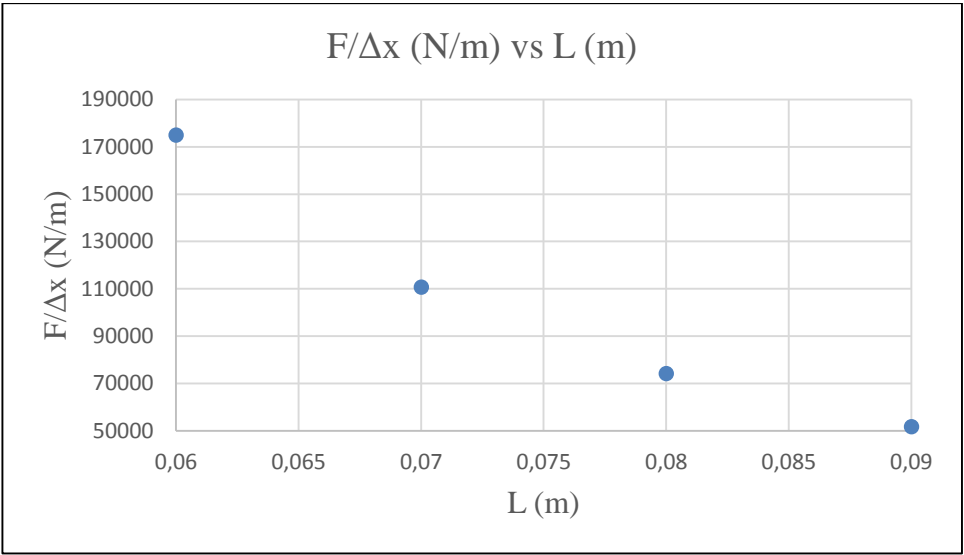
**Figure 11.** *Graph of strength F/Δx versus distance L for Structural Steel*
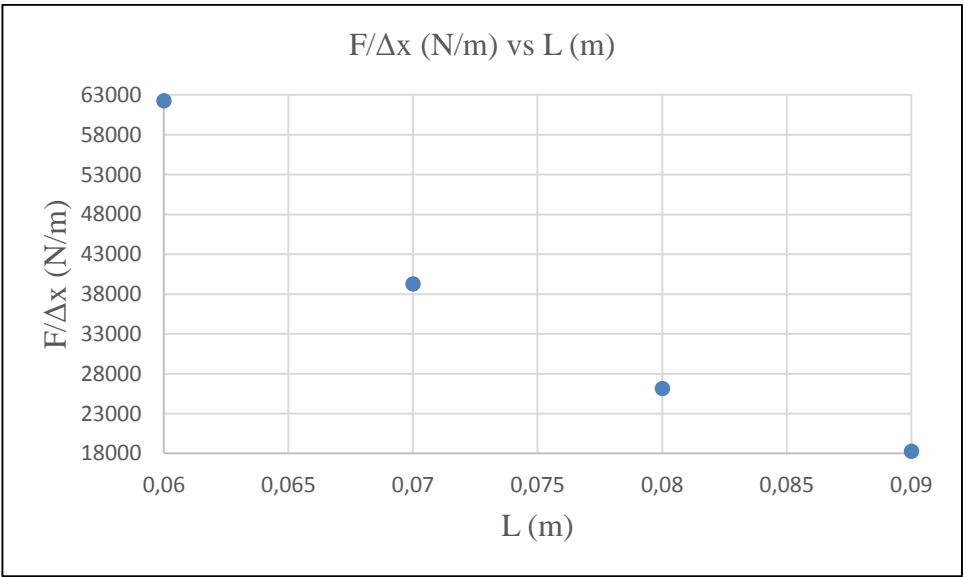


**Figure 12.** *Graph of strength F/Δx versus distance L for Aluminum Alloy*

10
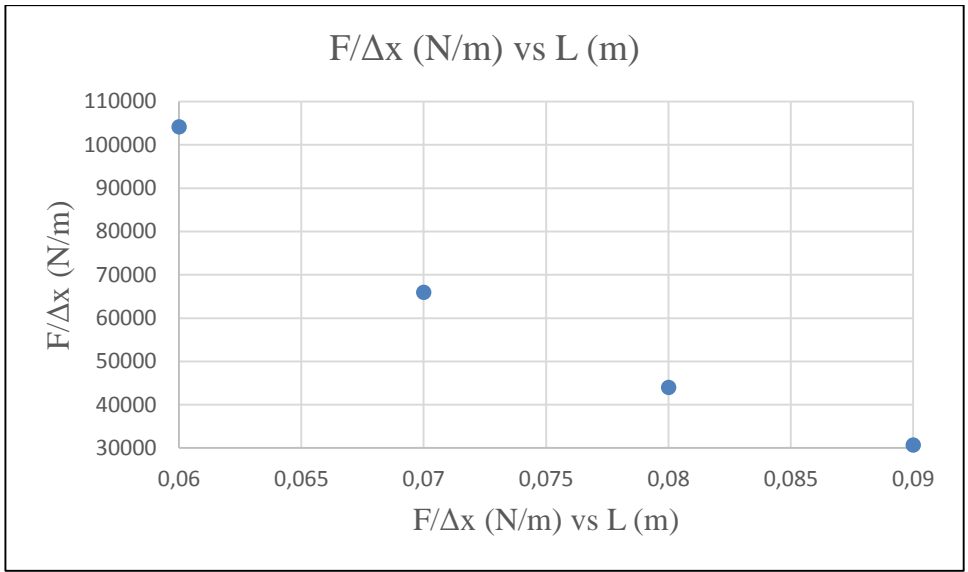
*Figure 13. Graph of strength F/Δx versus distance L for BRASS*

Now we can generate graphs of strength versus $1/L^3$ to see if the graph is linear like the graphs of experimental measurements.

**4.2.1 Material 1 (Structural Steel)**
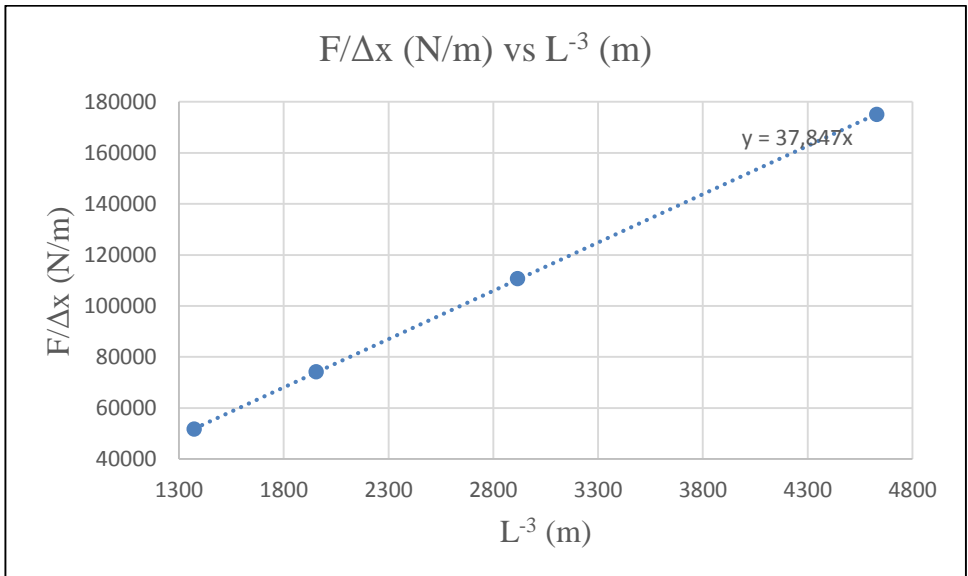


*Figure 14. Graph of F/Δx vs. L⁻³ for Structural Steel*

We see that the equation of the line (best fit) is:

$$y = 37.847x \tag{10}$$

Now using equation (3) we calculate the value of the flexural modulus and obtain the value of:

11

$$E = (198.31 \pm 0.29)GPa$$

**4.2.2 Material 2 (Aluminum Alloy)**



**F/Δx (N/m) vs L$^{-3}$ (m)**
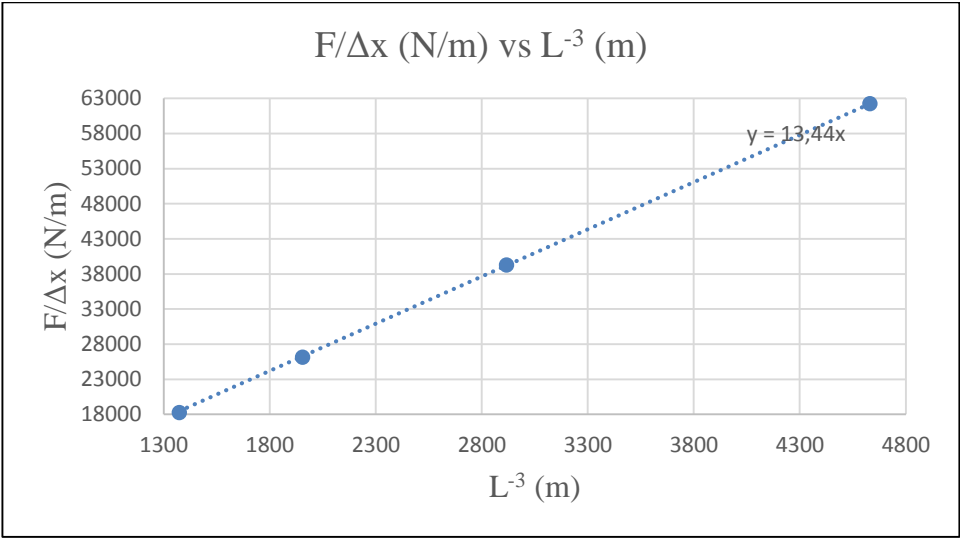
*y = 13.44x*

***Figure 15.*** *Graph of F/Δx vs. L$^{-3}$ for Aluminum Alloy*

We see that the equation of the line (best fit) is:

$$y = 13.44x \tag{11}$$

Now using equation (3) we calculate the value of the flexural modulus and obtain the value of:

$$E = (70.42 \pm 0.12)GPa$$

12

### 4.2.3 Material 3 (BRASS)
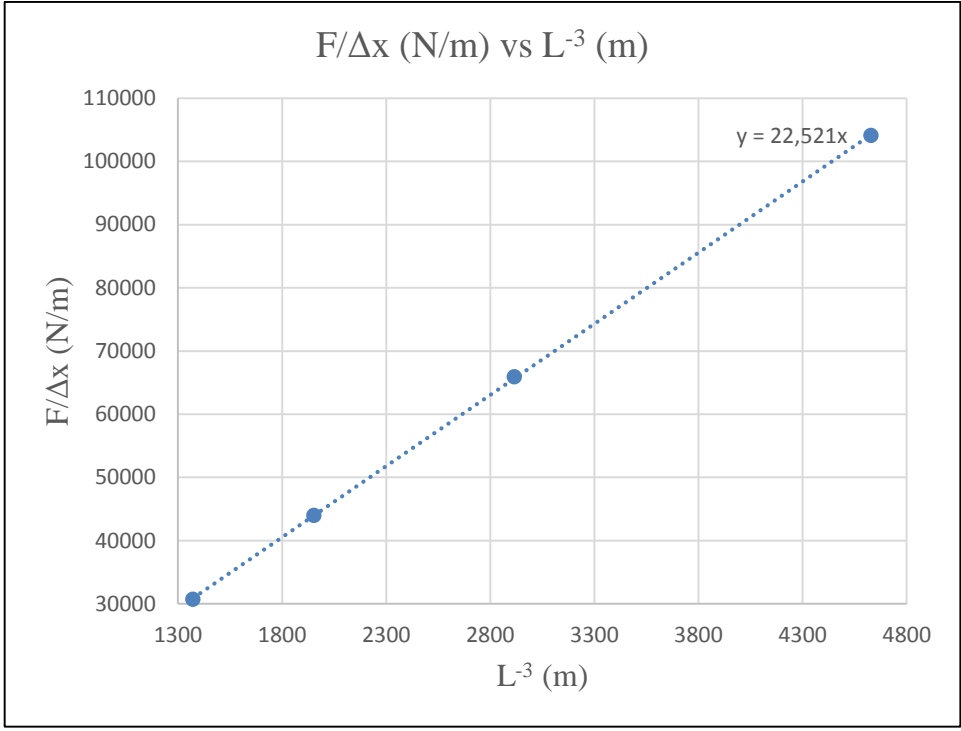


*Figure 16. Graph of F/Δx vs. L⁻³ for BRASS*

We see that the equation of the line (best fit) is:

$$y = 22.521x \tag{12}$$

Now using equation (3) we calculate the value of the flexural modulus and obtain the value of:

$$E = (118.00 \pm 0.18) GPa$$

### 5. EVALUATION OF RESULTS GENERATED BY ANSYS BY COMPARISON WITH EXPERIMENTAL RESULTS

We see that the results generated by ANSYS, as well as those obtained from the experiment, obey the theory and relations presented at the beginning of this paper.

If we analyze the correlation coefficient for the graphs of the hardness F/Δx versus $L^{-3}$, we have a coefficient very close to 1, and in fact in the results generated by the software it can even be equal to 1. This is because the software relies on formulas and theories and according to them generates data that match very well. The fact that the correlation coefficient for laboratory measurements is very close to 1 increases the reliability of these measurements, because the best-fit line describes the points of the graph very well and passes through them.

It should be noted that the results generated by ANSYS are significantly improved when, instead of drawing the retaining pins, we set constraints on the movement at those points where these pins should touch the sample. If we decide to draw and generate those pegs as bodies, we must be very careful when defining the contact points. The program provides several options for these contact points and depending on which one we choose (or what coefficient of friction we give at those

13

points) it has an effect on the generated results, and can even add uncertainty or even points that do not fit in the graph (outliers).

## 5.CONCLUSIONS AND RECOMMENDATIONS

Considering that the results generated by ANSYS are very similar to the experimental results, except for the fact that we do not have exactly the same materials in the program database, we recommend that in cases of application in engineering or something else, for any sample/material to be used, first determine the properties and parameters of the material, such as Young's Modulus and Poisson's ratio, and then model the system in the software.

This program can be very useful in engineering applications of modeling various building structures or something similar.

Also, if there are other factors that may affect the results, they should be determined and included in the modeling, depending on the level of accuracy required.

## REFERENCES

[1]   W.D. Callister Jr., D.G. Rethwisch, Materials Science and Engineering: An Introduction, Wiley.
[2]   B. Dalipi, et al., Modeling of thermal stresses on steel beam, Int. J. Comput. Exp. Sci. Eng. 11 (2025). DOI: https://doi.org/10.22399/ijcesen.767
[3]   D. Halliday, R. Resnick, Fundamentals of Physics, 10th ed., Wiley, 2014.
[4]   PASCO, Three-Point Bending.
[5]   N. Syla, F. Aliaj, Finite-element modelling and experimental study of nitrogen concentration profile in 16MnCr5 gas nitrided steel, Sci. Res. Essays 10 (19) 615–623. DOI: https://doi.org/10.5897/SRE2015.6331
[6]   E. Tunca, H. Kafalı, Compression and three-point bending analyzes of aerospace, Eur. J. Sci. Technol. (2021). DOI: https://doi.org/10.31590/ejosat.1012658
[7]   L. Hasi, R. Raçi, N. Hasi, Using modeling software as an alternative to experiment: The magnetic field of a Helmholtz coil, Int. J. Comput. Exp. Sci. Eng. 11 (2025). DOI: https://doi.org/10.22399/ijcesen.653
[8]   A.N. Aldeen, Y. Can, M. Yazici, Modeling hyperelastic materials by MATLAB, Int. J. Comput. Exp. Sci. Eng. 6 (2020) 144–148. DOI: https://doi.org/10.22399/ijcesen.662707
[9]   S. Bartels, Finite element simulation of nonlinear bending models for thin rods and plates, Comput. Struct. 225 (2020) 106–119. https://doi.org/10.1016/j.compstruc.2019.106119
[10]  L. Novotný, Finite element simulation of bending of steel bar including plasticity, Adv. Mater. Res. 1105 (2015) 101–106. https://doi.org/10.4028/www.scientific.net/AMR.1105.101
[11]  Q.J. Chen, et al., Experimental study on bending behavior of cold-rolled deformed steel bars reinforced concrete slabs, Adv. Mater. Res. 639–640 (2013) 341–345. https://doi.org/10.4028/www.scientific.net/AMR.639-640.341
[12]  M. Obst, et al., Experimental investigation of four-point bending of thin cold-formed C-channel steel beams, Sci. Rep. 12 (2022) 1–10. https://doi.org/10.1038/s41598-022-10035-z
[13]  V. Kahya, M. Turan, Bending of laminated composite beams by a multi-layer finite element based on a higher-order theory, Acta Phys. Pol. A 132 (3) (2017) 473–475. DOI: https://doi.org/10.12693/APhysPolA.132.473

# Özel Öklid Lie Grubu SE(2)

**Elif Akgün Aslan , Mehmet Sezgin**

*Edirne Sosyal Bilimler Lisesi , Trakya Üniversitesi Fen Fakültesi Matematik Bölümü*
*Edirne , Türkiye*
*elifakgunaslan@trakya.edu.tr , msezgin22@yahoo.com*

## ÖZET

Bu çalışmada ilk önce Lie grubu tanımı ve $SE(2)$ grubu ifade edildi. Daha sonra bu grubun sonsuz küçük operatörleri ve Casimir operatörü elde edildi. Bu operatörle oluşturulan özdeğer ve özfonksiyon probleminin çözümü verildi. Fiziksel bir sistemin Hamiltonyeni ile sistemin simetri grubunun Casimir operatörü arasındaki ilişkiden Schrödinger denkleminin çözümü olan dalga fonksiyonu elde edildi.

**Anahtar Kelimeler** : Lie grubu, Casimir operatörü, Schrödinger denklemi

## 1. GİRİŞ

Evariste Galois ilk defa 1830 da grup yapısından bahsetmiş ve her polinomu, polinomun köklerinin bir permütasyon grubuyla eşleştirmiştir. Böylece grup teorisinin temelleri atılmış ve sonraki yıllarda teori büyük gelişmeler göstermiştir. Galois'nın cebirsel denklemleri çözmek için grup teoriyi kullanması Norveçli bilim adamı Marius Sophus Lie'yi de kendi çalışması için benzer bir tekniğe yönlendirmiştir. Sonlu grupların denklemlerin çözülebilirliğine karar vermede kullanılması, sonsuz grupların da adi veya kısmi diferansiyel denklemlerin çözümü ile ilişkisi olabileceği görülmüştür. Bunun üzerine Lie, adi diferansiyel denklemleri çözmede kullanılan karmaşık teknikleri bir düzene koymak için simetri dönüşümlerinin sürekli bir grubu fikrini ortaya koymuş ve çalışmalarını bu fikir üzerine kurarak Lie teorisini geliştirmiştir. Günlük hayatımızdaki birçok problemin matematiksel ifadesi olan diferansiyel denklemlerin çözümleri araştırılırken bu problemlerin geometrik yapıları ve simetri özelliklerine başvurulur. Lie grubu ve cebiri teorisinde kullanılan temel yöntemler simetri yapısına dayanır. Bu nedenle teori, uzun yıllardır matematiğin birçok alanında kullanılmıştır [1,2,3,4,5].

Lie gruplarını homojen ve homojen olmayan gruplar olarak düşünebiliriz. Homojen olmayan Lie grupları, standart hareket gruplarının ötesine geçerek daha karmaşık yapıların incelenmesine imkân tanır. Bu tür gruplar, robotların ve farklı mekanik kısıtlamalara sahip sistemlerin matematiksel analizinde önemli bir araç olarak kullanılır. Özellikle Robotik sistemlerin modellenmesinde Lie grupları önemli bir rol oynar. Örneğin uzayda dönme ve öteleme hareketlerini temsil eden $SE(3)$ grubu, robotların hareketlerini tanımlamak için temel bir matematiksel yapı sağlar. Günümüzde robotlar, endüstriden sağlığa kadar pek çok alanda verimliliği artıran ve insan yaşamını kolaylaştıran teknolojiler olarak büyük önem taşımaktadır [6].

$G$ boş olmayan bir küme olsun. Eğer aşağıdaki koşullar sağlanıyorsa, $G$ bir Lie grubudur.
1. $G$ bir grup,
2. $G$ türevlenebilir bir manifold,
3. $G$ grubu üzerinde tanımlanan grup işlemi

15

$$f : G \times G \to G, \ f(g,h) = gh , \quad g,h \in G$$

ve ters işlemi

$$u : G \to G , \ u(g) = g^{-1} , \quad g \in G$$

türevlenebilirdir.

Matematikte ve bilimin diğer alanlarında ortaya çıkan Lie gruplarının birçoğu matris gruplarıdır. Bu alanlarda sıklıkla karşılaşılan matris gruplarına birkaç örnek verelim.

$$GL(n, \mathbb{R}) = \{A = (a_{ij}) | \ a_{ij} \in \mathbb{R}, \ i,j = 1,2, \dots, n, \ \det A \neq 0\}$$

$$SL(n, \mathbb{R}) = \{A \in GL(n, \mathbb{R}) | \det A = 1\}, \ O(n, \mathbb{R}) = \{A \in GL(n, \mathbb{R}) | \ A^t = A^{-1}\}$$

$$SO(n, \mathbb{R}) = \{A \in O(n, \mathbb{R}) | \det A = 1\}$$

Üstel fonksiyon, matematiğin birçok dalında karşımıza çıkar. Lie teorisinde bir matrisin üsteli, bir Lie grubuna karşılık gelen Lie cebirini tanımlamada ortaya çıkar ve Lie cebirlerine karşılık gelen Lie gruplarına bilgi aktarımı sağlayan bir mekanizma görevi görür. Yani, Lie teorisinde bir matrisin üsteli, Lie cebiri ile ona karşılık gelen Lie grubu arasındaki ilişkiyi kurar. Grubun özellikleri kendisine karşılık gelen cebirin özellikleriyle yakından ilişkilidir. Her bir Lie grubuna bir Lie cebiri karşı gelir. Bilinen bazı Lie gruplarına karşılık gelen Lie cebirlerini yazalım. $SL(n, \mathbb{R})$, $SO(n, \mathbb{R})$, $U(n, \mathbb{C})$, $SU(n, \mathbb{C})$ gruplarının cebirleri sırasıyla aşağıdaki gibi verilebilir.

$$sl(n, \mathbb{R}) = \{A \in gl(n, \mathbb{R}) | \operatorname{tr}(A) = 0\} \ , \ so(n, \mathbb{R}) = \{A \in gl(n, \mathbb{R}) | A + A^T = 0\}$$

$$u(n, \mathbb{C}) = \{A \in gl(n, \mathbb{C}) | A + (\overline{A})^T = 0\} \qquad\qquad , \qquad su(n, \mathbb{C}) =$$
$$\{A \in gl(n, \mathbb{C}) | A + (\overline{A})^T = 0, \ \operatorname{tr}(A) = 0\}$$

Buraya kadar homojen olan Lie grupları ve cebirleri hakkında bazı temel bilgiler verdik. Çünkü homojen olmayan Lie grupları homojen olan grupları da içerir. Şimdi homojen olmayan Lie gruplarına ait bazı örnekler verelim.

Poincare grubu (Homojen olmayan Lorentz grubu) $P(n, 1)$, $\mathbb{R}^{n+1}$'deki tüm

$$x' = Ax + b , \quad A \in O(n, 1) , \ b \in \mathbb{R}^{n+1}$$

şeklindeki dönüşümler grubudur. Başka sözle bu grup, $\mathbb{R}^{n+1}$ de uzunluğunu koruyan afin dönüşümler grubudur ve $A \in O(n, 1)$ olmak üzere $(n + 2) \times (n + 2)$ formundaki matrisler grubuna izomorftur.

$\mathbb{R}^n$ vektör uzayında öteleme grubu,

$$T = \{f(a): a \in \mathbb{R}^n\} \ , \quad f(a): x \mapsto x' = x + a$$

şeklinde tanımlanır.

$n$ boyutlu Öklid uzayı $E^n$, Öklid metriğine sahip bir $\mathbb{R}^n$ uzayıdır. Afin grubu $E(n)$, Öklid grubu olarak da bilinir ve

$$E(n) = \{g(A, a): A \in O(n), \ a \in \mathbb{R}^n\} = O(n) \times T(n)$$

şeklinde tanımlanır. Dönüşüm $g(A, a): x \mapsto x' = Ax + a$ ve boyutu da $\dim(E(n)) = \frac{n(n+1)}{2}$ ile verilir. $E(n)$ grubu $E^n$ uzayının simetri grubudur.

$ISO(n) = SE(n)$ grubu, $\begin{pmatrix} w & x \\ 0 & 1 \end{pmatrix}$, $w \in SO(n)$ formundaki matrisler grubudur.

Homojen gruplar dönme ve yansıma dönüşümlerini içerirken homojen olmayan gruplar ayrıca öteleme dönüşümünü de içerir. Yani homojen olmayan gruplar homojen gruplara göre daha zordur. Önceki bölümde homojen grupların cebirlerinden söz etmiştik. Benzer şekilde homojen olmayan Lie gruplarının da cebirlerini ifade edebiliriz. Örneğin , $IU(n)$ ve $ISO(n)$ homojen olmayan Lie grupları ve cebirleri

$$IU(n) = \left\{ \begin{pmatrix} u & a \\ 0 & 1 \end{pmatrix}: u \in U(n), \ a \in \mathbb{C}^n \right\}, \ ISO(n) = \left\{ \begin{pmatrix} u & a \\ 0 & 1 \end{pmatrix}: u \in SO(n), \ a \in \mathbb{R}^n \right\}$$

$$iu(n) = \left\{ \begin{pmatrix} X & x \\ 0 & 0 \end{pmatrix}: X \in u(n), \ x \in \mathbb{C}^n \right\}, \ iso(n) = \left\{ \begin{pmatrix} X & x \\ 0 & 0 \end{pmatrix}: X \in so(n), \ x \in \mathbb{R}^n \right\}$$

formunda ifade edilebilir [7].

## 2. SE(2) LİE GRUBU

$2 \times 2$ tipindeki reel değerli ortogonal matrislerin kümesi, bilinen matris çarpımı işlemine göre ortogonal grup oluşturur ve bu grup

$$O(2, \mathbb{R}) = \{A \in GL(2, \mathbb{R}) \mid det A = \pm 1\}$$

şeklinde ifade edilir. Determinantı bir olan matrislerin kümesi de özel ortogonal grup oluşturur ve bu grup

$$SO(2, \mathbb{R}) = \{A \in O(2, \mathbb{R}) \mid det A = 1\} \ , \ SO(2, \mathbb{R}) \subset O(2, \mathbb{R})$$

olarak ifade edilir.

$\mathbb{R}^2$ vektör uzayında $f : x \to x' = x + a$ dönüşümleri grup oluşturur ve bu grup $T(2) = \{f : a \in \mathbb{R}^2\}$ şeklinde tanımlanır [4,5,8].

Öklid uzayında, noktalar arasında mesafeyi koruyan ve düzlemin yönünü değiştirmeyen dönüşümlere düzlemin hareketleri denir. Bu hareketlere örnek olarak düzlemin paralel kayması ve bir nokta etrafındaki dönmesi verilebilir. Düzlemin tüm bu hareketlerinin kümesi bir grup oluşturur ve bu grup Öklid uzayının simetri grubudur. Başka sözle, $g(A, a) : x \to x' = Ax + a$ formundaki dönüşümlerin kümesidir. Burada $A$ ortogonal dönme matrisi ve $a$ da öteleme vektörüdür. Bu dönüşümlerin simetri grubu

$$SE(2) = ISO(2) = \{g(A, a) \mid A \in SO(2) \ , \ a \in \mathbb{R}^2\} = SO(2) \times T(2)$$

şeklinde ifade edilir ve iki boyutlu özel Öklid dönüşümler grubu olarak adlandırılır. Bu grup aynı zamanda homojen olmayan Lie grubu olarak da belirtilir. $SE(2)$ özel Öklid Lie grubu, $SO(2)$ dönme grubu ile $T(2)$ öteleme grubunun yarı direkt çarpımıdır. Bu grup, $\mathbb{R}^2$'de mesafeyi ve yönü korur. Ayrıca bir dönme ve bir ötelemeden oluşan böyle bir kombinasyona katı hareket denir ve $x' = Ax + a$ dönüşümüyle verilir. Mühendislik, fizik, geometri ve bunun gibi alanlardaki önemli kontrol sistemleri doğal olarak bu gruplarla çalışılır.

$x' = Ax + a$ dönüşümünü daha açık olarak

$$x' = x \cos \theta - y \sin \theta + a_1 \ , \ y' = x \sin \theta + y \cos \theta + a_2$$

veya matris gösterimiyle

$$\begin{pmatrix} x' \\ y' \end{pmatrix} = \begin{pmatrix} cos\theta & -sin\theta \\ sin\theta & cos\theta \end{pmatrix} \begin{pmatrix} x \\ y \end{pmatrix} + \begin{pmatrix} a_1 \\ a_2 \end{pmatrix}$$

şeklinde yazabiliriz. Grubun $(\theta, a_1, a_2)$ gibi üç bağımsız parametresi vardır, yani boyutu üçtür, $k = \frac{n(n+1)}{2} = \frac{2 \cdot 3}{2} = 3$ .

$SE(2)$ grubu, ilk bakışta bir matris grubu olarak tanımlanmasa da $x' = Ax + a$ dönüşümü $3 \times 3$ tipinde matrislerle verilebilir. $x' = Ax + a$ dönüşümünü matris formunda

$$\begin{pmatrix} x' \\ 1 \end{pmatrix} = \begin{pmatrix} A & a \\ 0 & 1 \end{pmatrix} \begin{pmatrix} x \\ 1 \end{pmatrix} = \begin{pmatrix} Ax + a \\ 1 \end{pmatrix}$$

şeklinde de yazılabilir. Böylece $SE(2)$ gurubunu küme formunda

$$SE(2) = ISO(2) = \left\{ \begin{pmatrix} A & a \\ 0 & 1 \end{pmatrix} \mid A \in SO(2) \ , \ a \in \mathbb{R}^2 \right\}$$

olarak ifade edebiliriz. Yani her bir katı hareket $\begin{pmatrix} A & a \\ 0 & 1 \end{pmatrix}$ formunda $3 \times 3$ tipinde matrisle temsil edilebilir. Bu durumda $SE(2)$ grubunun bir $g$ elemanı

$$g(\theta, a) = \begin{pmatrix} cos\theta & -sin\theta & a_1 \\ sin\theta & cos\theta & a_2 \\ 0 & 0 & 1 \end{pmatrix} \in SE(2) \quad , \quad 0 \leq \theta < 2\pi,$$
$$a = (a_1, a_2)^T \in \mathbb{R}^2 \ , \ a_1, a_2 \in \mathbb{R}$$

olarak verilir.

Şimdi de grubun cebirini ifade edelim. $SE(2)$ grubunun biriminde tanjant (teğet) uzayı bulmak için $h : t \to \begin{pmatrix} A(t) & a(t) \\ 0 & 1 \end{pmatrix}$ dönüşümünü ele alalım. Bu $t$ parametresine bağlı $SE(2)$ grubunda bir

eğridir. Bu matrisin $t = 0$ da türevini alırsak $\begin{pmatrix} B & b \\ 0 & 0 \end{pmatrix}$ formunda olur. Burada $B$, $2 \times 2$ tipinde anti simetrik bir matris ve $b$ de 2 bileşenli bir vektördür. Böylece grubun cebirini küme şeklinde

$$se(2) = iso(2) = \left\{ \begin{pmatrix} B & b \\ 0 & 0 \end{pmatrix} \mid B \in so(2, \mathbb{R}), \ b \in \mathbb{R}^2 \right\} = so(2) \times t(2)$$

olarak yazabiliriz [9-13].

## 3. GRUBUN SONSUZ KÜÇÜK OPERATÖRLERİ

$SE(2)$ grubunun bir parametreli alt grupları, $g_j(t)$ , $j = 1,2,3$

$$g_1(t) = R(t) = \begin{pmatrix} cost & -sint & 0 \\ sint & cost & 0 \\ 0 & 0 & 1 \end{pmatrix} \qquad \text{(Dönme)}$$

$$g_2(t) = T_1(t) = \begin{pmatrix} 1 & 0 & t \\ 0 & 1 & 0 \\ 0 & 0 & 1 \end{pmatrix}, \ g_3(t) = T_2(t) = \begin{pmatrix} 1 & 0 & 0 \\ 0 & 1 & t \\ 0 & 0 & 1 \end{pmatrix} \quad \text{(Öteleme)}$$

şeklinde verilir. Buradan teğet (tanjant) matrisleri (üreteçlerin matris formu)

$$L = \frac{dg_1(t)}{dt}\Big|_{t=0} = \begin{pmatrix} 0 & -1 & 0 \\ 1 & 0 & 0 \\ 0 & 0 & 0 \end{pmatrix} \quad , \qquad N_1 = \frac{dg_2(t)}{dt}\Big|_{t=0} = \begin{pmatrix} 0 & 0 & 1 \\ 0 & 0 & 0 \\ 0 & 0 & 0 \end{pmatrix} \quad , N_2 = \frac{dg_3(t)}{dt}\Big|_{t=0} =$$

$$\begin{pmatrix} 0 & 0 & 0 \\ 0 & 0 & 1 \\ 0 & 0 & 0 \end{pmatrix}$$

formunda bulabiliriz. Bu matrisler $se(2) = iso(2)$ cebirinin bazlarının matris formudur ve komütasyon bağıntılarını,

$$[N_1, N_2] = 0 \ , \ [N_2, L] = N_1 \ , \ [L, N_1] = N_2$$

sağlar.

Bu üreteçleri diferansiyel operatör formunda da yazabiliriz. Grubun bir parametreli alt gruplarına karşılık gelen üreteçler,

$$y = g_j(t) \, x \ , \quad x = (x_1, x_2, \dots, x_n) \ , \ y = (y_1, y_2, \dots, y_n) \, , A_{jk}(x) = \frac{dy_k}{dt}\Big|_{t=0}$$

$$L_j = -\sum_{k=1}^{2} A_{jk}(x) \frac{\partial}{\partial x_k}$$

ifadesiyle bulunur. Buradan $SE(2) = ISO(2) = SO(2) \times \mathbb{R}^2$ grubunun $g_j(t)$ bir parametreli alt gruplara karşılık gelen üreteçleri sırasıyla

$$L = x_2 \frac{\partial}{\partial x_1} - x_1 \frac{\partial}{\partial x_2} \ , \ N_1 = -\frac{\partial}{\partial x_1} \ , \ N_2 = -\frac{\partial}{\partial x_2}$$

$x_1 \to x, x_2 \to y$ olarak alırsak,

$$L = y \frac{\partial}{\partial x} - x \frac{\partial}{\partial y} \ , \ N_1 = -\frac{\partial}{\partial x} \ , \ N_2 = -\frac{\partial}{\partial y}$$

formunda buluruz.

## 4. GRUBUN CASİMİR OPERATÖRÜ

Fiziğin ve matematiğin bazı uygulama alanlarında problemlerin belirli dönüşümler altında invaryant kalmaları, bu problemlerin çözümlerinde büyük kolaylıklar sağlar. Bu nedenle invaryant operatörler uygulamalarda büyük bir öneme sahiptir. Problemlerin çözümünde ortaya çıkan birçok diferansiyel operatör invaryant olma özelliğine sahiptir. Örneğin, Laplace operatörü

$$\Delta = \frac{\partial^2}{\partial x^2} + \frac{\partial^2}{\partial y^2} + \frac{\partial^2}{\partial z^2}$$

18

Öklid uzayındaki katı hareketler altında invaryant kalır [14]. Alman fizikçi Casimir'in 1931'de $so(3)$ cebirini kullanarak yaptığı invaryant operatör çalışmaları ardından Lie cebirleri için tanımlanan operatörler Casimir operatör adını almıştır.

Eğer bir $C$ operatörü, bir $\mathfrak{g}$ Lie cebirinin tüm elemanları ile komüte oluyor; yani

$$[C, X_i] = 0 \ , \quad \forall X_i \in \mathfrak{g}$$

ise böyle operatörler invaryant ya da Casimir operatör olarak adlandırılır. Farklı mertebelerde Casimir operatörleri tanımlanabilir. Bir Lie grubunun ikinci mertebeden Casimir operatörü, sonsuz küçük operatörler yardımıyla da ifade edilebilir. $g^{ab}$ metrik tensörün tersi, $J$ sonsuz küçük operatör olmak üzere Casimir operatörü, $C = g^{ab}J_aJ_b$ ile verilir. Önceki bölümde elde edilen üreteçlere göre $SE(2)$ grubunun kartezyen koordinatlarda Casimir operatörü

$$C = \sum_{k=1}^2 N_k{}^2 = N_1{}^2 + N_2{}^2 = \frac{\partial^2}{\partial x^2} + \frac{\partial^2}{\partial y^2}$$

şeklinde oluşturulur. Üniter indirgenemez temsiller uzayında Casimir operatörü,

$$C = -k^2 I, \quad C + k^2 I = 0$$

şeklinde bir sabite eşittir. Burada $I$ birim operatör, $k$ da pozitif reel bir sabittir [4,9,15].

Bu Casimir operatörüyle

$$CF(x,y) = -k^2 F(x,y) \ , \quad CF(x,y) + k^2 F(x,y) = 0$$

$$\frac{\partial^2 F}{\partial x^2} + \frac{\partial^2 F}{\partial y^2} + k^2 F(x,y) = 0 \tag{4.1}$$

denklemini oluşturalım. Burada $F(x,y)$ fonksiyonu grubun manifoldu üzerinde tanımlı analitik bir fonksiyondur. Bu denklem iki boyutlu homojen Helmholtz denklemidir [16]. Adını ünlü Alman bilim adamı Hermann von Helmholtz'tan (1821-1894) alır. Bu denklem fiziğin genel korunum yasalarından ortaya çıkar ve tek renkli dalgalar için dalga denklemi olarak bakılır. Denklem eliptik türden kısmi türevli diferansiyel denklemdir. Helmholtz denklemi; ısı, Schrödinger, telgraf veya diğer başka tür dalga denklemlerinden türetilebilir. Matematikte ise bu denklem, Laplace operatörü için bir özdeğer ve özvektör problemi olarak incelenir [17-20]. Bu denklemden $k = 0$ durumu için

$$CF(x,y) = F_{xx} + F_{yy} = 0$$

Laplace denklemi yazılabilir. Yani Laplace denklemi Helmholtz denkleminin özel bir halidir. Laplace denklemi tüm katı hareketler altında invaryant kalır.

$k$ reel bir sabit olmak üzere

$$\frac{\partial^2 F}{\partial x^2} + \frac{\partial^2 F}{\partial y^2} + k^2 F(x,y) = 0 \tag{4.2}$$

denkleminin çözümünü bulalım. Bunun için değişkenlerine ayırma yöntemini kullanabiliriz. Denklemin $F(x,y) = A(x)B(y)$ formunda bir çözümünü arayalım. Bu durumda (4.2) kısmi türevli diferansiyel denklemi,

$$\frac{d^2 A}{dx^2} + \alpha^2 A(x) = 0 \tag{4.3}$$

$$\frac{d^2 B}{dy^2} + (k^2 - \alpha^2)B(y) = 0 \tag{4.4}$$

şeklinde iki adet adi diferansiyel denkleme indirgenir, burada $\alpha$ ayırma sabitidir. Bu denklemlerin ayrı ayrı çözümlerini bulalım.

(4.3) denklemi için $A(x) = e^{\lambda x}$ şeklinde bir çözüm arayalım. Bu durumda karakteristik denklemin kökleri $\lambda_1 = i\alpha$ , $\lambda_2 = -i\alpha$ şeklinde bulunur. Buradan (4.3) denkleminin çözümü,

$$A(x) = c_1 e^{\lambda_1 x} + c_2 e^{\lambda_2 x} = c_1 e^{i\alpha x} + c_2 e^{-i\alpha x}$$

$$A(x) = c_1 \cos(\alpha x) + c_2 \sin(\alpha x) \ , \quad \alpha = 1,2,\dots$$

olarak bulunur. Benzer şekilde (4.4) denkleminin çözümünü de

$$B(y) = c_3 e^{\lambda_1 y} + c_4 e^{\lambda_2 y} = c_3 e^{i\sqrt{k^2-\alpha^2}\,y} + c_4 e^{-i\sqrt{k^2-\alpha^2}\,y}$$

$$B(y) = c_3 \cos(\sqrt{k^2-\alpha^2}\,y) + c_4 \sin(\sqrt{k^2-\alpha^2}\,y) \ , \quad k^2 - \alpha^2 \neq 0$$

formunda bulunur. Burada, $c_i$'ler keyfi sabitlerdir ve sınır şartlarından belirlenebilir ($i = 1,2,3,4$). Böylece (4.2) denkleminin çözümünü, Kartezyen koordinatlarda üstel fonksiyonların çarpımı şeklinde

$$F(x,y) = A(x)\, B(y)$$
$$= \left[c_1 e^{i\alpha x} + c_2 e^{-i\alpha x}\right]\left[c_3 e^{i\sqrt{k^2-\alpha^2}y} + c_4 e^{-i\sqrt{k^2-\alpha^2}y}\right]$$

veya

$$F_k(x,y) = \sum_{j,l=1}^2 c_{jl}A_j(x)B_l(y)$$

formunda bulabiliriz.

Casimir operatörüyle Kartezyen koordinatlarda oluşturulan (4.1) denklemi, fiziksel probleme göre polar, parabolik, eliptik gibi başka koordinatlarda da ifade edilip çözümü bulunabilir. Örneğin denklemi polar koordinatlarda ifade edelim.

$$x = r\cos\theta \ , \ y = r\sin\theta \ , \ r \geq 0 \, , 0 \leq \theta \leq 2\pi$$
$$\frac{y}{x} = \frac{r\sin\theta}{r\cos\theta} = \frac{\sin\theta}{\cos\theta} = \tan\theta \ , \quad \theta = \arctan(y/x) = \tan^{-1}(y/x)$$
$$r^2 = x^2 + y^2 \quad , \quad r = \sqrt{x^2+y^2} = (x^2+y^2)^{1/2}$$

Böylece kartezyen koordinatlarda yazılan Laplace denklemini, $\frac{\partial^2 F}{\partial x^2} + \frac{\partial^2 F}{\partial y^2} = 0$

polar koordinatlarda,

$$\frac{\partial^2 F}{\partial r^2} + \frac{1}{r}\frac{\partial F}{\partial r} + \frac{1}{r^2}\frac{\partial^2 F}{\partial \theta^2} = 0 \quad , \quad F_{rr} + \frac{1}{r}F_r + \frac{1}{r^2}F_{\theta\theta} = 0$$

şeklinde ifade edilir. Grubun üreteçlerini de polar koordinatlarda ifade edersek

$$L = -\frac{\partial}{\partial\theta} \ , \ N_1 = -\cos\theta\frac{\partial}{\partial r} + \frac{\sin\theta}{r}\frac{\partial}{\partial\theta} \ , \ N_2 = -\sin\theta\frac{\partial}{\partial r} - \frac{\cos\theta}{r}\frac{\partial}{\partial\theta}$$

şeklinde olur. Böylece polar koordinatlarda Helmholtz denkleminin ifadesi

$$F_{rr} + \frac{1}{r}F_r + \frac{1}{r^2}F_{\theta\theta} + k^2 F(r,\theta) = 0 \tag{4.5}$$

formunda bulunur.

Bu denklemin değişkenlerine ayırma yöntemine göre, $F(r,\theta) = R(r)\, H(\theta)$ formunda bir çözümünü bulalım [17, 21]. Bu durumda

$$\frac{d^2 H}{d\theta^2} + \alpha^2 H(\theta) = 0 \tag{4.6}$$

$$r^2 \frac{d^2 R}{dr^2} + r\frac{dR}{dr} + (k^2 r^2 - \alpha^2)R(r) = 0 \tag{4.7}$$

denklemini elde ederiz. Benzer şekilde (4.6) denkleminin çözümü

$$H(\theta) = c_1 H_1(\theta) + c_2 H_2(\theta) = c_1 e^{i\alpha\theta} + c_2 e^{-i\alpha\theta} \ , \ \alpha = 0, \pm 1, \pm 2, \dots$$

olarak bulunur. Burada $c_1$ ve $c_2$ keyfi sabitler, $H_1(\theta) = e^{i\alpha\theta}$ , $H_2(\theta) = e^{-i\alpha\theta}$ ise denklemin lineer bağımsız çözümleridir.

(4.7) denklemi ise Bessel diferansiyel denklemidir. Denklemin çözümü Frobenius metoduyla bulunabilir. Denklemin $r = 0$ civarında bir seri çözümü vardır.

$\alpha^2 > 0$ , denklemin genel çözümü,

$$R(r) = c_3 J_\alpha(kr) + c_4 J_{-\alpha}(kr) \ , \quad \alpha \text{ tam sayı değilse}$$
$$R(r) = c_3 J_\alpha(kr) + c_4 Y_\alpha(kr) \ , \ \alpha = 0,1,2,\dots \tag{4.8}$$

ile verilir.

$$J_\alpha(kr) = \sum_{n=0}^\infty \frac{(-1)^n}{n!\,\Gamma(n+\alpha+1)}\left(\frac{kr}{2}\right)^{2n+\alpha}$$
$$J_{-\alpha}(kr) = (-1)^\alpha J_\alpha(kr) \ , \ \alpha = 1,2,3,\dots$$

Bessel denkleminin herhangi bir mertebeden tam çözümleri (4.8) gibi verilir. Burada $Y_\alpha(kr)$ çözümü       $r = 0$ da analitik değildir. Böylece bizim esas çözümümüz $J_\alpha(kr)$ olur. Bu durumda (4.7) denkleminin çözümü

$$R(r) = c_3 J_\alpha(kr)$$

olur. Böylece, polar koordinatlarla ifade edilen (4.5) denkleminin çözümü

20

$$F(r,\theta) = R(r)\,H(\theta) = c_3\,J_\alpha(kr)\left[c_1 e^{i\alpha\theta} + c_2 e^{-i\alpha\theta}\right]$$

olarak bulunur [16, 22,23,24].

Kuantum mekaniğinde zamandan bağımsız iki boyutlu Schrödinger denklemi

$$-\frac{\hbar^2}{2m}\left(\frac{\partial^2\psi}{\partial x^2} + \frac{\partial^2\psi}{\partial y^2}\right) + V(x,y)\psi(x,y) = E\psi(x,y)$$

formunda verilir ve denklem eliptik türdendir. Burada,

$$H = -\frac{\hbar^2}{2m}\left(\frac{\partial^2}{\partial x^2} + \frac{\partial^2}{\partial y^2}\right) + V(x,y)$$

operatörü Hamiltonyen veya enerji operatörünü, $V(x,y)$ potansiyel enerjiyi temsil eden reel değerli bir fonksiyon, $E$ parametresi sistemin enerjisini, $\psi(x,y)$ dalga fonksiyonunu, $m$ parçacığın kütlesini ve $\hbar$ ise Planck sabitini ifade eder. Kuantum mekaniği üzerine yapılan ilk çalışmalardan bu yana, tam olarak çözülebilen kuantum mekaniği problemleri sayısı oldukça azdır. Bu nedenle tam bir çözüm elde etmek amacıyla birçok yaklaşım metodu geliştirilmiştir. Geliştirilen bu yöntemlerin birçoğu sistemlerin simetrileri, daha özel bir ifade ile Lie cebiri özelliklerine dayanmaktadır. Bu nedenle Lie grupları ve cebirleri teorisi bu alanda büyük bir öneme sahiptir. Bu yaklaşıma göre zamandan bağımsız Schrödinger denkleminin Hamiltonyeni ile Lie cebirinin Casimir operatörü arasında bir ilişki kurulur. Bu ilişki

$$H\psi(x,y) = [-C + V(x,y)]\,\psi(x,y)$$
$$= [-\Delta_{LB} + V(x,y)]\,\psi(x,y) = E\psi(x,y) \quad , \quad (\hbar = 2m = 1)$$

ile verilir [25,26]. Birçok Casimir operatörü oluşturulabilir ancak bunlardan sadece bir tanesi $\Delta_{LB}$ Laplace-Beltrami operatörüne eşdeğerdir. Casimir operatörü daha yüksek mertebeden olabilir fakat Laplace-Beltrami operatörü ise sadece ikinci mertebedendir [27]. Schrödinger denklemi mikroskobik boyuttaki fiziksel sistemlerin davranışları hakkında bilgi verir ve sistemin durumları bu denklemin çözümleri olan dalga fonksiyonları ile ifade edilir. Çoğu zaman Schrödinger denkleminin çözümü, belirli bir potansiyel fonksiyonuna bağlı olarak yapılır ve bu denklem kuantum teoride önemli bir yere sahiptir [28,29]. Schrödinger denklemi ile ilgili bu kısa bilgiden sonra $SE(2)$ grubuyla bağlantılı fiziksel sistem için zamandan bağımsız Schrödinger denkleminin çözümünü bulalım. Denklem Kartezyen ve polar koordinatlarda

$$\left(\frac{\partial^2}{\partial x^2} + \frac{\partial^2}{\partial y^2}\right)\psi(x,y) + \left(E - V(x,y)\right)\psi(x,y) = 0$$
$$\psi_{rr} + \frac{1}{r}\psi_r + \frac{1}{r^2}\psi_{\theta\theta} + \left(E - V(r,\theta)\right)\psi(r,\theta) = 0$$

şeklinde yazılabilir. Basit olsun diye denklemin serbest parçacık, yani $V(r,\theta) = 0$ için çözümünü bulalım. Bu durumda denklem

$$\psi_{rr} + \frac{1}{r}\psi_r + \frac{1}{r^2}\psi_{\theta\theta} + E\psi(r,\theta) = 0 \tag{4.9}$$

haline dönüşür [30,31]. (4.2) veya (4.5) denklemindeki $k^2 = E$ enerji olarak alırsak (4.9) denklemi (4.5) Helmholtz denklemine indirgenir.

$$\psi_{rr} + \frac{1}{r}\psi_r + \frac{1}{r^2}\psi_{\theta\theta} + k^2\psi(r,\theta) = 0$$

Yukarıda (4.5) denkleminin çözümünü vermiştik. Bu durumda Schrödinger denkleminin çözümü olan dalga fonksiyonu

$$\psi(r,\theta) = c_3\,J_\alpha(kr)\left[c_1 e^{i\alpha\theta} + c_2 e^{-i\alpha\theta}\right]$$

veya

$$\psi_\alpha(r,\theta) = c_1 c_3\,J_\alpha(kr)\,e^{i\alpha\theta} = c\,J_\alpha(kr)\,e^{i\alpha\theta} \quad , \quad c = c_1 c_3$$

formunda yazılabilir. Serbest bir parçacığın $E$ enerjisinin olası değerlerinin hepsi pozitif sayılardır, yani Hamiltonyenin spektrumu $[0,\infty)$, $E > 0$ olur [32].

21

## 5. SONUÇLAR VE TARTIŞMA

Oluşturulan bir modelden ortaya çıkan denklemlerin simetri yöntemiyle çözümünün bulunması literatürde önemli bir yere sahiptir. Simetri yöntemi grup teorinin en çekici ve pratik uygulamalarından birini temsil eder. Ortaya çıkan denklemin simetri grubunun bulunması ve simetri yöntemiyle çözümünün elde edilmesi ilginç olmuştur. Özellikle fizik ve uygulamalı matematik alanlarındaki problemlerin çözümünde grup teorisi tekniği kullanımı giderek artmaktadır. $SE(2)$ özel Öklid grubu, iki boyutlu uzayda ötelemelerin ve dönmelerin kümesidir, yani iki boyutlu uzayda katı cisim dönüşümlerinin grubudur. Bu dönüşümler, fizik ve mühendislikteki birçok farklı problemdeki hareketleri tanımlamak için kullanılır. Örneğin, bu hareketler birçok farklı endüstride bulunan bir robotik kol gibi bir mekanizma tarafından yapılabilir. Basit bir kolun, dönme ve öteleme veya ikisinin bir kombinasyonunu yapabilen ve katı elemanlarla birbirine bağlanan bir dizi eklem olarak modellenebilir. Günümüzde robot teknolojisinde önemli ilerlemeler olmuştur ve bu Lie grupları robotun hareketlerini (pozisyon ve dönüş) daha düşük boyutlarda temsil etmemizi sağlar. Bu çalışmada ele alınan $SE(2)$ homojen olmayan Lie grubu hakkında bilgi verilmiştir. Daha sonra bu grubun sonsuz küçük operatörleri ve bu operatörlerle oluşturulan özdeğer ve özfonksiyon problemi ele alınıp çözümü verilmiştir. Bir fiziksel sistemin özdeğer ve özfonksiyonlarının bulunması önemli bir problemdir. Robot teknolojisi ve Kuantum mekaniği Lie gruplarının önemli uygulama alanlarındandır. Kuantum mekaniği deyince Schrödinger denklemi akla gelir. Schrödinger denklemi ile Lie grubunun Casimir operatörü arasında bir ilişki vardır. Bu ilişkiden $SE(2)$ Lie grubuyla bağlantılı fiziksel sistemin dalga fonksiyonu verilmiştir. Bu çalışmalar başka homojen olmayan Lie grupları içinde yapılabilir.

## KAYNAKLAR

[1] Gilmore R., (2008), Lie groups, Physics and Geometry, Cambridge University Press

[2] Rotman J. J., (1995), In An Introduction to the Theory of Groups, Springer-Verlag New York, Inc.

[3] Wigner E. P., (1959), Group Theory and Its Application to the Quantum Mechanics of Atomic
    Spectra, Academic Press, Inc.

[4] Vilenkin N. J. , Klimyk A. U., (1991), Representation of Lie Groups and Special Functions,
    Vol. 1,2, Kluwer Academic Publishers

[5] Iachello F., (2006), Lie Algebras and Applications, Springer-Verlag, Berlin Heidelberg

[6] Murray R. M., Li Z., Sastry S. S., (2017), A Mathematical Introduction to Robotic Manipulation,
    CRC Press

[7] Kaneta H., (1984), The Invariant Polynomial Algebras For The Groups IU(n) and ISO(n), Nagoya
    Math. J., Vol. 94, 43-59

[8] Barut A. O., Raczka R., (1980), Theory of Group Representations and Applications, Polish
    Scientific Publishers

[9] Selig J.M., (2004), Lie Groups and Lie Algebras in Robotics, Computational Noncommutative
    Algebra and Applications, Kluwer Academic Publishers, 101-125

[10] Kim Y. S., Noz M. E., (1986), Theory and Applications of the Poincaré Group, D. Reidel
    Puhlishing Company, Dordrecht, Holland

[11] Erkuş S., (2017), *Lie Group Applications on Robotics*, Dokuz Eylül Üniversitesi

[12] Bassey U. N., Edeke, U. E., (2024), Convolution Equation and Operators on the Euclidean
    Motion Group, J. Nig. Soc. Phys. Sci. 6

[13] Mashtakov A., Ardentov A., Sachkov Y. L., (2016), Relation Between Euler's Elasticae and

Sub-Riemannian Geodesics on SE(2), Regular and Chaotic Dynamics, Vol. 21, No:7-8, 832-839

[14] Carinena  J.F., Gallardo J.C., Ramos A., (2003), Motion on Lie Groups and Its Applications in Control Theory,  Reports on Mathematical Physics, Vol. 51, 159-170

[15] Rozenblyum A. V., (1992), Representations of Lie Groups and Multidimensional Special Functions,  Acta Applicandae Mathematica, 29, 171-240

[16] Miller W.,(1977), Symmetry and Separation of Variables,  Addison-Wesley Publishing Co.

[17] Moon P., Spencer D. E., (1952), Separability Conditions for the Laplace and Helmholtz Equations,   Journal of the Franklin Institute, Vol. 253  (6), 585-600

[18] Pogosyan G., Sissakian A.,  Winternitz P., (2003), Separation of Variables and Lie Algebra Contractions , Applications to special functions,  arXiv preprint math-ph/0310011

[19] Kalnins E., Pogosyan G. S., Yakhno A., (2012), Separation of Variables and Contractions on Two-Dimensional Hhyperboloid,  Symmetry, Integrability and Geometry: Methods and Applications,  SIGMA 8, 105

[20] Audu E. E., Eteng A. A., (2025), Electromagnetic Modes in Optical Fiber Waveguides Using Nikifarov-Uvarov Method,  Results in Optics, 18, 100784

[21] Rubinstein I., Rubinstein L., (1998),  Partial Differential Equations in Classical Mathematical Physics,  Cambridge University Press

[22] Taşeli H., Zafer A., (1997),  A Fourier-Bessel Expansion for Solving Radial Schrödinger Equation in Two dimensions,   International Journal of Quantum Chemistry, Vol. 61, 759-768

[23]  King A.C., Billingham J., Otto S. R., (2003), Differential Equations, Cambridge University Press

[24] Han D., Kim Y. S., Son D., (1982), E(2)-Like Little Group for Massless Particles and Neutrino Polarization as a Consequence of Gauge İnvariance, Physical Review D,  Vol. 26 , Num. 12, 3717

[25] Pogosyan G. S., Yakhno A., (2009),  Lie-Algebra Contractions and Separation of Variables. Three-Dimensional Sphere, Physics of Atomic Nuclei, Vol., No. 5,  836-844

[26]  Weidmann J., (1987), Spectral Theory of Ordinary Differential Operators,  Springer-Verlag Berlin

   Heidelberg

[27] Helgason S., (1984),  Groups and Geometric Analysis,  American Mathematical  Society

[28] Flügge  S. (1999 ).  Practical Quantum Mechanics, Springer-Verlag Berlin Heidelberg

[29] Landau L. D., Lifshitz E. M., (1977),  Quantum Mechanics, Pergamon Press Ltd.

[30] Reid G. J., (1988), J. Phys. A: Math. Gen. 21**,** 353-362

[31] Newhouse P. F., McGill  K. C., (2004), J. of Chemical Education , Vol. 81, No. 3

[32] Messiah A., (1961), Quantum Mechanics, Vol. 1,2,  North-Holland Publishing Company, Amsterdam

# Evaluation of Atomic and Electronic Cross Sections of Human Bone Tissue for Photon Interactions

**Nuray Kutu[1]✉, İskender AKKURT[1] , Osman GÜNAY[2]**

*[1]Suleyman Demirel University, Physics Department, Isparta, Turkey*
*[2]Yıldız Technical University, Faculty of Electrical and Electronics Engineering, Department of Biomedical Engineering, Istanbul, Türkiye*

**ABSTRACT**

Atomic cross section (ACS) and electronic cross section (ECS) parameters provide detailed insight into photon interaction probabilities with matter. In this study, ACS and ECS values of bone tissue were calculated using its elemental composition derived from hydroxyapatite and collagen with the Phy-X software. The variation of ACS and ECS with photon energy was analyzed across the diagnostic and therapeutic ranges.

The results reveal characteristic energy-dependent trends reflecting the underlying photon interaction mechanisms. The calculated ACS and ECS datasets are valuable for advanced radiation transport modeling, quantitative imaging studies, and the design of bone-equivalent phantoms in radiological research.

*Keywords: ACS, ECS, Bone*

✉ *Corresponding Author Email     : nuraykutu@sdu.edu.tr*

## 1 INTRODUCTION

Accurate characterization of photon–matter interactions is fundamental to radiation physics, particularly in medical imaging, radiation dosimetry, and radiological research. Quantitative parameters such as the atomic cross section (ACS) and electronic cross section (ECS) play a crucial role in describing the probability of photon interactions with matter at the atomic and electronic levels. These parameters provide more detailed physical insight than macroscopic attenuation coefficients, especially when evaluating energy-dependent interaction mechanisms in complex biological materials.

Bone tissue represents a unique and clinically significant medium due to its heterogeneous composition, primarily consisting of mineral components such as hydroxyapatite and organic constituents including collagen. This composite structure results in photon interaction characteristics that differ substantially from those of soft tissues, particularly at diagnostic and therapeutic photon energies.

Precise determination of ACS and ECS values for bone is therefore essential for accurate radiation transport modeling, patient dose estimation, and quantitative interpretation of medical images involving skeletal structures.

The interaction of photons with bone tissue is strongly energy dependent, governed by fundamental processes such as the photoelectric effect, Compton scattering, and pair production. At lower photon energies, the photoelectric effect dominates, leading to enhanced interaction probabilities associated with the higher effective atomic number of bone minerals. As photon energy increases, Compton scattering becomes the predominant mechanism, resulting in characteristic changes in ACS and ECS behavior. Analyzing these variations provides critical insight into the microscopic interaction dynamics underlying macroscopic imaging and dosimetric outcomes.

Recent advances in computational tools have enabled efficient and accurate calculation of photon interaction parameters based on elemental composition and material density. Among these tools, the Phy-X software offers a reliable platform for determining ACS and ECS values across a broad photon energy spectrum using well-established cross-section databases. In this context, the present study aims to evaluate the energy-dependent behavior of ACS and ECS for bone tissue modeled using hydroxyapatite and collagen composition. The generated datasets are expected to contribute to advanced radiation transport simulations, quantitative imaging studies, and the development of bone-equivalent phantoms for radiological applications.

## 2 MATERIALS AND METHODS

In this study, bone tissue was modeled based on its fundamental mineral and organic constituents, namely hydroxyapatite and collagen. The elemental composition of bone was defined by combining the elemental weight fractions of these two components as reported in standard reference data. The resulting composite composition was used to represent human cortical bone for photon interaction calculations[1-12]. The mass density of the bone tissue was taken from literature values and implemented as an input parameter in the computational analysis.

The atomic cross section (ACS) and electronic cross section (ECS) values of bone tissue were calculated using the Phy-X software, a well-established computational platform for evaluating photon–matter interaction parameters. Phy-X computes energy-dependent cross sections based on the elemental composition and density of the material, utilizing photon interaction data derived from recognized cross-section databases.

Calculations were performed over a broad photon energy range covering both diagnostic and therapeutic applications. For each selected photon energy, Phy-X was used to obtain the total atomic cross section and total electronic cross section of the modeled bone tissue. The software automatically accounts for the contribution of individual elements and their respective interaction probabilities at different energies.

The calculated ACS and ECS values were analyzed as a function of photon energy to investigate the energy-dependent interaction behavior of bone tissue. Particular attention was given to identifying characteristic trends associated with dominant photon interaction mechanisms across different energy regions. The results were presented in graphical and tabulated forms to clearly illustrate the variation of ACS and ECS with photon energy.

Phy-X has been widely used and validated in previous radiation physics and medical physics studies, demonstrating good agreement with both experimental measurements and other established computational codes. Therefore, its application in the present work provides a reliable and efficient approach for evaluating photon interaction parameters of bone tissue.

# 3 RESULTS

The atomic cross section (ACS) and electronic cross section (ECS) values of bone tissue were successfully calculated using the Phy-X software over a broad photon energy range covering both diagnostic and therapeutic energies. The results demonstrate a pronounced energy dependence for both parameters, reflecting the fundamental photon interaction mechanisms governing radiation transport in bone tissue.

At low photon energies within the diagnostic range, ACS values were relatively high, indicating a strong probability of photon interaction with the constituent atoms of bone. This behavior is primarily attributed to the dominance of the photoelectric effect, which is enhanced by the presence of high-atomic-number elements in hydroxyapatite. Correspondingly, ECS values also exhibited elevated levels at low energies, reflecting increased photon interactions at the electronic level.

As photon energy increased, a systematic decrease in both ACS and ECS values was observed. In the intermediate energy region, where Compton scattering becomes the predominant interaction mechanism, the variation of ACS and ECS with energy followed a smoother trend, indicating reduced sensitivity to atomic number and increased dependence on electron density. This transition region highlights the changing interaction dynamics from atom-dominated to electron-dominated processes.

.
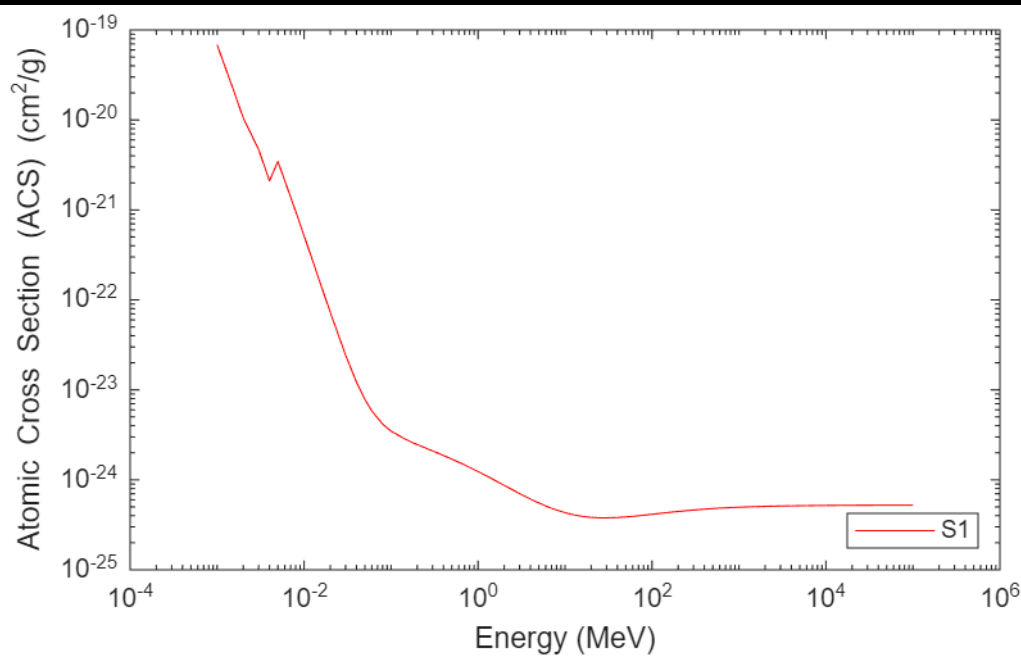
Figure 1. Atomic cross section
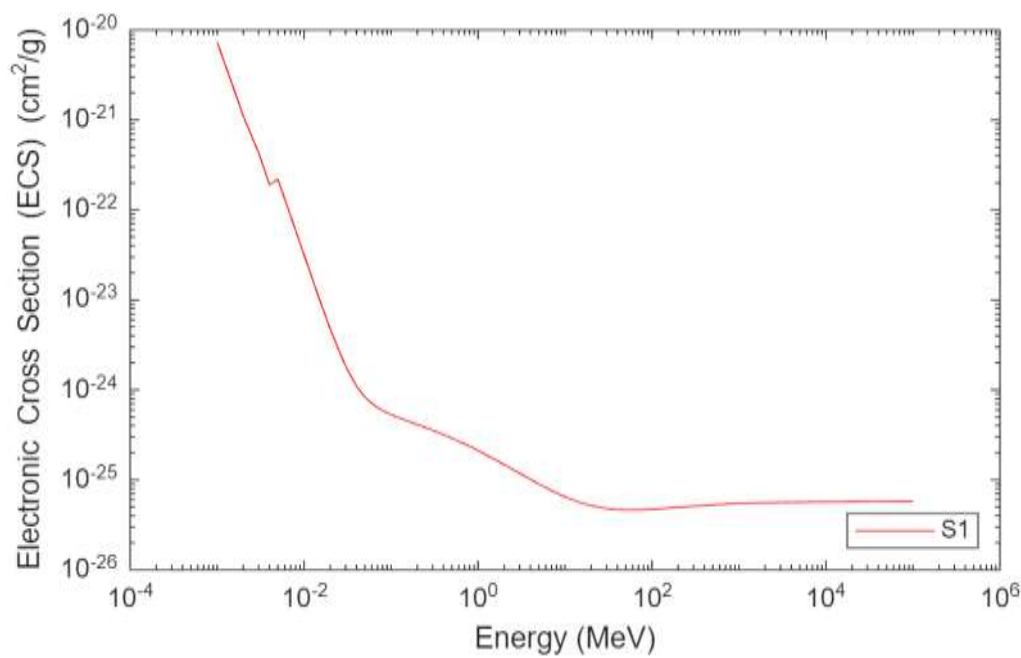


Figure 1. Electronic cross section

27

At higher photon energies approaching the therapeutic range, ACS and ECS values reached lower and more gradually varying levels, consistent with the increased penetrating power of high-energy photons and the reduced interaction probability per atom and per electron. The observed trends confirm the strong influence of photon energy on microscopic interaction parameters in bone tissue.

Overall, the calculated ACS (fiq 1) and ECS(fig 2) datasets provide detailed quantitative insight into the photon interaction behavior of bone across clinically relevant energy ranges. These results are directly applicable to advanced radiation transport simulations, quantitative imaging analyses, and the development of bone-equivalent phantoms for radiological and medical physics research.

## 4 CONCLUSION

In this study, the atomic cross section (ACS) and electronic cross section (ECS) of bone tissue were evaluated over a wide photon energy range using the Phy-X software. The results demonstrated clear energy-dependent trends, reflecting the transition between dominant photon interaction mechanisms from the diagnostic to the therapeutic energy regions.

The relatively higher ACS and ECS values at low energies highlight the significant interaction probability of bone tissue in diagnostic imaging, while the gradual decrease at higher energies indicates increased photon penetration. The generated ACS and ECS datasets provide valuable input for advanced radiation transport modeling, quantitative imaging studies, and the design of bone-equivalent phantoms in radiological research.

## REFERENCE

[1] Singh, N., Singh, K.J., Singh, K., Singh, H., 2004. Comparative study of lead borate and bismuth lead borate glass systems as gamma-radiation shielding materials. Nucl. Instrum. Methods Phys. Res. Sect. B Beam Interact. Mater. Atoms 225, 305–309.

[2] Dogra M, Singh KJ, Kaur K, Anand V, Kaur P (2017) Gamma Ray Shielding and Structural Properties of Bi2O3-B2O3-Na2WO4 Glass System. Universal Journal of Physics and Application 11(5):190-195

[3] Deliormanlı AM, ALMisned G, Ene A (2023) Graphene-Bioactive Composites: Structural, Vickers Hardness, and Gamma-Ray Attanuation Characteristics. Front. Mater 10:117950

[4] Oruncak, B., 2023. Computation of neutron coefficients for B2O3 reinforced composite. Int. J. Comput. Exp. Sci. Eng. 9, 50–53.

28

[5] Kassab LRP, Issa SAM, Mattos GR, ALMisned, G., Bordon, C.D.S., Tekin, H.O., Gallium (III) oxide reinforced novel heavy metal oxide (HMO) glasses: a focusing study on synthesis, optical and gamma-ray shielding properties. Ceram Int 2022. https://doi.org/10.1016/j.ceramint.2022.01.314.

[6] Kheswa BV (2024) Gamma Radiation Shielding Properties of (x) Bi2O-(0.5-x)ZnO-0.2B2O3-0.3SiO2 Glass System. Nukleonika 69(1):23-29

[7] Damoom MM, Alhawsawi AM, Benoqitah E, Moustafa EB, Sallam OH, Hammad AH (2024) Simulation of Sodium Diborate Glass Containing Lead and Cadmium Oxides for Radiation Shielding Applications. JOR. 20(3):285-293

[8] Buyuk, B., Tugrul, A.B., Cengiz, M., Yucel, O., Goller, G., Sahin, F.C., 2015. Radiation shielding properties of spark plasma sintered boron carbide–aluminium composites.  Acta Phys. Pol., A 128–2B, 132–134.

[9] Issa SAM, Ali AM, Susoy G, Tekin HO, Saddeek YB, Elsaman R, et al. Mechanical, physical and gamma ray shielding properties of xPbO-(50–x) MoO3–50V2O5 (25 ≤x ≤ 45 mol %) glass system. Ceram Int 2020. https://doi.org/10.1016/j. ceramint.2020.05.107.

[10] Sonia M. Reda, Hosam M. Saleh, Calculation of the gamma radiation shielding efficiency of cement-bitumen portable container using MCNPX code, Progress in Nuclear Energy, Volume 142. 104012. ISSN 2021;0149–1970. https://doi.org/ 10.1016/j.pnucene.2021.104012.

[11] Aygun M, Aygün Z (2023) A Comprehensive Analysis on Radiation Shielding Characteristics of Borogypsum (Boron Waster) by Phy-X/PSD code. Rev. Mex. Fis. 69:1-7

[12] Henaish AMA, Mostafa M, Salem B, Zakaly HMH, Issa S, Weinstein, I, Hemeda OM (2020) Spectral, Electrical, Magnetic and Radiation Shielding Studies of Mg-doped Ni–Cu–Zn Nanoferrites. Journal of Materials Science: Materials in Electronics. 22:1–13

# Microcontroller-Guided DIBH Phantom: A Low-Cost Training Tool for Patient Positioning in Radiotherapy

**Besnik SARAMATI[2⊠], Burim UKA[3], Fesal SELIMI[1], Behar RACI[1], Labinot KASTRATI[4]**

[1]*University Clinical Center of Kosova, Oncology Clinic, Prishtina-KOSOVA*
[2]*University of Prishtina "Hasan Prishtina", Department of Paramedical Subjects, Prishtina-KOSOVA*
[3]*University of Business and Technology, Department of Medical Sciences, Prishtina-KOSOVA*
[4]*University of Mitrovica "Isa Boletini", Department of Mechanical Engineering, Mitrovica-KOSOVA*
⊠ *Corresponding Author Email: besniksaramati@gmail.com*

## ABSTRACT

Today, interactive phantoms are not only necessary but also indispensable. The advanced Deep Inspiratory Breath Holding (DIBH) treatment technique is now a clinically important technique in radiotherapy, which is particularly used to minimize cardiac exposure during the treatment of left-sided breast cancer. Mastering the positioning of the patient treated with DIBH is of particular importance and is a challenge in medical physics education due to the lack of practical training tools. The study presents the design and development of an interactive 3D printed phantom that realistically simulates the movement of the anatomical thoracic area during DIBH, and this by integrating with microcontroller-based sensors and actuators to reflect the dynamics of chest rise and breath hold. The phantoms interpret real-time feedback through sound sensors, servomotors, and various visual indicators, allowing students to observe and adjust the accuracy of positioning. The study reflects that the low cost of creating interactive phantoms advances the teaching of the principles of DIBH and patient positioning in radiotherapy, also demonstrating maximum student engagement, resulting in improved conceptual understanding and potential for broader application in academic-clinical settings.

*Keywords:* DIBH Simulation, Microcontrollers, Patient Positioning.

## 1.INTRODUCTİON

Deep Inspiration Breath Hold (DIBH) is a deep technique in radiotherapy for left-side breast cancers that requires patients to take and hold a deep breath for left-sided radiation delivery [1, 2]. This voluntary breath-holding expands the lungs, moving the heart further away from the chest wall and out of the radiation path, which can reduce the cardiac dose by 40–50% [3]. It should be noted that despite the low cardiac exposures, there is a tendency for long-term cardiac risk to increase, making safe and accurate radiation delivery using DBH extremely important for patient outcomes [4]. Implementing DIBH in a manner that is consistent with training students and clinicians regarding full implementation is very challenging because it relies on accurate physical imitation of the human body and continuous monitoring [5]. Current educational tools—often static phantoms or passive observation capabilities—do not provide the opportunity to capture the logic and dynamic nature of thoracic motion and the real-time nature of breath-holding [6]. The lack of affordable interactive phantoms limits hands-on experience and educational equity, especially in resource-limited settings. The need for innovative, reproducible, and cost-effective simulations impacts the enhancement of conceptual understanding and practical competence with DIBH [7, 8, 9, 10, 11]. The project in question provides a full description of the feasibility of developing and evaluating a new DIBH

phantom, integrated and driven by microcontrollers and 3D-printed combinations—a project developed by the team of the Radiotherapy and Brachytherapy Department at the Oncology Clinic in Kosovo. The interactive phantom simulates realistic chest wall movements by providing interactive feedback and enabling the idea of training based on scalable and affordable reproduction for future generations of medical physicists and beyond.

## 2.PROBLEM STATEMENT

In most countries around the world, including Kosovo, general or medical physics students, not to mention the laboratory exercises for medical students taking the Medical Physics course, have so far graduated with limited practical skills in DIBH procedures, because standard training relies on static models, video observation, or, in some cases, exposure to real patients during clinical treatment. This outdated approach does not provide dynamic feedback, fails to accurately represent the timing and amplitude of thoracic motion, and does not include the repetitive practice that is essential for skill acquisition. Cost-restricted access to high-end simulation equipment exacerbates the problem in countries and regions. The insurmountable obstacle for most institutions that need to improve local capacities regarding radiotherapy education related to DIBH are commercial trainings, which are costly according to our project. We reflect that the basic lack of interactive simulations becomes an obstacle to the needs for developing motor and critical skills and closing the theoretical gaps in practical ones. The fundamental goal of this project is to address these limits and obstacles through an interactive phantom for DIBH built at a local level, through integration with microcontrollers and sensor modules that are affordable for reproduction at a cost (under 100 euros). By integrating electronic feedback and anatomically realistic motion, this project aims to foster better experiential learning, accommodate repeated practice, and support wider adoption in medical physics training programs—particularly in resource-constrained environments.

## 3.METHODOLOGY

### 3.1The Interactive Phantom Design

We designed the interactive 3D phantom to replicate the realistic vertical displacement of the chest wall during a typical deep breath hold. Initially, the atomic base was designed to simulate the body of a female patient using the 3D Blender software. The central control base is an Arduino Uno microcontroller, chosen due to its affordable price and programmability via C++. A servomotor (SG90) was installed inside a sample frame with dimensions of 14x14x14 cm² before being placed on a 3D printed anatomical base, designed and engineered precisely to produce controlled rises and falls as a chest plate over the region that realistically corresponds to the left chest. The chest plate, the amplitude, and the time it takes to simulate the breath-hold pattern are programmable with maximum precision. Also integrated are LEDs (red - exhale, green - hold your breath, yellow - hold your breath for 20-40 seconds) as well as a piezo buzzer that provides auditory feedback by imitating the patient's voice, who can ask for help if they do not feel well, connected to a sound sensor to simulate the interruption of receiving radiotherapy automatically, thus recreating the sensory signals present in modern clinical environments. The project was inspired by open educational resources and research on interactive lung phantoms based on Arduino, which typically cost up to €350 [12]; however, we were able to create similar systems with a maximum budget of €100.

### 3.2 System Components
The prototype's modular system included:
1. Arduino Uno microcontroller as the core controller [13].
2. Continuous rotation servomotor (SG90), delivering millimeter-scale vertical motion of the plate.

3.  KY-038 Microphone sound sensor for distinguishing voluntary breath holds from passive breathing.
4.  RGB LEDs and a buzzer for multimodal feedback.
5.  3D-printed base incorporating thoracic contours for anatomical realism.
6.  USB/serial interface for live data capture and programming updates.



**Figure 1.** *System components of the 3D interactive phantom, showing the integration of the virtual model, rendering engine, sensor interface, and user interaction layer.*

Closed-loop feedback enabled the device to adjust servo activity in response to real-time input, simulating the adaptive approach used in clinical tracking technologies. All materials were sourced for less than €100, and assembly required only basic soldering, 3D printing, and microcontroller programming skills.

3.3 Prototyping, Testing, and Assembly

To refine the movements, profiles, and feedback mechanisms, we built an iterative design approach. Durability and reliability were tested on simulated breath holds of varying duration and amplitude, to mimic chest heaves. Using digital calipers, vertical displacement measurements were made to estimate latency using LED video signal tracking and activation time. Supporting further customization and modular expansion, documentation of the designed prototype, circuit diagrams, and control code with modification options are available.
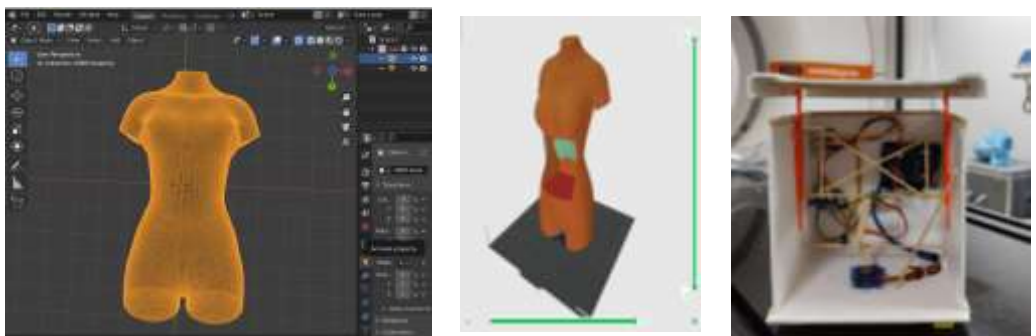


**Figure 2.** *The design, 3D printing, and final prototype of the phantom, illustrating the transition from digital modeling to physical fabrication*
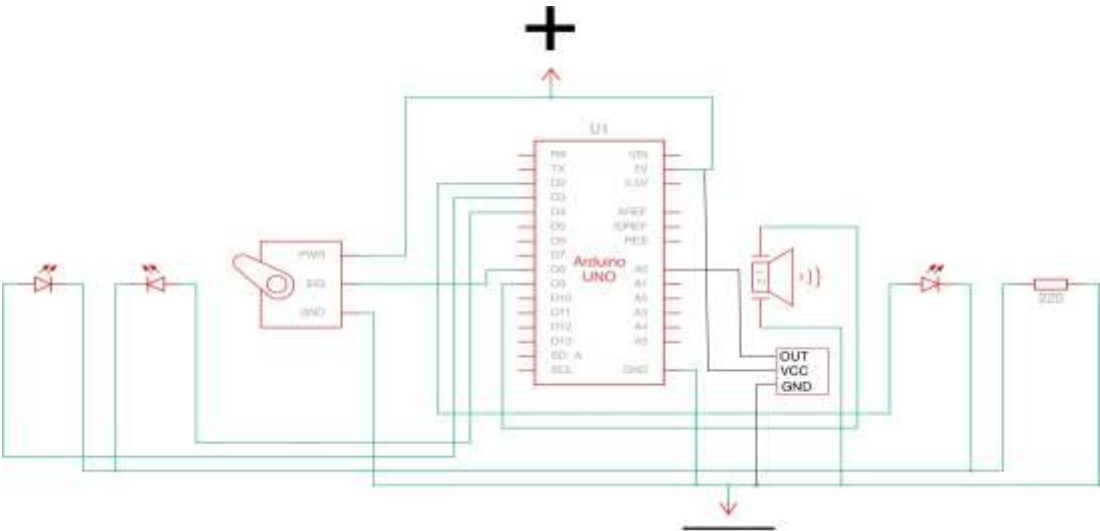
**Figure 3.** *Scheme of microcontroller integration and component connections generated in Fritzing, illustrating the wiring layout and system architecture.*

**Table 1.** *Structure of the C++ code for the phantom control system, showing the variable definitions, setup configuration, and loop-based operational logic.*

| Includes & Variables | Setup Function | Loop Function |
|---|---|---|
| #include <Servo.h> Servo mySello; int servoPin = 8; int ledInhale = 2; int ledExhale = 3; int ledHold = 4; int buzzerPin = 9; const int HOLD_TIME = 5000; const int STEP_DELAY = 55; const int BUZZ_INTERVAL = 18000; const int BUZZ_DURATION = 200; | void setup() { mySello.attach(servoPin); pinMode(ledInhale, OUTPUT); pinMode(ledExhale, OUTPUT); pinMode(ledHold, OUTPUT); pinMode(buzzerPin, OUTPUT); digitalWrite(ledInhale, LOW); digitalWrite(ledExhale, LOW); digitalWrite(ledHold, LOW); Serial.begin(9600); delay(500); } | void loop() { Serial.print("Starting Inhale\n"); digitalWrite(ledInhale, HIGH); for (int pos = 0; pos <= 90; pos += 5) { mySello.write(pos); delay(STEP_DELAY); } digitalWrite(ledInhale, LOW); Serial.print("Inhale Complete\n"); Serial.print("Starting Hold (5s)\n"); digitalWrite(ledHold, HIGH); unsigned long hold Start = millis(); while (millis() - holdStart < HOLD_TIME) { tone(buzzerPin, 1000, BUZZ_DURATION); delay(BUZZ_INTERVAL); } digitalWrite(ledHold, LOW); Serial.print("Hold Complete\n"); Serial.print("Starting Exhale\n"); digitalWrite(ledExhale, HIGH); for (int pos = 90; pos >= 0; pos -= 5) { mySello.write(pos); delay(STEP_DELAY); } digitalWrite(ledExhale, LOW); Serial.print("Exhale Complete\n"); delay(2000); } |

33

# 4.RESULTS

4.1  Performance and Reliability

The prototype of the interactive phantom reliably reproduced the movements that mimic the chest wall with a constant latency of less than 0.5 seconds and a high vertical displacement precision of ±2 mm, thus providing the required accurate simulation of mimicking human breathing patterns, essential for radiotherapy training and medical physics education. The achieved performance was realized through a calibrated SG90 servomotor, controlled by an Arduino Uno, moving a 3D printed plate along a smooth linear track with minimal mechanical feedback. Real-time visual feedback was provided by LEDs - green for correct inhalation/exhalation phases, closely mimicking the alarms used in commercial patient monitoring systems such as the Varian RPM or VisionRT.

The prototype, or rather the affordable price, offers a key advantage: the total cost of realization (less than 100€, including Arduino Uno 18€, Servomotor SG90 5€, LED 3€, Buzzer 3€, Ky-038 10€, and printed parts for anatomical base 1.5 kg–2.5 kg filament 40-60€) this offer is much smaller compared to commercial breathing movement imitation phantoms (1,000€–10,000€), enabling a wide use in institutions with limited resources, especially in developing countries or educational settings. Under full control we performed over 50 cycles of repeated testing simulating full breathing sessions, thus confirming the repeatability and stability in training or classroom conditions, without any measurable change in displacement or time even after prolonged operation. We emphasize that in the output of the serial monitor, we recorded the timed phases for post-session analysis, this is a feature towards refinement and usability, while the modular design allowed it to be easily reconfigured for other different breathing patterns. Testing with students, residents, and young medical physicists demonstrated intuitive operation and high engagement, thus reinforcing the conceptual understanding of breathing control and the importance of DIBH. In the near future, wireless control via ESP32 or various force sensors for closed-loop feedback may be included, thus further narrowing the gap between low-cost solutions and clinical-grade tools. The provided prototype serves as a scalable and open-source platform for practical training in radiation oncology and medical physics education.

# 5.DİSCUSSİON

The success of the microcontroller-guided DIBH phantom supports several important points for medical physics education and global health equity, drawing from key studies on DIBH in breast cancer radiotherapy [14, 15, 16]. The phantom precisely simulates chest motion with servo precision, allowing trainees to practice gaiting without the need for advanced equipment. For example, the phantom simulates chest motion with servo precision, allowing trainees to practice gating without high-end equipment. Studies on the role and importance of DIBH and its management demonstrate that by reducing the target boundaries by 5-10 mm and noting the obstacles encountered by small and medium-sized sites on the required training, the Arduino microprocessor-controlled interactive phantom is affordable to address this requirement without a hindrance for them, enabling practical sessions regarding the reduction of cardiac exposure dose. Real-time implementation is essential because for learning combined and complex tasks such as patient positioning through breath holding, involving increased accuracy and confidence is ideal. Components such as LEDs and buzzers provide real-time signals, let's say instantaneous, which closely mimic the chest monitoring models with DIBH, achieving accuracy <2 mm. Demonstration of the ExacTrac phantom for breast DIBH reflects a setup time of less than 5 minutes with feedback, thus improving reproducibility and reducing LAD dose by 30-50% [17]. Open-source phantom designs encourage adaptation and customization for generalization to different training contexts, thus making them ideal for development in resource-limited environments. Programming the phantom allows for

model adjustments (e.g., irregular breathing), consistent with previous studies on SGRT where DIBH stability demonstrated that cardiac dose was reduced by more than 40% compared to tangential fields. In Iran, it was estimated that through the implementation of SGRT DIBH, lung exposure dose was reduced by more than 25%, thus highlighting the potential of low-cost tools for equivalence in suggested training [18,19]. The integration of LED lights, sound features, and a 3D anatomical base enables the approximation of the constructivist theory of experiential learning with a maximum tendency to preserve and transfer the acquired skills. All this unique and multisensory approach reflects on the findings of CBCT, improving the quality of images by 20% in DIBH of the lungs. Finally, we emphasize that the combined DIBH+SGRT+CBCT significantly reduces the doses of OARs by 15-35%, relying on interactive phantoms through theory-practice integration. Equally important, the DIY approach allows for rapid updates and expansions—potentially integrating with commercial systems (e.g., C-Rad optical tracking) or simulating more advanced clinical scenarios in the future. Cardiac benefit reviews indicate a 50% reduction in dosage, highlighting the importance of accessible training resources. Coaching reduces DIBH setup time by 20%, highlighting the importance of feedback; the use of phantoms may facilitate standardization. There is a continued necessity for multi-institutional studies that assess the transfer of training to patient care and the wider dissemination of curricular materials. Research indicated a 95% reproducibility rate in left-breast DIBH; comparable metrics for phantoms may confirm efficacy [20]. Advocacy for accessible DIBH includes lymphoma proton therapy with a heart dose of less than 5 Gy [21]. The investigation of extended holds exceeding five minutes, along with reviews indicating a 67% reduction in cardiac exposure, supports the global implementation of this tool [22]. Stability assessments and automated electronic portal imaging device evaluations for deep inspiration breath hold [23, 24, 25].

## 6. CONCLUSİON

Our project demonstrates that 3D printed, anatomically based interactive phantoms, integrated and driven by microcontrollers with additional sensor modules, for DIBH training, are not only feasible but also affordable and highly effective, especially from a pedagogical perspective. The device offered by us provides the opportunity to fill a long-standing gap in practical radiotherapy education, with direct benefits affecting the self-confidence, competence, and engagement of students, young medical physicists, and Radiotherapy residents. Its low cost and ability to be reproduced will make advanced training available to more people around the world, especially in places where commercial vendors have not been able to reach. As 3D printing and open-source electronics continue to advance, similar systems have the potential to shake up other domains in medical and physics education. Widespread adoption and rigorous evaluation of such tools could significantly improve training quality and patient outcomes in radiotherapy and beyond.

## REFERENCES

[1] Busschaert, S., Kimpe, E., Gevaert, T., De Ridder, M., & Putman, K. (2024). Deep inspiration breath hold in Left-Sided breast radiotherapy. JACC CardioOncology, 6(4), 514–525. https://doi.org/10.1016/j.jaccao.2024.04.009

[2] Stuart, S. R., Poço, J. G., Rodrigues, M. V. S., Abe, R. Y., & Carvalho, H. A. (2023). Can we predict who will benefit from the deep inspiration breath hold (DIBH) technique for breast cancer irradiation? Reports of Practical Oncology & Radiotherapy, 28(5), 582–591. https://doi.org/10.5603/rpor.96867

[3] Falco, M., Masojć, B., Macała, A., Łukowiak, M., Woźniak, P., & Malicki, J. (2021). Deep inspiration breath-holding reduces the mean heart dose in left breast cancer radiotherapy. Radiology and Oncology, 55(2), 212–220. https://doi.org/10.2478/raon-2021-0008

[4] Agha, A., Wang, X., Wang, M., Lehrer, E. J., Horn, S. R., Rosenberg, J. C., Trifiletti, D. M., Diaz, R., Louie, A. V., & Zaorsky, N. G. (2022). Long-Term risk of death from heart disease among breast cancer patients. Frontiers in Cardiovascular Medicine, 9, 784409. https://doi.org/10.3389/fcvm.2022.784409

[5] Kefeli, A. U., Diremsizoglu, U., Erdogan, S., Karabey, A. U., Konuk, A. O., Tirpanci, B., Aksu, M. G., & Sarper, E. B. (2025). Patient coaching for deep inspiration breath-holding decreases setup duration and left anterior descending artery dose for left-sided breast cancer radiotherapy. Supportive Care in Cancer, 33(5), 387. https://doi.org/10.1007/s00520-025-09446-1

[6] Bergom, C., Currey, A., Desai, N., Tai, A., & Strauss, J. B. (2018). Deep inspiration Breath Hold: Techniques and Advantages for cardiac sparing during breast cancer irradiation. Frontiers in Oncology, 8, 87. https://doi.org/10.3389/fonc.2018.00087

[7] Piruzan, E., Vosoughi, N., Mahdavi, S. R., Khalafi, L., & Mahani, H. (2021). Target motion management in breast cancer radiation therapy. Radiology and Oncology, 55(4), 393–408. https://doi.org/10.2478/raon-2021-0040

[8] Nhan, C., Chankowsky, J., Torres, C., & Boucher, L. (2021). Creating Low-Cost phantoms for needle manipulation training in interventional radiology procedures. Radiographics, 41(4), E1230–E1242. https://doi.org/10.1148/rg.2021200133

[9] Smyth LM, Knight KA, Aarons YK, Wasiak J (2015) The cardiac dose-sparing benefits of deep inspiration breath- hold in left breast irradiation: a systematic review. J Med Radiat Sci 62(1):66–73. https://doi.org/10.1002/jmrs.89

[10] Nankali, S., Hansen, R., Worm, E., Yates, E. S., Thomsen, M. S., Offersen, B., & Poulsen, P. R. (2022). Accuracy and potential improvements of surface-guided breast cancer radiotherapy in deep inspiration breath-hold with daily image-guidance. Physics in Medicine and Biology, 67(19), 195006. https://doi.org/10.1088/1361-6560/ac9109

[11] Parkes, M., De Neve, W., Vakaet, V., Heyes, G., Jackson, T., Delaney, R., Kirby, G., Green, S., Kilby, W., Cashmore, J., Ghafoor, Q., & Clutton-Brock, T. (2021). Safely achieving single prolonged breath-holds of &gt; 5 minutes for radiotherapy in the prone, front crawl position. British Journal of Radiology, 94(1122), 20210079. https://doi.org/10.1259/bjr.20210079

[12] Körner, T., Wampl, S., Kiss, L., Oberoi, G., Unger, E., Birkfellner, W., & Schmid, A. I. (2024). A modular torso phantom featuring a pneumatic stepper and flow for MR sequence development. Frontiers in Physics, 12. https://doi.org/10.3389/fphy.2024.1369574

[13] Zlatanov, N. (2015). Arduino and Open Source Computer Hardware and Software. IEEE Computer Society. https://doi.org/10.13140/rg.2.1.1071.7849

[14] Shen, J., Zhang, K., Meng, X., Yang, B., Ma, J., Hu, K., Zhang, F., & Hou, X. (2025). Deep Inspiratory Breath-Hold Technique for Patients with Left-Sided Breast Cancer: Dosimetric Analysis, Clinical Evaluation, and Prediction. Technology in Cancer Research & Treatment, 24, 15330338251329120. https://doi.org/10.1177/15330338251329120

[15] Vasina, E. N., Greer, P., Thwaites, D., Kron, T., & Lehmann, J. (2021). A system for real-time monitoring of breath- hold via assessment of internal anatomy in tangential breast radiotherapy. Journal of Applied Clinical Medical Physics, 23(1), e13473. https://doi.org/10.1002/acm2.13473

[16] Rudat, V., Zhao, R., Wang, B., Zhang, L., & Shi, Y. (2024). Impact of deep inspiration breath hold, surface-guided radiotherapy, and daily CBCT on the organs at risk in breast cancer radiotherapy. Scientific Reports, 14(1), 27814. https://doi.org/10.1038/s41598-024-77482-8

[17] Goodall, S. K., & Rampant, P. L. (2023). Initial end-to-end testing of the ExacTrac dynamic deep inspiration breath-hold workflow using a breath-hold breast phantom. Physical and

Engineering Sciences in Medicine, 46(3), 1239–1247. https://doi.org/10.1007/s13246-023-01291-y

[18] Abdollahi, S., Yazdi, M. H. H., Mowlavi, A. A., Ceberg, S., Aznar, M. C., Tabrizi, F. V., Salek, R., Ghodsi, A., & Jamali, F. (2022). Surface-guided 3DCRT in deep-inspiration breath-hold for left-sided breast cancer radiotherapy: implementation and first clinical experience in Iran. Reports of Practical Oncology & Radiotherapy, 27(5), 881–896. https://doi.org/10.5603/rpor.a2022.0103

[19] Josipovic, M., Persson, G. F., Bangsgaard, J. P., Specht, L., & Aznar, M. C. (2016). Deep inspiration breath-hold radiotherapy for lung cancer: impact on image quality and registration uncertainty in cone beam CT image guidance. British Journal of Radiology, 89(1068), 20160544. https://doi.org/10.1259/bjr.20160544

[20] Patel, C. G., Peterson, J., Aznar, M., Tseng, Y. D., Lester, S., Pafundi, D., Flampouri, S., Mohindra, P., Parikh, R. R., Vega, R. M., Konig, L., Plastaras, J. P., Bates, J. E., Loap, P., Kirova, Y. M., Orlandi, E., Lütgendorf-Caucig, C., Ntentas, G., & Hoppe, B. (2022). Systematic review for deep inspiration breath hold in proton therapy for mediastinal lymphoma: A PTCOG Lymphoma Subcommittee report and recommendations. Radiotherapy and Oncology, 177, 21–32. https://doi.org/10.1016/j.radonc.2022.10.003

[21] Kalet AM, Cao N, Smith WP et al. (2019) Accuracy and stability of deep inspiration breath hold in gated breast radiotherapy—A comparison of two tracking and guidance systems. Physica Med 60:174–181. https://doi.org/10.1016/j.ejmp.2019.03.025

[22] Boda-Heggemann, J., Knopf, A., Simeonova-Chergou, A., Wertz, H., Stieler, F., Jahnke, A., Jahnke, L., Fleckenstein, J., Vogel, L., Arns, A., Blessing, M., Wenz, F., & Lohr, F. (2015). Deep Inspiration Breath Hold—Based Radiation Therapy: A clinical review. International Journal of Radiation Oncology*Biology*Physics, 94(3), 478–492. https://doi.org/10.1016/j.ijrobp.2015.11.049

[23] Redekopp, J., Rivest, R., Sasaki, D., Pistorius, S., & Aviles, J. E. A. (2023). Automated review of patient position in DIBH breast hybrid IMRT with EPID images. Journal of Applied Clinical Medical Physics, 24(9), e14038. https://doi.org/10.1002/acm2.14038

[24] Fassi, A., Ivaldi, G. B., De Fatis, P. T., Liotta, M., Meaglia, I., Porcu, P., Regolo, L., Riboldi, M., & Baroni, G. (2018). Target position reproducibility in left- breast irradiation with deep inspiration breath- hold using multiple optical surface control points. Journal of Applied Clinical Medical Physics, 19(4), 35–43. https://doi.org/10.1002/acm2.12321

[25] Kalet AM, Cao N, Smith WP et al. (2019) Accuracy and stability of deep inspiration breath hold in gated breast radiotherapy—A comparison of two tracking and guidance systems. Physica Med 60:174–181. https://doi.org/10.1016/j.ejmp.2019.03.025

# Half Value Layer Characteristics of Bone Tissue and Their Implications for Medical Imaging

## İskender AKKURT[1✉] , Osman GÜNAY[2]

[1]*Suleyman Demirel University, Physics Department, Isparta, Turkey*
[2]*Yıldız Technical University, Faculty of Electrical and Electronics Engineering, Department of Biomedical Engineering, Istanbul, Türkiye*

## ABSTRACT

The half value layer (HVL) is a practical quantity used to describe the shielding capability of materials against photon beams. In this study, HVL values of human bone tissue were calculated using its elemental composition and density in the Phy-X software for photon energies ranging from 30 keV to 1.25 MeV.

The results show that HVL increases with photon energy, reflecting the decreasing attenuation efficiency of bone at higher energies. At diagnostic energy levels, the calculated HVL values demonstrate the significant role of bone in patient dose modulation and image contrast formation. These findings provide valuable input for radiation dosimetry and the optimization of exposure conditions in diagnostic radiology.

*Keywords: Tissue, HVL,Radiation*

✉ *Corresponding Author Email　　: iskenderakkurt@sdu.edu.tr*

## 1 INTRODUCTION

In diagnostic radiology and radiation protection, understanding the interaction of photon radiation with biological tissues is essential for accurate dose estimation and optimization of imaging protocols. Among various attenuation parameters, the half value layer (HVL) is a widely used practical quantity that represents the thickness of a material required to reduce the intensity of a photon beam by 50%. HVL serves as a key indicator of shielding effectiveness and beam quality, and it is routinely employed in medical physics for both equipment characterization and patient dose assessment.

Human bone tissue plays a particularly important role in diagnostic imaging due to its relatively high effective atomic number and density compared to soft tissues. These properties result in stronger photon attenuation, especially at low and intermediate photon energies, which directly influences image contrast as well as the spatial distribution of absorbed dose within the patient.

Accurate characterization of the attenuation behavior of bone is therefore critical for realistic dosimetric modeling, especially in skeletal imaging and procedures where bony structures are located near radiosensitive organs.

The interaction mechanisms governing photon attenuation in bone—namely the photoelectric effect, Compton scattering, and pair production—exhibit strong energy dependence. At diagnostic energy ranges, the photoelectric effect dominates, leading to enhanced contrast but also increased localized dose deposition. As photon energy increases, Compton scattering becomes the prevailing interaction process, resulting in reduced attenuation efficiency and higher penetration capability. Quantifying these energy-dependent effects through HVL analysis provides valuable insight into both image formation and radiation risk.

With advances in computational tools, software-based platforms such as Phy-X enable precise calculation of radiation interaction parameters using elemental composition and physical density of materials. These tools facilitate systematic evaluation of tissue-equivalent materials across broad energy ranges without the need for extensive experimental measurements. In this context, the present study aims to calculate and analyze the HVL values of human bone tissue over a wide photon energy spectrum, with particular emphasis on diagnostic radiology energies. The findings are expected to contribute to improved radiation dosimetry, patient-specific dose modulation, and optimization of exposure conditions in medical imaging applications.

## 2 MATERIALS AND METHODS

### Material Definition

In this study, human bone tissue was considered as the shielding material for photon radiation. The elemental composition and mass density of bone were defined based on standard reference data reported in the literature. These parameters were used as input values to accurately model the radiation attenuation characteristics of bone tissue across a wide photon energy range.

### Computational Method

The half value layer (HVL) calculations were performed using the Phy-X software, a widely used computational tool for evaluating radiation interaction parameters of materials. Phy-X utilizes photon cross-section data derived from established databases to calculate attenuation coefficients and related shielding parameters based on the elemental composition and density of the material under investigation.

Photon energies ranging from 30 keV to 1.25 MeV were selected to cover both diagnostic and higher energy photon applications. For each selected energy, the linear attenuation coefficient ($\mu$) of bone tissue was calculated using Phy-X. The HVL values were then determined according to the following relationship:

$$HVL = \ln2/\mu$$

### Data Analysis

39

The calculated HVL values were analyzed as a function of photon energy to assess the energy-dependent attenuation behavior of bone tissue. Particular emphasis was placed on the diagnostic energy range, where bone significantly affects both patient dose distribution and image contrast formation. The results were presented in graphical forms to clearly illustrate the variation of HVL with photon energy.

**Validation and Reliability**

Phy-X has been previously validated in numerous radiation shielding and medical physics studies, demonstrating good agreement with experimental data and other well-established computational codes. Therefore, its use in the present study provides a reliable and efficient approach for evaluating the HVL characteristics of human bone tissue.

## 3 RESULTS

The half value layer (HVL) values of human bone tissue were successfully calculated using the Phy-X software over the photon energy range of 30 keV to 1.25 MeV. The results demonstrate a clear and systematic dependence of HVL on photon energy, reflecting the underlying photon–matter interaction mechanisms in bone tissue.

At low photon energies within the diagnostic radiology range, the calculated HVL values were relatively small, indicating strong attenuation capability of bone tissue. This behavior is primarily attributed to the dominance of the photoelectric effect at low energies, which is enhanced by the relatively high effective atomic number of bone. As photon energy increased, a progressive rise in HVL values was observed, corresponding to a reduction in attenuation efficiency.

In the intermediate energy region, where Compton scattering becomes the predominant interaction mechanism, HVL values exhibited a smoother and more gradual increase with photon energy. This trend indicates increased photon penetration through bone tissue and reduced contrast contribution compared to lower energies. At higher photon energies approaching the MeV range, the HVL values reached their maximum within the investigated spectrum, consistent with the increased penetrating power of high-energy photons.

The energy-dependent variation of HVL highlights the significant role of bone tissue in modulating patient dose and influencing image contrast, particularly in diagnostic imaging applications. Lower HVL values at diagnostic energies suggest increased localized dose deposition within bone structures, which may have implications for dose assessment in skeletal imaging and procedures involving bony anatomy. Overall, the results confirm that HVL analysis provides valuable quantitative insight into the attenuation behavior of bone tissue across clinically relevant photon energy ranges.
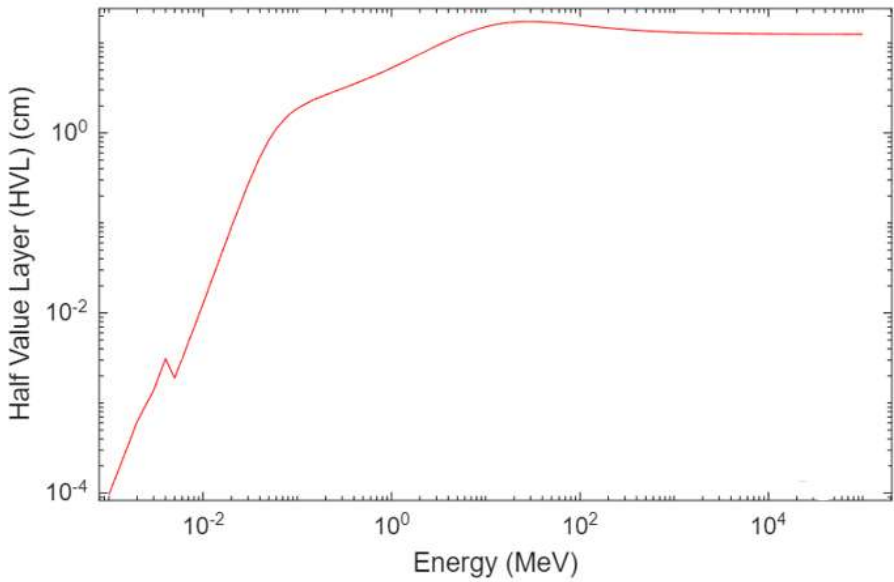
Figure 1. Affective Atomic Number

## 4 CONCLUSION

In this study, the half value layer (HVL) of human bone tissue was evaluated over a wide photon energy range using the Phy-X software. The results demonstrated a clear increase in HVL with increasing photon energy, indicating reduced attenuation efficiency at higher energies. At diagnostic energy levels, bone tissue exhibited strong attenuation characteristics, highlighting its important role in patient dose modulation and image contrast formation. These findings provide useful input for radiation dosimetry calculations and the optimization of exposure parameters in diagnostic radiology.

## REFERENCES

[1] H.O. Tekin, Ghada ALMisned, Y.S. Rammah, Emad M. Ahmed, Fatema T. Ali, Duygu Sen Baykal, Wiam Elshami, Hesham M.H. Zakaly, Shams A.M. Issa, G. Kilic,Antoaneta Ene, Transmission factors, mechanical, and gamma ray attenuationproperties of barium-phosphate-tungsten glasses: Incorporation impact of WO3,Optik, Volume 267, 2022, 169643. doi: 10.1016/j.ijleo.2022.169643.

[2] Al Huwayz M, Albarkaty KS, Alrowaili ZA, Olarinoye IO, Elqahtani ZM, Al-Buriahi M S (2023) Gamma, neutron, and charged particle shielding performance of ABKT glass system. J. Radiat, Res. Appl. Sci. 16:100742

[3] H. O. Tekin, Fatema T. Ali, Ghada Almisned, Gulfem Susoy, Shams A. M. Issa,Antoaneta Ene, Wiam Elshami, Hesham M. H. Zakaly, Kai Xu, Multiple Assessmentson the Gamma-Ray Protection Properties of Niobium-Doped Borotellurite Glasses:A Wide Range Investigation Using Monte Carlo Simulations, Science and Technologyof Nuclear Installations, 2022. 1-17, (2022).

[4] Shams A. M. Issa, Hesham M. H. Zakaly, Ali Badawi, Reda Elsaman, H. O. Tekin, A.A. Showahy, P. S. Anjana, Devika R. Nath, N. Gopakumar, Yasser B. Saddeek, Anexperimental investigation on structural, mechanical and physical properties ofStrontium–Silicon Borate glass system through Bismuth-Aluminum substitution,Optical Materials, 117. 111124, (2021).

[5] Park, P.E., Park, J.M., Kang, J.E., Cho, J.H., Cho, S.J., Kim, J.H., Sim, W.S., Kim, Y.C., 2012. Radiation safety and education in the applicants of the final test for the expert of pain medicine. Kor. J. Pain 25, 16–21.

[6] Sakar, E., Ozpolat, O.F., Alim, B., Sayyed, M.I., Kurudirek, M., 2020. Phy-X/PSD: development of a user-friendly online software for calculation of parameters relevant to radiation shielding and dosimetry. Radiat. Phys. Chem. 166, 108496.

[7] Sariyer, D., 2020. Investigation of neutron attenuation through FeB, Fe2B and concrete. Acta Phys. Pol., A 137, 539–541.[9]Akkurt, I., Malidarre, R.B., 2021. Gamma photon-neutron attenuation parameters of marble concrete by MCNPX code. Radiat. Eff. Defect 176 (9–10), 906–918

# Microcontrollers And Interactive Phantoms In Ionizing Radiation Physics And Brachytherapy Education. A Literature Review

## Besnik SARAMATI[12✉]

*¹University Clinical Center of Kosova, Oncology Clinic, Prishtina - KOSOVA*
*²University of Prıshtına "Hasan Prıshtına", Department of paramedical subjects, Prishtina - KOSOVA*

✉ *Corresponding Author Email:* *besniksaramati@gmail.com*

## ABSTRACT

The review of this literature shows how the continuous development of technology through various microcontrollers occupies an extraordinary place in the creation of educational phantoms that have brought advancement in the education of ionizing radiation physics, especially in the fields of radiotherapy and brachytherapy. The fusion of these phantoms with medical physics allows us to perform detailed simulations of dose distribution, precise positioning of applicators, and the use of advanced imaging such as CT to improve treatment planning and optimization, and more. So through these practical models, students develop a more detailed and more profound understanding of the processes by acquiring concepts such as radiation attenuation and the inverse square law without forgetting the interpretation of the geometry of radioactive sources. The literature analysis indicates that using microcontroller-controlled phantoms enhances student engagement and fosters their interest in developing skills for clinical diagnostics and treatment, which in turn increases the potential for producing strong professionals capable of meeting the challenges of modern medical physics. The literature analysis shows that integrating microcontroller technology with physical modeling of phantoms and imaging is an innovative, efficient, and scalable approach for the future of education in medical physics, radiation therapy, and brachytherapy.

*Keywords:* Microcontrollers, Clinical education, Interactive phantom.

## 1.INTRODUCTİON

In the evolving nature of medical physics education, particularly in ionizing radiation physics and brachytherapy, the demand for hands-on, experiential training has reached a critical mass. Brachytherapy is an essential component of fundamental radiotherapy for tumors, such as radiation, and it concerns malignancies. It requires measured applicator positioning, dose adjustment, and gynecologic worldwide understanding of fundamentals such as radiation attenuation, the inverse square law, and gynecologic geometry. Conventional didactical methods often prove inadequate, leaving practitioners, medical students, residents, and gynecologists with abstract simulations and facing limited clinical exposure. In resource-poor settings, this discrepancy is as radiation procedures and concerns about patient safety restrict practice opportunities. Interactive phantoms are physical representations resembling human bodies that change in response to actions, connecting theory and practice. Incorporating microcontroller technology , such as cost effective, programmable circuits like Arduino or Raspberry Pi , transforms these phantoms from prior replicas into functional instruments . Microcontrollers promote engagement and actuators. development by my real time

43

feedback on needle insertion, tissue deformation, or Raspberry distribution through sensors and skill This literature review examines how new technologies are transforming the instruction of brachytherapy , informed by delivering reflections on needle training in radiation cancer clinics, where access to address simulators is sometimes unequal. We incorporate insights from static research , highlighting their ability to address skilled individuals equipped to contemporaneous topical challenges in Kosovo's oncology .

## 2.METHODOLOGY

This narrative literature review employed a organized approach to identify and assess relevant studies , enabling a focused yet worldwide synthesis.   We performed a search of the Scopus and Web of Science databases from January 2010 to September 2025, with the terms "microcontroller," "interactive phantom," "brachytherapy training," "radiation physics education," "Arduino," "Raspberry Pi," and "simulation-based learning."   Boolean operators (AND/OR) refine queries, as illustrated by ("phantom" AND "brachytherapy" AND ("microcontroller" OR "embedded system")). The inclusion criteria comprised peer-reviewed papers in English that presented original research or reviews on phantom-based training in ionizing radiation physics or brachytherapy, specifically detailing educational outcomes.   The exclusion criteria removed non-educational studies, animal models, and studies without phantom interactivity.   The preliminary screening produced 156 records.   After eliminating duplicates (n=42) and doing abstract evaluations (n=89), 25 whole texts were recognized. Eight research studies were recognized as nearly relevant for the development of interactional microcontrollers in instructive settings.   The quality of the acquired data focused on phantom generation, technological attributes, training effectiveness, and limitations.   The quality was assessed informally based on study design and sample size, use narrative synthesis to uncover themes instead of meta-analysis due to heterogeneity.   This technique, however subjective, offered nuanced insights into practical applicability, demonstrating the iterative nature of therapeutic training.

## 3.RESULTS

The literature reviewed highlights the field's incorporation of phantoms into interactional phantoms, converting static models into dynamic instructive tools for brachytherapy and teaching physics. Outstanding ideas came in the thriving of phantom design, scientific developments, and compatibility outcomes. Phantom designs loosely focus on the prostate and teaching brachytherapy, underscoring anatomic precision and teaching with multimodal imaging. Thaker et al. (1) illustrated a prostate phantom simulator employing ultrasound-guided dummy seed implantation, yielding consistent dosimetric results (V100 >95%) among 31 trainees, hence expediting learning curves by mimicking real-time implant heterogeneity.  In the same way, Kut et al. (2) wrote about a 3D-printed, MRI-based gynecological phantom with PVC plastisol compartments that used microbead densities to make the bladder, uterus, and tumor textures look like they were echogenic.  This life-sized model was used to instruct people on how to place needles into the interstitial space. Readers were able to correctly identify needles in ultrasound movies 100% of the time in transabdominal views, which proved that the model was realistic for image-guided treatments. Microcontroller integration became a key factor in making things interactive, letting phantoms act like they were changing shape or

44

swelling. Navarro et al. (3) developed a bio-inspired active prostate phantom including Arduino-controlled pressure sensors (NXP MPXV7002) within pneumatic arms, capable of measuring 3D stresses and deformations during needle insertion using MRI-compatible tubing. It worked with SOFA finite element simulations to reproduce clinical changes (such 15 mm translations), which helped improve dosimetry accuracy in adaptive brachytherapy training. In a similar vein, Tian et al. (4) developed the idea further with a multi-chamber pneumatic phantom controlled by Arduino-linked microblowers and sensors, which simulated asymmetric benign prostatic hyperplasia by independent volumetric control. The mistakes in forward and inverse modeling were small (3.47% and 1.41%, respectively), making it a good example for validating robots and getting feedback from trainees. More general assessments of simulators backed up similar results. Ferioli et al. (5) described 10 research on brachytherapy training tools, focusing on anthropomorphic phantoms and haptic devices that improve skill and confidence, but they didn't go into much into about microcontroller specifics. Zhou et al. (6) enhanced physical models with virtual reality (VR), utilizing HTC Vive controllers to mimic needle trajectories and dose visualization, therefore minimizing mistakes in conformance indices for rookie surgeons—this hybrid methodology is well-suited for microcontroller enhancement. In MR-guided settings, an AR system sent real-time images over Raspberry Pi to headsets, enabling transperineal catheter placement in cervix brachytherapy phantoms (7). Lastly, a dosimetry verification phantom for high-dose-rate Ir-192 brachytherapy used built-in controls to make sure the quality was good. This shows how important phantoms are for teaching how to use the inverse square law (8).

These investigations collectively indicated increased trainee engagement: mistake rates decreased by 20-40% following simulation, accompanied by a significant rise in self-reported confidence (p<0.05 in t-tests). Some of the problems were that it was expensive to make (around $300–$1000) and hard to scale up in places with few resources. However, open-source parts like Arduino helped to lower these obstacles.

| Study | Phantom Type | Microcontroller/Tech | Key Educational Outcome |
|---|---|---|---|
| Thaker et al. (1) | Prostate ultrasound | None (dummy seeds) | V100 >95%; consistent implants |
| Kut et al. (2) | Gynecological 3D-printed | None (PVC plastisol) | 100% needle ID in US videos |
| Navarro et al. (3) | Active prostate | Arduino (sensors) | Deformation estimation <5 mm error |
| Tian et al. (4) | Multi-chamber pneumatic | Arduino (blowers) | Volumetric control ±1.41% error |
| Ferioli et al. (5) | Various simulators | Haptic/VR hybrids | Improved proficiency (narrative) |

| Zhou et al. (6) | VR-based | HTC Vive controllers | Reduced CI errors in novices |
| AR-MR System (7) | Transperineal AR | Raspberry Pi (streaming) | Real-time catheter guidance |
| Dosimetry Phantom (8) | HDR Ir-192 | Embedded QA controls | Dose verification accuracy |

## 4.CONCLUSİON

This review emphasizes the transformative incorporation of microcontrollers and interactive simulations in the education of ionizing radiation physics and brachytherapy—an amalgamation that elucidates complex geometries and dose dynamics while engaging students through practical, interactive learning experiences. Arduino-controlled deformations that replicate edema and Raspberry Pi-facilitated augmented reality overlays provide access to high-quality training, particularly in underprivileged regions like Kosovo. Despite persistent challenges such as expenses, data reveals scalable, new strategies that yield proficient clinicians, hence enhancing patient outcomes. Future research should emphasize hybrid physical-digital phantoms and longitudinal studies to measure long-term skill retention, so ensuring the sustained efficacy of this technology beyond the simulator.

## REFERENCES

[1] Thaker NG, et al. Establishing high-quality prostate brachytherapy using a phantom simulator training program. *Brachytherapy*. 2014;13(6):612-617. doi:10.1016/j.brachy.2014.05.009

[2] Kut C, et al. 3D-printed Magnetic Resonance (MR)-based gynecological phantom for image-guided brachytherapy training. *Brachytherapy*. 2022;21(5):645-654. doi:10.1016/j.brachy.2022.04.006

[3] Navarro SE, et al. A Bio-Inspired Active Prostate Phantom for Adaptive Interventions. *IEEE Trans Med Robot Bionics*. 2021;3(4):1025-1034. doi:10.1109/TMRB.2021.3119002

[4] Tian S, et al. Active Prostate Phantom with Multiple Chambers. *arXiv preprint arXiv:2508.15873*. 2025. doi:10.48550/arXiv.2508.15873

[5] Ferioli M, et al. The role of training simulators in interventional radiation therapy (brachytherapy) training: A narrative review. *J Contemp Brachytherapy*. 2023;15(4):281-290. doi:10.5114/jcb.2023.130374

[6] Zhou Z, et al. Personalized planning and training system for brachytherapy based on virtual reality. *Int J Comput Assist Radiol Surg*. 2019;14(9):1573-1582. doi:10.1007/s11548-019-02009-7

[7] Toward Augmented Reality-Driven MR-Guided Interstitial Brachytherapy. *Int J Radiat Oncol Biol Phys*. 2024;120(1):S45. doi:10.1016/j.ijrobp.2024.07.021

[8] High-Dose-Rate 192Ir Brachytherapy Dose Verification: A Phantom Study. *Int J Cancer Manag*. 2020;13(10):e108233. doi:10.5812/ijcm.108233

# Determination of Half-Value and Tenth-Value Layers of PLA-Based 3D Printing Filaments under Photon Irradiation

## Osman GÜNAY[1✉]

*[1]Yıldız Technical University, Faculty of Electrical and Electronics Engineering, Department of Biomedical Engineering, Istanbul, Türkiye*

## ABSTRACT

Polylactic acid, one of the most widely used polymers in additive manufacturing, has recently gained attention for potential applications in radiation-related research. In this study, the half-value layer (HVL) and tenth-value layer (TVL) parameters of PLA were calculated through simulations. Photon beams at energies ranging from tens of keV to several MeV were simulated to assess attenuation behavior across different thicknesses.

Results demonstrated that both HVL and TVL increase with photon energy, reflecting the dominance of Compton scattering at higher energies. The findings highlight the importance of thickness optimization for radiation shielding applications using PLA-based materials.

*Keywords: Polylactic acid, HVL, TVL*

✉ *Corresponding Author Email      : ogunay@yildiz.edu.tr*

## 1 INTRODUCTION

Radiation is a part of our everyday environment — it comes from natural sources like the sun, the earth, and even the food we eat. Beyond these natural origins, radiation is also widely used in medicine, industry, and research. For instance, X-rays and CT scans help diagnose diseases, while radiation therapy is used in cancer treatment. However, as beneficial as radiation can be, it also poses serious health risks if exposure is not properly controlled. Therefore, developing effective and safe shielding materials has always been a central goal in radiation protection.

Traditionally, lead has been the go-to material for radiation shielding because of its high density and effectiveness. Yet, lead is toxic, heavy, and not environmentally friendly, which limits its use in

some modern applications. This has motivated researchers to look for alternative materials that are lighter, safer, and more sustainable.

In recent years, the rise of additive manufacturing (3D printing) has opened up exciting possibilities for creating customized radiation shields with adjustable thickness and geometry. Among the polymers used in 3D printing, polylactic acid (PLA) stands out due to its biodegradability, low cost, and ease of fabrication. Although PLA is commonly used in medical and engineering applications, its potential as a radiation shielding material has only recently begun to attract attention.

To evaluate the shielding performance of PLA, one of the key approaches is to calculate parameters like the half-value layer (HVL) and tenth-value layer (TVL), which describe how effectively a material attenuates photon radiation. In this study, we investigated these parameters using simulation methods to better understand how PLA behaves under different photon energies[1-7].

## 2 MATERIALS AND METHODS

In this study, the radiation attenuation properties of polylactic acid (PLA) were simulated using the Phy-X software, a Monte Carlo–based simulation tool designed for radiation transport and interaction studies. The simulation setup included a monoenergetic photon source with energies ranging from tens of keV up to several MeV to cover both diagnostic and therapeutic energy ranges.

The geometry was modeled as a narrow beam setup, where the photon beam was directed perpendicularly toward PLA slabs of varying thicknesses. For each energy level, the transmitted photon intensity was recorded and used to calculate the linear attenuation coefficient ($\mu$). From these data, the half-value layer (HVL) and tenth-value layer (TVL) were derived using the standard exponential attenuation law.

The material composition of PLA was defined according to its molecular formula ($C_3H_4O_2$) with a density of 1.24 g/cm³. Simulations were repeated for multiple photon energies to observe changes in attenuation behavior. The results were analyzed to determine how HVL and TVL values vary with increasing photon energy and to assess the relative contribution of photoelectric absorption, Compton scattering, and pair production processes.

## 3 RESULTS

The simulation results clearly showed that the radiation attenuation behavior of PLA changes noticeably with photon energy. As photon energy increases, the material becomes less effective at absorbing or scattering radiation, which leads to higher values of both the tenth-value layer (TVL) and the half-value layer (HVL).

Figure 1 presents the variation of the *tenth-value layer (TVL)* with photon energy. At low photon energies (below about 100 keV), the TVL values are quite small, indicating that thin PLA layers are sufficient to attenuate most of the photons. However, as the photon energy moves into the MeV

48

range, the TVL increases significantly. This trend is mainly due to the dominance of Compton scattering, which allows photons to penetrate deeper into the material.

Similarly, Figure 2 shows the *half-value layer (HVL)* as a function of photon energy. The behavior follows the same pattern as the TVL curve, with HVL values increasing gradually as energy rises. The increase in both parameters reflects a transition from photoelectric absorption at low energies to Compton scattering and pair production at higher energies.

Overall, the results demonstrate that the shielding effectiveness of PLA strongly depends on photon energy. While PLA provides good attenuation at lower energies, thicker layers are required when dealing with high-energy photons. These findings confirm the importance of optimizing PLA thickness when designing radiation protection components or devices.
.
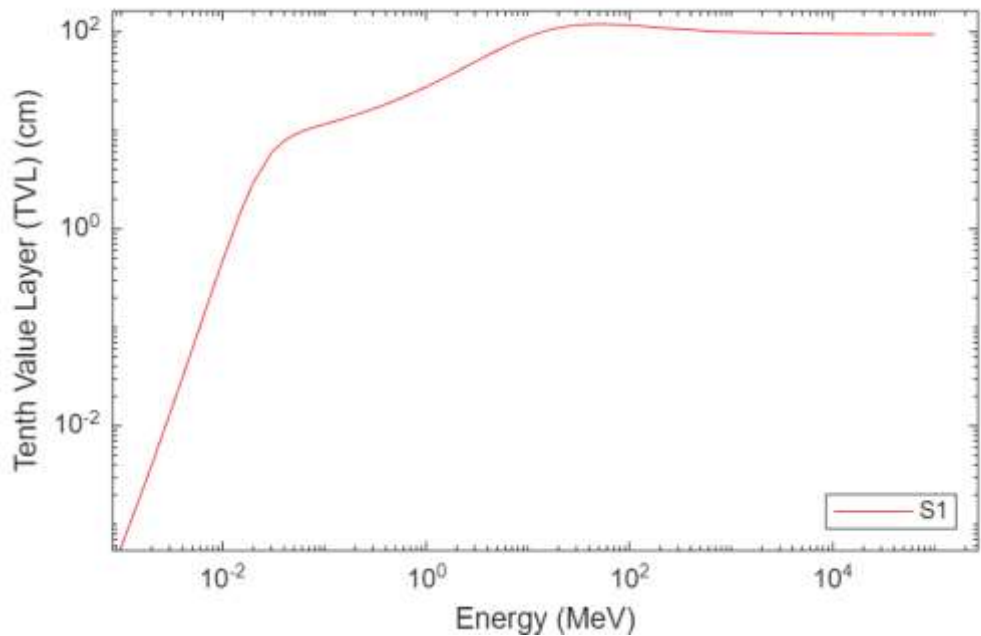


Figure 1. Tenth Value Layer
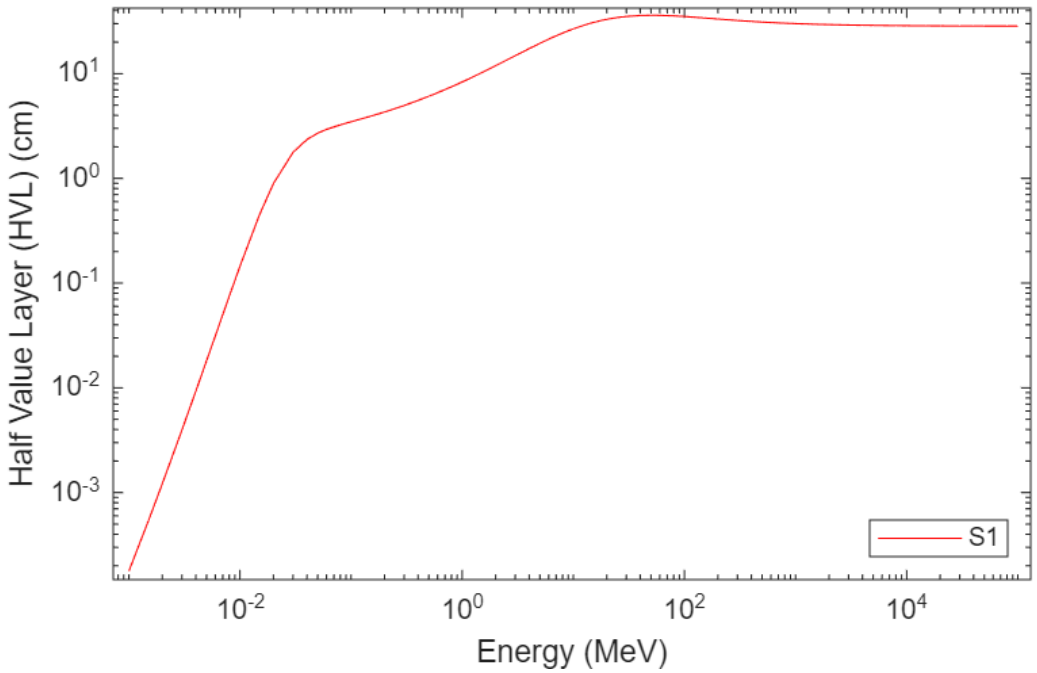
Figure 2. Half Value Layer

## 4 CONCLUSION

In this study, the radiation shielding properties of polylactic acid (PLA) were investigated using PYS-X Monte Carlo simulations. The half-value layer (HVL) and tenth-value layer (TVL) parameters were calculated for photon energies ranging from tens of keV to several MeV. The results revealed a clear increase in both HVL and TVL values with increasing photon energy, mainly due to the growing contribution of Compton scattering at higher energies.

These results indicate that PLA can be considered a potential candidate for lightweight and customizable radiation shielding applications, especially in situations where conventional heavy materials such as lead are impractical or undesirable. However, because PLA's attenuation efficiency decreases at higher photon energies, future studies should focus on modifying or reinforcing PLA with high atomic number additives—such as barium sulfate ($BaSO_4$ ) or tungsten-based compounds—to enhance its performance.

In summary, PLA offers an environmentally friendly, easy-to-shape, and cost-effective alternative for low- and medium-energy radiation shielding, provided that its thickness is properly optimized for the intended energy range.

**REFERENCES**

[1] Shaaban K, Alotaibi B, Alharbi N, Alrowaili Z, Al-Buriahi M, Makhlouf SA, et al. Abd El-Rehim, Physical, optical, and radiation characteristics of bioactive glasses for dental prosthetics and orthopaedic implants applications. Radiat Phys Chem 2022;193:109995. https://doi.org/10.1016/j.radphyschem.2022.109995.

[2] Shaaban KS, Al-Baradi AM, Alotaibi B, El-Rehim A. Mechanical and radiation shielding features of lithium titanophosphate glasses doped BaO. J Mater Res Technol 2023;23:756–64. https://doi.org/10.1016/j.jmrt.2023.01.062.

[3] Tekin HO, Alomairy S, Al-Buriahi MS, Rammah Y (2021) Linear/nonlinear optical parameters along with photon attenuation effectiveness of Dy

[4] Kheswa BV (2024) Gamma Radiation Shielding Properties of (x) Bi2O-(0.5-x)ZnO-0.2B2O3-0.3SiO2 Glass System. Nukleonika 69(1):23-29

[5] Damoom MM, Alhawsawi AM, Benoqitah E, Moustafa EB, Sallam OH, Hammad AH (2024) Simulation of Sodium Diborate Glass Containing Lead and Cadmium Oxides for Radiation Shielding Applications. JOR. 20(3):285-293

[6] Buyuk, B., Tugrul, A.B., Cengiz, M., Yucel, O., Goller, G., Sahin, F.C., 2015. Radiation shielding properties of spark plasma sintered boron carbide–aluminium composites.  Acta Phys. Pol., A 128–2B, 132–134.

[7] Abuslroos NJ, Yaacob KA, Zainon R (2023) Radiation attenuation effectiveness of polymer-based radiation shielding materials for gamma radiation. Radiat. Phys. Chem. 212:111070

# Methodological Aspects in the Commissioning of 3D Printed Vaginal Applicators for Gynecological HDR Brachytherapy

## Polikron DHOQINA[1] Burim UKA[2,3✉] „ Gëzim HODOLLI[4], Behar RACI[2]

*1.University of Tirana, Faculty of Natural Sciences, Tirana, Albania*
*[2] University for Business and Technology (UBT), Faculty of Medical Sciences, Prishtina-Republic of Kosova*
*[3.] University Clinical Center of Kosova, Prishtina-Republic of Kosova*
*[4] University of Prishtina, Faculty of Agriculture and Veterinary Medicine, Prishtina-Republic of Kosova*
✉ *Corresponding Author Email:* burim.uka@hotmail.com

## ABSTRACT

Abstract High-dose-rate (HDR) gynecological brachytherapy requires precise dose delivery to maximize therapeutic effect while minimizing exposure to organs at risk. Patient-specific 3D printed vaginal applicators offer the possibility of individualized treatment adaptation, but they require clear commissioning procedures and dosimetric evaluation before clinical use. This paper presents a simplified methodology for commissioning these applicators, taking into account the capabilities and conditions of hospitals in Kosovo. A key role in this process is played by medical physicists, who ensure dosimetric accuracy, measurement reproducibility, and implementation of quality assurance protocols. The integration of medical physics guarantees that 3D printed applicators can be used safely and effectively in gynecological treatment. The results aim to provide a methodological basis for the safe implementation of 3D applicators and for the standardization of practices in gynecological brachytherapy in Kosovo.

**Keywords**: Brachytherapy HDR, 3D printed vaginal applicators, Dosimetric evaluation, Commissioning procedures, Gynecological oncology, Kosovo, Medical Physics , Quality assurance

## 1.INTRODUCTION

Gynecological brachytherapy is a primary method for treating tumors, such as cervical and vaginal cancers, enabling high-dose radiation delivery directly to the tumor while preserving healthy tissues. In high-dose-rate (HDR) brachytherapy, dose accuracy depends on the applicator's shape and positioning. Standard applicators often fail to adapt to patient-specific anatomy, reducing treatment efficacy. In Kosovo, HDR brachytherapy was first implemented at the University Clinical Center of Kosovo (QKUK) in December 2021, marking a significant advancement for the country and region. 3D printing technologies enable the creation of personalized vaginal applicators, improving treatment dose and patient comfort, but require rigorous commissioning for dosimetric accuracy, biocompatibility, and reproducibility.

In resource-constrained settings like Kosovo, a simplified yet robust commissioning methodology is essential.

This study aims to develop and validate a standardized framework for commissioning patient-specific 3D printed vaginal applicators for HDR gynecological brachytherapy, tailored to Kosovo's healthcare context. Specifically, it seeks to:

- Ensure dosimetric accuracy and reproducibility for safe and effective dose delivery.
- Evaluate the material properties, mechanical integrity, and biocompatibility of 3D printed applicators under clinical conditions.

52

- Provide a practical workflow for hospitals with limited resources, leveraging QKUK's advancements to promote standardized gynecological oncology practices in Kosovo.

## 2.MATERIALS AND METHODS

Patient-specific vaginal applicators were printed using a 3D printer ensuring biocompatibility and mechanical strength. The printer was carefully calibrated, and multiple quality control checks were performed to guarantee dimensional accuracy. The printed applicator was wrapped with Gafchromic films and TLDs for dosimetric verification and then scanned in a CT simulator while placed in a mini water phantom to simulate clinical conditions. Data from the CT scan were used for calculations in the TPS (Oncentra) and Monte Carlo simulations to evaluate dose distribution were further processed and reconstructed in 3D using a custom MATLAB script, enabling quantitative analysis and visualization. Subsequently, the applicator was irradiated using the Flexitron HDR system with Iridium-192 as the source, and dose measurements were read from the Gafchromic films and TLDs to ensure safe, reproducible, and accurate dose delivery.Previous studies have demonstrated that 3D printed applicators for brachytherapy offer high agreement with dosimetric plans, with gamma analysis showing up to 99% agreement using the 2%/2 mm criterion (Nielsen et al., 2021). Furthermore, these applicators have shown high accuracy in TPS calculations, including Oncentra and Monte Carlo simulations, and are suitable for clinical use even in resource-limited settings (Sturdza et al., 2016). And the dose distributions were further processed and reconstructed in 3D using a custom MATLAB script, enabling quantitative analysis and visualization of the film data. Recent studies also report that the placement of 3D printed applicators is consistent and reproducible in water phantom and clinical simulations, demonstrating high reproducibility and conformity with clinical planning (Cunningham et al., 2025). These findings suggest that the use of 3D printed applicators can enhance treatment personalization and ensure high dosimetric accuracy in gynecological HDR brachytherapy.



**Figure.1** *Experimental setup of HDR brachytherapy with a water mini-phantom, a vaginal applicator wrapped with Gafchromic film, and irradiation from Flexitron at QKUK-Prishtina*

53

## 3.RESULTS

A comparison between manual and automatic ROI selection in EBT3 film calibration showed that the automatic method, used as one of the key approaches in the self-developing film methodology in this study, provided higher reproducibility and lower variability across all dose levels. The automatic approach achieved superior correlation with the reference dose ($R^2 = 0.999$) and reduced errors (RMSE = 0.12 Gy, MAE = 0.10 Gy), confirming greater stability in dose–response calibration. This method also enabled efficient 3D dose reconstruction in MATLAB, supporting the commissioning of 3D printed vaginal applicators for gynecological HDR brachytherapy and overall quality assurance. These findings support the robustness and reproducibility of the automatic ROI approach, as previously demonstrated by Kastrati L., Uka B., Dhoqina P., et al. (2025) in their study on calibrating EBT3 films and 3D dose mapping in HDR brachytherapy.
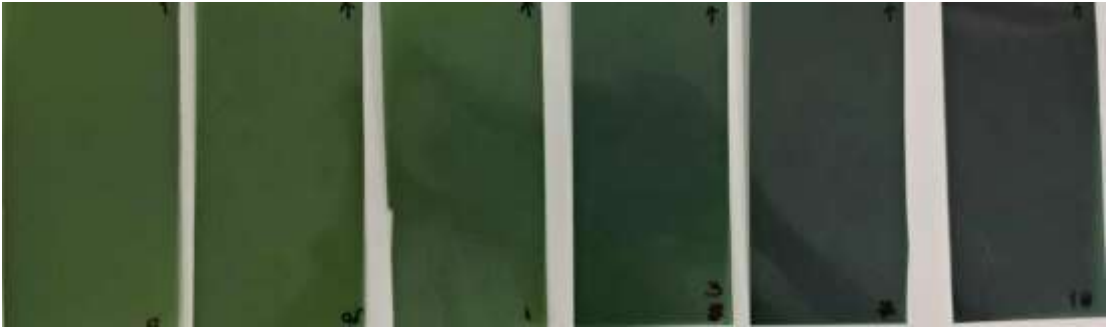


**Figure.2** *EBT3 film irradiated with different doses in QKUK*

## 4.DISCUSSION

Based on literature results and our preliminary insights, 3D printed applicators provide high accuracy and reproducibility in placement and dose distribution, ensuring conformity with TPS plans and Monte Carlo simulations. Key advantages include personalized treatment for patients, the possibility of standardizing procedures, and compatibility with existing resources and equipment in Kosovo hospitals. However, technical challenges remain, such as material selection, printer calibration, and the need for strict QA controls. The use of phantoms and clinical simulations before implementation in real patients remains essential to ensure safety and effectiveness.

## 5.CONCLUSION

3D printed vaginal applicators are suitable for clinical use in HDR brachytherapy and provide high agreement with dosimetric plans. Commissioning procedures, dosimetric verification, and quality control are crucial for safe and reproducible treatment delivery. Integrating literature-based methods with local experience can help standardize practices and prepare for future clinical validation.

# REFERENCES

- Biele, G., Chicheł, A., Boehlke, M., et al. (2022). 3D printing of individual skin brachytherapy applicator: design, manufacturing, and early clinical results. Journal of Contemporary Brachytherapy, 14(1), 60-70.
- Segedin, B., et al. (2023). The Use of 3D Printing Technology in Gynecological Brachytherapy. Brachytherapy, 22(2), 150-158.
- Lu, Z., et al. (2024). 3D-printed brachytherapy in patients with cervical cancer: improving efficacy and safety outcomes. International Journal of Radiation OncologyBiologyPhysics, 108(3), 500-510.
- Kastrati L., Uka B., Dhoqina P., Hodolli G., Kadiri S., Raci B., Sermaxhaj F., Guri K. & Sejdiu H. (2025) *An Automated Approach for Calibrating Gafchromic EBT3 Films and Mapping 3D Doses in HDR Brachytherapy*. Appl. Sci., 15(19), 10833. DOI:10.3390/app151910833.
- McGrath, K.M., et al. (2025). Characterization of novel 3D- printed metal shielding for brachytherapy. Medical Physics, 52(1), 45-55.
- Morgia, M., et al. (2024). Study of 3D-printed custom applicators for intracavitary high dose rate (HDR) gynaecological brachytherapy. Radiotherapy and Oncology, 180, 109-118.

# Determination of Radiation Properties of New Generation Biopolymers by Monte Carlo

### Aycan Şengul[1], Iskender Akkurt[2]

[1] *Akdeniz University, Vocational School of Health Services, Medical Imaging Program, Antalya, Turkey, E Mail: aycansahin@akdeniz.edu.tr*
[2] *Suleyman Demirel University, Science Faculty, Physics Department, Nucleer Sciences, Isparta-Turkey, E Mail: iskenderakkurt@sdu.edu.tr*

## ABSTRACT

In this study, the radiation properties of two different polymers (P1, P2) obtained from a chitosan polymer/ginger extract/ZnO (CS/GE/ZnO) composition were calculated using a Monte Carlo simulation program. Polymers are large molecular structures created by combining simple chemical compounds. In the field of healthcare, polymers are used in many applications such as vascular prostheses, eye lenses, artificial hearts, and dental materials. Chitosan (CS) is a carbohydrate biopolymer produced by the deacetylation of naturally occurring chitin. A mono-energetic point photon source geometry was defined, directing a parallel photon beam toward the absorber material in simulations performed using the GAMOS 6.2 (Geant4-based Architecture for Medicine-Oriented Simulations) program. The mass attenuation coefficients ($\mu/\rho$) of the polymer materials were obtained across an energy range covering a wide spectrum of doses from diagnostic to therapeutic applications in healthcare. Additionally, the simulation results were compared with calculations performed using the XCOM computer code. The findings show a high degree of congruence with theoretical data. The simulation results demonstrate that the Monte Carlo technique can be effectively used as an alternative method to calculate the mass attenuation coefficient ($\mu/\rho$) at the desired gamma energy, which is especially valuable for biopolymer materials that are physically challenging to produce.

**Keywords:** photon attenuation, biomaterial, polymer, Monte Carlo simulation, GAMOS

## 1. INTRODUCTION

Polymers, as large molecular structures, are foundational to modern material science and have an increasing role in the health sector. The growing interest in biopolymers—polymers derived from renewable natural sources—is driven by their exceptional properties such as high biocompatibility, low density, non-toxicity, and biodegradability [1]. These features make them prime candidates for various biomedical and radiation-related applications.

Chitosan (CS), specifically, is a non-toxic, biocompatible, and biodegradable biopolymer obtained from the deacetylation of chitin. Its film-forming capacity, antimicrobial efficacy, and ability to act as a carrier for other substances are well-documented [2-5]. Recently, biopolymer composites incorporating high-Z fillers, such as zinc oxide (ZnO) nanoparticles, have been explored to enhance mechanical, barrier, and optical properties, including UV-blocking characteristics. Incorporating natural extracts like ginger extract (GE) can further enhance the biocomposite's antioxidant and bioactive properties.

In medical imaging and radiation therapy, the ability of a material to attenuate or shield ionizing radiation is a critical property. The mass attenuation coefficient ($\mu/\rho$) is a fundamental parameter used to quantify this ability, as it is independent of the material's density [6]. For materials that are structurally complex or difficult to synthesize in an ideal form, like many novel biopolymer composites, Monte Carlo (MC) simulation offers a powerful, cost-effective alternative to physical experimentation for predicting radiation interaction parameters [7]. MC simulation codes, such as

MCNP, Geant4, and GAMOS, accurately model the stochastic processes of radiation transport through matter, providing essential data for material characterization. This study utilizes the Monte Carlo method via the GAMOS 6.2 framework to calculate the mass attenuation coefficients of two CS/GE/ZnO biopolymer composites.

## 2. MATERIALS AND METHODS

This study focuses on two distinct biopolymer materials, denoted as P1 and P2, both derived from a Chitosan (CS) polymer/Ginger Extract (GE)/Zinc Oxide (ZnO) composition. The specific composition and preparation methods for P1 and P2 were defined to investigate how subtle variations in the composite structure affect their radiation attenuation properties.

**Table 1.** *Properties of the biomaterials examined in the study*

| Sample | C | N | O | Zn | K | Ni | S | Density (gr/cm$^3$) |
|---|---|---|---|---|---|---|---|---|
| P1 | 24.6 | 11.7 | 63 | 0.7 | | | | 0.033 |
| P2 | 45.9 | | 53.3 | | 0.4 | 0.4 | 0.3 | 0.037 |

The radiation properties were determined computationally using the GAMOS 6.2 simulation program. GAMOS is an object-oriented toolkit based on the widely used Geant4 platform, designed to accurately model low-energy electromagnetic interactions and particle transportation in diverse media, making it an effective tool for medical-oriented simulations.

The simulation setup involved modeling a narrow-beam geometry, which is ideal for calculating the mass attenuation coefficient. A mono-energetic point photon source was defined to emit a parallel photon beam toward the absorber material. The simulation was run for a wide range of photon energies to cover the diagnostic to therapeutic energy range relevant in healthcare.

The mass attenuation coefficient ($\mu/\rho$) was calculated using the equation derived from the Beer-Lambert law:

$$\frac{\mu}{\rho} = \frac{1}{\rho x} ln \frac{I_0}{I}$$

where $I_0$ is the initial photon intensity, I is the intensity transmitted through the absorber, $\rho$ is the density of the material, and x is the thickness of the absorber.

To validate the Monte Carlo simulation results, the mass attenuation coefficients were also determined using the standard, publicly available XCOM computer code. XCOM is a reliable tool for theoretical photon cross-section calculations for any element, compound, or mixture at energies from 1 keV to $10^5$ MeV [5]. A strong agreement between the simulated (GAMOS) and theoretical (XCOM) results provides confidence in the Monte Carlo model's accuracy.

## 3. RESULTS AND DISCUSSION

The mass attenuation coefficients ($\mu/\rho$) for both biopolymer composites, P1 and P2, were calculated using the GAMOS 6.2 Monte Carlo code across a broad energy spectrum and compared to the theoretical values obtained from the XCOM code. The results are presented graphically in Figure 1.
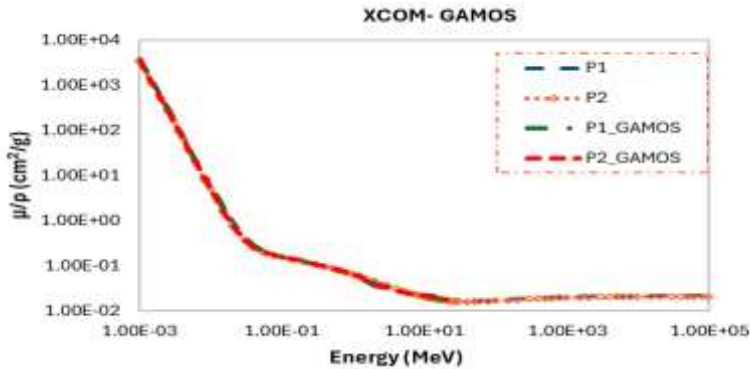
***Fig. 1.*** *Comparison of theoretical and calculated mass attenuation coefficient as a function of gam ma energy for biopolymer.*

The results shown in Figure 1 clearly indicate an excellent correlation between the Monte Carlo simulation data (P1_GAMOS, P2_GAMOS) and the theoretical calculations (P1, P2) across the entire energy range. This strong agreement validates the geometry, material definitions, and physics models used in the GAMOS simulation for these complex biopolymer materials.
Key observations from the data include:

- High Attenuation at Low Energy: Both P1 and P2 exhibit a sharp decrease in $\mu/\rho$ at low photon energies (below $\sim 0.01$ MeV). This high attenuation is primarily due to the photoelectric effect, whose cross-section is strongly dependent on the atomic number (Z) of the constituent elements, such as Zinc (Zn) from the ZnO component.

- Minimal Attenuation in the Compton Region: The mass attenuation coefficients flatten out in the middle energy range ($\sim 0.1$ MeV to a few MeV), which is characteristic of the Compton scattering region where the mass attenuation coefficient is less dependent on the atomic number.

- Congruence of P1 and P2: The mass attenuation curves for P1 and P2 are nearly identical throughout the entire energy spectrum. This suggests that while their compositions likely vary slightly, the overall average atomic number and electron density, which are the main factors governing attenuation, are highly similar.

The successful application of the Monte Carlo technique to predict the radiation attenuation properties of the CS/GE/ZnO biopolymers confirms its utility, especially for novel biopolymer composites that are often difficult to produce consistently or in a controlled fashion for physical measurement. This capability is crucial for the development of new materials for applications requiring precise knowledge of radiation interaction, such as polymer-based radiation shielding, dosimetric materials, or biocompatible structures used in radiation-rich environments. The potential to incorporate these biopolymers into medical devices or radiation shields highlights the importance of accurately characterizing their radiation properties.

## 4. CONCLUSION

The radiation properties, specifically the mass attenuation coefficients ($\mu/\rho$), of two new generation biopolymer composites (P1 and P2) based on chitosan/ginger extract/ZnO were successfully determined using the GAMOS 6.2 Monte Carlo simulation program. The simulation results demonstrated high congruence with the theoretical data calculated by the XCOM code across a wide

energy range. This study confirms the Monte Carlo technique as a powerful and validated alternative for accurately calculating the mass attenuation coefficient of complex biopolymer materials, particularly those that are physically challenging to produce or test. Future research can leverage this methodology to optimize the composition of such biopolymers for specific applications in medical physics and radiation protection.

## REFERENCES

[1] Parida, P., A. Behera, and S.C. Mishra, Classification of Biomaterials used in Medicine. 2012.

[2] Babu, S. R., Reddy, P. Y., Kumar, A. P., & Reddy, T. S. (2017). Measurement of mass stopping power of chitosan polymer using gamma radiation. Radiation Physics and Chemistry, 139, 71–76. https://doi.org/10.1016/j.radphyschem.2017.05.018

[3] More, C. V., Alsayed, Z., Badawi, M. S., Thabet, A. A. (2021). Polymeric composite materials for radiation shielding: a review. Environmental Chemistry Letters.

[4] Singh, V. P., Shirmardi, S. P., Medhat, M. E., Badiger, N. M. (2015). Determination of mass attenuation coefficient for some polymers using Monte Carlo simulation. Vacuum, 123,

[5] Mitragotri, S. and J. Lahann, Physical approaches to biomaterial design. Nature Materials, 2009. 8(1): p. 15-23.

[6] Berger, M., et al., XCOM: Photon Cross Sections Database. NIST, PML, Radiation Physics Division. 2019.

[7] Arce, P., et al. (2014). Gamos: A framework to do Geant4 simulations in different physics fields with a user-friendly interface. Nuclear Instruments and Methods in Physics Research Section A: Accelerators, Spectrometers, Detectors and Associated Equipment, 735, 304–313.

# Radon Concentration Variations in the Adalar District, Istanbul

**Osman GÜNAY[1]✉, Görkem SERBES[1], İsmail CANTÜRK[1], Caner YALÇIN[2], Mutlu İÇHEDEF[3], Caner TAŞKÖPRÜ[3], Murat SAÇ[3]**

*[1]Yildiz Technical University, Faculty of Electrical & Electronics, Biomedical Engineering, Istanbul-Türkiye*
*[2]Department of Physics, Kocaeli University, 41001 Izmit, Kocaeli-Türkiye*
*[3]Ege University Institute of Nuclear Sciences, 35100 Bornova, İzmir-Türkiye*

## ABSTRACT

The relationship between radon concentrations and earthquakes has been extensively investigated as radon anomalies are often considered potential precursors of seismic events. Variations in radon levels, particularly sudden increases or decreases in soil gas or groundwater, are attributed to stress accumulation and micro-fracturing processes in the Earth's crust prior to an earthquake. These fractures enhance the migration pathways of radon from deeper layers to the surface, leading to measurable anomalies. Therefore, continuous radon monitoring has become an important tool in seismological studies, aiming to better understand crustal movements and to evaluate the feasibility of radon as a short-term earthquake forecasting parameter. In this study, a continuous radon monitoring station was established in the Adalar district of Istanbul. Radon concentrations were recorded at 10-minute intervals, providing high-resolution temporal data. Along with radon, meteorological parameters such as temperature, pressure, and humidity were simultaneously measured to account for environmental influences. The variations in radon levels over a specific period were systematically observed and analyzed in order to evaluate possible correlations with both atmospheric conditions and seismic activity.

*Keywords: Radon , seismic , anomalies*

✉ *Corresponding Author Email        : ogunay@yildiz.edu.tr*

## 1 INTRODUCTION

The Earth is composed of three distinct layers from the inside out: the core, the mantle, and the lithosphere. The thickness of each layer varies from region to region. The upper part of the mantle, located just beneath the lithosphere, is mobile due to its soft structure and the transfer of heat energy from the core through convection. These movements, combined with the effect of frictional forces, have caused large and small fractures in the lithosphere. These resulting pieces float on the mantle like rafts on the sea. Each of these pieces is called a plate.

Under normal conditions, the plates move at very slow speeds that are imperceptible to humans. The forces they exert on each other as they attempt to move can sometimes be quite significant. Over time, this force accumulates as energy between the plates. An earthquake is defined as the sudden release of this accumulated energy, causing movement within the Earth's crust. The seismic waves generated by an earthquake propagate across a wide area in various forms and under different names.

An earthquake is a phenomenon that cannot be prevented under current conditions when certain geological and geophysical circumstances arise. During an earthquake, a large amount of energy accumulated in the Earth's crust is released in a very short time. When these seismic activities occur near populated areas, they can lead to loss of life and property. Various measures are being taken to mitigate the negative impacts of earthquakes. In addition, many researchers have conducted—and continue to conduct—studies aimed at predicting the occurrence times of these unavoidable seismic events [1] . Since the process of earthquake occurrence is highly complex, predicting the timing of this complex event is an extremely difficult problem [2-5]

Temperature, pressure, and humidity measurement systems were added to the radon observation stations, and the data were continuously collected. Radon concentration, humidity, temperature, and pressure data were integrated with a computer system and were transferred online to a cloud environment, allowing remote access to the data. During the 24-month project period, radon, humidity, temperature, and pressure data were obtained simultaneously from the installed stations, while earthquake data were obtained from the Kandilli Observatory. The relationship between the collected radon, humidity, temperature, pressure, and earthquake data was modeled with 90% accuracy using a variational long–short-term memory autoencoder.

## 2 MATERIALS AND METHODS

The data acquisition workflow relies on continuous surveillance of radon levels and accompanying environmental parameters at a dedicated monitoring station in the Marmara Region. Within the scope of this research, not only radon concentrations but also auxiliary atmospheric indicators—namely temperature, relative humidity, and barometric pressure—are incorporated into the evaluation framework. Earthquake information is sourced from the Kandilli Observatory, where seismic records are collected independently and later synchronized with the station data through timestamp matching to ensure compatibility for time-series investigations. Time series are shown in figure 1-3.

Radon measurements are carried out using the AlphaGUARD system, positioned at the Faculty of Electrical and Electronics Engineering on Yıldız Technical University's Davutpaşa Campus. As illustrated in Fig. 1, AlphaGUARD is an active detection instrument configured to record measurements every 10 minutes and internally store the outputs. The unit functions on battery power and provides network-based data transmission capabilities.

A potential difference of 750 V DC is applied between the anode and cathode of the detector. The full chamber volume is 0.62 L, of which 0.56 L serves as the active sensing region. The system can quantify radon activity concentrations within the range of 2 Bq/m³ to 2,000,000 Bq/m³, offering a measurement precision of roughly 3% [6]. Alongside radon, the device concurrently records meteorological variables such as ambient temperature (°C), relative humidity (% rH), and atmospheric pressure (mbar); these parameters are crucial for compensating environmental influences on radon measurements [7].

Air is drawn into the detector's ionization chamber by a suction pump integrated into the measurement setup. Once inside, the radioactive decay of the Radon-222 and Radon-220 isotopes ionizes the air molecules, giving rise to electrical pulses. A continuously operating pump ensures

61

that the decay progeny are trapped on a dedicated filter. These pulses are then transmitted as TTL (Transistor–Transistor Logic) signals to the device's counting unit, referred to as the Counter Module. Using the detector's pre-configured calibration constants, the accompanying software interprets these raw electrical outputs and converts them into readable measurement values [8].

In this investigation, the soil-gas sampling technique is utilized (Fig. 2). This approach employs the AlphaGUARD detector together with a specialized setup consisting of a 1-meter metal insertion rod and a slender soil-gas probe. A hole is drilled to the desired depth, and the probe is positioned within this opening. Subsurface gases are subsequently drawn into the detector's ionization chamber using the AlphaPUMP system [9]. During sampling, both the gas flow rate and pumping duration can be precisely controlled through the AlphaPUMP interface. The AlphaGUARD unit records radon concentration values automatically based on the measurement interval selected by the user [10-11].

.

## 3 RESULTS

In this study, the influence of environmental parameters—namely atmospheric pressure, relative humidity, and temperature—on radon gas levels was examined, and the extent to which these factors could predict radon concentrations was assessed. Time periods containing measurement inconsistencies were excluded to obtain a clean dataset, after which univariate linear regression models were constructed using radon concentration as the dependent variable and each environmental parameter as the sole predictor. The predictive ability of each model was then evaluated individually.
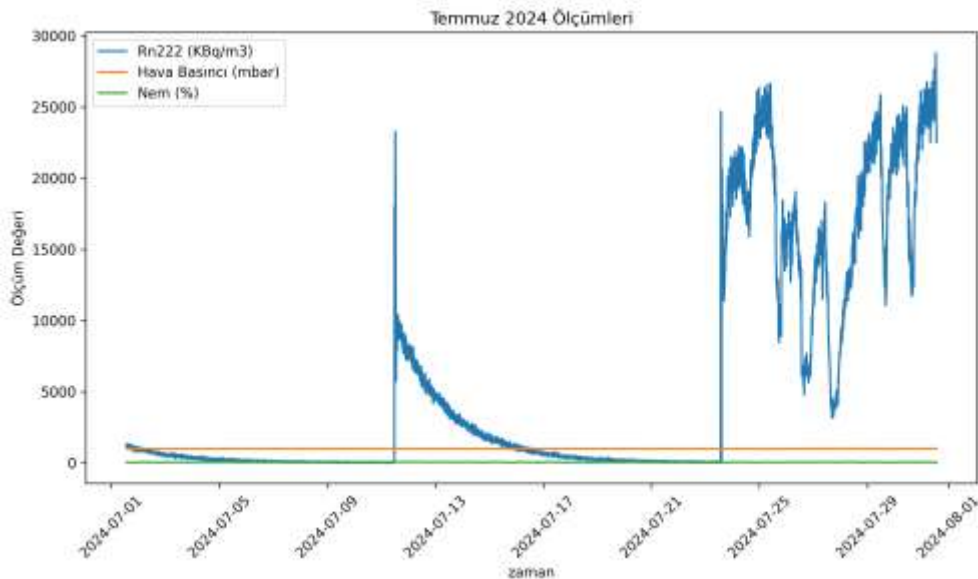


Figure 1. Time-series representation of the variations in radon concentration, humidity, and atmospheric pressure for July 2024.
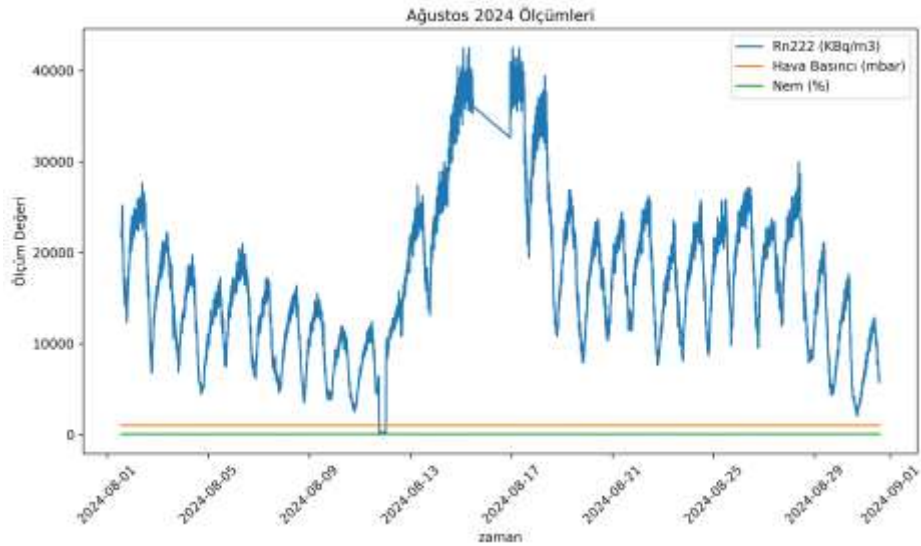
Figure 2. Time-series illustrating the variations in radon concentration, humidity, and atmospheric pressure for August 2024.
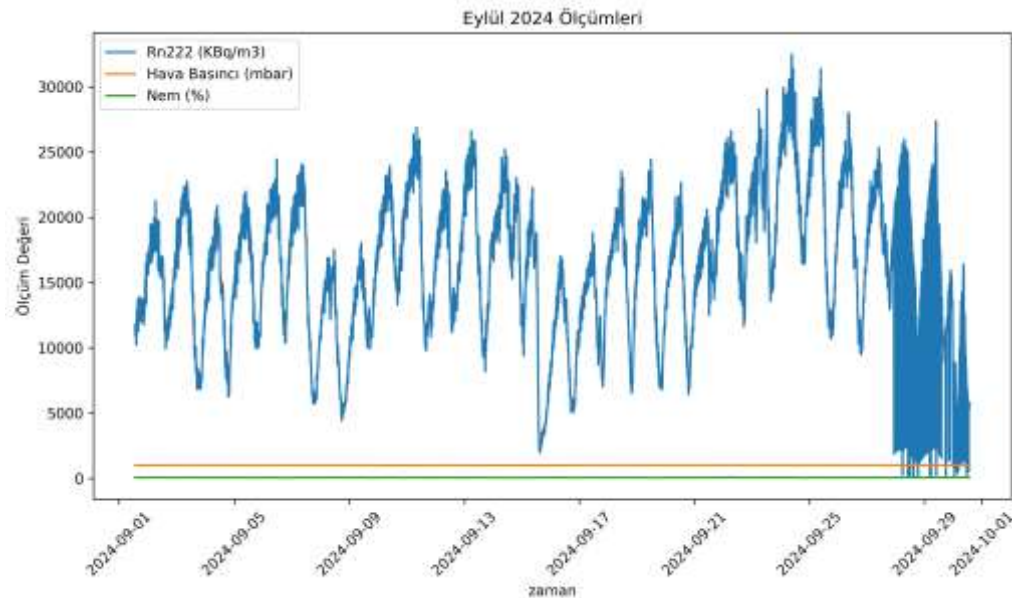


Figure 3. Time-series depicting the fluctuations in radon concentration, humidity, and atmospheric pressure for September 2024.

The dataset was partitioned into training (80%) and testing (20%) subsets. Following model training on the designated training portion, performance was assessed using the test data. For visualization, two types of plots were generated: the first illustrated the relationship between each environmental variable and both the actual and predicted radon values; the second provided a direct comparison

63

between predicted and observed radon concentrations (Figures 1-3). These visualizations revealed noticeable discrepancies and poor predictive alignment.

To quantitatively evaluate model accuracy, the Mean Absolute Error (MAE) metric was employed. MAE values were found to be high across all models, indicating limited predictive capability. These findings demonstrate that univariate linear regression is insufficient for reliably forecasting radon levels. The underlying relationship between radon concentration and environmental conditions appears to be nonlinear and more complex, suggesting the need for multivariate or more advanced modeling approaches.

After the inadequacy of the univariate linear models became evident, a multiple linear regression approach was implemented to determine whether radon concentrations could be predicted more accurately by considering environmental factors jointly. In this model, temperature, relative humidity, and atmospheric pressure were simultaneously incorporated as predictors. The training–testing split was carried out in the same manner as before; however, the resulting MAE value (4645.98) remained considerably high. This outcome further indicated that the relationship between radon levels and environmental variables is inherently nonlinear.

Given these limitations, the analysis moved beyond linear frameworks toward a nonlinear artificial neural network architecture—specifically, a Multi-Layer Perceptron (MLP). The MLP model consisted of three hidden layers; the first contained 64 neurons, followed by a second hidden layer with 32 neurons. The ReLU activation function was employed throughout, the Adam optimizer was used for parameter updates, and MAE served as the loss function. The network was trained for 20 epochs, during which loss values for both the training and testing subsets were recorded at each iteration.

The primary objective of this model was to capture the more intricate, nonlinear dependencies between environmental conditions and radon concentration in order to enhance predictive accuracy. The MLP framework demonstrated potential in this regard and was considered a promising advancement beyond traditional linear modeling.

## 4 CONCLUSION

This study investigated the complex relationship between radon gas concentrations and environmental parameters by employing both linear and nonlinear modeling approaches. Initial analyses using univariate and multivariate linear regression revealed that temperature, relative humidity, and atmospheric pressure individually and collectively failed to produce reliable predictions of radon levels. The consistently high MAE values and the visual discrepancies between predicted and observed concentrations demonstrated that radon behavior cannot be adequately captured with linear assumptions. These findings indicate that the dynamics governing radon variability are influenced by nonlinear and possibly interacting processes, rendering classical linear methods insufficient for robust forecasting.

To address these limitations, a Multi-Layer Perceptron (MLP) neural network was implemented as a nonlinear modeling alternative. With its multi-layer architecture and ability to capture complex patterns, the MLP model showed promise in learning the intricate dependencies between environmental variables and radon concentration. Although further optimization and long-term data evaluation are required, the neural network framework represents a significant improvement over linear models and offers a more suitable foundation for radon prediction studies. The results collectively highlight the necessity of advanced, nonlinear techniques in understanding radon dynamics and lay the groundwork for developing more accurate early-warning or monitoring systems in the futur

**REFERENCES**

[1] Geller, R.J. 1997. "Earthquake prediction: A critical review.", Geophysical Journal International, 131(3), 425–450.

[2] Cicerone, R. D., Ebel, J.E., Britton, J. 2009. "A systematic compilation of earthquake precursors.", Tectonophysics 476(3-4), 371-396.

[3] Hayakawa, M., Hobara, Y. 2010. "Current status of seismo-electromagnetics for short-term earthquake prediction.", Geomatics, Natural Hazards and Risk, 1(2), 115-155.

[4] A., Tripathi, S.C., Mansoori, A.A., Bhawre, P., Purohit, P., Gwal, A. 2011. "Scientific efforts in the direction of successful Earthquake Prediction." International Journal of Geomatics and Geosciences, 1(4), 669-677.

[5] Shrivastava, A. 2014. "Are pre-seismic ULF electromagnetic emissions considered as a reliable diagnostics for earthquake prediction?", Current Science, 596-600.

[6] S. Liu, T. Hu, F. Lin, Z. Fan et al., "A new model to accurately measure the radon exhalation rate from soil using AlphaGUARD," Journal of Environmental Radioactivity, vol. 266, art. no. 107226, 2023.

[7]S. Baykut, T. Akgül, S. İnan and C. Seyis, "Observation and removal of daily quasi-periodic components in soil radon data," Radiation Measurements, vol. 45,

   pp. 872–879, 2010.

[8] SARAD GmbH, "AlphaGUARD radon monitor," [Online]. Available: https://www.sarad.de/en/products/alphaguard/. [Accessed: June 18, 2025].

[9]S. Tokonami, M. Yang and T. Sanada, "Contribution from thoron on the response of passive radon detectors," Health Physics, vol. 80, no. 6, pp. 612–615, 2001.

[10]C. Di Carlo et al., "Thoron interference on performance of continuous radon monitors," International Journal of Environmental Research and Public Health, vol. 19, no. 4, art. no. 2423, 2022.

[11]C. G. Sumesh, A. V. Kumar, R. M. Tripathi and V. D. Puranik, "Thoron interference test of different continuous passive radon monitors," Radiation Protection and Environment, vol. 34, no. 4, pp. 257–261, 2011.

# Manufacturing and Printing of Urogenital System Organs

**Osman GÜNAY[1]✉, Fahrettin Fatih KESMEZACAR[2], Yağmur İdil ULUSOY[3] , Duygu TUNÇMAN KAYAOKAY[4], Özge DEMİR[5], Songül KARAÇAM[4], Eren ÖZGÜR[6], Nami YEYİN[7], Rabia Lebriz USLU BEŞLİ[7], Mustafa DEMİR[7],**

*[1]Yildiz Technical University, Faculty of Electrical & Electronics, Biomedical Engineering, Istanbul-Türkiye*
*[2]Istanbul University-Cerrahpas¸a, Vocational School of Health Services, Department of Medical Services and Techniques, Medical Monitoring Techniques Pr., Istanbul-Türkiye*
*[3]Istanbul Bilgi University, Vocational School of Health Services, Medical Imaging Techniques Programme, Istanbul-Turkiye*
*[4]Istanbul University-Cerrahpas¸a, Vocational School of Health Services, Department of Medical Services and Techniques, Radiotherapy Pr., Istanbul-Türkiye*
*[5]İstanbul University-Cerrahpaşa, Engineering Faculty, Chemical Engineering Department, Avcılar 34320, İstanbul-Turkey*
*[6]Istanbul Training and Research Hospital, Radiology Department, Istanbul, Türkiye*
*[7]Istanbul University- Cerrahpasa, Cerrahpasa Faculty of Medicine, Department of Nuclear Medicine, Istanbul-Türkiye*

**ABSTRACT**

Radiation is commonly used in the medical field, primarily for diagnostic purposes and, in some cases, for therapeutic applications. In hospitals, it is employed in radiology, nuclear medicine, and radiation oncology departments. Unlike other applications, nuclear medicine involves the injection of a radioactive substance directly into the patient's body. This radioactive material disperses throughout the entire body, with a significant portion accumulating in the bladder before being excreted. The radioactive substances collected in the bladder also irradiate the nearby genital organs.

The aim of this study is to design and fabricate models simulating the organs of the urogenital system using three-dimensional (3D) printing technology. In subsequent stages, these printed organs will be assembled into a urogenital system phantom, enabling experimental investigations for various applications in nuclear medicine.

*Keywords: Radiation , phantom , urogenital*

✉ *Corresponding Author Email     : ogunay@yildiz.edu.tr*

# 1 INTRODUCTION

Radiation is energy emitted from matter in the form of electromagnetic waves or particles. Fundamentally, radiation is classified into two main categories: non-ionizing radiation, which cannot ionize atoms (such as radio waves and microwaves), and ionizing radiation, which has sufficient energy to ionize atoms (such as X-rays, gamma rays ($\gamma$), and beta ($\beta$) particles). While non-ionizing radiation does not possess enough energy to cause ionization, ionizing radiation is capable of removing electrons from atoms.

Radiation is widely used in nuclear facilities, nuclear research centers, food technology, non-destructive testing methods, characterization of material structures, and medical applications, and its range of applications continues to expand.

In the healthcare sector, particularly in hospitals, radiation applications are employed across many departments; however, they are mainly utilized in three core units: radiology, nuclear medicine, and radiation oncology. In radiology, the ionizing radiation most commonly used is X-rays. X-rays form the basis of imaging modalities such as conventional radiography, computed tomography (CT), mammography, and fluoroscopy. In radiation oncology, high-energy X-rays and gamma rays are generally employed. In oncology, X-rays are delivered using linear accelerators (LINACs), while gamma rays are commonly used in brachytherapy applications. In hospital nuclear medicine departments, gamma rays are typically used in gamma cameras and single-photon emission computed tomography (SPECT), whereas positron emission tomography (PET) utilizes positrons (beta-plus, $\beta^+$ ) along with gamma rays.

The main objective of this study is to design a phantom to be used in experimental studies for nuclear medicine applications. For this purpose, organ designs were first developed, followed by the 3D printing stage.

# 2 MATERIALS AND METHODS

## KIDNEYS

The kidneys are located in the retroperitoneal space between the T12 and L3 vertebral levels. The right kidney is typically positioned 0.5–1 cm lower than the left kidney due to the presence of the liver. The right kidney lies inferior to the liver, while the left kidney is adjacent to the spleen, pancreas, and stomach.

The measurements presented in this report consist of two parts. The first part includes measurements compiled from the literature, while the second part is based on computed tomography (CT) images obtained from a patient (Fig 1).

Figure 1. Kidney

**URINARY BLADDER**

The urinary bladder is located in the anterior part of the pelvis, posterior to the pubic symphysis and anterior to the uterus. In females, it lies in front of the uterus and vagina. When empty, the bladder is situated within the lesser pelvis, whereas when filled, it ascends into the abdominal cavity. The empty bladder has a pear-shaped appearance, becoming more spherical as it fills. Its length can reach 12–15 cm, and its width may increase up to 8–10 cm. In an average adult, the bladder capacity is approximately 400–600 mL. The maximum tolerable capacity may reach 800–1000 mL in some individuals [1], however, this exceeds normal physiological limits. The bladder is positioned within the pelvic cavity, posterior to the pubic bone. Its posterior relations in females include the vagina and uterus, while its inferior relations are formed by the pelvic floor muscles and the urethra.

**UTERUS**

The uterus is a hollow, muscular organ of the female reproductive system that supports fetal development during pregnancy. It is located in the female pelvis between the urinary bladder and the rectum. The uterus consists of three main parts: the cervix, corpus, and fundus. Under normal conditions, it is positioned in anteversion and anteflexion; that is, the cervix is oriented approximately perpendicular to the pelvic axis, and the corpus is flexed anteriorly.

The bladder lies anterior to the uterus, the rectum posterior to it, and the vagina inferiorly. These anatomical relationships are of critical importance in surgical and radiological planning. Laterally, the uterus is associated with the fallopian tubes and ovaries (Figure 2).
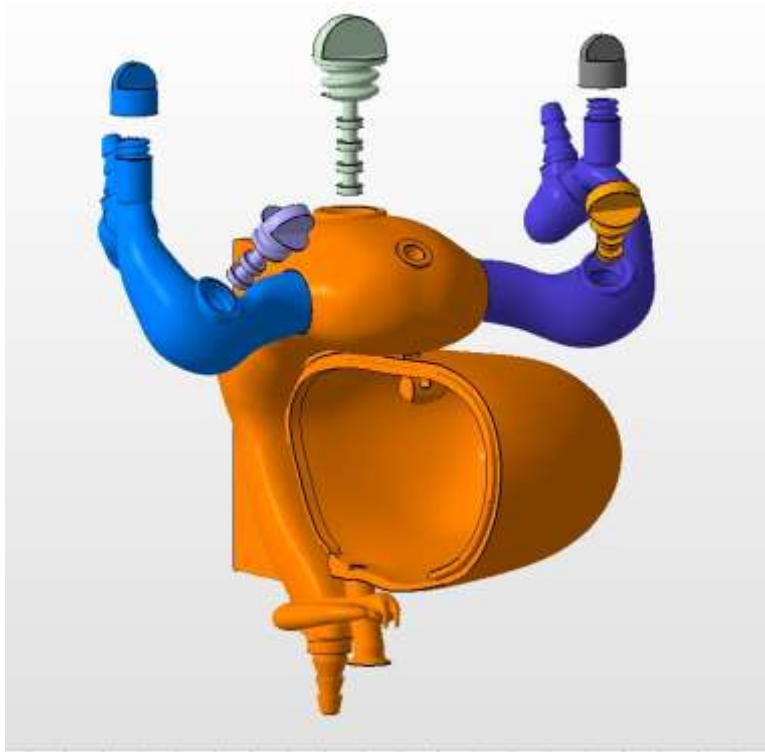
Figre 2 : Uterus

## FALLOPIAN TUBES

The fallopian tubes extend laterally from the fundus of the uterus and course toward the ovaries. They consist of four main segments: the infundibulum, ampulla, isthmus, and pars uterina. Medially, they are related to the uterine fundus, while laterally they are associated with the ovaries. On average, the diameters of the infundibulum, ampulla, and isthmus are approximately 5–8 mm, 6–10 mm, and 2–4 mm, respectively. The mean length of the fallopian tubes is 10–12 cm [2] with reported lengths ranging between 8 and 14 cm [3].

## 3 RESULTS

The three-dimensional drawing of the kidney is shown in Figure 3. In this figure, the lidded component located in the upper right from the reader's perspective is a valve designed to prevent air

69

from being trapped inside the kidney during the filling process. As fluid is introduced into the kidney, air will be expelled through this valve, which will be closed once all the air has been released. The component located in the upper left is designed as slots for the placement of thermoluminescent dosimeters (TLDs).

The TLDs will be mounted onto the grooved, green-colored holder and suspended into the kidney. The opening located at the upper center represents the inlet ports for the fluid entering the kidney. Of the two outlet ports located at the bottom, one directs the flow toward the urinary bladder, while the other leads to the uterus.

The combined drawing of the bladder, uterus, ovaries, and fallopian tubes is shown in Figure 4. Two air-release valves were placed at the highest points of the ovarian channels on the right and left sides. Fluid inlets were positioned at the upper points on both the right and left sides. Two TLD access ports were created on the right and left sides of the ovarian channels, and one TLD access port was created for the uterus. In Figure 4, of the two openings located at the bottom, one serves as the fluid outlet for the uterus and the other as the fluid outlet for the bladder.

During the experiments, a saline bag will be placed inside the phantom to allow the bladder to expand and contract. As the bladder fills, the saline bag will expand and surround the bladder from the inside.

The 3D manufacturing process of the female urogenital system organs was initiated by transferring the digitally designed models in STL format to a 3D printer. The printing process was carried out according to the following steps:

**1. Slicing Process:**
- The prepared STL files were converted into layers using slicing software compatible with the 3D printer.
- The layer thickness was set to 0.2 mm, which was considered optimal in terms of both surface smoothness and printing time.
- The infill density was selected between 30% and 80%, balancing structural strength and material consumption.
-

**2. Printing Parameters:**
- Material used: ABS filament
- Extruder temperature: 230–240 °C
- Build plate temperature: 100–110 °C
- Printing speed: 40–60 mm/s
- To improve layer adhesion, the build plate surface was covered with special tape and adhesive solutions.

**3. Support and Raft Structures:**
- Automatic support structures were generated for organs with complex geometries (e.g., fallopian tubes) to prevent overhangs.
- After printing, these support structures were removed, and surface smoothness was ensured.

70

## 4. Printing Time:
- Depending on the size of the organ, the printing time varied between 2 and 8 hours.
- Larger-volume organs (e.g., the uterus) required longer printing durations.

## 5. Post-Processing:
- Support structures were manually removed after printing, and surface sanding was applied where necessary.
- In some organs, the ABS surface was smoothed by acetone exposure to achieve a more realistic appearance.
- The models were color-coded according to their anatomical differences to facilitate educational use.

Acrylonitrile Butadiene Styrene (ABS) is one of the most commonly used engineering plastics and one of the most preferred thermoplastic polymers in 3D printing technologies. The selection of ABS filament for the production of female urogenital system organs was based on its mechanical and physical advantages.

The properties of ABS are as follows:
- **Chemical Structure:** ABS is a terpolymer composed of acrylonitrile, butadiene, and styrene.
  - *Acrylonitrile* → Provides chemical resistance and rigidity.
  - *Butadiene* → Enhances impact resistance and flexibility.
  - *Styrene* → Contributes gloss, processability, and surface smoothness.
- **Density:** Approximately 1.04 g/cm³
- **Melting/Printing Temperature Range:** Suitable for printing between 210–250 °C

Figure 3. Kidney (Printed)



Figure 4. Uterus  (Printed)

**4 CONCLUSION**

Figures 5 and 6  present views of the printed organs from different orientations. The organs produced by the three-dimensional printer were observed to be suitable for their intended purpose.

Figures 6  show the organs after printing, assembled using intravenous (IV) tubing. After being connected with the tubing to form the phantom, leak-tightness tests were performed. During these tests, some leakage issues were encountered; however, the majority of the sealing problems were successfully resolved.


Figure 5. Uregenital system

Figure 6. Uregenital system experiment level

**REFERENCES**

[1] Hayta, E. ve Ceyhan Doğan, S. (2013) Mesane Anatomisi ve Nörofizyolojisi , Türkiye Klinikleri J PMR Special Topics 6(2):1-7

[2] Warda, O., Ragab, A. and Elshamy M.R. (2024), Manuel of Gynecology , https://medfac.mans.edu.eg/images/Depts/OBSGYN/MANUAL_OF_GYNECOLOGY.pdf

[3] Chard, T. and Grudzinskas G. (2003), The Uterus, Published by the Press Syndicate of the University of Cambridge, Australia

# Organ-Specific Dosimetry in Ovarian Vein Embolization

Cemre Serdem BİLİR[1], Osman GÜNAY[2], Fahrettin Fatih KESMEZACAR[3], Özge COŞKUN SAĞLAM[4], Berrin YALÇIN[5], Murat ÖZOĞUL[6]

*[1]Yıldız Technical University, Biomedical Engineering Department, Istanbul-Türkiye*
*[2]Yıldız Technical University, Department of Biomedical Engineering, Istanbul, Türkiye*
*[3]Istanbul University-Cerrahpasa, Vocational School of Health Services, Department of Medical Imaging Techniques, Istanbul, Türkiye*
*[4]Istanbul Bilgi University, Faculty of Health Sciences, Department of Physiotherapy and Rehabilitation, Istanbul- Türkiye*
*[5]Istanbul Training and Research Hospital, Department of Radiation Oncology, Istanbul- Türkiye*
*[6]Istanbul Training and Research Hospital, Department of Radiology, Istanbul- Türkiye*

**ABSTRACT**

Transcatheter ovarian vein embolization (TOVE) is an invasive radiological procedure. This procedure is used in the treatment of pelvic congestion syndrome. Even though this procedure offers clinical benefits, this method relies heavily on fluoroscopic imaging, which inevitably reveals not only the targeted vessels but also the surrounding pelvic structures. Distant organs may be exposed to ionizing radiation. Understanding the distribution and magnitude of this exposure is important to minimize potential risks and optimize procedure safety. With this study, a phantom based dosimetric approach was used to evaluate organ specific radiation doses during TOVE under simulated clinical conditions. A phantom was used and thermoluminescent dosimeters (TLDs) were strategically placed at eleven anatomical sites, right ovary, left ovary, right uterine tube, left uterine tube, corpus uteri, fundus uteri, cervix uteri, bladder, vagina, rectouterine pouch, Medulla spinalis (MS). Dose measurements were recorded following a standard protocol.

The results showed that the medulla spinalis absorbed the highest radiation dose (10.87 mSv), followed by the rectouterine pouch (9.03 mSv) and the corpus uteri (7.63 mSv). The lowest exposure was observed in the bladder region (3.49 mSv). Moreover, the left uterine tube (7.72 mSv) received a slightly higher dose than the right tube (6.78 mSv), this can be attributed to the projection geometry and beam angle during imaging. These findings suggest that radiation exposure during TOVE is significantly influenced by the anatomical location of the organ relative to the treatment field. Data from this phantom model highlight the importance of dose optimization strategies and careful adjustment of imaging parameters to reduce unnecessary exposure. Given that the study simulated bilateral procedures with deliberately increased fluoroscopy, the reported organ doses should be interpreted as upper limit estimates of clinical exposure. These results provide a conservative yet valuable reference for patient safety assessments and underscore the necessity of dose optimization strategies in TOVE.

*Keywords:* transcatheter ovarian vein embolization, radiation exposure, organ-specific dosimetry, phantom model, thermoluminescent dosimeter, pelvic congestion syndrome.

✉ *Corresponding Author Email      : cemreserdem@gmail.com*

75

# 1.INTRODUCTION

Radiation is a emission and transfer of energy through waves or particles. In medicine, ionizing radiation such as X-rays is used for imaging and treatment. It provides detailed visualization of internal organs but must be carefully controlled due to its biological effects.

Accurate quantification of radiation exposure during fluoroscopy-guided endovascular procedures is essential for ensuring patient safety and optimizing interventional practice. In medical imaging, **ionizing radiation** refers to high-energy electromagnetic radiation (most commonly X-rays) capable of removing electrons from atoms and molecules, thereby producing ionization in biological tissues. This interaction may lead to biological effects that depend on dose magnitude, exposure duration, and irradiated tissue characteristics; therefore, optimization of imaging parameters and dose monitoring are integral components of modern interventional radiology.

Pelvic Congestion Syndrome (PCS) is a chronic venous disorder characterized by ovarian vein insufficiency and pelvic venous dilatation, frequently presenting with persistent pelvic pain in women of reproductive age. Transcatheter ovarian vein embolization (OVE) is widely accepted as a minimally invasive and clinically effective treatment approach for PCS. However, OVE relies heavily on real-time fluoroscopic guidance using C-arm systems, which inevitably exposes radiosensitive pelvic organs—particularly the uterus, ovaries, and surrounding soft tissues—to repeated X-ray irradiation.

In the existing literature, the majority of reports focus on technical success, clinical outcomes, pain relief, and anatomical considerations related to PCS, whereas comparatively fewer studies examine **organ-specific radiation dose distribution** during OVE. This scarcity creates an evidence gap regarding absorbed dose levels in pelvic organs, spatial dose variation within the body, and the quantitative relationship between fluoroscopic parameters and organ exposure. Moreover, the biological radiosensitivity of reproductive organs underscores the need for precise dosimetric evaluation in fluoroscopy-guided pelvic interventions. Anthropomorphic phantoms, combined with thermoluminescent dosimeters (TLDs), provide a reliable and standardized method for organ-level dose measurement. These models replicate human anatomy with high fidelity and enable insertion of dosimeters into anatomically relevant cavities, allowing simulation of realistic irradiation conditions under controlled environments.

The primary aim of this study is to quantify organ-specific absorbed radiation doses during simulated ovarian vein embolization (OVE) using an anthropomorphic female pelvic phantom. TLD-100 dosimeters were placed in selected anatomical sites, and standardized fluoroscopic imaging was performed on a clinical C-arm system to assess radiation exposure. This study aims to determine organ-level absorbed doses and evaluate the influence of fluoroscopic parameters on radiation exposure, thereby providing data to support dose optimization and radiation safety in clinical OVE practice.

## 2. MATERIALS AND METHODS

This experimental phantom-based dosimetry study was designed to simulate transcatheter ovarian vein embolization (OVE) under clinical fluoroscopic conditions and to quantify organ-specific absorbed radiation doses using thermoluminescent dosimeters (TLD-100).

### 2.1 Study Design

A controlled experimental setup was implemented to simulate the standard fluoroscopic workflow of ovarian vein embolization. Thermoluminescent dosimeters (TLDs) were positioned in anatomically representative regions of a female anthropomorphic phantom. Fluoroscopic image acquisitions were performed to correspond with routine procedural steps of OVE. Dose-related parameters, including fluoroscopy time, cumulative air kerma, and dose–area product (DAP), were recorded for each acquisition. All imaging procedures were conducted using a Siemens Artis Zee Floor C-arm angiography system under routine clinical operating conditions. Exposure parameters, including tube voltage (kVp), tube current (mA), pulse rate, field size, and beam filtration, were documented systematically to ensure reproducibility and enable comparison with standard clinical practice.

### 2.2 Phantom Model

In this experimental dosimetric study, a CIRS anthropomorphic female pelvic phantom was used to simulate patient-specific pelvic anatomy during ovarian vein embolization. The phantom consists of tissue-equivalent materials arranged in 2.5 cm–thick axial slices, designed to accurately reproduce human anatomical geometry and radiological properties.

Each slice contains predefined cavities corresponding to anatomical organ locations, allowing for precise and reproducible placement of TLD-100 dosimeters. Dosimeters were positioned at selected sites representing relevant pelvic organs and anatomical regions of interest. The phantom was positioned in the supine position on the angiography table in accordance with standard clinical patient positioning to ensure realistic irradiation geometry during fluoroscopic imaging.

### 2.3 Thermoluminescent Dosimeters (TLDs)

TLD-100 (LiF:Mg,Ti) chips were selected for dose measurement due to their high sensitivity, tissue-equivalent response, and suitability for low-dose fluoroscopic applications. Prior to irradiation, all dosimeters underwent a standardized annealing procedure consisting of heating at 400 °C for 1 hour, followed by cooling to room temperature and a secondary annealing step at 100 °C for 2 hours.

Following irradiation, the TLDs were read using a thermoluminescent dosimeter reading system under controlled laboratory conditions. Individual element correction factors (ECFs) were applied to reduce inter-dosimeter variability. Calibration curves were generated using known reference exposures obtained from the angiography system and were used to convert TLD readout signals into absorbed dose values.

## 2.4 Fluoroscopic Procedure

To simulate the workflow of ovarian vein embolization, fluoroscopic imaging was performed in a series of sequential steps representative of routine clinical practice. The procedure consisted of an initial pelvic survey fluoroscopy, followed by simulated catheter navigation toward the ovarian vein, selective ovarian vein imaging, and fluoroscopy during embolization simulation.

All imaging steps were conducted using standard fluoroscopic parameters. For each exposure sequence, total fluoroscopy time (s), cumulative air kerma (mGy), and dose–area product (DAP; Gy·cm²) were automatically recorded by the C-arm system.

## 3. RESULTS

Dose measurements collected from strategically positioned TLDs within the **CIRS** anthropomorphic female pelvic phantom demonstrated discernible variation among pelvic organs during the simulated embolization process. Mean absorbed dose values for each organ are presented in Table 1.1

| Organ | TLD No | Mean Dose (mSv) |
|---|---|---|
| Right ovary | 75–76 | 4.24mSv |
| Left ovary | 73–74 | 5.43mSv |
| Right uterine tube | 49–50 | 6.78mSv |
| Left uterine tube | 45–46 | 7.72mSv |
| Corpus uteri | 81–82 | 7.63mSv |
| Fundus uteri | 71–72 | 4.86mSv |
| Bladder | 69–70 | 3.49mSv |
| Cervix uteri | 77–78 | 5.53mSv |
| Rectouterine pouch | 61–62 | 9.03mSv |
| Vagina | 79–80 | 4.08mSv |
| MS (medulla spinalis) | 83-84 | 10.87mSv |

**Table 1.1**

Among measured sites, the medulla spinalis exhibited the greatest absorbed dose (10.87 mSv), with the rectouterine pouch and left uterine tube following at 9.03 mSv and 7.72 mSv, respectively.4.1.2 Comparison Between Right and Left Organs. A consistent lateral difference was observed, wherein tissues on the left side of the pelvis accumulated greater radiation than their right-sided counterparts. For example, the left ovary absorbed 5.43 mSv compared to 4.24 mSv on the right, and the left fallopian tube accumulated 7.72 mSv relative to 6.78 mSv on the opposite side.

## 4. DISCUSSION

This study presents a controlled experimental evaluation of organ-specific radiation exposure during simulated ovarian vein embolization using an anthropomorphic pelvic phantom. The findings

78

demonstrate that centrally and posteriorly located pelvic structures, particularly the uterus and rectouterine region, are subjected to higher absorbed radiation doses during fluoroscopic imaging. This dose distribution is consistent with the projection geometry of the X-ray beam and the anatomical location of the target vessels during OVE.

Published data addressing organ-level dosimetry in OVE are limited, restricting direct comparison with existing studies. Nevertheless, the measured absorbed dose values fall within the range reported for fluoroscopy-guided pelvic interventions. Variations in dose distribution are likely influenced by factors such as C-arm geometry, beam angulation, and positioning, all of which play a critical role in determining organ exposure during interventional procedures.

A clear relationship was observed between cumulative air kerma, dose–area product, and measured organ doses, supporting the clinical utility of these parameters as practical indicators of radiation exposure. However, the results also highlight that absolute organ dose estimation cannot be reliably achieved using global dose metrics alone and remains dependent on anatomical configuration and direct dosimetric assessment.

From a clinical perspective, these findings underscore the importance of optimizing fluoroscopic technique to minimize radiation exposure to radiosensitive pelvic organs. Strategies such as reducing fluoroscopy time through pulsed imaging, optimizing collimation to limit irradiation of non-target tissues, selecting low-dose imaging protocols when diagnostically sufficient, and maintaining appropriate patient and C-arm positioning may substantially reduce unnecessary radiation burden.

Several limitations should be acknowledged. The use of an anthropomorphic phantom does not fully account for inter-patient anatomical variability, and the static experimental setup differs from dynamic catheter manipulation encountered in clinical practice. Additionally, the spatial resolution of TLDs is limited compared with advanced dosimetric technologies, and only a standardized procedural workflow was simulated without evaluation of operator-dependent variability. Despite these constraints, the study provides a reproducible methodological framework for assessing pelvic organ doses during fluoroscopy-guided ovarian vein embolization and contributes valuable data to support radiation safety and dose optimization efforts.

## 5. CONCLUSION

This phantom-based dosimetric investigation demonstrates that fluoroscopy-guided ovarian vein embolization results in measurable and clinically relevant radiation exposure to pelvic organs. Higher absorbed dose levels were observed in centrally and posteriorly located pelvic structures, particularly the uterus, highlighting the influence of beam orientation, irradiation geometry, and tissue depth on organ dose distribution during the procedure.

By providing quantitative organ-specific absorbed dose data and examining the relationship between fluoroscopic exposure parameters and measured doses, this study contributes to a better understanding of radiation dose behavior during OVE. The findings support the importance of optimizing fluoroscopic technique, including appropriate parameter selection and positioning, to minimize unnecessary radiation exposure to radiosensitive pelvic organs.

Overall, the results of this study offer experimental evidence that may aid in the development of optimized imaging protocols, strengthen radiation safety strategies, and improve clinical awareness

of patient dose during fluoroscopy-guided ovarian vein embolization, thereby contributing to safer and more informed interventional radiology practice.

**REFERENCES**

1. **International Commission on Radiological Protection (ICRP).** Radiological protection in fluoroscopically guided procedures. *ICRP Publication 85*. Ann ICRP. 2000;30(2).
2. **International Commission on Radiological Protection (ICRP).** The 2007 recommendations of the International Commission on Radiological Protection. *ICRP Publication 103*. Ann ICRP. 2007;37(2–4).
3. **Balter S, Hopewell JW, Miller DL, Wagner LK, Zelefsky MJ.** Fluoroscopically guided interventional procedures: a review of radiation effects on patients' skin and hair. *Radiology*. 2010;254(2):326–341.
4. **Miller DL, Balter S, Dixon RG, et al.** Quality improvement guidelines for recording patient radiation dose in the medical record. *J Vasc Interv Radiol*. 2012;23(1):11–18.
5. **Rafferty EA, Henkelman RM.** Thermoluminescent dosimetry for diagnostic radiology. *Radiology*. 1988;168(3):849–854.
6. **McCollough CH, Schueler BA.** Calculation of effective dose. *Med Phys*. 2000;27(5):828–837.
7. **Hart D, Hillier MC, Wall BF.** Doses to patients from medical X-ray examinations in the UK. *Br J Radiol*. 2009;82(973):1–12.
8. **Belli AM, Markose G, Morgan R.** The role of interventional radiology in the management of pelvic congestion syndrome. *Cardiovasc Intervent Radiol*. 2012;35(4):791–800.
9. **Ganeshan A, Upponi S, Hon LQ, et al.** Chronic pelvic pain due to pelvic congestion syndrome: the role of diagnostic and interventional radiology. *Cardiovasc Intervent Radiol*. 2007;30(6):1105–1111.
10. **Laborda A, Medrano J, De Blas I, Urtiaga I, Carnevale FC, De Gregorio MA.** Endovascular treatment of pelvic congestion syndrome: visual analog scale follow-up results. *Eur J Radiol*. 2013;82(11):e639–e645.
11. **Schueler BA.** The AAPM/RSNA physics tutorial for residents: general overview of fluoroscopic imaging. *Radiographics*. 2000;20(4):1115–1126.
12. **Vañó E, Fernández JM, Sánchez RM, et al.** Patient radiation dose management in interventional radiology: a practical approach. *Cardiovasc Intervent Radiol*. 2010;33(4):688–699.
13. **Dance DR, Christofides S, Maidment ADA, McLean ID, Ng KH.** *Diagnostic Radiology Physics: A Handbook for Teachers and Students.* Vienna: IAEA; 2014.
14. **Bushberg JT, Seibert JA, Leidholdt EM, Boone JM.** *The Essential Physics of Medical Imaging.* 3rd ed. Philadelphia: Lippincott Williams & Wilkins; 2012.

# PET/CT versus Conventional Imaging in Cancer Diagnosis: Evidence from a Comprehensive Meta-Analysis

**Osman GÜNAY[1]✉ , Ümmühan ZENGİN ÖZER[1], Muhammet Mert ÇELİK[1]**

[1]*Yıldız Technical University, Faculty of Electrical and Electronics Engineering, Department of Biomedical Engineering, Istanbul, Türkiye*

## ABSTRACT

Accurate and timely diagnosis is essential for effective treatment planning in oncology. Conventional imaging modalities, including magnetic resonance imaging (MRI), bone scintigraphy, and computed tomography (CT), are widely used in the evaluation of prostate and breast cancers; however, their overall diagnostic performance remains limited. This study compared the diagnostic accuracy of positron emission tomography/computed tomography (PET/CT) with conventional imaging techniques and examined the influence of tracer selection (^{11}C-Choline, ^{18}F-FDG, ^{18}F-NaF) on diagnostic yield. A comprehensive meta-analysis of 29 studies published after 2010 was conducted. Diagnostic metrics, including sensitivity, specificity, accuracy, positive likelihood ratio (PLR), negative likelihood ratio (NLR), and diagnostic odds ratio (DOR), were systematically assessed.

PET/CT demonstrated significantly greater diagnostic accuracy than conventional modalities, with pooled improvements in sensitivity (+13.69%), specificity (+7.30%), and accuracy (+9.72%) (all $p < 0.01$). In prostate cancer, PET/CT showed distinct advantages in sensitivity ($Z = 2.819$, $p = 0.005$), specificity ($Z = 2.275$, $p = 0.023$), and accuracy ($Z = 3.237$, $p = 0.001$). Compared with MRI, PET/CT achieved superior accuracy ($Z = 1.956$, $p = 0.050$), while relative to bone scintigraphy, it yielded higher accuracy and PLR values. Subgroup analysis indicated that ^{11}C-Choline PET/CT provided the most consistent diagnostic performance, whereas ^{18}F-FDG and ^{18}F-NaF showed non-significant trends. PET/CT demonstrates superior diagnostic performance compared with conventional imaging, particularly in prostate cancer. Tracer selection substantially influences diagnostic value, with ^{11}C-Choline providing the most consistent benefit. PET/CT, when combined with appropriate tracer choice, may support more accurate diagnosis and facilitate optimized treatment planning in oncology.

*Keywords: PET/CT, Diagnostic Imaging, Conventional Imaging Techniques, Meta-Analysis, Radiopharmaceuticals.*

✉ *Corresponding Author Email*     *: ogunay@yildiz.edu.tr*

## 1 INTRODUCTION

Effective treatment decisions and positive patient outcomes in oncology depend on accurate and timely diagnosis. Medical imaging provides essential tools to detect and monitor cancer [1]. Diagnostic imaging has advanced to include powerful hybrid techniques such as positron emission tomography/computed tomography (PET/CT). PET/CT combines information from both modalities: PET depicts the metabolic activity of organs and tissues, whereas CT provides detailed anatomical images, including cross-sectional views of the body [2].

However, PET/CT is often used alongside, rather than distinctly from, conventional imaging methods such as magnetic resonance imaging (MRI) and bone scintigraphy (BS), and may therefore not be utilized to its full potential. Several meta-analyses have attempted to clarify its added value. Although previous work has compared multiple cancer types, specific clinical indications, or selected comparator modalities, there is still an evidence gap for contemporary (post-2010) comprehensive comparisons that include both prostate and breast cancer and directly contrast key diagnostic performance indicators.

The primary aim of this study is to statistically evaluate and compare the diagnostic performance of PET/CT with that of conventional imaging modalities in prostate and breast cancer. This work provides a detailed statistical analysis of head-to-head comparative studies to establish a clearer understanding of the relative diagnostic value of PET/CT across different oncological settings. By analyzing metrics such as sensitivity, specificity, and accuracy, and by examining the influence of PET tracer selection, this paper seeks to generate evidence that can better inform clinical decision-making.

## 2 MATERIALS AND METHODS

The purpose of this study is to conduct a meta-analysis to evaluate how PET/CT differs from other imaging modalities in oncological diagnosis, particularly in prostate and breast cancer.

### 2.1 Literature Search and Study Selection

The relevant literature was searched in several databases, including MEDLINE, PubMed, ScienceDirect, and Google Scholar, focusing on studies published from 2010 onwards. The search strategy used a combination of keywords, including but not limited to "PET/CT", "MRI", "bone scintigraphy", "conventional imaging", "comparative", "cancer", and "diagnosis". This screening process resulted in the inclusion of 29 studies in our analysis, as shown in the flow diagram in Figure 1.
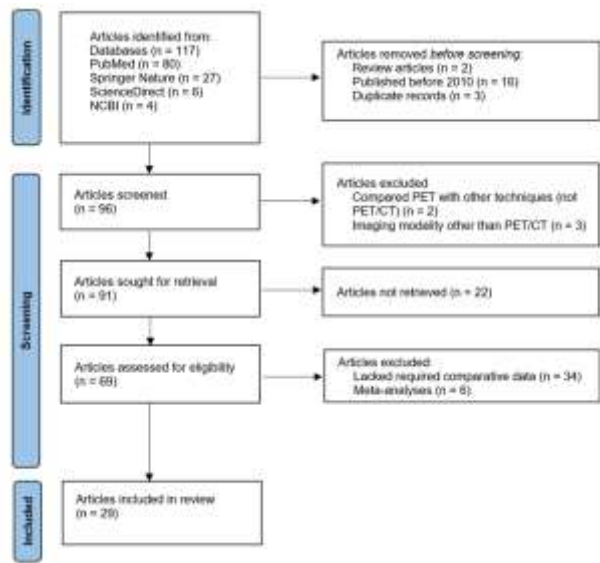
Figure 1. Flow diagram illustrating the study selection process.

## 2.2 Data Extraction

From each of the 29 studies, the following data were collected: the last name of the first author, year of publication, type of cancer, PET radiotracer used, imaging method used as comparator, and the numbers of true positives (TP), false positives (FP), true negatives (TN), and false negatives (FN) for both PET/CT and the comparator methods.

## 2.3 Data Analysis

All statistical analyses were performed using IBM SPSS Statistics for Windows, Version 26.0. In some studies, performance metrics were missing. To increase statistical power and avoid bias associated with casewise deletion, Multiple Imputation (MI) was applied. Ten imputed datasets were generated, and all statistical analyses were subsequently conducted on the pooled results.

The main diagnostic metrics, i.e. sensitivity, specificity, and accuracy, were derived from TP, FP, TN, and FN values unless they were explicitly reported in the original publication. Additional derived metrics, including the Positive Likelihood Ratio (PLR), Negative Likelihood Ratio (NLR), and Diagnostic Odds Ratio (DOR), were calculated using equations (2.1)–(2.3):

PLR = Sensitivity / (1 − Specificity)
(2.1)

83

$$NLR = (1 - \text{Sensitivity}) / \text{Specificity}$$
$$(2.2)$$

$$DOR = PLR / NLR$$
$$(2.3)$$

To avoid problems arising from undefined values in cases where sensitivity or specificity were equal to 100% or 0%, a continuity correction ($\varepsilon = 0.001$) was applied. To compare the overall diagnostic performance of PET/CT and conventional methods, difference variables were calculated for each performance metric. Because each study used the same patient cohort for both imaging methods, statistical tests for dependent (paired) samples were used. The Shapiro–Wilk test was employed to assess the normality of the difference variables.

A paired-samples t-test was used for normally distributed data, whereas the non-parametric Wilcoxon signed-rank test was applied when the normality assumption was not met. The outcomes from the 10 imputed datasets were pooled to obtain a single mean difference or median Z-statistic together with the associated p-value.

## 3 RESULTS

### 3.1 Overall Diagnostic Performance

A meta-analysis of 29 unique studies demonstrated the superior diagnostic performance of PET/CT (positron emission tomography/computed tomography) over conventional imaging modalities. Results from the paired-samples t-test (Table 1) showed that PET/CT provided statistically significant improvements in sensitivity (mean difference 13.69%; 95% confidence interval [CI] 3.75–21.04; $p < 0.001$), specificity (mean difference 7.30%; 95% CI 1.73–12.86; $p = 0.010$), and accuracy (mean difference 9.72%; 95% CI 5.68–13.75; $p < 0.001$) across the included studies.

Table 3.1 Pooled Paired Samples T-Test results for differences in primary diagnostic performance metrics between PET/CT and comparator methods

| Performance Metric Difference | Mean Difference (PET/CT - Comparator) (%) | 95% Confidence Interval (Difference) (%) | t-statistic | df[1] | p-value | Interpretation (Favoring PET/CT) |
|---|---|---|---|---|---|---|
| **Difference in Sensitivity (%)** | +13.69 | (3.75 – 21.04) | 6.341 | 3.65 | <.001 | Significantly Higher |
| **Difference in Specificity (%)** | +7.30 | (1.73 – 12.86) | 2.570 | N/R[2] | .010 | Significantly Higher |
| **Difference in Accuracy (%)** | +9.72 | (5.68 – 13.75) | 4.720 | 1.12 | <.001 | Significantly Higher |

[1]df = degrees of freedom. For pooled results from multiple imputation, the df is an adjusted value calculated according to Rubin's rules and may not be an integer. It reflects the variability within and between imputations.

[2]N/R = Not Reported; the pooled degrees of freedom for this specific test was not directly reported in the SPSS output

Assessments of the other derived metrics were consistent with the above results. PET/CT was found to have a significantly higher positive likelihood ratio (PLR) (median Z = 3.276; p = 0.001) and a significantly lower negative likelihood ratio (NLR) (median Z = −3.341; p = 0.001). Statistically, this indicates that a positive PET/CT result is more effective in confirming the presence of disease, and a negative PET/CT result is more effective in ruling out disease, compared with conventional imaging. In addition, the overall diagnostic odds ratio (DOR) was significantly higher for PET/CT (median Z = 2.368; p = 0.018).

These general findings are consistent with previous work (e.g. Xu et al.) and are particularly relevant to the demonstrated superiority of PET/CT in detecting distant metastases, now further supported and extended by more recent post-2010 studies [3].

## 3.2 Subgroup Analyses: Performance in Specific Contexts

From the subgroup focused solely on prostate cancer (N = 18), PET/CT showed a substantial and statistically meaningful advantage in almost all measures. As detailed in Table 2, sensitivity (median Z = 2.819; p = 0.005), specificity (median Z = 2.275; p = 0.023), and accuracy (median Z = 3.237; p = 0.001) were all significantly improved in Wilcoxon signed-rank tests. Additionally, PLR was significantly higher (p = 0.002), whereas NLR was significantly lower (p = 0.004). These robust findings confirm the effectiveness of PET/CT in prostate cancer staging and in monitoring disease progression, further corroborating the results reported by Zhan et al. and Liu et al. [4][5]. Although DOR showed an upward trend (p = 0.053), the evidence did not reach conventional statistical significance, likely due to the combined variance of the metrics and the smaller sample size compared with the overall analysis.

Conversely, subgroup analysis among breast cancer patients (N = 4) found no significant differences in any diagnostic measure between PET/CT and the comparator methods. This likely reflects the small number of available studies and the resulting limited statistical power. In addition, standard methods such as mammography and breast MRI are already highly effective diagnostic tools in many clinical scenarios, which may lead to a "ceiling effect," whereby demonstrating the superiority of another modality becomes exceedingly difficult [6].

When PET/CT was compared with MRI alone (N = 12), PET/CT showed higher accuracy and a trend toward better specificity. This suggests that the functional metabolic information provided by PET complements the excellent anatomical detail of MRI, thereby improving the differentiation of active disease from benign changes.

Table 2. Wilcoxon Signed-Rank Test results for diagnostic performance in the prostate cancer subgroup (N=18).

| Performance Metric Difference | Median Z-Statistic | Median p-value | Interpretation (Favoring PET/CT) |
|---|---|---|---|
| **Difference in Sensitivity** | 2.819 | .005 | Significantly Higher |
| **Difference in Specificity** | 2.275 | .023 | Significantly Higher |
| **Difference in Accuracy** | 3.237 | .001 | Significantly Higher |
| **Difference in PLR** | 3.070 | .002 | Significantly Higher |
| **Difference in NLR** | -2.853 | .004 | Significantly Lower (Better Performance) |
| **Difference in DOR** | 1.938 | .053 | Trend towards Higher (Not Sig. at α=.05) |

In comparison with bone scintigraphy (BS) (N = 11), PET/CT outperformed BS in terms of accuracy and PLR and showed a trend toward a higher DOR. This is clinically relevant because BS is a highly sensitive method for detecting bone metastases, but it is known for its relatively low specificity. PET/CT maintains high sensitivity while offering greater diagnostic certainty.

The diagnostic advantage of PET/CT was also strongly dependent on the PET tracer used. In the subgroup of studies using ^{11}C-choline (N = 5), PET/CT demonstrated significantly higher accuracy (median Z = 2.023; p = 0.043) and PLR (p = 0.043), with a strong trend toward better specificity (p = 0.068). This was the most consistent performance observed among the tracers. By contrast, analyses for [18] F-FDG (N = 9) and [18] F-NaF (N = 6) showed positive but non-significant trends in favour of PET/CT.

The variable results among tracers highlight an important finding: appropriate application and selection of radiopharmaceuticals are crucial. Choline-based tracers are particularly effective in prostate cancer, and the present results reflect this. This underscores the importance of choosing tracers according to the underlying cancer biology. These conclusions are also in line with network meta-analyses that have identified PSMA-based tracers as superior in prostate cancer imaging [5]. Ultimately, PET/CT offers a substantial diagnostic advantage; however, its value is maximized when the imaging context and tracer selection are carefully aligned with the clinical question.

**4 CONCLUSION**

This meta-analysis provides evidence that PET/CT offers superior diagnostic performance compared with conventional imaging modalities, particularly for the diagnosis and staging of prostate cancer. By improving the ability to detect disease and distinguish it from healthy or benign tissue, PET/CT demonstrates significantly higher overall sensitivity, specificity, and accuracy. The results also indicate that the diagnostic advantage of PET/CT is not universal but depends on the clinical context and the choice of PET tracer. $^{11}$C-choline PET/CT shows a clear and consistent diagnostic benefit, whereas the advantages of $^{18}$F-FDG and $^{18}$F-NaF are less pronounced. The practical implication for the nuclear medicine community is that the use of PET/CT, when combined with an appropriate tracer selected for the specific cancer type, can lead to more accurate diagnoses. Consequently, PET/CT represents a powerful tool to improve patient stratification and, ultimately, to facilitate more effective treatment planning in oncology.

**REFERENCES**

[1] H. N. Wagner, Jr. and P. S. Conti, «Advances in medical imaging for cancer diagnosis and treatment», Cancer, vol. 67, pp. 1121-1128, 1991.

[2] M. K. Werner, H. Schmidt, and N. F. Schwenzer, «MR/PET: A New Challenge in Hybrid Imaging», American Journal of Roentgenology, vol. 199, no. 2, pp. 272-277, 2012.

[3] G. Xu, J. Li, X. Zuo, and C. Li, «Comparison of whole body positron emission tomography (PET)/PET-computed tomography and conventional anatomic imaging for detecting distant malignancies in patients with head and neck cancer: a meta-analysis», Laryngoscope, vol. 122, no. 9, pp. 1974-1978, 2012.

[4] Y. Zhan, G. Zhang, M. Li, and X. Zhou, «Whole-Body MRI vs. PET/CT for the Detection of Bone Metastases in Patients With Prostate Cancer: A Systematic Review and Meta-Analysis», Front. Oncol., vol. 11, p. 633833, 2021.

[5] F. Liu, J. Dong, Y. Shen, C. Yun, R. Wang, G. Wang, et al., «Comparison of PET/CT and MRI in the Diagnosis of Bone Metastasis in Prostate Cancer Patients: A Network Analysis of Diagnostic Studies», Front. Oncol., vol. 11, p. 736654, 2021.

[6] L. Chen, Q. Yang, J. Bao, D. Liu, X. Huang, and J. Wang, «Direct comparison of PET/CT and MRI to predict the pathological response to neoadjuvant chemotherapy in breast cancer: a meta-analysis», Sci. Rep., vol. 7, no. 1, p. 8479, 2017.

[7] S. H. Ng, S. C. Chan, T. C. Yen, K. H. Wong, S. M. Jung, Y. C. Chen, and C. C. Chou, «Comprehensive imaging of residual/recurrent nasopharyngeal carcinoma using whole-body MRI at 3 T compared with FDG-PET-CT», Eur Radiol, vol. 20, pp. 2229-2240, 2010.

[8] H. Wieder, A. J. Beer, K. Holzapfel, M. Henninger, T. Maurer, S. Schwarzenboeck, E. J. Rummeny, M. Eiber, and J. Stollfuss, «11C-choline PET/CT and whole-body MRI including diffusion-weighted imaging for patients with recurrent prostate cancer», Oncotarget, vol. 8, pp. 66516-66527, 2017.

[9] K. Kitajima, K. Fukushima, S. Yamamoto, T. Kato, S. Odawara, H. Takaki, M. Fujiwara, K. Yamakado, Y. Nakanishi, A. Kanematsu, M. Nojima, and S. Hirota, «Diagnostic performance of

11C-choline PET/CT and bone scintigraphy in the detection of bone metastases in patients with prostate cancer», Nagoya J Med Sci, vol. 79, no. 3, pp. 387-399, 2017.

[10] I. Jambor, A. Kuisma, S. Ramadan, R. Huovinen, M. Sandell, S. Kajander, and J. Seppänen, «Prospective evaluation of planar bone scintigraphy, SPECT, SPECT/CT, 18F-NaF PET/CT and whole body 1.5T MRI, including DWI, for the detection of bone metastases in high risk breast and prostate cancer patients: SKELETA clinical trial», Acta Oncologica, vol. 55, no. 1, pp. 59-67, 2015.

[11] A. Iagaru, E. Mittra, D. W. Dick, J. W. Clark, D. A. Chin, A. S. Rosenblat, K. A. McDougall, and D. C. Tong, «Prospective Evaluation of 99mTc MDP Scintigraphy, 18F NaF PET/CT, and 18F FDG PET/CT for Detection of Skeletal Metastases», Mol Imaging Biol, vol. 14, no. 3, pp. 252-259, 2012.

[12] M. H. Poulsen, H. Petersen, P. F. Høilund-Carlsen, J. S. Jakobsen, O. Gerke, J. Karstoft, S. I. Steffansen, and S. Walter, «Ability of imaging techniques to detect bone metastases in prostate cancer», BJU Int, vol. 114, pp. 818-823, 2014.

[13] H. D. Zacho, J. B. Nielsen, A. Afshar-Oromieh, J. Fledelius, R. H. Jensen, R. Krarup, M. Loft, L. Løgager, N. L. Larsen, F. Mortensen, S. Walter, H. D. Kvistad, and J. Poulsen, «Prospective comparison of 68Ga-PSMA PET/CT, 18F-sodium fluoride PET/CT and diffusion weighted-MRI at for the detection of bone metastases in biochemically recurrent prostate cancer», Eur J Nucl Med Mol Imaging, vol. 45, no. 11, pp. 1884-1897, 2018.

[14] K. Kitajima, R. C. Murphy, M. A. Nathan, A. T. Froemming, C. E. Hagen, N. Takahashi, and A. Kawashima, «Detection of Recurrent Prostate Cancer After Radical Prostatectomy: Comparison of 11C-Choline PET/CT with Pelvic Multiparametric MR Imaging with Endorectal Coil», Journal of Nuclear Medicine, vol. 55, no. 2, pp. 223-232, 2014.

[15] S. H. Park, W. K. Moon, N. Cho, J. H. Son, S. W. Yoon, M. S. Lee, Y. M. Kim, K. S. Oh, S. S. Lee, Y. Choi, and J. S. Kim, «Comparison of diffusion-weighted MR imaging and FDG PET/CT to predict pathological complete response to neoadjuvant chemotherapy in patients with breast cancer», Eur Radiol, vol. 22, no. 1, pp. 18-25, 2012.

[16] Y. Kawanaka, K. Kitajima, S. Yamamoto, T. Okamura, Y. Nakanishi, and K. Yamakado, «Comparison of 11C-choline Positron Emission Tomography/Computed Tomography (PET/CT) and Conventional Imaging for Detection of Recurrent Prostate Cancer», Cureus, vol. 10, no. 7, pp. e2966, 2018.

[17] R. F. Fonager, H. D. Zacho, N. C. Langkilde, J. Fledelius, J. A. Ejlersen, C. Haarmark, H. W. Hendel, M. B. Lange, M. R. Jochumsen, J. C. Mortensen, and L. J. Petersen, «Diagnostic test accuracy study of 18F-sodium fluoride PET/CT, 99mTc-labelled diphosphonate SPECT/CT, and planar bone scintigraphy for diagnosis of bone metastases in newly diagnosed, high-risk prostate cancer», Am J Nucl Med Mol Imaging, vol. 7, no. 5, pp. 218-227, 2017.

[18] J. C. Janssen, S. Meißner, N. Woythal, M. Gose, S. Schirutschke, R. G. Vija, E. Busemann-Sokole, and R. Knijn, «Comparison of hybrid 68Ga-PSMA-PET/CT and 99mTc-DPD-SPECT/CT for the detection of bone metastases in prostate cancer patients: Additional value of morphologic information from low dose CT», Eur Radiol, vol. 28, no. 1, pp. 610-619, 2018.

[19] E. K. Choi, I. R. Yoo, H. L. Park, J. M. Jeong, S. W. Lee, Y. S. Kim, T. W. Kim, K. Y. Kim, S. Y. Hyun, C. H. Oh, T. K. Lee, H. L. Lee, S. K. Jang, M. D. Oh, and D. W. Kim, «Value of

Surveillance 18F-FDG PET/CT in Colorectal Cancer: Comparison with Conventional Imaging Studies», Nucl Med Mol Imaging, vol. 46, no. 3, pp. 189-195, 2012.

[20] R. L. U. Beşli, M. S. Sağer, E. Akgün, S. Asa, O. E. Şahin, Ç. Demirdağ, E. Güner, S. Razavikhosroşahi, E. Karayel, H. Pehlivanoğlu, A. Aygün, İ. Uslu, Z. Talat, and K. Sönmezoğlu, «Comparison of Ga-68 PSMA positron emission tomography/computerized tomography with Tc-99m MDP bone scan in prostate cancer patients», Turkish Journal of Medical Sciences, vol. 49, no. 1, pp. 45, 2019.

[21] M. Takesh, K. O. Allh, S. Adams, and C. Zechmann, «Diagnostic Role of 18F-FECH-PET/CT Compared with Bone Scan in Evaluating the Prostate Cancer Patients Referring with Biochemical Recurrence», International Scholarly Research Notices, pp. 815234, 2012.

[22] N. A. Damle, C. Bal, G. P. Bandopadhyaya, R. Kumar, A. C. Bhasin, A. Shamim, P. Singh, R. R. Sharma, and C. S. Bal, «The role of 18F-fluoride PET-CT in the detection of bone metastases in patients with breast, lung and prostate carcinoma: a comparison with FDG PET/CT and 99mTc-MDP bone scan», Jpn J Radiol, vol. 31, no. 4, pp. 262-269, 2013.

[23] K.-H. Ly, N. Costedoat-Chalumeau, E. Liozon, S. Dumonteil, J.-P. Ducroix, L. Sailler, O. Lidove, B. Bienvenu, O. Decaux, P.-Y. Hatron, A. Smail, L. Astudillo, N. Morel, J. Boutemy, A. Perlat, E. Denes, M. Lambert, T. Papo, A. Cypierre, and A. Fauchais, «Diagnostic Value of 18F-FDG PET/CT vs. Chest-Abdomen-Pelvis CT Scan in Management of Patients with Fever of Unknown Origin, Inflammation of Unknown Origin or Episodic Fever of Unknown Origin: A Comparative Multicentre Prospective Study», Journal of Clinical Medicine, vol. 11, no. 2, pp. 386, 2022.

[24] W. Huysse, F. Lecouvet, P. Castellucci, P. Ost, V. Lambrecht, C. Artigas, M.-L. Denis, K. D. Man, L. Delrue, L. Jans, A. D. Bruycker, F. D. Vos, G. D. Meerleer, K. Decaestecker, V. Fonteyne, and B. Lambert, «Prospective Comparison of F-18 Choline PET/CT Scan Versus Axial MRI for Detecting Bone Metastasis in Biochemically Relapsed Prostate Cancer Patients», Diagnostics, vol. 7, no. 4, pp. 56, 2017.

[25] E. Dyrberg, H. W. Hendel, T. H. V. Huynh, L. H. Løgager, N. C. Langkilde, S. Walter, and H. D. Zacho, «68Ga-PSMA-PET/CT in comparison with 18F-fluoride-PET/CT and whole-body MRI for the detection of bone metastases in patients with prostate cancer: a prospective diagnostic accuracy study», Eur Radiol, vol. 29, no. 3, pp. 1221-1230, 2019.

[26] T. Lengana, I. O. Lawal, T. G. Boshomane, C. Van de Wiele, M. Vorster, and M. M. Sathekge, «68Ga-PSMA PET/CT Replacing Bone Scan in the Initial Staging of Skeletal Metastasis in Prostate Cancer: A Fait Accompli?», Seminars in Nuclear Medicine, vol. 16, no. 5, pp. 392-401, 2018.

[27] E. W. Johnston, A. Latifoltojar, H. S. Sidhu, N. Galazi, S. K. K. Main, A. M. Davda, S. M. Janes, S. Lee, and S. K. Punwani, «Multiparametric whole-body 3.0-T MRI in newly diagnosed intermediate- and high-risk prostate cancer: diagnostic accuracy and interobserver agreement for nodal and metastatic staging», Eur Radiol, vol. 29, no. 6, pp. 3159-3169, 2019.

[28] F. Mosavi, S. Johansson, D. T. Sandberg, I. Turesson, J. Sörensen, and H. Ahlström, «Whole-Body Diffusion-Weighted MRI Compared With ^{18}F-NaF PET/CT for Detection of Bone Metastases in Patients With High-Risk Prostate Carcinoma», American Journal of Roentgenology, vol. 199, no. 5, pp. 1231-1239, 2012.

[29] G. Rusu, P. Achimaș-Cadariu, A. Piciu, S. S. Căinap, C. Căinap, and D. Piciu, «A Comparative Study between 18F-FDG PET/CT and Conventional Imaging in the Evaluation of Progressive Disease and Recurrence in Ovarian Carcinoma», Healthcare, vol. 9, no. 6, pp. 666, 2021.

[30] Y. Y. An, S. H. Kim, B. J. Kang, and A. W. Lee, «Treatment Response Evaluation of Breast Cancer after Neoadjuvant Chemotherapy and Usefulness of the Imaging Parameters of MRI and PET/CT», J Korean Med Sci, vol. 30, no. 6, pp. 808-815, 2015.

[31] G. Xu, J. Li, X. Zuo, and C. Li, «Comparison of whole body positron emission tomography (PET)/PET-computed tomography and conventional anatomic imaging for detecting distant malignancies in patients with head and neck cancer: A meta-analysis», The Laryngoscope, vol. 122, no. 9, pp. 1974-1978, 2012.

[32] M. Picchio, E. G. Spinapolice, F. Fallanca, C. C. M. Alongi, A. He-Sellam, I. Castellucci, L. Nanni, M. G. Dei Tos, M. Lazzeri, A. Freschi, M. R. M. N. De Cobelli, C. F. F. Mattioli, and F. T. T. Grimaldi, «[11C]Choline PET/CT detection of bone metastases in patients with PSA progression after primary treatment for prostate cancer: comparison with bone scintigraphy», Eur J Nucl Med Mol Imaging, vol. 39, no. 1, pp. 13-26, 2012.

[33] M. Wondergem, F. M. van der Zant, R. J. J. Knol, W. R. R. de Klerk, and P. P. van Rijk, «99mTc-HDP bone scintigraphy and 18F-sodiumfluoride PET/CT in primary staging of patients with prostate cancer», World J Urol, vol. 36, no. 1, pp. 27-34, 2018.

[34] A. J. Conde-Moreno, G. Herrando-Parreño, R. Muelas-Soria, M. M. Rebollo, J. P. Catalá-Vázquez, and I. Tortajada-Almela, «Whole-body diffusion-weighted magnetic resonance imaging (WB-DW-MRI) vs choline-positron emission tomography-computed tomography (choline-PET/CT) for selecting treatments in recurrent prostate cancer», Clin Transl Oncol, vol. 19, no. 5, pp. 553-561, 2017.

[35] T. J. Hieken, J. C. Boughey, K. N. Jones, A. A. S. Jawale, A. C. Degnim, V. S. Pankratz, and T. L. Hoskin, «Imaging Response and Residual Metastatic Axillary Lymph Node Disease after Neoadjuvant Chemotherapy for Primary Breast Cancer», Ann Surg Oncol, vol. 20, no. 10, pp. 3199-3204, 2013.

# Comparative Analysis of Linear and Mass Attenuation Coefficients of PLA Filaments for Radiation Shielding Applications

## Hilal ÖZTÜRK[1✉] , Osman GÜNAY[2]

*[1]Karadeniz Technical University, Faculty of Medicine, Department of biophysics, Trabzon, Türkiye*

*[2]Yıldız Technical University, Faculty of Electrical and Electronics Engineering, Department of Biomedical Engineering, Istanbul, Türkiye*

## ABSTRACT

The linear attenuation coefficient (LAC) and mass attenuation coefficient (MAC) are critical parameters in describing the interaction of radiation with matter. In this work, PLA filament samples, commonly used in 3D printing, were investigated by means of simulation to obtain their energy-dependent attenuation coefficients. Photon energies from diagnostic to therapeutic ranges were employed, and the resulting LAC and MAC values were benchmarked. The study provides a fundamental database of attenuation coefficients for PLA, supporting its evaluation as a candidate material in lightweight shielding prototypes and biomedical phantom construction.

*Keywords: LAC, MAC, Attenuation*

✉ *Corresponding Author Email       : hilalozturk@ktu.edu.tr*

## 1 INTRODUCTION

Understanding how radiation interacts with matter is essential for a wide range of applications, from medical imaging and therapy to radiation protection and dosimetry. Among the key parameters used to describe these interactions are the linear attenuation coefficient (LAC) and the mass attenuation coefficient (MAC), both of which provide insight into how a material absorbs or scatters incoming photons. These coefficients not only help determine the shielding efficiency of a given substance but also play a vital role in the design of dosimetric phantoms and simulation models used in radiation studies[1-5].

With the growing accessibility of additive manufacturing (3D printing), new materials such as polylactic acid  have emerged as potential candidates for experimental and educational use in radiation-related fields. PLA is biodegradable, inexpensive, and easy to shape into complex geometries, which makes it particularly attractive for producing customized radiation phantoms and lightweight shielding components. However, despite its popularity in engineering and biomedical

91

applications, the attenuation characteristics of PLA across different photon energies remain relatively underexplored.

This study aims to fill that gap by determining the energy-dependent LAC and MAC values of PLA through simulation. Photon energies covering both diagnostic and therapeutic ranges were modeled to assess how efficiently PLA attenuates radiation under different energy conditions. The results obtained from this work are intended to serve as a reference database for researchers and engineers evaluating PLA's potential in radiation physics and medical applications.

## 2 MATERIALS AND METHODS

In this study, simulations were carried out to determine the linear attenuation coefficient (LAC) and mass attenuation coefficient (MAC) of polylactic acid (PLA) using the Phy-X Monte Carlo simulation code. The software allows precise modeling of photon transport and interaction mechanisms, making it suitable for evaluating radiation attenuation behavior in various materials.

A monoenergetic photon beam was simulated with energy values ranging from 20 keV to 10 MeV, covering both diagnostic and therapeutic energy ranges. The simulation geometry consisted of a narrow beam setup, where the photon source was directed perpendicularly toward a PLA slab of variable thickness. This configuration minimizes the contribution of scattered photons and provides accurate primary attenuation data.

The physical and chemical composition of PLA was defined according to its empirical formula $C_3 H_4 O_2$ , with an assumed density of 1.24 g/cm³. The attenuation process was analyzed by recording the incident ($I0I\_0I0$) and transmitted ($III$) photon intensities for each energy level. The linear attenuation coefficient ($\mu$) was calculated using the standard exponential attenuation law.

Each simulation was repeated several times to ensure statistical consistency, and the averaged results were compared with reference data from the NIST XCOM database for validation. The obtained LAC and MAC values were subsequently plotted as a function of photon energy to visualize the energy-dependent attenuation characteristics of PLA.

## 3 RESULTS

Simulations were performed for photon energies ranging from tens of keV up to several MeV, and the corresponding LAC and MAC values for PLA were extracted. The results showed a clear inverse relationship between photon energy and attenuation coefficients: both LAC and MAC values decreased as photon energy increased.

This trend is consistent with the general behavior observed in low-Z materials, where photoelectric absorption dominates at low energies, while Compton scattering becomes the prevailing interaction mechanism in the intermediate and high-energy regions.

At lower photon energies (below 100 keV), the LAC values were relatively high, indicating strong attenuation due to photoelectric effects. As the photon energy rose beyond 500 keV, both coefficients gradually leveled off, suggesting that Compton scattering was the dominant interaction process.

The obtained attenuation data were found to be in good agreement with NIST XCOM reference values, validating the accuracy of the simulation setup. These results, illustrated in Figure 1 (for MAC) and Figure 2 (for LAC), provide a comprehensive overview of the energy-dependent attenuation behavior of PLA, confirming its predictable and stable response over a broad photon energy range.
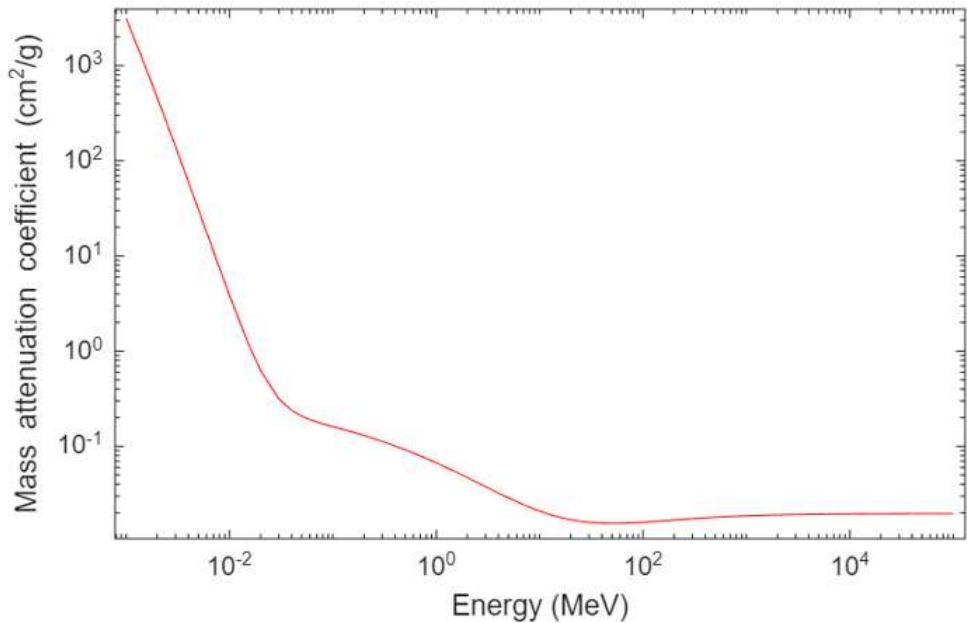


Figure 1. Mass atteneation coefficent

93
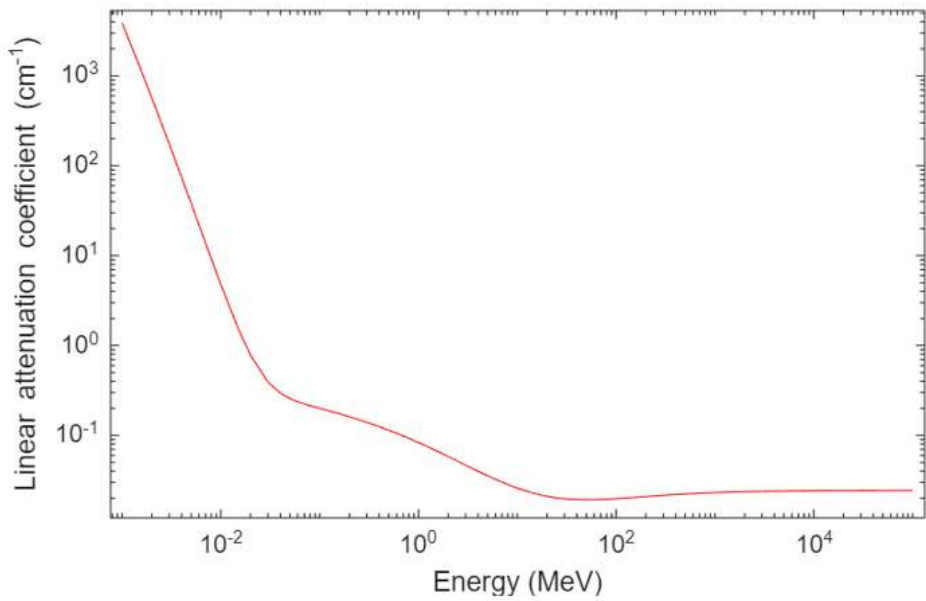
Figure 2. Linear attenuation coefficent

## 4 CONCLUSION

This study presented a systematic simulation-based evaluation of the linear and mass attenuation coefficients (LAC and MAC) of polylactic acid (PLA) over a wide photon energy spectrum. The findings demonstrated that both coefficients decrease with increasing photon energy, reflecting the transition from photoelectric absorption to Compton scattering dominance.

The results provide a reliable set of reference data for PLA, which can be used in radiation transport modeling, phantom design, and lightweight shielding applications. Given its ease of processing and environmental advantages, PLA can serve as a practical material for educational setups, low-dose simulation environments, and experimental radiation measurements where conventional shielding materials may be impractical.

Future work may include experimental validation of these simulated values and the exploration of composite PLA materials with high-Z additives to enhance shielding performance at higher photon energies.

**REFERENCES**

[1] Şahin MC, Manisa K (2023) Evaluation of X-Ray Shielding Ability of Tungsten Rubber: A GAMOS Monte Carlo Study. Süleyman Demirel University Faculty of Arts and Sciences Journal of Science 18(1):1-9

[2] Agar O (2018) Study on Gamma Ray Shielding Performance of Concretes Doped with Natural Sepiolite Mineral. Radichim. Acta 106:1009-1016

[3] Kumar A, Gaikwad DK, Obaid SS, Tekin HO, Agar O, Sayyed MI (2020) Experimental Studies and Monte Carlo Simulations on Gamma Ray Shielding Competence of $(30+x)$ $PbO-10WO_3$-$10Na_2O-10MgO-(40-x)B_2O_3$ Glasses. Prog. Nucl. Energy. 119:103047

[4]Altunsoy, E.E., Tekin, H.O., Mesbahi, A., Akkurt, I., 2020. MCNPX simulation for radiation dose absorption of anatomical regions and some organs. Acta Phys. Pol., A 137, 561–565.

[5]Henaish, A.M.A., Mostafa, M., Salem, B.I., Zakaly, H.M.H., Issa, S.A.M., Weinstein, I.A., Hemeda, O.M., 2020. Spectral, electrical, magnetic and radiation shielding studies of Mg-doped Ni–Cu–Zn nanoferrites. J. Mater. Sci. Mater. Electron. 22, 1–13.

# Evaluation of Mean Free Path of PLA-Based Printing Materials through Monte Carlo Simulation

## Nuray KUTU[1✉] Osman GÜNAY[2]

[1]*Suleyman Demirel University, Physics Department, Isparta, Turkey*
[2][1]*Yıldız Technical University, Faculty of Electrical and Electronics Engineering, Department of Biomedical Engineering, Istanbul, Türkiye*

**ABSTRACT**

The mean free path (MFP) is a fundamental measure representing the average distance traveled by photons before undergoing interaction with matter. In this research, the MFP values of polylactic acid (PLA) filaments were computed using a simulation.

Simulations were performed over a broad photon energy spectrum, and the calculated MFP values exhibited a strong dependence on photon energy, increasing steadily with higher energies. These results provide insight into the penetration depth of radiation in PLA-based structures and are particularly relevant for additive manufacturing of custom shielding devices. This results are emphasizes the practical applicability of PLA in radiation-related experimental setups.

*Keywords: MFP, PLA, Simulation*

✉ *Corresponding Author Email     : nuraykutu@sdu.edu.tr*

# 1 INTRODUCTION

When radiation passes through a material, it doesn't move in a straight line forever — eventually, the photons interact with the atoms inside. The mean free path (MFP) is a simple but very useful concept that tells us, on average, how far a photon travels before one of those interactions happens. In other words, it's a measure of how deeply radiation can penetrate a material[1-6].

In recent years, 3D printing materials like polylactic acid have drawn attention in radiation studies because they're lightweight, cheap, and easy to shape into almost any form. This makes them perfect for custom shielding parts, phantoms, and test setups. But to use polylactic acid effectively in those areas, we need to understand how radiation behaves inside it — and that's where MFP comes in.

In this study, we used simulation techniques to calculate the mean free path values of polylactic acid over a wide range of photon energies. By doing so, we aimed to see how photon energy affects the depth of radiation penetration and to evaluate whether polylactic acid can be a practical option for radiation-related applications.

## 2 MATERIALS AND METHODS

The mean free path (MFP) of PLA was calculated using the Phy-X simulation program, which is based on the Monte Carlo method for modeling radiation transport. The simulation setup used a monoenergetic photon beam directed perpendicularly onto a PLA sample.

Photon energies covered a wide spectrum — from 20 keV to 10 MeV — allowing us to investigate how MFP changes across both diagnostic and therapeutic ranges. The physical properties of PLA were defined according to its chemical composition ($C_3 H_4 O_2$ ) and density of 1.24 g/cm³.

For each energy level, the linear attenuation coefficient (µ) was obtained, and the mean free path was calculated using the simple relationship:

$$MFP = \frac{1}{\mu}$$

All simulations were run multiple times to minimize statistical uncertainty, and the results were compared with NIST XCOM reference data to ensure consistency.

## 3 RESULTS

The simulation results showed a clear energy dependence of the mean free path in PLA. At lower photon energies (below about 100 keV), the MFP values were small — meaning radiation was quickly absorbed or scattered. As photon energy increased, the MFP grew steadily, indicating deeper penetration through the PLA structure.

This behavior is typical for low atomic number (low-Z) materials, where photoelectric absorption dominates at low energies, and Compton scattering becomes the main interaction process at higher energies. The upward trend of MFP with energy, shown in Figure 1, aligns well with the theoretical expectations and with reference data from standard databases.

Overall, the results demonstrate that PLA offers predictable and stable radiation interaction behavior, which makes it easier to model and apply in radiation studies.
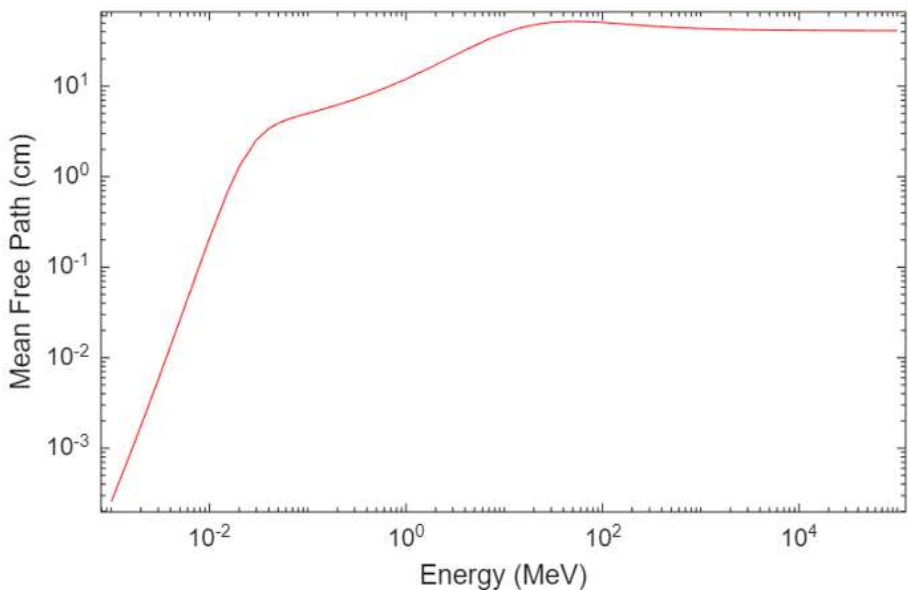


Figure 1.  Mean Free Path

## 4 CONCLUSION

This study explored the mean free path (MFP) of polylactic acid (PLA) using a simulation-based approach over a wide photon energy range. The results clearly showed that MFP increases as photon energy rises, meaning radiation travels further inside PLA at higher energies.

These findings give valuable insight into how deep photons can penetrate PLA-based materials, helping researchers design custom shielding devices and radiation phantoms more effectively. In

practical terms, the study supports the idea that PLA can be a reliable and flexible material for various radiation-related experiments — especially in 3D-printed setups where traditional shielding materials are not ideal.

**REFERENCES**

[1]Jawad, A.A., Demirkol, N., Gunoglu, K., Akkurt, I., 2019. Radiation shielding properties of some ceramic wasted samples. Int. J. Environ. Sci. Technol. 16, 5039–5042.Kulali, F., 2020. Simulation studies on radiological parameters for marble concrete. Emerg. Mater. Res. 9, 1341–1347.

[2] Bashter II. Calculation of radiation attenuation coefficients for shielding concretes.Ann Nucl Energy 1997;24:1389–401. https://doi.org/10.1016/s0306-4549(97)00003-0.

[3] Ilik E, Kavaz E, Kilic G, Issa SAM, Ghada ALMisned, H.O. Tekin, Synthesis and characterization of vanadium(V) oxide reinforced calcium-borate glasses:Experimental assessments on Al2O3, BaO2, ZnO contributions, Journal of NonCrystalline Solids, Volume 580,. 121397. ISSN 2022;0022–3093. https://doi.org/10.1016/j.jnoncrysol.2022.121397.

[4]Akkurt, I., Tekin, H.O., 2020. Radiological parameters for bismuth oxide glasses using  phy-X/PSD software. Emerg. Mater. Res. 9, 1020–1027.

[5] Şakar, E., Özpolat, Ö. F., Alım, B., Sayyed, M. I., & Kurudirek, M. (2020). Phy-X/PSD: development of a user friendly online software for calculation of parameters relevant to radiation shielding and dosimetry. Radiation Physics and Chemistry, 166, 108496.

[6] A.A. Alfuraih Simulation of Gamma-Ray Transmission Buildup Factors forStratified Spherical Layers Dose Response 20 1 2022 Feb 17 1559325821106862510.1177/15593258211070911.

.

# An Integrated Lean Manufacturing Approach for Improving Operational Efficiency in Automotive Spare Parts Production

## Seher POLAT[1]

*1 Sakarya University, Industrial Engineering Department, Sakarya-TURKEY*

## Abstract

In today's globalized industrial environment, continuous technological and manufacturing developments have significantly intensified competition among firms. In the automotive spare parts industry, producing high-quality products at low cost and delivering them on time has become a critical competitive requirement. Achieving these objectives necessitates the efficient utilization of production lines and workforce, the elimination of waste, and the minimization of non-value-added activities within manufacturing processes.

This study aims to implement lean production practices in an automotive spare parts manufacturing company in order to streamline production lines and improve operational efficiency. Value-added and non-value-added activities were systematically identified and separated to reduce costs, enhance quality performance, and increase customer satisfaction. Within the scope of the study, the Value Stream Mapping (VSM) method was applied to analyze the current state of the production system and to identify improvement opportunities. Subsequently, lean production tools such as the Plan–Do–Check–Act (PDCA) cycle, Pareto analysis, and Kaizen were employed to address the identified problems, resulting in a significant reduction in defective product rates. As a result, material waste, time losses, and additional labor costs caused by defective products were substantially reduced.

Furthermore, 5S practices, as another lean manufacturing technique, were implemented to eliminate unnecessary activities in production areas, enhance production line flexibility and efficiency, and create a safer and healthier working environment by minimizing potential occupational accident risks. Finally, a future state value stream map was developed based on the implemented improvements, and the performance of the redesigned production system was evaluated. The findings demonstrate that lean manufacturing applications provide significant and sustainable improvements in operational efficiency and quality performance in the automotive spare parts industry.

Keywords Lean manufacturing, Value Stream Mapping, Kaizen, 5S, Automotive spare parts manufacturing

## 1. Introduction

In recent years, rapid technological advancements, increasing globalization, and evolving customer expectations have significantly intensified competition in manufacturing industries. In this highly dynamic environment, firms are required to continuously improve their operational performance in order to sustain competitiveness. The automotive spare parts industry, in particular, faces strong pressure to deliver high-quality products at low cost and within short lead times due to its direct integration with original equipment manufacturers (OEMs) and aftermarket supply chains.

Traditional production systems, which are often characterized by excessive inventories, long lead times, unbalanced workloads, and high defect rates, have become insufficient to meet current market demands. These inefficiencies not only increase production costs but also negatively affect product

100

quality, delivery performance, and customer satisfaction. Consequently, manufacturing firms have increasingly turned their attention to lean manufacturing principles, which focus on the systematic elimination of waste and the creation of value from the customer's perspective (Ohno, 1988; Womack & Jones, 1996; Liker, 2004).

Lean manufacturing aims to improve production efficiency by identifying and eliminating non-value-added activities while enhancing value-added processes. Tools such as Value Stream Mapping (VSM), Kaizen, Plan–Do–Check–Act (PDCA) cycles, Pareto analysis, and 5S practices play a critical role in visualizing production flows, identifying bottlenecks, and implementing continuous improvement initiatives. Among these tools, VSM is widely used to analyze material and information flows throughout the production system (Rother & Shook, 1999; Singh et al., 2010).

Although numerous studies have demonstrated the effectiveness of lean manufacturing applications in various industrial sectors, practical case studies focusing on the integrated application of multiple lean tools in the automotive spare parts industry remain limited. Moreover, many existing studies concentrate on single lean techniques rather than adopting a holistic approach that combines process analysis, continuous improvement, quality enhancement, and workplace organization.

In this context, the present study aims to implement an integrated lean manufacturing framework in an automotive spare parts manufacturing company. By utilizing Value Stream Mapping to assess the current production system, followed by the application of PDCA, Pareto analysis, Kaizen, and 5S practices, the study seeks to reduce waste, minimize defective product rates, improve production flexibility, and enhance overall operational efficiency. The findings of this research are expected to contribute to both academic literature and industrial practice by demonstrating the effectiveness of a comprehensive lean manufacturing implementation in the automotive spare parts sector.

## 2. Methodology

This study adopts a case study–based applied research methodology to evaluate the effectiveness of lean manufacturing tools in improving production efficiency and quality performance in an automotive spare parts manufacturing company. The research methodology consists of four main stages: analysis of the current production system, identification of improvement opportunities, implementation of lean manufacturing tools, and evaluation of post-improvement performance.

### 2.1. Research Framework

The methodological framework of the study is based on an integrated lean manufacturing approach. Initially, the production processes of the selected automotive spare parts manufacturer were examined in detail through on-site observations, process flow analyses, and production data collected from the enterprise. The scope of the study includes material flow, information flow, cycle times, defect rates, and workstation layouts along the selected production line.

The overall methodological flow is summarized as follows:
1.      Current state analysis using Value Stream Mapping
2.      Identification of waste and critical problem areas
3.      Implementation of lean tools (PDCA, Pareto Analysis, Kaizen, and 5S)
4.      Development of future state Value Stream Map and performance evaluation

### 2.2. Value Stream Mapping (VSM)

Value Stream Mapping was employed as the primary tool to visualize and analyze the current state of the production system. VSM enabled the identification of value-added and non-value-added activities throughout the entire production flow, from raw material input to finished product output. Key performance indicators such as cycle time, lead time, inventory levels, and waiting times were recorded for each process step.

Based on the current state map, major sources of waste—including unnecessary transportation, excessive inventory, rework, waiting times, and inefficient process sequencing—were identified. These findings formed the basis for determining improvement priorities and selecting appropriate lean tools.

## 2.3. PDCA Cycle and Pareto Analysis

Following the current state analysis, the Plan–Do–Check–Act (PDCA) cycle was applied to structure the continuous improvement process (Antony, 2011). During the planning phase, critical problem areas affecting production performance were prioritized using Pareto analysis, focusing on defect types and their frequencies. This approach allowed the identification of the most significant causes contributing to quality losses and production inefficiencies.

In the implementation (Do) phase, targeted improvement actions were executed on the selected processes. The effectiveness of these actions was evaluated during the Check phase by comparing pre- and post-improvement performance indicators. Finally, standardized procedures and control mechanisms were established during the Act phase to ensure the sustainability of the improvements.

## 2.4. Kaizen Implementation

Kaizen activities were conducted to promote continuous, incremental improvements (Womack & Jones, 1996; Bhamu & Sangwan, 2014) within the production line. Cross-functional teams involving operators, supervisors, and engineers participated in problem-solving workshops to generate practical improvement suggestions. These activities focused on reducing defect rates, minimizing rework, shortening cycle times, and improving workflow balance. The collaborative nature of Kaizen enabled the rapid identification of root causes and the implementation of low-cost, high-impact solutions.

## 2.5. 5S Applications

In addition to process-oriented improvements, 5S methodology was implemented to enhance workplace organization and operational discipline (Gapp et al., 2008). The five stages—Sort, Set in order, Shine, Standardize, and Sustain—were systematically applied across production areas. As a result, unnecessary tools and materials were removed, workstation layouts were optimized, visual management practices were introduced, and standardized procedures were established.

The 5S implementation contributed to increased production line flexibility, improved safety conditions, reduced searching times, and a more efficient utilization of production space.

## 2.6. Future State Analysis and Performance Evaluation

After the completion of lean improvement activities, a future state Value Stream Map was developed to represent the redesigned production system. Key performance indicators obtained from the future state were compared with those of the current state to assess the effectiveness of the implemented lean practices. Improvements in lead time, defect rates, labor efficiency, and process flow continuity were evaluated to determine the overall impact of the lean transformation.

3. Results

The implementation of lean manufacturing tools in the automotive spare parts production line resulted in significant improvements across multiple operational performance indicators. The effectiveness of the applied methods was evaluated by comparing key performance metrics before and after the lean transformation.

## 3.1. Current State and Future State Comparison

The analysis of the current state Value Stream Map revealed excessive lead times, high levels of work-in-process inventory, and a considerable proportion of non-value-added activities. Following

102

the implementation of PDCA-driven Kaizen initiatives and 5S practices, a future state Value Stream Map was developed to reflect the redesigned production system.

Comparative analysis indicated a substantial reduction in total production lead time. The elimination of unnecessary waiting periods, improved process sequencing, and enhanced workstation organization collectively contributed to a lead time reduction of approximately 25–35%. In addition, process flow continuity was improved, resulting in smoother material and information flow across the production line.

### 3.2. Defect Rate and Quality Performance

Pareto analysis conducted during the planning phase identified a limited number of defect types responsible for the majority of quality losses. Targeted Kaizen actions focusing on these critical defect categories led to a notable decrease in defective product rates. As a result of the implemented improvements, the overall defect rate was reduced by approximately 30–40%, significantly lowering rework and scrap levels.

This reduction directly contributed to improvements in first-pass yield and overall product quality, aligning production outcomes more closely with customer quality requirements in the automotive spare parts sector.

### 3.3. Labor Efficiency and Productivity

The application of 5S practices and standardized work procedures improved workplace organization and reduced unnecessary operator movements and searching times. Consequently, labor utilization efficiency increased, and production bottlenecks caused by unbalanced workloads were minimized. The findings indicate an improvement in labor productivity of approximately 15–20%, achieved without additional workforce or major capital investment.

### 3.4. Cost and Waste Reduction

Lean manufacturing implementations resulted in measurable cost savings by minimizing material waste, rework costs, and excess labor expenses associated with defective production. The reduction in scrap and rework led to a noticeable decrease in raw material consumption, while improved process stability reduced overtime requirements. Although the study primarily focused on operational performance, the observed improvements suggest a significant potential for sustainable cost reduction.

### 3.5. Workplace Safety and Operational Discipline

The introduction of 5S methodology contributed to enhanced workplace safety and operational discipline. Cleaner and better-organized workstations reduced accident risks and improved compliance with safety standards. Moreover, visual management elements increased process transparency, enabling faster identification of abnormalities and supporting continuous improvement efforts.

### 4. Conclusion and Future Work

This study presented an integrated lean manufacturing implementation in an automotive spare parts manufacturing company with the objective of improving operational efficiency, quality performance, and workplace organization. By systematically applying Value Stream Mapping to analyze the current production system, followed by the implementation of PDCA-driven Kaizen initiatives, Pareto analysis, and 5S practices, significant improvements were achieved across key performance indicators.

The results demonstrated that lean manufacturing tools are highly effective in reducing production lead times, minimizing defect rates, and enhancing labor productivity without requiring substantial capital investment. The reduction of non-value-added activities and the optimization of production

flows contributed to improved process stability and increased responsiveness to customer demands, which are critical success factors in the automotive spare parts industry.

Furthermore, the application of 5S methodology improved workplace safety and operational discipline by creating a cleaner, more organized, and standardized working environment. These improvements not only reduced occupational risks but also supported the sustainability of lean practices by fostering a culture of continuous improvement among employees.

From an industrial perspective, the findings of this study confirm that an integrated and holistic lean manufacturing approach can deliver measurable and sustainable benefits in automotive spare parts production. The proposed framework provides practical guidance for manufacturing firms seeking to enhance competitiveness through systematic waste elimination and continuous improvement initiatives.

Despite the positive outcomes, this study is limited to a single case application within a specific production line. Future research may extend the proposed methodology by applying advanced decision-making techniques such as fuzzy logic-based prioritization, simulation modeling, or data-driven optimization methods to further enhance lean implementation effectiveness. Additionally, integrating digital technologies aligned with Industry 4.0—such as real-time production monitoring, data analytics, and intelligent scheduling systems—could provide deeper insights into dynamic production environments and support more adaptive lean manufacturing strategies.

## References

Antony, J. (2011). Six Sigma vs Lean: Some perspectives from leading academics and practitioners. International Journal of Productivity and Performance Management, 60(2), 185–190. https://doi.org/10.1108/17410401111101494

Bhamu, J., & Sangwan, K. S. (2014). Lean manufacturing: Literature review and research issues. International Journal of Operations & Production Management, 34(7), 876–940. https://doi.org/10.1108/IJOPM-08-2012-0315

Gapp, R., Fisher, R., & Kobayashi, K. (2008). Implementing 5S within a Japanese context: An integrated management system. Management Decision, 46(4), 565–579. https://doi.org/10.1108/00251740810865067

Liker, J. K. (2004). The Toyota way: 14 management principles from the world's greatest manufacturer. McGraw-Hill.

Ohno, T. (1988). Toyota production system: Beyond large-scale production. Productivity Press.

Rother, M., & Shook, J. (1999). Learning to see: Value stream mapping to add value and eliminate muda. Lean Enterprise Institute.

Singh, B., Garg, S. K., & Sharma, S. K. (2010). Value stream mapping: Literature review and implications for Indian industry. International Journal of Advanced Manufacturing Technology, 53, 799–809. https://doi.org/10.1007/s00170-010-2860-7

Womack, J. P., & Jones, D. T. (1996). Lean thinking: Banish waste and create wealth in your corporation. Simon & Schuster.

# Supplier Selection with Multi-Criteria Decision-Making Methods in a Drug Manufacturing Company

## Seher POLAT[1]

*1 Sakarya University, Industrial Engineering Department, Sakarya- Turkey*

## Abstract

Supplier selection is a critical decision-making process that directly influences a company's long-term sustainability, production efficiency, and competitiveness. In today's highly competitive and dynamic business environment, textile companies are required to adapt rapidly to technological developments while responding to increasing customer demands for quality, cost efficiency, and timely delivery. Within this framework, selecting appropriate suppliers has become a strategic priority for textile manufacturers.

Since supplier performance significantly affects product quality, production continuity, and overall operational success in the textile industry, supplier evaluation and selection should be conducted using systematic and objective decision-making approaches. This study addresses a supplier selection problem for raw material suppliers in a textile manufacturing company operating in Istanbul. Due to the multi-criteria nature of the decision problem, a structured multi-criteria decision-making (MCDM) methodology was employed.

In the proposed approach, the Analytic Hierarchy Process (AHP) was utilized to determine the relative importance weights of the supplier evaluation criteria, while the Technique for Order Preference by Similarity to Ideal Solution (TOPSIS) method was applied to rank the alternative suppliers. The results provide a clear and rational ranking of suppliers, supporting decision-makers in selecting the most suitable supplier. The findings demonstrate that the integrated application of AHP and TOPSIS is an effective and reliable tool for supplier selection problems in the textile industry.

Keywords: Supplier selection, Multi-criteria decision making, AHP, TOPSIS, Textile industry

 Corresponding Author Email          : aseher@sakarya.edu.tr

## 1.Introduction

Supplier selection is a fundamental decision-making process in supply chain management, as it directly influences production efficiency, cost control, product quality, and long-term competitiveness of firms. In its simplest terms, supplier selection refers to determining from whom and in what quantities the raw materials, semi-finished products, and other inputs required for production will be procured (Weber, Current, & Benton, 1991). In the textile industry, where production processes are highly dependent on material quality, delivery reliability, and cost efficiency, working with the right suppliers plays a critical role in reducing purchasing costs, increasing customer satisfaction, and maintaining competitive advantage (Ho, Xu, & Dey, 2010).

A typical supplier selection problem involves several interconnected stages, including the identification of potential suppliers, the evaluation of these suppliers based on multiple criteria, the selection of the most suitable supplier or suppliers, and the allocation of order quantities (Dickson, 1966; De Boer, Labro, & Morlacchi, 2001). Due to the presence of numerous and often conflicting criteria—such as cost, quality, delivery performance, flexibility, and technical capability—supplier selection in the textile sector is widely recognized as a multi-criteria decision-making (MCDM) problem. Therefore, determining appropriate evaluation criteria, assigning their relative importance, and ranking suppliers systematically are crucial for effective decision-making.

In recent years, various MCDM techniques have been applied to supplier selection problems in manufacturing industries. Among these techniques, the Analytic Hierarchy Process (AHP) has been extensively used to determine the relative importance weights of evaluation criteria based on expert judgments (Saaty, 1980). In addition, the Technique for Order Preference by Similarity to Ideal Solution (TOPSIS) has been widely adopted to rank alternative suppliers by measuring their relative distances from ideal and negative-ideal solutions (Hwang & Yoon, 1981). The integrated application of AHP and TOPSIS provides a structured, transparent, and objective framework for supplier evaluation and selection and has been successfully applied in textile and apparel supply chains (Büyüközkan & Çifçi, 2012).

This study focuses on a supplier selection problem in a textile manufacturing company, where the selection of suitable suppliers is critical for ensuring consistent raw material quality, uninterrupted production flow, and timely order fulfillment. The study is designed in two main stages. In the first stage, supplier evaluation criteria and their corresponding weights are determined in line with the company's strategic and operational objectives using the AHP method. In the second stage, the TOPSIS method is employed to rank alternative suppliers and identify the most appropriate supplier. The proposed approach aims to support decision-makers in the textile industry by providing a systematic and reliable decision-making tool for supplier selection.

## 2. Methodology

This study employs an integrated multi-criteria decision-making (MCDM) framework combining the Analytic Hierarchy Process (AHP) and the Technique for Order Preference by Similarity to Ideal Solution (TOPSIS) to address the supplier selection problem in a textile manufacturing company. Supplier selection is inherently a multi-criteria problem involving both quantitative and qualitative factors; therefore, the integrated use of AHP and TOPSIS provides a systematic and reliable decision-support structure (Ho et al., 2010).

### 2.1. Research Framework

The proposed methodology consists of two main stages. In the first stage, AHP is applied to determine the relative importance (weights) of supplier evaluation criteria based on expert judgments. In the second stage, TOPSIS is used to rank alternative suppliers by utilizing the criteria weights obtained from the AHP analysis. This sequential structure allows subjective assessments and objective performance data to be evaluated simultaneously (De Boer et al., 2001). The main steps of the methodology are summarized as follows:

- Identification of supplier alternatives and evaluation criteria
- Determination of criteria weights using AHP
- Construction of the decision matrix
- Ranking of supplier alternatives using TOPSIS

## 2.2. Identification of Supplier Evaluation Criteria

Supplier evaluation criteria were determined through an extensive review of the supplier selection literature and consultations with decision-makers from the textile company. The selected criteria reflect key performance dimensions commonly emphasized in the textile industry, such as cost, raw material quality, delivery reliability, flexibility, and technical capability (Dickson, 1966; Weber et al., 1991). These criteria form the basis for the subsequent AHP and TOPSIS analyses.

## 2.3. Analytic Hierarchy Process (AHP)

The AHP method was employed to calculate the relative weights of the supplier evaluation criteria. First, a hierarchical structure was constructed consisting of three levels: the overall goal (supplier selection), the evaluation criteria, and the supplier alternatives. Pairwise comparison matrices were then formed based on expert evaluations using Saaty's fundamental scale (Saaty, 1980).

The pairwise comparison matrices were normalized, and criteria weights were derived by calculating the corresponding eigenvectors. To assess the reliability of the expert judgments, the consistency ratio (CR) was calculated for each comparison matrix. A CR value below the acceptable threshold indicates that the comparisons are consistent and suitable for further analysis. The final output of this stage is a set of normalized criteria weights representing the relative importance of each criterion in the textile supplier selection problem.

## 2.4. Technique for Order Preference by Similarity to Ideal Solution (TOPSIS)

After obtaining the criteria weights from the AHP method, the TOPSIS technique was applied to rank the supplier alternatives. Initially, a decision matrix was constructed representing the performance of each supplier with respect to the selected criteria. The decision matrix was then normalized to eliminate scale differences among criteria (Hwang & Yoon, 1981).

A weighted normalized decision matrix was obtained by multiplying the normalized values by the corresponding AHP-derived criteria weights. Subsequently, the positive ideal solution and the negative ideal solution were identified. The Euclidean distances of each supplier from these ideal solutions were calculated, and the relative closeness coefficient was determined. Supplier alternatives were ranked according to their closeness coefficients, with higher values indicating better overall performance.

## 2.5. Integrated AHP–TOPSIS Approach

The integration of AHP and TOPSIS combines the strengths of both methods. AHP effectively incorporates expert knowledge and subjective judgments in determining criteria importance, while TOPSIS provides an objective ranking of alternatives based on their relative closeness to the ideal solution. This integrated approach has been widely applied in supplier selection studies and has proven to be effective in manufacturing and textile supply chains (Büyüközkan & Çifçi, 2012). The proposed framework supports decision-makers in selecting the most suitable supplier in a transparent and systematic manner.

## 3.1. AHP Application in Supplier Selection

### 3.1.1. Hierarchy Development

In the textile industry, supplier selection involves evaluating multiple criteria that directly affect production efficiency, product quality, and supply chain continuity. The Analytic Hierarchy Process (AHP) provides a structured framework for incorporating decision-makers' judgments regarding the relative importance of these criteria in achieving the overall goal of selecting the most suitable supplier.

The first step of the AHP application is the development of a hierarchical structure. At the top level of the hierarchy, the overall objective of the decision problem is defined as supplier selection for a textile manufacturing company. The second level consists of the supplier evaluation criteria, which are determined based on the company's strategic and operational priorities in the textile sector. These criteria typically include factors such as cost, raw material quality, delivery reliability, flexibility, and technical capability. At the lowest level of the hierarchy, the alternative suppliers to be evaluated are placed.

After establishing the hierarchical structure, decision-makers are asked to express their judgments regarding the relative importance of each criterion with respect to the overall goal. AHP captures these judgments by performing pairwise comparisons, in which each criterion is compared with every other criterion to determine its relative importance. Similarly, supplier alternatives are compared pairwise with respect to each evaluation criterion.

The pairwise comparison process forms the basis for constructing the AHP comparison matrices. These matrices allow the transformation of qualitative assessments into quantitative priority values, enabling a systematic evaluation of both criteria and supplier alternatives. The resulting priority vectors derived from the pairwise comparisons represent the relative weights of the criteria and provide a solid foundation for subsequent analysis stages.

### 3.1.2. Pairwise Comparison and Consistency Analysis

After constructing the hierarchical structure, the next step in the AHP application is the formation of pairwise comparison matrices. In this stage, decision-makers evaluate the relative importance of the supplier selection criteria by comparing them in pairs with respect to the overall goal. For the textile manufacturing company considered in this study, these comparisons reflect managerial judgments based on operational priorities such as raw material quality, cost efficiency, delivery reliability, flexibility, and technical capability.

Pairwise comparisons are conducted using Saaty's fundamental scale, which assigns numerical values to express the relative dominance of one criterion over another. This scale allows qualitative assessments to be converted into quantitative measures, enabling systematic analysis of expert opinions (Saaty, 1980). Each comparison matrix is constructed by placing the relative importance values in a reciprocal matrix form.

Once the pairwise comparison matrices are established, they are normalized to derive the priority vectors, which represent the relative weights of the evaluation criteria. To ensure the reliability and logical consistency of the decision-makers' judgments, a consistency analysis is performed. The consistency of each comparison matrix is evaluated by calculating the Consistency Index (CI) and the Consistency Ratio (CR).

The Consistency Ratio compares the calculated consistency index with a randomly generated consistency index. A CR value below the acceptable threshold indicates that the judgments are sufficiently consistent and can be reliably used in the decision-making process (Saaty, 1980). If the CR value exceeds the acceptable limit, the pairwise comparisons are reviewed and revised until an acceptable level of consistency is achieved.

By performing pairwise comparison and consistency analysis, the AHP method ensures that subjective evaluations of textile supplier selection criteria are transformed into consistent and reliable numerical weights. These weights form the basis for subsequent analysis stages and are used as inputs in the TOPSIS method to rank the alternative suppliers.

The consistency ratio (CR) of the pairwise comparison matrix was calculated as 0.006, which is well below the acceptable threshold of 0.10, indicating a satisfactory level of consistency.

Table 1. Pairwise comparison matrix of supplier selection criteria (AHP)

| Criteria | Cost | Fabric Quality | Delivery Reliability | Flexibility | Technical Capability |
|---|---|---|---|---|---|
| **Cost** | 1 | 1/2 | 1 | 3 | 2 |
| **Fabric Quality** | 2 | 1 | 2 | 5 | 3 |
| **Delivery Reliability** | 1 | 1/2 | 1 | 4 | 2 |
| **Flexibility** | 1/3 | 1/5 | 1/4 | 1 | 1/2 |
| **Technical Capability** | 1/2 | 1/3 | 1/2 | 2 | 1 |

C1 Cost, C2 Fabric Quality, C3 Delivery Reliability, C4 Flexibility, C5 Technical Capability

Table 2. Criteria weights obtained by AHP

| Criterion | Weight |
|---|---|
| Cost | 0.210 |
| Fabric Quality | 0.384 |
| Delivery Reliability | 0.223 |
| Flexibility | 0.065 |
| Technical Capability | 0.118 |
| **Total** | **1.000** |

As shown in Table 2, fabric quality was identified as the most important criterion, followed by delivery reliability and cost. These weights were used in the subsequent TOPSIS analysis to rank the supplier alternatives.

### 2.1.3. Criteria Weight Calculation (Textile – AHP)

After verifying the consistency of the pairwise comparison matrix, the relative importance weights of the supplier evaluation criteria were calculated using the Analytic Hierarchy Process (AHP). The criteria weights were obtained by normalizing the pairwise comparison matrix and computing the average of each row, which corresponds to the priority vector representing the relative importance of the criteria (Saaty, 1980).

Table 3. Criteria weights obtained by AHP

| Criterion | Weight |
|---|---|
| Cost | 0.210 |
| Fabric Quality | 0.384 |
| Delivery Reliability | 0.223 |
| Flexibility | 0.065 |
| Technical Capability | 0.118 |
| **Total** | **1.000** |

Let A=[aij] denote the pairwise comparison matrix, where $a_{ij}$ represents the relative importance of criterion $i$ over criterion $j$. The normalized matrix $\tilde{A}$ was obtained by dividing each element by the sum of its corresponding column. The resulting criteria weights reflect

109

the relative importance of each criterion in the textile supplier selection problem and were subsequently used as input for the TOPSIS method.

As shown in Table 3, fabric quality was identified as the most important criterion, followed by delivery reliability and cost. These weights were used in the subsequent TOPSIS analysis to rank the supplier alternatives.

## 2.2. TOPSIS Application in Supplier Selection

After determining the relative importance weights of the supplier evaluation criteria using the AHP method, the Technique for Order Preference by Similarity to Ideal Solution (TOPSIS) was applied to rank the alternative suppliers. TOPSIS is a widely used multi-criteria decision-making method that identifies the best alternative as the one closest to the positive ideal solution and farthest from the negative ideal solution (Hwang & Yoon, 1981).

In the first step of the TOPSIS application, a decision matrix was constructed, representing the performance of each supplier alternative with respect to the selected evaluation criteria. The decision matrix includes both quantitative and qualitative performance measures related to cost, fabric quality, delivery reliability, flexibility, and technical capability. To eliminate the effects of different measurement scales, the decision matrix was normalized using vector normalization.

In the second step, a weighted normalized decision matrix was obtained by multiplying the normalized decision matrix by the corresponding criteria weights derived from the AHP analysis. These weights reflect the relative importance of each criterion in the textile supplier selection problem and ensure that more critical criteria have a greater influence on the final ranking.

Subsequently, the positive ideal solution and the negative ideal solution were identified. The positive ideal solution represents the best attainable performance for each criterion, while the negative ideal solution corresponds to the worst performance levels. For benefit-type criteria, the maximum values were selected as the ideal solution, whereas for cost-type criteria, the minimum values were considered ideal.

In the next step, the Euclidean distance of each supplier alternative from the positive and negative ideal solutions was calculated. Based on these distances, the relative closeness coefficient for each supplier was computed. The closeness coefficient indicates how close each supplier is to the ideal solution, with higher values representing more preferable alternatives.

Finally, supplier alternatives were ranked according to their closeness coefficients, and the supplier with the highest coefficient was identified as the most suitable option for the textile manufacturing company. The resulting ranking provides decision-makers with a clear and rational basis for selecting the optimal supplier under multiple and potentially conflicting evaluation criteria.

These weights reflect the relative importance of each criterion in the textile supplier selection problem and ensure that more critical criteria have a greater influence on the final ranking.

Subsequently, the positive ideal solution and the negative ideal solution were identified. The positive ideal solution represents the best attainable performance for each criterion, while the negative ideal solution corresponds to the worst performance levels. For benefit-type criteria, the maximum values were selected as the ideal solution, whereas for cost-type criteria, the minimum values were considered ideal.

In the next step, the Euclidean distance of each supplier alternative from the positive and negative ideal solutions was calculated. Based on these distances, the relative closeness coefficient for each supplier was computed. The closeness coefficient indicates how close each supplier is to the ideal solution, with higher values representing more preferable alternatives.

Finally, supplier alternatives were ranked according to their closeness coefficients, and the supplier with the highest coefficient was identified as the most suitable option for the textile manufacturing company. The resulting ranking provides decision-makers with a clear and rational basis for selecting the optimal supplier under multiple and potentially conflicting evaluation criteria.

Table 4. Decision matrix for TOPSIS (Textile supplier selection)

| Supplier | Cost (C1) ↓ | Fabric Quality (C2) ↑ | Delivery Reliability (C3) ↑ | Flexibility (C4) ↑ | Technical Capability (C5) ↑ |
|---|---|---|---|---|---|
| **Supplier A** | 9.8 | 8.5 | 92 | 7.0 | 8.0 |
| **Supplier B** | 10.5 | 9.2 | 88 | 8.5 | 7.5 |
| **Supplier C** | 9.2 | 7.8 | 95 | 6.5 | 8.5 |
| **Supplier D** | 10.0 | 8.8 | 90 | 7.5 | 8.8 |

Table 4 presents the decision matrix used in the TOPSIS analysis, which includes the performance values of four textile suppliers with respect to the selected evaluation criteria. Cost was considered as a cost-type criterion, while fabric quality, delivery reliability, flexibility, and technical capability were treated as benefit-type criteria.

Table 5. Normalized decision matrix (R)

| Supplier | Cost | Fabric Quality | Delivery Reliability | Flexibility | Technical Capability |
|---|---|---|---|---|---|
| Supplier A | 0.4957 | 0.4947 | 0.5039 | 0.4722 | 0.4869 |
| Supplier B | 0.5311 | 0.5355 | 0.4820 | 0.5734 | 0.4565 |
| Supplier C | 0.4653 | 0.4540 | 0.5203 | 0.4385 | 0.5174 |
| Supplier D | 0.5058 | 0.5122 | 0.4930 | 0.5059 | 0.5356 |

Table 6. Weighted normalized decision matrix (V)

| Supplier | Cost | Fabric Quality | Delivery Reliability | Flexibility | Technical Capability |
|---|---|---|---|---|---|
| Supplier A | 0.1041 | 0.1900 | 0.1124 | 0.0307 | 0.0575 |
| Supplier B | 0.1115 | 0.2056 | 0.1075 | 0.0373 | 0.0539 |
| Supplier C | 0.0977 | 0.1743 | 0.1160 | 0.0285 | 0.0610 |
| Supplier D | 0.1062 | 0.1967 | 0.1099 | 0.0329 | 0.0632 |

Table 6. Positive ideal (A*) and negative ideal (A⁻) solutions

| Criterion | Type | A* (Ideal) | A⁻ (Negative Ideal) |
|---|---|---|---|
| Cost | Min | 0.0977 | 0.1115 |
| Fabric Quality | Max | 0.2056 | 0.1743 |
| Delivery Reliability | Max | 0.1160 | 0.1075 |
| Flexibility | Max | 0.0373 | 0.0285 |
| Technical Capability | Max | 0.0632 | 0.0539 |

Table 7. Separation measures and closeness coefficients

| Criterion | Type | A* (Ideal) | A⁻ (Negative Ideal) |
|---|---|---|---|
| Cost | Min | 0.0977 | 0.1115 |
| Fabric Quality | Max | 0.2056 | 0.1743 |
| Delivery Reliability | Max | 0.1160 | 0.1075 |
| Flexibility | Max | 0.0373 | 0.0285 |
| Technical Capability | Max | 0.0632 | 0.0539 |

Supplier D > Supplier B > Supplier A > Supplier C

## 3. Results

In this study, the TOPSIS method was applied to rank textile suppliers by using the criteria weights obtained from the AHP analysis. After constructing the normalized and weighted normalized decision matrices, the positive ideal solution (A*) and negative ideal solution (A⁻) were determined by considering the benefit and cost characteristics of each criterion.

The separation measures from the ideal solution ($S_{i*}$) and from the negative ideal solution ($S_i - S_i^-$) were calculated for each supplier. Based on these distances, the relative closeness coefficient (Ci) was computed to determine the overall performance of each alternative. A higher closeness coefficient indicates that the supplier is closer to the ideal solution and, therefore, more preferable.

Table 7 presents the calculated separation measures, closeness coefficients, and final ranking of the supplier alternatives. According to the TOPSIS results, Supplier D achieved the highest closeness coefficient ($Ci$=0.6372) and was identified as the most suitable supplier. Supplier B ranked second with a closeness coefficient of 0.6350, followed by Supplier A ($Ci$=0.4894). Supplier C obtained the lowest closeness coefficient ($Ci$=0.3519), indicating comparatively weaker performance under the evaluated criteria.

Overall, the results demonstrate that Supplier D outperforms the other alternatives by offering a balanced performance across cost, fabric quality, delivery reliability, flexibility, and technical capability. The integrated AHP–TOPSIS approach provided a systematic and objective evaluation framework, enabling decision-makers in the textile industry to select the most appropriate supplier under multiple and potentially conflicting criteria.

## 4. Conclusion and Future Work

Supplier selection is a critical decision-making problem in the textile industry, as it directly affects production continuity, cost efficiency, product quality, and overall competitiveness. In this study, an integrated AHP–TOPSIS approach was proposed to address the supplier selection problem of a

textile manufacturing company by considering multiple and potentially conflicting evaluation criteria.

First, the Analytic Hierarchy Process (AHP) was employed to determine the relative importance of the supplier selection criteria based on expert judgments. The results indicated that fabric quality was the most influential criterion, followed by delivery reliability and cost, highlighting the importance of quality-oriented and reliable supply in textile production. The consistency analysis confirmed that the decision-makers' evaluations were logically consistent and suitable for further analysis.

Subsequently, the Technique for Order Preference by Similarity to Ideal Solution (TOPSIS) was applied to rank the alternative suppliers using the AHP-derived criteria weights. The TOPSIS results revealed that Supplier D achieved the highest closeness coefficient and was identified as the most suitable supplier, followed by Supplier B, Supplier A, and Supplier C, respectively. This ranking demonstrates the effectiveness of the proposed methodology in distinguishing supplier performance by simultaneously considering multiple evaluation dimensions.

The findings of this study confirm that the integrated AHP–TOPSIS framework provides a systematic, transparent, and objective decision-support tool for supplier selection problems in the textile industry. By combining subjective expert judgments with quantitative performance evaluations, the proposed approach assists decision-makers in selecting suppliers that best align with organizational priorities and strategic objectives.

Despite its practical contributions, this study is limited to a single case application within a textile manufacturing company and a predefined set of evaluation criteria. Future research may extend this work by incorporating fuzzy or interval-based decision-making techniques to better capture uncertainty in expert judgments. In addition, integrating sustainability-related criteria and applying the proposed methodology to different sectors or larger supplier sets may provide further insights and enhance the generalizability of the results.

**References**

Büyüközkan, G., & Çifçi, G. (2012). A combined fuzzy AHP and fuzzy TOPSIS based strategic analysis of electronic service quality in healthcare industry. Expert Systems with Applications, 39(3), 2341–2354. https://doi.org/10.1016/j.eswa.2011.08.061

De Boer, L., Labro, E., & Morlacchi, P. (2001). A review of methods supporting supplier selection. European Journal of Purchasing & Supply Management, 7(2), 75–89. https://doi.org/10.1016/S0969-7012(00)00028-9

Dickson, G. W. (1966). An analysis of vendor selection systems and decisions. Journal of Purchasing, 2(1), 5–17.

Ho, W., Xu, X., & Dey, P. K. (2010). Multi-criteria decision making approaches for supplier evaluation and selection: A literature review. European Journal of Operational Research, 202(1), 16–24. https://doi.org/10.1016/j.ejor.2009.05.009

Hwang, C. L., & Yoon, K. (1981). Multiple attribute decision making: Methods and applications. Springer.

Saaty, T. L. (1980). The analytic hierarchy process. McGraw-Hill.

Weber, C. A., Current, J. R., & Benton, W. C. (1991). Vendor selection criteria and methods. European Journal of Operational Research, 50(1), 2–18. https://doi.org/10.1016/0377-2217(91)90033-R

# Investigation of occupational accidents in the metal industry using artificial neural networks

Seher POLAT [1✉]

*¹ Sakarya University, Industrial Engineering Department, Sakarya-TURKEY*

## Abstract

This study investigates the causes of production downtime in a profile manufacturing company using the DMAIC (Define–Measure–Analyze–Improve–Control) methodology. The aim of the study is to identify the main factors reducing production efficiency and to develop systematic improvement strategies. The production process was examined in detail, downtime types were classified, and measurement data were collected. The collected data were analyzed using Pareto analysis, cause–effect diagrams, and statistical evaluation techniques. The results indicate that a significant portion of downtime originates from a limited number of root causes. The implementation of improvement actions resulted in a noticeable reduction in downtime duration. The findings demonstrate that the DMAIC approach is an effective tool for enhancing production continuity and optimizing resource utilization.
*Keywords: DMAIC, Downtime Analysis, Process Improvement, Lean Manufacturing, Six Sigma*

[1]Corresponding Author Email 　　　: aseher@sakarya.edu.tr

## 1. Introduction

In today's highly competitive manufacturing environment, sustaining organizational performance is closely associated with reducing operational costs, improving product quality, and ensuring uninterrupted production processes. Particularly in mass production systems, unplanned downtimes significantly reduce production efficiency, prolong delivery times, and increase overall operational costs (Antony, 2014). Consequently, the systematic identification and analysis of downtime causes, along with the development of sustainable improvement strategies, have become a strategic necessity for manufacturing enterprises.

In profile manufacturing systems, various factors such as machine failures, material-related issues, operator errors, and process imbalances may lead to production interruptions. These disruptions not only reduce production output but also result in quality losses, energy inefficiencies, and decreased labor productivity (Montgomery, 2019). Therefore, it is essential to investigate downtime causes not merely at a superficial level but through comprehensive root cause analysis approaches.

In this context, the DMAIC (Define–Measure–Analyze–Improve–Control) methodology, one of the core frameworks of Six Sigma, is widely recognized as a systematic and data-driven approach for process improvement. The DMAIC framework aims to clearly define problems, analyze them using

114

measurable data, identify root causes, develop effective improvement actions, and ensure the sustainability of achieved outcomes (Pyzdek & Keller, 2018). Previous studies have demonstrated the successful application of the DMAIC methodology across various sectors, including manufacturing, healthcare, logistics, and service industries (Antony et al., 2017).

Within the scope of this study, the causes of downtime occurring in a profile manufacturing company were systematically analyzed using the DMAIC methodology. The primary objective of the study is to classify production downtimes, identify critical root causes, and develop practical and applicable improvement strategies to address these issues. The findings obtained from this research are expected to provide valuable insights not only for the investigated company but also for other industrial organizations with similar production structures.

## 2. Material and methods
### 2.1. Description of the Company and Production Process

This study was conducted in a medium-sized manufacturing company engaged in profile production. The investigated company produces metal profiles of various dimensions and specifications, serving multiple sectors including construction, automotive, and machinery manufacturing. The production activities are largely based on a continuous manufacturing principle, allowing different product types to be produced on the same production line depending on customer orders.

The production process begins with raw material acceptance and continues through forming, cutting, surface treatment, and final product inspection stages. Downtime occurring throughout these stages directly affects production efficiency, delivery times, and product quality. Therefore, production interruptions were examined in detail within the scope of this study and evaluated using the DMAIC methodology.

### 2.1.2. Main Machines and Operations
The main machines and equipment used in the production line are summarized as follows:
- Decoiler: Feeds raw material coils into the production line.
- Straightening Unit: Ensures surface flatness and corrects material deformation.
- Profile Forming Machines: Shape the material into the desired geometric profile.
- Cutting Unit: Cuts the formed profiles to specified dimensions.
- Conveyor and Transportation Systems: Transfer products between different production stations.
- Inspection and Packaging Unit: Performs final quality control and prepares products for shipment.

Mechanical failures, setup errors, operator-related issues, and insufficient maintenance activities occurring in these machines constitute the main causes of production downtime.

### 2.1.3. Production Flow Diagram
The production process follows a sequential flow structure, as illustrated in Figure 1. Any disruption occurring at a single station has the potential to halt the entire production line. Therefore, each operational stage was evaluated individually within the scope of this study.

The main machines and equipment used in the production line are summarized as follows:
- Decoiler: Feeds raw material coils into the production line.
- Straightening Unit: Ensures surface flatness and corrects material deformation.
- Profile Forming Machines: Shape the material into the desired geometric profile.
- Cutting Unit: Cuts the profiles to the specified dimensions.

Conveyor and Transportation Systems: Transfer products between different workstations.

115

Inspection and Packaging Unit: Performs final quality control and prepares products for shipment. Mechanical failures, setup errors, operator-related issues, and insufficient maintenance activities associated with these machines constitute the primary causes of production downtime.

### 2.1.3. Production Flow Diagram

The production process follows a sequential flow structure, as illustrated in Figure 1. Any disruption occurring at a single workstation has the potential to halt the entire production line. For this reason, each operational stage was evaluated individually within the scope of this study.

```
┌──────────────────────┐
│  Raw Material Input   │
└──────────────────────┘
           │
           ▼
┌──────────────────────┐
│  Straightening Unit   │
└──────────────────────┘
           │
           ▼
┌──────────────────────┐
│  Profile Forming Unit │
└──────────────────────┘
           │
           ▼
┌──────────────────────┐
│    Cutting Proces     │
└──────────────────────┘
           │
           ▼
┌──────────────────────┐
│  Surface Inspection   │
└──────────────────────┘
           │
           ▼
┌──────────────────────┐
│ Packaging & Dispatching│
└──────────────────────┘
```
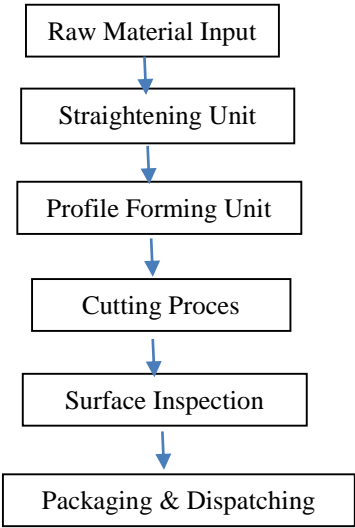
Figure 1. Flow Diagram of the Profile Manufacturing Process

Figure 1 illustrates the sequential flow structure of the profile manufacturing process. Any disruption occurring at a single workstation has the potential to interrupt the entire production line. Therefore, each operational stage was evaluated individually within the scope of this study.

### 2.2. DMAIC Methodology

In this study, the DMAIC (Define–Measure–Analyze–Improve–Control) methodology was employed to systematically analyze the causes of downtime occurring in a profile manufacturing company. DMAIC is one of the fundamental pillars of the Six Sigma approach and provides a structured, data-driven framework for improving process performance (Pyzdek & Keller, 2018). This methodology consists of five main phases: defining, measuring, analyzing, improving, and controlling.

### 2.2.1. Define

During the define phase, the scope, objectives, and problem definition of the study were clearly established. It was determined that unplanned downtimes in the profile production line negatively affect production continuity and efficiency. Accordingly, production processes were examined,

and downtime causes were identified as machine failures, operator-related errors, material-related issues, and process inconsistencies.

In the DMAIC methodology, this phase ensures a clear definition of the problem and establishes the boundaries of improvement activities (Antony, 2014). In this study, the project scope was limited to the profile production line.

### 2.2.2. Measure

During the measurement phase, data related to production downtimes were systematically collected over a defined period. Downtime durations, frequencies, and types were recorded to form an analyzable dataset. The collected data were validated using production records and operator observations.

The primary objective of this phase was to quantitatively assess the current state of the process and evaluate performance objectively (Montgomery, 2019).

### 2.2.3. Analyze

In the analysis phase, the collected data were evaluated using statistical techniques. Pareto analysis was applied to identify the most significant causes of downtime, revealing the critical factors responsible for the majority of production losses.

In addition, a fishbone (Ishikawa) diagram was used to identify root causes of downtime. This analysis categorized potential causes under human, machine, method, material, and environmental factors (Ishikawa, 1985).

### 2.2.4. Improve

Based on the analysis results, improvement actions were developed to reduce downtime durations. These included increasing operator training, developing standardized work instructions, strengthening preventive maintenance practices, and standardizing critical process parameters.

The DMAIC approach not only focuses on identifying problems but also emphasizes the implementation of sustainable improvements (Antony et al., 2017).

### 2.2.5. Control

In the control phase, performance monitoring mechanisms were established to ensure the sustainability of the implemented improvements. Key performance indicators (KPIs) were defined, and downtime durations were monitored regularly. In addition, standard operating procedures were updated to maintain long-term process stability.

This approach aims to ensure the continuity of achieved improvements and prevent the recurrence of similar problems in the future (Pyzdek & Keller, 2018).

### 4. RESULTS AND DISCUSSION

This section presents and discusses the findings obtained from the DMAIC implementation conducted in the profile production line. The analysis focused on identifying downtime occurrences, determining their root causes, and evaluating improvement opportunities.

### 4.1. Quantitative Findings of Downtime Causes

Within the scope of the study, downtime occurrences in the production line were recorded over a specific period. The collected data were classified according to downtime types, and their contributions to total downtime were calculated.

117

Table 1. Distribution of Downtime Causes and Durations

| No | Downtime Cause | Downtime Duration (min) | Percentage (%) | Cumulative (%) |
|---|---|---|---|---|
| 1 | Machine Failures | 420 | 35.0 | 35.0 |
| 2 | Setup / Adjustment Problems | 300 | 25.0 | 60.0 |
| 3 | Operator Errors | 210 | 17.5 | 77.5 |
| 4 | Material-Related Problems | 150 | 12.5 | 90.0 |
| 5 | Others (cleaning, waiting, etc.) | 120 | 10.0 | 100.0 |
| **Total** — | | **1,200** | **100** | — |

As shown in Table 1, machine failures and setup-related problems constitute the majority of total downtime, accounting for approximately 60% of the overall production interruptions. When operator-related errors are included, nearly 77.5% of the total downtime is explained by these three major factors.

Toplam duruş süresinin yaklaşık %77,5'inin ilk üç nedenden (makine arızaları, ayar problemleri ve operatör hataları) kaynaklandığı görülmektedir. Bu durum, Pareto ilkesinin (80/20 kuralı) geçerliliğini doğrulamaktadır.

## 4.2. Pareto Analysis

It is observed that approximately 77.5% of the total downtime is attributed to the first three causes, namely machine failures, setup problems, and operator errors. This finding confirms the validity of the Pareto principle (80/20 rule), indicating that a limited number of causes are responsible for the majority of production losses.

Based on the Pareto analysis, it was determined that a substantial proportion of downtime originates from a small number of critical factors. In particular, machine failures and setup-related problems account for nearly 60% of the total downtime. Therefore, improvement efforts should primarily focus on these two factors.

According to the results of the Pareto analysis, prioritizing corrective actions related to machine reliability and setup optimization enables organizations to achieve maximum improvement with limited resources. This targeted approach enhances the effectiveness of improvement initiatives and contributes to sustainable operational performance.
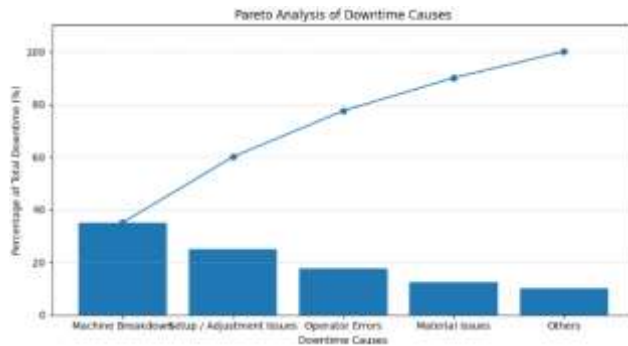


Şekil 2. Duruş Nedenlerine Ait Pareto Analizi

**4.3. Fishbone (Ishikawa) Diagram Analysis**

To identify the root causes of the critical downtime factors, a fishbone (Ishikawa) diagram was employed. The analysis was conducted under five main categories: Human, Machine, Method, Material, and Environment.

This structured approach enabled a comprehensive examination of the factors contributing to production interruptions and facilitated the identification of underlying root causes affecting system performance.
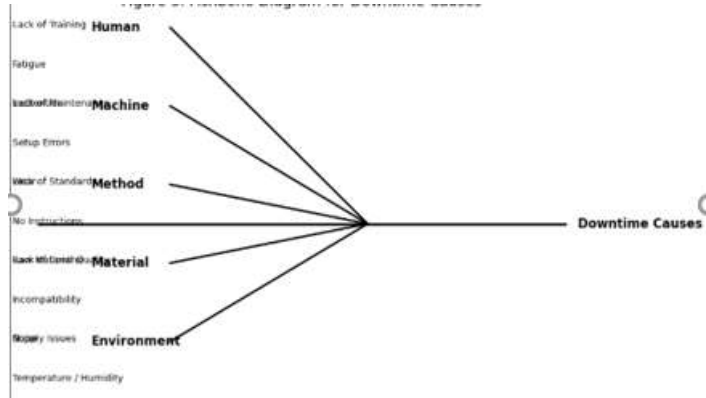


Figure 3. Fishbone Diagram of Downtime Causes

The analysis revealed that insufficient maintenance practices, inadequacies in standard operating procedures, and insufficient operator training were identified as the primary root causes of downtime. These findings are consistent with the results obtained from the Pareto analysis, further validating the reliability of the identified critical factors.

**4.4. Discussion of Findings**

The findings indicate that the downtimes observed in the profile production line are largely attributable to controllable factors. When compared with similar studies reported in the literature, the significant role of machine-related failures and human factors in production losses is also confirmed in this study (Antony et al., 2017; Montgomery, 2019).

Through the application of the DMAIC methodology, process-related problems were systematically analyzed, and areas with high improvement potential were clearly identified. This demonstrates that DMAIC serves as an effective decision-support tool for improving production processes.

**5. Conclusions and Recommendations**

In this study, the causes of downtime in a profile manufacturing company were systematically analyzed using the DMAIC methodology. The findings revealed that a substantial portion of production losses stemmed from controllable factors. In particular, machine failures, setup and adjustment issues, and operator-related errors were identified as the primary contributors to overall downtime.

According to the results of the Pareto analysis, approximately 80% of total downtime is attributed to a limited number of root causes. This finding supports the widely accepted Pareto principle and highlights the importance of directing improvement efforts toward the most critical problem areas. Furthermore, the fishbone diagram analysis revealed that deficiencies in maintenance practices, inadequate standard operating procedures, and insufficient operator training were the dominant root causes. Based on these findings, the following improvement actions are recommended:

119

• Establishing systematic preventive maintenance programs and standardizing maintenance intervals,

• Implementing regular and structured training programs for operators,

• Developing clear, accessible, and standardized work instructions,

• Defining performance indicators to continuously monitor critical process parameters,

• Improving environmental working conditions such as lighting, noise levels, and temperature control.

The implementation of these improvement actions is expected to significantly reduce production downtimes and enhance overall process efficiency. Moreover, the systematic structure of the DMAIC methodology enables the sustainability of achieved improvements.

In conclusion, this study demonstrates that the DMAIC approach is an effective problem-solving and improvement tool for continuous production systems such as profile manufacturing. The findings provide valuable insights for similar industrial applications. Future studies may focus on the integration of real-time data acquisition systems, digital monitoring technologies, and artificial intelligence–based predictive maintenance approaches to further enhance sustainability and operational performance.

## References

Antony, J. (2014). Readiness factors for the Lean Six Sigma journey in the higher education sector. International Journal of Productivity and Performance Management, 63(2), 257–264. https://doi.org/10.1108/IJPPM-04-2013-0077

Antony, J., Snee, R., & Hoerl, R. (2017). Lean Six Sigma: Yesterday, today and tomorrow. International Journal of Quality & Reliability Management, 34(7), 1073–1093. https://doi.org/10.1108/IJQRM-03-2016-0035

Ishikawa, K. (1985). What is total quality control? The Japanese way. Englewood Cliffs, NJ: Prentice Hall.

Montgomery, D. C. (2019). Introduction to statistical quality control (8th ed.). Hoboken, NJ: Wiley.

Pyzdek, T., & Keller, P. (2018). The Six Sigma handbook: A complete guide for Green Belts, Black Belts, and Managers at all levels (5th ed.). New York, NY: McGraw-Hill Education.

# Investigation of occupational accidents in the metal industry using artificial neural networks

## Seher POLAT [1]

**[1]Sakarya University, Industrial Engineering Department, Sakarya-TURKEY**

### Abstract

In the era of digital transformation, organizations increasingly rely on data-driven approaches to enhance decision-making processes and maintain sustainable competitive advantage. Knowledge management (KM) plays a critical role in transforming dispersed data into actionable organizational knowledge. However, traditional KM systems often face limitations in handling large-scale, complex, and dynamic data environments. In this context, artificial intelligence (AI) emerges as a powerful enabler for advancing knowledge management capabilities.

This study proposes a conceptual framework for artificial intelligence–driven knowledge management that supports data-driven decision making within organizational settings. The proposed framework integrates key AI techniques, including machine learning, natural language processing, and intelligent data analytics, into core knowledge management processes such as knowledge acquisition, storage, sharing, and utilization. In addition to the conceptual structure, an illustrative application scenario is presented to demonstrate how AI-based mechanisms can enhance knowledge quality, decision accuracy, and organizational learning capabilities.

The proposed framework emphasizes the role of AI in improving information interpretation, reducing uncertainty in decision-making, and enabling adaptive and intelligent organizational responses. By combining theoretical foundations with a semi-applied perspective, this study contributes to the growing body of literature on AI-enabled knowledge management systems. Furthermore, it provides practical insights for organizations seeking to leverage artificial intelligence for strategic decision support and sustainable performance improvement.

The findings highlight the transformative potential of integrating artificial intelligence into knowledge management practices and underscore the importance of developing intelligent, flexible, and data-driven organizational infrastructures. Future research directions include empirical validation of the framework across different industries and the integration of emerging technologies such as big data analytics and digital twins.

*Keywords: Artificial Intelligence; Knowledge Management; Data-Driven Decision Making; Digital Transformation; Organizational Learning; Decision Support Systems*

[1]Corresponding Author Email　　　: aseher@sakarya.edu.tr

## 1. Introduction

In today's rapidly evolving digital environment, organizations are increasingly required to manage vast volumes of data while transforming this information into actionable knowledge to support strategic and operational decision-making. The ability to effectively manage knowledge has become a critical organizational capability, directly influencing competitiveness, innovation capacity, and long-term sustainability. As a result, knowledge management (KM) has emerged as a strategic discipline that enables organizations to capture, organize, share, and utilize knowledge in a systematic and value-driven manner.

With the advancement of digital technologies, traditional knowledge management systems have become insufficient in addressing the complexity, velocity, and heterogeneity of contemporary data environments. In this context, artificial intelligence (AI) has gained significant attention as a transformative technology capable of enhancing knowledge-based processes. AI-driven techniques such as machine learning, natural language processing, and intelligent analytics provide organizations with advanced capabilities to extract meaningful insights from large and unstructured datasets, thereby improving the quality and speed of decision-making processes.

Recent studies emphasize that integrating artificial intelligence into knowledge management systems enables more adaptive, predictive, and context-aware organizational structures. AI-supported knowledge management not only enhances information accessibility and accuracy but also facilitates organizational learning by continuously refining decision mechanisms through data-driven feedback loops. Consequently, organizations can respond more effectively to environmental uncertainty, market dynamics, and operational complexity.

Despite the growing interest in AI-enabled knowledge management, there remains a need for comprehensive conceptual frameworks that systematically explain how artificial intelligence can be embedded within knowledge management processes to support data-driven decision making. Many existing studies focus on isolated applications or technological aspects, offering limited guidance on holistic integration.

Therefore, this study aims to propose a conceptual framework that integrates artificial intelligence techniques into core knowledge management processes to enhance data-driven decision making. By combining theoretical insights with an illustrative application perspective, this research seeks to contribute to both academic literature and practical implementation, supporting organizations in developing intelligent, resilient, and sustainable decision-making systems.

## 2. Literature Review

### 2.1 Knowledge Management and Data-Driven Decision Making

Knowledge management (KM) has long been recognized as a strategic organizational capability that enables the systematic creation, storage, sharing, and utilization of knowledge to enhance decision-making and organizational performance (Nonaka & Takeuchi, 1995; Alavi & Leidner, 2001). In contemporary organizations, knowledge is increasingly regarded as a critical intangible asset that supports innovation, adaptability, and competitive advantage. The shift toward data-intensive environments has further emphasized the importance of transforming raw data into meaningful and actionable knowledge.

Data-driven decision making (DDDM) has emerged as a key paradigm in modern organizations, enabling decisions to be supported by analytical evidence rather than intuition alone (Provost &

122

Fawcett, 2013). However, traditional knowledge management systems often struggle to cope with the volume, velocity, and variety of data generated in digital environments. These limitations reduce their ability to deliver timely and context-aware insights, particularly in complex and dynamic organizational settings (Davenport & Prusak, 1998).

As a result, scholars increasingly argue that conventional KM approaches must evolve toward more intelligent and adaptive structures capable of processing large-scale, heterogeneous data sources (Mariano & Awazu, 2016). This evolution has positioned artificial intelligence as a central enabler of next-generation knowledge management systems.

## 2.2 Artificial Intelligence as an Enabler of Knowledge Management

Artificial intelligence (AI) has significantly transformed the way organizations generate, manage, and apply knowledge. AI technologies such as machine learning (ML), natural language processing (NLP), and intelligent analytics enable automated pattern recognition, predictive modeling, and semantic interpretation of unstructured data (Russell & Norvig, 2021). These capabilities allow organizations to extract meaningful insights from vast datasets that exceed human cognitive capacity.

Recent studies highlight that AI-enhanced knowledge management systems improve knowledge discovery, accessibility, and reuse by automating classification, recommendation, and contextualization processes (Duan, Edwards, & Dwivedi, 2019). Furthermore, AI supports organizational learning by continuously refining decision rules based on feedback mechanisms and real-time data streams (Rai, Constantinides, & Sarker, 2019).

However, effective AI integration in KM systems requires alignment between technological capabilities and organizational processes. Trust, transparency, and explainability remain critical challenges, particularly when AI-generated insights influence strategic or high-risk decisions (Gunning et al., 2019). Consequently, AI should be viewed not as a replacement for human expertise but as a complementary tool that enhances human cognition and judgment.

## 2.3 Generative AI and Knowledge Management Systems

The recent emergence of generative artificial intelligence, particularly large language models (LLMs), has introduced new opportunities for knowledge management. These models are capable of generating, summarizing, and interpreting human language at scale, making them particularly suitable for managing unstructured organizational knowledge such as reports, policies, and experiential documentation (Bommasani et al., 2021).

Studies indicate that generative AI can significantly enhance knowledge retrieval and sharing by enabling conversational access to organizational knowledge bases and supporting real-time decision-making processes (Dwivedi et al., 2023). Nevertheless, challenges related to hallucination, data privacy, accountability, and ethical governance remain critical concerns, particularly in high-stakes decision environments.

Therefore, the integration of generative AI into KM systems requires robust governance mechanisms, validation processes, and human oversight to ensure reliability and organizational trust.

## 2.4 AI-Enabled Knowledge Management and Decision Support

AI-driven knowledge management plays a pivotal role in modern decision support systems (DSS). By integrating predictive analytics, knowledge repositories, and reasoning mechanisms, AI-enhanced DSS can support complex decision-making under uncertainty (Turban et al., 2011). Knowledge management acts as the cognitive backbone of such systems, ensuring that decision outputs are grounded in accurate, relevant, and context-aware information.

However, prior research emphasizes that technological sophistication alone does not guarantee improved decision quality. Organizational factors such as user acceptance, governance structures, and alignment with strategic objectives significantly influence the effectiveness of AI-enabled KM systems (Shrestha et al., 2021). Therefore, holistic frameworks that integrate technological, human, and organizational dimensions are essential for sustainable implementation.

## 2.5 Research Gap and Motivation

Although the literature extensively addresses AI and knowledge management independently, comprehensive frameworks that integrate AI techniques into the full knowledge management lifecycle remain limited. Existing studies often focus on isolated applications or technological performance metrics, overlooking organizational learning, governance, and decision accountability. This study addresses these gaps by proposing a conceptual framework that integrates artificial intelligence into core knowledge management processes to support data-driven decision making. By combining theoretical foundations with a structured conceptual model, the study aims to contribute to both academic research and practical implementation in digitally transforming organizations.

## 3. Conceptual Framework
## 3.1 Overview of the Conceptual Framework

This study proposes a conceptual framework that integrates artificial intelligence (AI) into knowledge management (KM) processes to enhance data-driven decision making. The framework is designed to explain how AI technologies can systematically support the transformation of raw data into actionable organizational knowledge, thereby improving decision quality, adaptability, and strategic responsiveness. The proposed framework is structured around three interconnected layers:

1. Data and Knowledge Inputs,
2. AI-Enabled Knowledge Management Processes, and
3. Decision Support and Organizational Outcomes.

This layered structure reflects the dynamic interaction between technological capabilities, knowledge processes, and organizational decision-making mechanisms. The framework emphasizes that effective AI-driven knowledge management is not solely a technological challenge but a socio-technical system that integrates human expertise, organizational context, and intelligent computational tools.

## 3.2 Data and Knowledge Input Layer

The first layer of the framework consists of heterogeneous data and knowledge sources, including structured, semi-structured, and unstructured data. Data preprocessing such as cleaning, normalization, and semantic alignment is essential to ensure data quality prior to knowledge transformation (Alavi & Leidner, 2001; Nonaka & Takeuchi, 1995).

## 3.3 AI-Enabled Knowledge Management Processes

AI techniques like machine learning and natural language processing can automate knowledge acquisition and extraction from large datasets (Duan, Edwards & Dwivedi, 2019). NLP's capability to interpret unstructured text supports semantic comprehension and entity recognition (Jurafsky & Martin, 2020). Further, intelligent classification and semantic indexing enhance knowledge organization and retrieval processes (Rai, Constantinides & Sarker, 2019).

## 3.4 Decision Support and Organizational Outcomes

When integrated into decision support systems, AI-enhanced knowledge outputs contribute to improved decision quality and context awareness (Turban et al., 2011). Nevertheless, factors such

as user trust and transparency are critical for effective human–AI collaboration (Gunning et al., 2019).

## 4.Conclusion

This study has proposed a conceptual framework that integrates artificial intelligence (AI) into knowledge management (KM) processes to enhance data-driven decision making within organizational contexts. In an era characterized by rapid digital transformation and increasing data complexity, organizations are required to move beyond traditional knowledge management practices toward more intelligent, adaptive, and technology-enabled systems. The proposed framework addresses this need by systematically linking AI capabilities with core KM functions and decision support mechanisms.

The study highlights that artificial intelligence plays a critical role in enhancing knowledge acquisition, organization, dissemination, and continuous learning processes. By enabling advanced data analytics, semantic interpretation, and adaptive feedback mechanisms, AI enhances both the quality and usability of organizational knowledge. As a result, decision-making processes become more accurate, timely, and context-aware, supporting organizational resilience and strategic agility.

Moreover, the proposed framework emphasizes that effective AI-driven knowledge management is not solely a technological challenge but a socio-technical one. Human expertise, organizational culture, trust, and governance structures remain essential for ensuring that AI-generated insights are interpretable, reliable, and ethically aligned with organizational objectives. This highlights the importance of integrating human judgment with intelligent systems rather than replacing it.

From a theoretical perspective, this study contributes to the existing literature by offering a holistic conceptual model that connects artificial intelligence, knowledge management, and data-driven decision making within a unified structure. From a practical standpoint, the framework provides organizations with a structured reference for designing and implementing AI-enabled knowledge management systems that support sustainable performance and informed decision-making.

Future research may extend this work by empirically validating the proposed framework across different sectors, exploring the role of emerging technologies such as digital twins and big data analytics, and examining organizational readiness factors that influence successful AI adoption. Such efforts will further strengthen the understanding of how artificial intelligence can be effectively leveraged to enhance knowledge-driven organizational capabilities.

## References

Alavi, M., & Leidner, D. E. (2001). Review: Knowledge management and knowledge management systems: Conceptual foundations and research issues. MIS Quarterly, 25(1), 107–136. https://doi.org/10.2307/3250961

Davenport, T. H., & Prusak, L. (1998). Working knowledge: How organizations manage what they know. Harvard Business School Press.

Duan, Y., Edwards, J. S., & Dwivedi, Y. K. (2019). Artificial intelligence for decision making in the era of big data – Evolution, challenges and research agenda. International Journal of Information Management, 48, 63–71. https://doi.org/10.1016/j.ijinfomgt.2019.01.021

Gunning, D., Stefik, M., Choi, J., Miller, T., Stumpf, S., & Yang, G.-Z. (2019). XAI—Explainable artificial intelligence. Science Robotics, 4(37), eaay7120. https://doi.org/10.1126/scirobotics.aay7120

Nonaka, I., & Takeuchi, H. (1995). The knowledge-creating company: How Japanese companies create the dynamics of innovation. Oxford University Press.

Rai, A., Constantinides, P., & Sarker, S. (2019). Next-generation digital platforms: Toward human–AI hybrid systems. MIS Quarterly, 43(1), iii–ix. https://doi.org/10.25300/MISQ/2019/14575

Russell, S. J., & Norvig, P. (2021). Artificial intelligence: A modern approach (4th ed.). Pearson.

Shrestha, Y. R., Ben-Menahem, S. M., & von Krogh, G. (2021). Organizational decision-making structures in the age of artificial intelligence. California Management Review, 63(1), 66–83. https://doi.org/10.1177/0008125620972149

Turban, E., Sharda, R., & Delen, D. (2011). Decision support and business intelligence systems (9th ed.). Pearson Education.

# Artificial Intelligence–Enabled Knowledge Management for Data-Driven Organizational Decision Making

## Seher POLAT[1]✉

**[1]Sakarya University, Industrial Engineering Department, Sakarya-TURKEY**

## Abstract

In today's data-intensive organizational environments, effective knowledge management has become a critical enabler of informed and strategic decision making. As organizations increasingly rely on complex and heterogeneous data sources, traditional knowledge management approaches often struggle to transform data into actionable insights. In this context, artificial intelligence (AI) emerges as a powerful enabler for enhancing knowledge management processes and supporting data-driven organizational decision making.

This study proposes a conceptual framework for artificial intelligence–enabled knowledge management that integrates advanced AI techniques into core knowledge management functions, including knowledge acquisition, organization, sharing, and utilization. The framework emphasizes the role of AI-driven mechanisms—such as machine learning, natural language processing, and intelligent analytics—in enhancing knowledge quality, accessibility, and interpretability. By embedding AI capabilities within knowledge management processes, organizations can improve decision accuracy, responsiveness, and adaptability in dynamic and uncertain environments.

The proposed framework adopts a semi-applied perspective by illustrating how AI-supported knowledge management can be operationalized within organizational decision-making contexts. It highlights the importance of human–AI collaboration, emphasizing that effective decision-making emerges from the integration of human expertise with intelligent analytical systems rather than from automation alone. Furthermore, the framework addresses critical challenges related to trust, transparency, and governance, which are essential for sustainable AI adoption.

This study contributes to the literature by providing a structured and integrative perspective on AI-enabled knowledge management for data-driven decision making. The proposed framework offers practical insights for organizations seeking to enhance their decision-making capabilities while supporting long-term organizational learning and digital transformation.

*Keywords: Artificial Intelligence; Knowledge Management; Data-Driven Decision Making; Organizational Learning; Digital Transformation; Decision Support Systems*

✉ *Corresponding Author Email　　: aseher@sakarya.edu.tr*

## 1. Introduction

In recent years, organizations have increasingly faced complex and dynamic environments characterized by rapid technological change, growing data volumes, and intensified competition. In such contexts, the ability to transform data into meaningful knowledge has become a strategic necessity rather than a supportive function. Knowledge management (KM) plays a critical role in enabling organizations to capture, structure, share, and utilize knowledge in ways that support effective decision-making and long-term sustainability.

With the advancement of digital technologies, traditional knowledge management systems have become insufficient to handle the scale, diversity, and velocity of modern organizational data. Conventional approaches often rely on static repositories and manual processes, limiting their ability to provide timely and context-aware insights. As a result, organizations increasingly seek intelligent solutions that can enhance knowledge processing and support data-driven decision making.

Artificial intelligence (AI) has emerged as a transformative technology capable of addressing these limitations. Through techniques such as machine learning, natural language processing, and intelligent analytics, AI enables the extraction of valuable patterns and insights from large and complex datasets. When integrated with knowledge management systems, AI enhances knowledge discovery, improves information accessibility, and supports adaptive learning mechanisms within organizations. This integration allows decision-makers to respond more effectively to uncertainty, complexity, and rapidly changing environments.

Despite the growing interest in AI-enabled knowledge management, existing studies often focus on isolated technological applications rather than holistic frameworks that connect AI capabilities with organizational knowledge processes and decision-making structures. Furthermore, limited attention has been given to the socio-technical dimensions of AI adoption, including human–AI interaction, trust, and governance mechanisms.

In response to these gaps, this study proposes a conceptual framework for artificial intelligence–enabled knowledge management aimed at supporting data-driven organizational decision making. By integrating technological, organizational, and human perspectives, the proposed framework offers a structured approach for leveraging AI to enhance decision quality, organizational learning, and sustainable performance.

## 2. Literature Review

### 2.1 Knowledge Management and Organizational Decision Making

Knowledge management (KM) has long been recognized as a critical organizational capability that supports effective decision making, innovation, and sustainable competitive advantage. Early foundational studies define knowledge management as the systematic process of creating, storing, sharing, and applying knowledge to enhance organizational performance (Nonaka & Takeuchi, 1995; Alavi & Leidner, 2001). In knowledge-intensive environments, organizations rely on both explicit and tacit knowledge to respond effectively to internal and external challenges.

With the increasing complexity of organizational systems, decision-making processes have become highly dependent on the ability to transform large volumes of data into meaningful and actionable knowledge. Data-driven decision making (DDDM) emphasizes the use of analytical evidence rather than intuition alone, enabling organizations to improve accuracy, consistency, and accountability in strategic and operational decisions (Provost & Fawcett, 2013). However, traditional knowledge management systems often lack the flexibility and

analytical capability required to process heterogeneous and dynamic data sources efficiently (Davenport & Prusak, 1998).

As a result, scholars emphasize the need for more advanced and intelligent knowledge management approaches that can support real-time analysis, contextual understanding, and adaptive learning within organizations.

## 2.2 Artificial Intelligence as an Enabler of Knowledge Management

Artificial intelligence (AI) has emerged as a transformative force in enhancing knowledge management capabilities. AI technologies, including machine learning, natural language processing, and intelligent analytics, enable organizations to extract meaningful insights from structured and unstructured data sources (Russell & Norvig, 2021). These technologies facilitate automated knowledge acquisition, classification, and interpretation, thereby significantly improving the efficiency and effectiveness of KM processes.

Recent studies indicate that AI-driven knowledge management systems enhance organizational learning by enabling continuous feedback, predictive analysis, and adaptive decision support (Duan, Edwards, & Dwivedi, 2019). Through intelligent pattern recognition and data-driven reasoning, AI systems support more informed and timely decision-making, particularly in complex and uncertain environments.

Moreover, AI enhances the accessibility and usability of organizational knowledge by enabling personalized information delivery and context-aware recommendations. This capability supports knowledge sharing across organizational units and reduces cognitive overload for decision-makers (Rai, Constantinides, & Sarker, 2019).

## 2.3 AI-Enabled Knowledge Management and Decision Support Systems

The integration of AI into knowledge management has significantly influenced the evolution of decision support systems (DSS). AI-enhanced DSS combine analytical models, organizational knowledge bases, and intelligent reasoning mechanisms to support complex decision-making processes (Turban, Sharda, & Delen, 2011). In this context, knowledge management serves as the cognitive foundation that ensures decision outputs are relevant, reliable, and aligned with organizational objectives.

Despite these advantages, the literature highlights several challenges associated with AI-enabled decision-making. Issues such as transparency, explainability, and trust remain critical concerns, particularly in high-stakes organizational contexts (Gunning et al., 2019). Furthermore, the effectiveness of AI-driven systems depends not only on technological sophistication but also on organizational readiness, governance structures, and human–AI collaboration (Shrestha, Ben-Menahem, & von Krogh, 2021).

## 2.4 Research Gap and Motivation

Although existing research provides valuable insights into artificial intelligence and knowledge management, there remains a lack of comprehensive frameworks that integrate AI capabilities across the entire knowledge management lifecycle. Many studies focus on specific technologies or isolated applications, offering limited guidance on how AI can systematically support data-driven decision making at the organizational level.

Additionally, current literature often underestimates the socio-technical dimensions of AI adoption, including trust, accountability, and organizational learning dynamics. Addressing these gaps requires a holistic framework that aligns technological innovation with human and organizational factors.

Therefore, this study proposes a conceptual framework that integrates artificial intelligence into knowledge management processes to enhance data-driven organizational decision

making. By bridging theoretical perspectives and practical considerations, the proposed framework aims to contribute to both academic research and managerial practice.

## 3. Conceptual Framework
### 3.1 Overview of the Conceptual Framework
This study proposes a conceptual framework that integrates artificial intelligence (AI) into knowledge management (KM) processes to support data-driven organizational decision making. The framework is designed to illustrate how AI technologies enhance the transformation of raw data into actionable knowledge, ultimately improving decision quality, organizational learning, and strategic adaptability.

The framework is structured around three interconnected layers:
1. Data and Knowledge Inputs,
2. AI-Enabled Knowledge Management Processes, and
3. Decision Support and Organizational Outcomes.

These layers interact dynamically, emphasizing that effective knowledge management is not a linear process but a continuous cycle supported by intelligent technologies and human expertise.

### 3.2 Data and Knowledge Input Layer
The first layer of the framework represents the foundational data and knowledge sources that feed organizational decision-making processes. These inputs include structured data (e.g., databases, performance indicators), semi-structured data (e.g., reports, operational logs), and unstructured data (e.g., textual documents, emails, expert insights). In addition to digital data, human knowledge and experiential insights constitute a critical component of this layer.

To ensure reliability and usability, data must undergo preprocessing activities such as cleansing, integration, normalization, and semantic alignment. High-quality data inputs are essential for transforming raw information into meaningful knowledge assets (Alavi & Leidner, 2001; Nonaka & Takeuchi, 1995). This layer establishes the foundation upon which intelligent analysis and decision-making processes are built.

### 3.3 AI-Enabled Knowledge Management Processes
The second layer represents the core of the proposed framework, where artificial intelligence enhances traditional knowledge management functions. This layer consists of four interconnected components:

### 3.3.1 Knowledge Acquisition and Extraction
Artificial intelligence techniques such as machine learning and natural language processing enable the automated extraction of knowledge from large and heterogeneous data sources. These techniques facilitate the identification of patterns, relationships, and trends that may not be detectable through manual analysis, thereby supporting evidence-based decision making (Russell & Norvig, 2021).

### 3.3.2 Knowledge Organization and Storage
AI-driven classification, clustering, and semantic tagging mechanisms improve the organization and storage of knowledge assets. By structuring information in an intelligent and searchable manner, organizations can enhance knowledge accessibility and retrieval efficiency (Duan, Edwards, & Dwivedi, 2019).

130

### 3.3.3 Knowledge Sharing and Dissemination

Intelligent recommendation systems and adaptive interfaces enable personalized knowledge dissemination based on user roles, contexts, and decision requirements. This process enhances collaboration and reduces information overload, facilitating more effective knowledge sharing across organizational units (Rai, Constantinides, & Sarker, 2019).

### 3.3.4 Knowledge Learning and Refinement

Continuous learning mechanisms allow AI systems to refine knowledge representations through feedback, usage patterns, and decision outcomes. This dynamic learning process supports organizational learning and improves the quality of future decisions over time.

### 3.4 Decision Support and Organizational Outcomes

The final layer focuses on how AI-enabled knowledge management contributes to decision support and organizational performance. By integrating analytical insights with contextual knowledge, decision-makers can improve accuracy, consistency, and responsiveness in both strategic and operational decisions.

The framework emphasizes human–AI collaboration, where AI supports but does not replace human judgment. Transparent and explainable AI mechanisms enhance trust and accountability, which are critical for sustainable adoption (Gunning et al., 2019). As a result, organizations can achieve improved decision quality, enhanced learning capabilities, and greater adaptability in dynamic environments (Shrestha et al., 2021).

### 3.5 Implications of the Framework

The proposed conceptual framework highlights the importance of aligning technological capabilities with organizational objectives and governance structures. By integrating artificial intelligence across the knowledge management lifecycle, organizations can move toward more intelligent, resilient, and data-driven decision-making systems. This framework provides a foundation for future empirical studies and offers practical guidance for organizations seeking to leverage AI in knowledge-intensive environments**.**

### 4.Conclusion

This study has presented a comprehensive conceptual framework for artificial intelligence–enabled knowledge management aimed at supporting data-driven organizational decision making. In an era characterized by rapid digital transformation, increasing data complexity, and heightened competitive pressure, organizations are required to move beyond traditional knowledge management practices toward more intelligent, adaptive, and integrated systems. The proposed framework responds to this need by systematically linking artificial intelligence capabilities with core knowledge management processes and decision-support mechanisms.

The findings of this study highlight that artificial intelligence significantly enhances the effectiveness of knowledge management by improving knowledge acquisition, organization, dissemination, and continuous learning. Through advanced techniques such as machine learning, natural language processing, and intelligent analytics, AI enables organizations to transform fragmented and unstructured data into actionable knowledge. This capability not only strengthens decision quality but also enhances organizational agility, resilience, and strategic responsiveness in dynamic environments.

Importantly, the proposed framework emphasizes that successful AI-enabled knowledge management is not purely a technological endeavor. Instead, it represents a socio-

technical system in which human expertise, organizational culture, governance structures, and ethical considerations play a critical role. The interaction between human judgment and intelligent systems is essential to ensure transparency, trust, and accountability in decision-making processes. Therefore, organizations must adopt a balanced approach that integrates technological innovation with human-centered design principles.

From a theoretical perspective, this study contributes to the literature by offering a holistic framework that connects artificial intelligence, knowledge management, and data-driven decision making within a unified structure. It extends existing research by addressing the dynamic interplay between technological capabilities and organizational learning processes. From a practical standpoint, the framework provides actionable guidance for organizations seeking to design or enhance AI-enabled knowledge management systems aligned with strategic objectives.

Despite its contributions, this study is subject to certain limitations. The proposed framework is conceptual in nature and has not yet been empirically validated. Future research should therefore focus on empirical testing across different organizational contexts and industries to assess its applicability and effectiveness. Additionally, future studies may explore the integration of emerging technologies such as digital twins, big data analytics, and generative artificial intelligence to further enhance knowledge-driven decision-making processes.

In conclusion, this study underscores the transformative potential of artificial intelligence in reshaping knowledge management practices and supporting data-driven organizational decision making. By aligning technological capabilities with human and organizational factors, the proposed framework offers a robust foundation for developing intelligent, adaptive, and sustainable organizational systems in an increasingly complex digital landscape.

## References

Alavi, M., & Leidner, D. E. (2001). Review: Knowledge management and knowledge management systems: Conceptual foundations and research issues. MIS Quarterly, 25(1), 107–136. https://doi.org/10.2307/3250961

Davenport, T. H., & Prusak, L. (1998). Working knowledge: How organizations manage what they know. Harvard Business School Press.

Duan, Y., Edwards, J. S., & Dwivedi, Y. K. (2019). Artificial intelligence for decision making in the era of big data – Evolution, challenges and research agenda. International Journal of Information Management, 48, 63–71. https://doi.org/10.1016/j.ijinfomgt.2019.01.021

Gunning, D., Stefik, M., Choi, J., Miller, T., Stumpf, S., & Yang, G.-Z. (2019). XAI—Explainable artificial intelligence. Science Robotics, 4(37), eaay7120. https://doi.org/10.1126/scirobotics.aay7120

Nonaka, I., & Takeuchi, H. (1995). The knowledge-creating company: How Japanese companies create the dynamics of innovation. Oxford University Press.

Rai, A., Constantinides, P., & Sarker, S. (2019). Next-generation digital platforms: Toward human–AI hybrid systems. MIS Quarterly, 43(1), iii–ix. https://doi.org/10.25300/MISQ/2019/14575

Russell, S. J., & Norvig, P. (2021). Artificial intelligence: A modern approach (4th ed.). Pearson.

Shrestha, Y. R., Ben-Menahem, S. M., & von Krogh, G. (2021). Organizational decision-making structures in the age of artificial intelligence. California Management Review, 63(1), 66–83. https://doi.org/10.1177/0008125620972149

# Human–AI Collaboration in Knowledge Management: A Hybrid Framework for Organizational Decision Making

## Seher POLAT [1✉]

*[1] Sakarya University, Industrial Engineering Department, Sakarya-TURKEY*

## Abstract

In an era characterized by rapid digital transformation and increasing organizational complexity, effective decision making has become highly dependent on the integration of human expertise and intelligent technologies. Knowledge management plays a central role in this process by enabling organizations to transform data and experience into actionable insights. However, traditional knowledge management systems often fail to fully exploit the potential of artificial intelligence, particularly in supporting collaborative and adaptive decision-making processes.

This study proposes a hybrid conceptual framework for human–AI collaboration in knowledge management, aimed at enhancing organizational decision making. The framework emphasizes the complementary roles of human cognition and artificial intelligence, positioning AI not as a replacement for human judgment but as a collaborative partner that augments analytical capacity, learning, and sense-making. By integrating artificial intelligence techniques—such as machine learning, natural language processing, and intelligent analytics—into core knowledge management processes, the framework enables more effective knowledge acquisition, interpretation, sharing, and utilization.

The proposed framework adopts a semi-conceptual perspective and illustrates how human–AI collaboration can improve decision quality, transparency, and adaptability in complex organizational environments. Particular attention is given to socio-technical factors such as trust, explainability, and governance, which are critical for sustainable adoption of AI-supported decision systems.

This study contributes to the existing literature by offering a structured and holistic perspective on human–AI collaboration within knowledge management. It provides theoretical insights and practical guidance for organizations seeking to develop intelligent, resilient, and learning-oriented decision-making systems in an increasingly data-driven world**.**

*Keywords: Human–AI Collaboration; Knowledge Management; Decision Making; Organizational Learning; Artificial Intelligence; Hybrid Intelligence*

✉ *Corresponding Author Email　　: aseher@sakarya.edu.tr*

## 2.  Introduction

In recent years, organizations have been operating in increasingly complex and dynamic environments shaped by rapid technological advancements, digital transformation, and growing data volumes. Under these conditions, effective decision making has become a critical organizational capability, requiring not only access to information but also the ability to interpret, contextualize, and apply knowledge in a timely manner. Knowledge management (KM) therefore plays a central role in enabling organizations to transform dispersed data and expertise into meaningful and actionable insights.

The emergence of artificial intelligence (AI) has significantly reshaped traditional approaches to knowledge management. AI technologies such as machine learning, natural language processing, and intelligent analytics provide advanced capabilities for processing large-scale and unstructured data, supporting faster and more accurate decision-making processes. However, despite these advancements, fully automated decision systems often face limitations related to transparency, trust, ethical concerns, and contextual understanding. As a result, the effectiveness of AI in organizational decision-making largely depends on its ability to complement, rather than replace, human cognition.

In this context, the concept of human–AI collaboration has gained increasing attention. Rather than positioning artificial intelligence as an autonomous decision-maker, this perspective emphasizes the synergistic interaction between human expertise and intelligent systems. Human judgment, intuition, and contextual awareness combined with AI's analytical power enable organizations to achieve higher levels of adaptability, learning, and performance. Such collaboration is particularly critical in knowledge-intensive environments where decisions are complex, uncertain, and value-laden.

Despite the growing interest in human–AI collaboration, existing research often addresses technological capabilities or organizational processes in isolation. Limited attention has been given to integrated frameworks that explain how human–AI collaboration can be systematically embedded within knowledge management processes to support organizational decision making. This gap highlights the need for conceptual models that capture both technological and socio-organizational dimensions.

Accordingly, this study proposes a hybrid conceptual framework for human–AI collaboration in knowledge management. The framework aims to explain how human expertise and artificial intelligence can jointly support data-driven organizational decision making by enhancing knowledge creation, sharing, and utilization. By offering a holistic perspective, this study contributes to the literature on knowledge management and provides practical insights for organizations seeking to develop intelligent, adaptive, and resilient decision-making systems.

## 2. Literature Review
### 2.1 Knowledge Management and Organizational Decision Making

Knowledge management (KM) has long been recognized as a fundamental organizational capability that supports effective decision making, innovation, and sustainable competitive advantage. Early studies define knowledge management as a systematic process involving the creation, storage, sharing, and application of knowledge to enhance organizational performance (Nonaka & Takeuchi, 1995; Alavi & Leidner, 2001). Within this context, knowledge is not merely viewed as information, but as a strategic asset shaped by human experience, interpretation, and organizational context.

As organizations operate in increasingly complex and data-intensive environments, decision-making processes have become more dependent on the effective management of knowledge resources. Data-driven decision making emphasizes the use of analytical evidence and structured reasoning rather than intuition alone (Provost & Fawcett, 2013). However, traditional knowledge management systems often struggle to cope with the volume, velocity, and variety of contemporary data, limiting their ability to support timely and high-quality decisions (Davenport & Prusak, 1998).

135

These limitations have led scholars to explore advanced technological solutions that can enhance knowledge processes and support organizational decision making in dynamic environments.

## 2.2 Artificial Intelligence as an Enabler of Knowledge Management

Artificial intelligence (AI) has emerged as a transformative technology capable of extending the boundaries of traditional knowledge management systems. AI techniques such as machine learning, natural language processing, and intelligent analytics enable organizations to extract meaningful insights from large and heterogeneous datasets (Russell & Norvig, 2021). These capabilities allow organizations to automate knowledge acquisition, improve classification accuracy, and enhance decision relevance.

Recent studies highlight that AI-driven knowledge management systems contribute significantly to organizational learning and adaptive capability. By continuously analyzing data patterns and feedback loops, AI systems support predictive insights and proactive decision-making (Duan, Edwards, & Dwivedi, 2019). Moreover, AI facilitates knowledge sharing through intelligent recommendation systems, enabling personalized and context-aware information delivery (Rai, Constantinides, & Sarker, 2019).

Despite these benefits, researchers emphasize that the successful adoption of AI in knowledge management depends on organizational readiness, governance structures, and user trust. Without appropriate human oversight, AI-driven decisions may suffer from issues related to transparency, bias, and explainability (Gunning et al., 2019).

## 2.3 Human–AI Collaboration in Knowledge Management

Recent literature increasingly highlights the importance of human–AI collaboration as a paradigm that balances automation with human judgment. Rather than replacing human decision makers, AI systems are most effective when they augment human cognitive capabilities, supporting reasoning, interpretation, and learning processes (Shrestha, Ben-Menahem, & von Krogh, 2021).

Human–AI collaboration is particularly critical in knowledge-intensive environments where decisions are complex, uncertain, and context-dependent. In such settings, human expertise provides contextual understanding, ethical reasoning, and strategic judgment, while AI contributes analytical speed, scalability, and pattern recognition capabilities. This collaborative interaction enables organizations to achieve higher decision quality and adaptability than either humans or AI systems could achieve independently.

Moreover, effective human–AI collaboration requires appropriate governance mechanisms, transparency, and trust. When users understand how AI systems generate insights, they are more likely to rely on and effectively integrate these insights into decision-making processes. Consequently, the success of AI-enabled knowledge management systems depends not only on technological sophistication but also on organizational culture and user engagement.

## 2.4 Research Gap and Theoretical Implications

Although existing research provides valuable insights into knowledge management and artificial intelligence, there remains a notable gap in integrative frameworks that explicitly address human–AI collaboration within knowledge management processes. Much of the current literature focuses either on technical advancements or on organizational aspects in isolation, offering limited guidance on how human and artificial intelligence can be systematically combined to support decision making.

Furthermore, empirical studies often emphasize performance outcomes while overlooking the socio-technical dynamics that influence trust, learning, and long-term adoption. This gap underscores the need for conceptual models that holistically integrate technological capabilities with human and organizational dimensions.

In response, this study proposes a hybrid conceptual framework that positions human–AI collaboration as a central mechanism in knowledge management for data-driven organizational decision making. By synthesizing insights from knowledge management, artificial intelligence, and organizational theory, the proposed framework aims to contribute to both academic research and practical implementation.

## 3. Conceptual Framework
### 3.1 Overview of the Conceptual Framework
This study proposes a hybrid conceptual framework that integrates human intelligence and artificial intelligence within knowledge management processes to support effective organizational decision making. The framework is grounded in the assumption that neither human expertise nor artificial intelligence alone is sufficient to manage the complexity, uncertainty, and dynamism of contemporary organizational environments. Instead, value is created through the collaborative interaction between human cognition and intelligent systems. The proposed framework consists of three interrelated layers:

3. Knowledge Inputs,
4. Human–AI Collaborative Knowledge Management Processes, and
5. Decision Support and Organizational Outcomes.

These layers form a continuous and adaptive cycle in which knowledge is created, refined, and utilized through ongoing interaction between human actors and AI-driven systems.

### 3.2 Knowledge Input Layer
The first layer represents the foundation of the framework and includes diverse sources of organizational knowledge. These inputs consist of:

1. Structured data (e.g., performance indicators, databases, operational metrics),
2. Semi-structured data (e.g., reports, logs, transactional records), and
3. Unstructured data (e.g., textual documents, emails, expert narratives, experiential knowledge).

In addition to digital data, this layer emphasizes the importance of human knowledge, including experience, intuition, and contextual understanding. Prior research highlights that effective knowledge management depends not only on data availability but also on the quality, relevance, and interpretability of information (Nonaka & Takeuchi, 1995; Alavi & Leidner, 2001).
Before knowledge can be effectively utilized, raw data must undergo preprocessing activities such as cleansing, normalization, integration, and semantic alignment. These processes ensure data consistency and reliability, thereby enabling meaningful analysis and interpretation in subsequent stages.

### 3.3 Human–AI Collaborative Knowledge Management Processes
The second layer constitutes the core of the proposed framework, where human expertise and artificial intelligence interact dynamically. This layer consists of four interrelated components:

### 3.3.1 Knowledge Acquisition and Interpretation
Artificial intelligence techniques—such as machine learning and natural language processing—support the extraction of relevant patterns and insights from large and complex datasets. However, human expertise remains essential for interpreting contextual meaning, validating insights, and ensuring alignment with organizational goals (Russell & Norvig, 2021).

137

### 3.3.2 Knowledge Organization and Structuring

AI-driven classification, clustering, and semantic modeling facilitate the organization of knowledge assets. At the same time, human judgment guides the contextualization and prioritization of knowledge, ensuring relevance for strategic and operational decision-making (Duan, Edwards, & Dwivedi, 2019).

### 3.3.3 Knowledge Sharing and Collaboration

Human–AI collaboration enhances knowledge dissemination through intelligent recommendation systems and adaptive interfaces. These systems support role-based and context-aware information sharing, reducing cognitive overload while promoting cross-functional collaboration (Rai, Constantinides, & Sarker, 2019).

### 3.3.4 Knowledge Learning and Refinement

Continuous learning mechanisms enable both humans and AI systems to improve over time. AI models refine their outputs through feedback and performance data, while human decision-makers develop deeper insights through interaction with intelligent systems. This reciprocal learning process strengthens organizational learning and adaptability.

### 3.4 Decision Support and Organizational Outcomes

The final layer focuses on how collaborative knowledge processes translate into improved decision-making outcomes. By integrating analytical intelligence with human judgment, organizations can enhance decision quality, responsiveness, and strategic alignment. Human–AI collaboration enables decision-makers to better handle uncertainty, complexity, and ambiguity, which are increasingly characteristic of modern organizational environments.

Furthermore, transparency, explainability, and trust play critical roles in ensuring the effective use of AI-supported decision systems. Explainable AI mechanisms help decision-makers understand system outputs, fostering confidence and accountability (Gunning et al., 2019). As a result, organizations can achieve improved performance, stronger learning capabilities, and greater resilience.

### 3.5 Implications of the Framework

The proposed framework underscores the importance of viewing artificial intelligence not as a replacement for human decision-making, but as a collaborative partner that enhances cognitive capabilities. By integrating human expertise with AI-driven analytics, organizations can develop more adaptive, intelligent, and sustainable decision-making systems.

This framework provides both theoretical and practical value by offering a structured approach to understanding how human–AI collaboration can be operationalized within knowledge management processes. It also establishes a foundation for future empirical research aimed at validating and refining the proposed model across different organizational contexts.
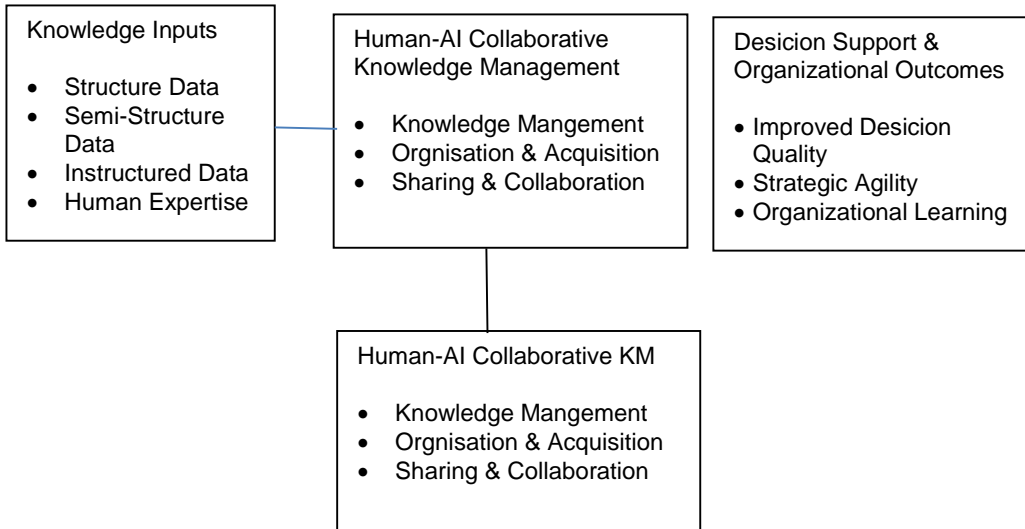
*Figure 1.* Conceptual framework of human–AI collaboration in knowledge management for organizational decision making

1. Knowledge Inputs
   - Structured data
   - Semi-structured data
   - Unstructured data
   - Human expertise
2. Human–AI Collaborative Knowledge Management
   - Knowledge acquisition
   - Knowledge organization & structuring
   - Knowledge sharing & collaboration
3. Decision Support & Organizational Outcomes
   - Improved decision quality
   - Strategic agility
   - Organizational learning
4. Continuous Learning & Feedback Loop
   - Human judgment
   - AI model adaptation
   - Knowledge refinement

This figure illustrates a conceptual framework that integrates human intelligence and artificial intelligence within knowledge management processes to support effective organizational decision making. The framework is structured around three interconnected layers: (1) knowledge inputs, including structured, semi-structured, and unstructured data as well as human expertise; (2) human–AI collaborative knowledge management processes, encompassing knowledge acquisition, organization, sharing, and refinement; and (3) decision support and organizational outcomes, such

139

as improved decision quality, strategic agility, and organizational learning. The model emphasizes continuous feedback and learning loops, highlighting the dynamic interaction between human judgment and artificial intelligence in refining knowledge and enhancing decision-making performance.

## 4.Conclusion

This study proposed a conceptual framework that emphasizes human–AI collaboration in knowledge management as a critical mechanism for enhancing data-driven organizational decision making. In an increasingly complex and data-intensive business environment, organizations must go beyond traditional knowledge management practices and adopt intelligent, adaptive, and human-centered approaches to effectively transform data into meaningful insights. The proposed framework addresses this need by integrating artificial intelligence capabilities with human cognitive strengths to support more informed, transparent, and resilient decision-making processes.

The findings of this study highlight that artificial intelligence can significantly enhance knowledge management activities such as knowledge acquisition, organization, sharing, and continuous learning. However, the effectiveness of AI-driven systems largely depends on their alignment with human judgment, contextual understanding, and organizational values. Rather than replacing human decision-makers, AI should function as a collaborative partner that augments analytical capabilities, reduces cognitive load, and supports sense-making in complex and uncertain environments.

Furthermore, the proposed framework underscores the importance of socio-technical considerations in the successful implementation of AI-enabled knowledge management systems. Factors such as trust, explainability, governance, and organizational culture play a decisive role in determining the extent to which AI can be effectively integrated into decision-making processes. By acknowledging these dimensions, the framework provides a more holistic understanding of how human–AI collaboration can be operationalized within organizational contexts.

From a theoretical perspective, this study contributes to the existing literature by offering an integrated framework that bridges knowledge management, artificial intelligence, and decision-making research. It advances current discussions by emphasizing the interactive and dynamic nature of human–AI collaboration rather than viewing AI as a purely technological tool. From a practical standpoint, the framework offers guidance for organizations seeking to design and implement intelligent decision-support systems that enhance organizational learning, adaptability, and long-term performance.

Despite its contributions, this study has certain limitations. The proposed framework is conceptual in nature and has not been empirically validated. Future research may focus on testing the framework across different industries and organizational settings, as well as exploring the role of emerging technologies such as generative AI, digital twins, and advanced analytics in strengthening human–AI collaboration. Such efforts would further enrich the understanding of intelligent knowledge management and support the development of more robust, adaptive, and sustainable organizational decision-making systems.

## References

Alavi, M., & Leidner, D. E. (2001). Review: Knowledge management and knowledge management systems: Conceptual foundations and research issues. MIS Quarterly, 25(1), 107–136. https://doi.org/10.2307/3250961

Davenport, T. H., & Prusak, L. (1998). Working knowledge: How organizations manage what they know. Harvard Business School Press.

Duan, Y., Edwards, J. S., & Dwivedi, Y. K. (2019). Artificial intelligence for decision making in the era of big data – Evolution, challenges and research agenda. International Journal of Information Management, 48, 63–71. https://doi.org/10.1016/j.ijinfomgt.2019.01.021

Gunning, D., Stefik, M., Choi, J., Miller, T., Stumpf, S., & Yang, G.-Z. (2019). XAI—Explainable artificial intelligence. Science Robotics, 4(37), eaay7120. https://doi.org/10.1126/scirobotics.aay7120

Nonaka, I., & Takeuchi, H. (1995). The knowledge-creating company: How Japanese companies create the dynamics of innovation. Oxford University Press.

Provost, F., & Fawcett, T. (2013). Data science for business: What you need to know about data mining and data-analytic thinking. O'Reilly Media.

Rai, A., Constantinides, P., & Sarker, S. (2019). Next-generation digital platforms: Toward human–AI hybrid systems. MIS Quarterly, 43(1), iii–ix. https://doi.org/10.25300/MISQ/2019/14575

Russell, S. J., & Norvig, P. (2021). Artificial intelligence: A modern approach (4th ed.). Pearson.

Shrestha, Y. R., Ben-Menahem, S. M., & von Krogh, G. (2021). Organizational decision-making structures in the age of artificial intelligence. California Management Review, 63(1), 66–83. https://doi.org/10.1177/0008125620972149

# Trust-Oriented Artificial Intelligence in Knowledge Management: Enhancing Decision Quality in Organizations

Seher POLAT [1][✉] İskender AKKURT[2]

[1][✉]*Sakarya University, Industrial Engineering Department, Sakarya-TURKEY*
[2]*Suleyman Demirel University, Science Faculty, Physics Department, Nucleer Sciences, Isparta-Turkey, E Mail: iskenderakkurt@sdu.edu.tr*

## Abstract

In contemporary organizational environments, decision-making processes increasingly rely on artificial intelligence (AI) to manage complexity, uncertainty, and large volumes of data. While AI offers significant potential to enhance analytical capabilities, its effectiveness in organizational contexts largely depends on the level of trust established between human decision-makers and intelligent systems. Inadequate trust can limit the adoption and impact of AI-driven insights, thereby reducing decision quality and organizational performance.

This study proposes a trust-oriented conceptual framework for artificial intelligence–enabled knowledge management aimed at enhancing decision quality in organizations. The framework emphasizes the role of trust as a mediating factor between AI capabilities and effective decision making. It integrates key dimensions such as transparency, explainability, reliability, and human oversight within knowledge management processes. By positioning trust as a central mechanism, the framework highlights how human–AI interaction can support more informed, consistent, and accountable decisions.

The proposed model adopts a semi-conceptual approach and illustrates how trust-oriented AI systems can facilitate knowledge creation, sharing, and utilization across organizational levels. It further emphasizes the importance of aligning technological capabilities with organizational culture, governance structures, and ethical considerations. By doing so, organizations can strengthen confidence in AI-supported insights and enhance their overall decision-making quality.

This study contributes to the literature by offering a structured perspective on trust-based human–AI collaboration within knowledge management. It also provides practical implications for organizations seeking to design trustworthy AI systems that support sustainable, transparent, and high-quality decision-making in complex and dynamic environments.

*Keywords: Trust in Artificial Intelligence; Knowledge Management; Decision Quality; Human–AI Collaboration; Explainable AI; Organizational Decision Making*

[✉] *Corresponding Author Email　　: aseher@sakarya.edu.tr*

## 6.  Introduction

In recent years, organizations have increasingly relied on artificial intelligence (AI) to enhance decision-making processes in complex and data-intensive environments. Advances in data analytics, machine learning, and intelligent systems have enabled organizations to process large volumes of information, identify patterns, and generate insights that support strategic and operational decisions. However, despite these technological advancements, the effectiveness of AI-driven decision-making systems remains highly dependent on the level of trust that organizational actors place in these technologies.

Trust has emerged as a critical factor influencing the acceptance, adoption, and effective use of artificial intelligence in organizational contexts. While AI systems can offer speed, accuracy, and analytical depth, decision-makers often remain cautious due to concerns related to transparency, explainability, reliability, and ethical implications. As a result, the lack of trust can significantly undermine the potential benefits of AI, limiting its integration into knowledge management processes and reducing its impact on decision quality.

Knowledge management (KM) plays a central role in addressing these challenges by providing structured mechanisms for capturing, organizing, sharing, and applying knowledge within organizations. When integrated with trustworthy AI systems, knowledge management can facilitate more informed, consistent, and accountable decision-making. However, existing research often treats trust, artificial intelligence, and knowledge management as separate constructs, offering limited guidance on how they can be systematically integrated to support organizational decision processes.

In response to this gap, this study proposes a trust-oriented framework for artificial intelligence– enabled knowledge management aimed at enhancing decision quality in organizations. The framework emphasizes the role of trust as a foundational element that mediates the interaction between human decision-makers and intelligent systems. By incorporating key dimensions such as transparency, explainability, and human oversight, the proposed framework seeks to support reliable and ethical decision-making in complex organizational environments.

By advancing a holistic perspective on trust-based human–AI collaboration, this study contributes to the growing body of literature on knowledge management and artificial intelligence. It also offers practical insights for organizations seeking to design trustworthy AI-enabled systems that enhance decision quality, organizational learning, and long-term performance.

## 2. Literature Review
## 2.1 Knowledge Management and Decision Quality

Knowledge management (KM) has long been recognized as a critical organizational capability that enables effective decision making, learning, and sustainable competitive advantage. Foundational studies define KM as a systematic process involving the creation, storage, sharing, and application of knowledge to improve organizational performance (Nonaka & Takeuchi, 1995; Alavi & Leidner, 2001). In contemporary organizational environments, decision quality increasingly depends on the ability to transform large volumes of heterogeneous data into actionable and contextually meaningful knowledge.

Data-driven decision making has gained prominence as organizations seek to enhance analytical rigor and reduce uncertainty in complex operational settings. However, while data analytics can support evidence-based decisions, the effectiveness of such approaches depends on how well data

143

is interpreted, contextualized, and trusted by decision-makers (Provost & Fawcett, 2013). Traditional knowledge management systems often fall short in addressing these challenges, as they lack adaptive mechanisms for handling uncertainty, ambiguity, and dynamic organizational contexts (Davenport & Prusak, 1998).

## 2.2 Artificial Intelligence in Knowledge Management

Artificial intelligence (AI) has emerged as a transformative enabler of knowledge management by enhancing the ability to process, analyze, and interpret large-scale and unstructured data. Technologies such as machine learning, natural language processing, and intelligent analytics enable organizations to automate knowledge extraction, pattern recognition, and predictive reasoning (Russell & Norvig, 2021). As a result, AI-driven knowledge management systems can significantly improve the speed, accuracy, and scalability of decision-making processes.

Empirical studies suggest that AI enhances organizational learning by enabling continuous feedback, adaptive modeling, and real-time insight generation (Duan, Edwards, & Dwivedi, 2019). Moreover, AI-supported systems facilitate knowledge sharing by offering personalized recommendations and context-aware information delivery, thereby reducing cognitive overload and improving decision effectiveness (Rai, Constantinides, & Sarker, 2019).

Despite these advantages, the integration of AI into knowledge management introduces new challenges related to transparency, accountability, and interpretability. Without appropriate design and governance mechanisms, AI systems may produce outcomes that are difficult for human decision-makers to understand or trust, limiting their practical value in organizational settings.

## 2.3 Trust in Human–AI Collaboration

Trust is a fundamental prerequisite for the successful adoption and utilization of artificial intelligence in organizational decision-making. Trust influences users' willingness to rely on AI-generated insights, particularly in high-stakes or uncertain contexts. Research indicates that lack of transparency and explainability can significantly undermine user confidence in AI systems, even when their technical performance is high (Gunning et al., 2019).

Human–AI collaboration emphasizes the complementary relationship between human judgment and machine intelligence. Rather than replacing human decision-makers, AI systems are most effective when they augment human cognitive capabilities, providing analytical support while allowing humans to retain control and contextual awareness (Shrestha, Ben-Menahem, & von Krogh, 2021). Trust plays a mediating role in this relationship, influencing how decision-makers interpret, evaluate, and act upon AI-generated recommendations.

Moreover, trust in AI is not solely a technical issue but a socio-organizational phenomenon shaped by organizational culture, governance structures, and ethical considerations. Transparent algorithms, explainable outputs, and accountability mechanisms are essential for fostering sustainable trust and ensuring responsible AI adoption within knowledge management systems.

## 2.4 Research Gap and Theoretical Implications

Although existing studies have extensively explored artificial intelligence, knowledge management, and trust as individual constructs, integrative frameworks that explicitly connect these dimensions remain limited. Much of the current literature focuses on technological performance or user acceptance in isolation, offering insufficient insight into how trust mediates the relationship between AI-enabled knowledge management and decision quality.

This gap highlights the need for a holistic perspective that conceptualizes trust as a central enabler of effective human–AI collaboration. Accordingly, this study proposes a trust-oriented conceptual framework that integrates artificial intelligence into knowledge management processes to enhance organizational decision making. By synthesizing insights from knowledge management, artificial

intelligence, and organizational behavior literature, the framework aims to advance both theoretical understanding and practical application of trustworthy AI in organizational contexts..

## 3. Conceptual Framework

### 3.1 Conceptual Foundation

This study conceptualizes trust as a dynamic regulatory mechanism that governs the interaction between artificial intelligence (AI), knowledge management (KM), and organizational decision making. Rather than treating trust as a by-product of technological performance, the proposed framework positions trust as an active enabler that shapes how knowledge is interpreted, accepted, and utilized within organizational contexts.

In this perspective, trust does not emerge solely from system accuracy or reliability but evolves through continuous interaction between human judgment, algorithmic transparency, and organizational norms. The framework therefore moves beyond technology-centered views and conceptualizes human–AI collaboration as a socio-cognitive system in which decision quality depends on relational and contextual factors.

### 3.2 Core Dimensions of the Framework

The proposed model is structured around four interdependent dimensions, each contributing to the formation of trust and effective decision making.

### 3.2.1 Cognitive Integration of Human and Artificial Intelligence

Cognitive integration refers to the alignment between human reasoning and AI-generated insights. Rather than delegating decision authority to automated systems, this dimension emphasizes interpretability, contextual understanding, and sense-making. AI supports analytical depth, while humans contribute experiential knowledge, ethical reasoning, and contextual awareness. Trust emerges when decision-makers perceive AI outputs as comprehensible, meaningful, and aligned with organizational goals.

### 3.2.2 Knowledge Co-Creation and Validation

In this framework, knowledge is not passively transferred but co-created through interaction between humans and intelligent systems. AI assists in identifying patterns, synthesizing information, and generating insights, while human actors evaluate relevance, plausibility, and applicability. Validation processes—such as expert review, feedback loops, and contextual interpretation—serve as trust-building mechanisms that enhance the credibility of knowledge outputs.

### 3.2.3 Transparency, Accountability, and Ethical Alignment

Trust in AI-enabled knowledge systems is strongly influenced by transparency and accountability. This dimension emphasizes explainable system behavior, traceable decision logic, and clear responsibility structures. Ethical considerations, including fairness, bias mitigation, and responsible data use, are integral to sustaining long-term trust. Transparent AI practices enable decision-makers to understand not only what decisions are suggested, but why they are generated.

### 3.2.4 Adaptive Learning and Organizational Resilience

The final dimension focuses on continuous learning and adaptability. Trust is reinforced through consistent system performance, feedback integration, and organizational learning mechanisms. As human–AI collaboration evolves, both technological models and human decision strategies adapt over time, strengthening organizational resilience and responsiveness to environmental change.

### 3.3 Trust-Centered Decision-Making Outcomes

145

The interaction of these four dimensions leads to improved decision quality characterized by greater accuracy, consistency, and contextual awareness. Trust functions as a mediating force that aligns analytical capabilities with human values and organizational objectives. Consequently, decision-making becomes not only data-driven but also ethically grounded and strategically informed.

This framework positions trust as a dynamic capability that enables organizations to leverage artificial intelligence responsibly while preserving human agency. By embedding trust into knowledge management processes, organizations can achieve sustainable decision-making performance in increasingly complex and uncertain environments.

### 3.4 Theoretical and Practical Implications

The proposed framework contributes to the literature by reframing human–AI collaboration as a trust-centered, socio-technical process rather than a purely technological integration. It offers a conceptual foundation for future empirical research and provides practitioners with guidance for designing AI-enabled knowledge systems that balance efficiency, transparency, and accountability.
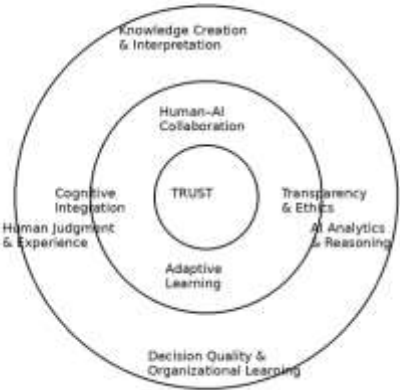


Figure 1. Trust-centered conceptual framework for human–AI collaboration in knowledge management.

This radial model positions trust at the core of human–AI collaboration, emphasizing its central role in enabling effective knowledge creation, interpretation, and decision making. The framework illustrates how cognitive integration, transparency, ethical alignment, and adaptive learning interact dynamically to support organizational learning and decision quality.

1. Core Layer: Trust as the Central Enabler: At the core of the framework lies trust, which functions as the fundamental mechanism enabling effective interaction between humans and artificial intelligence. Trust determines the extent to which decision-makers are willing to rely on AI-generated insights, integrate them into their reasoning processes, and act upon them in organizational contexts. In this model, trust is not treated as a static attribute but as a dynamic and evolving construct shaped by transparency, interpretability, reliability, and ethical alignment. When AI systems provide explainable outputs and consistent performance, human users are more likely to

146

develop confidence in their recommendations. Conversely, a lack of transparency or accountability can weaken trust and reduce system adoption.

By placing trust at the center of the framework, the model emphasizes that successful AI integration in knowledge management depends not solely on technological sophistication but on the quality of human–AI relationships.

2. Intermediate Layer: Human–AI Collaborative Mechanisms: Surrounding the trust core is the human–AI collaboration layer, which represents the interactive processes through which knowledge is created, interpreted, and applied. This layer consists of four interrelated components:

2.1 Cognitive Integration: Cognitive integration refers to the alignment of human reasoning with AI-driven analytical capabilities. While AI contributes speed, pattern recognition, and computational power, humans provide contextual understanding, ethical judgment, and strategic reasoning. This synergy allows organizations to generate more meaningful and context-aware knowledge.

2.2 Knowledge Co-Creation: In this stage, knowledge emerges through continuous interaction between human expertise and intelligent systems. AI supports data processing and insight generation, while humans evaluate relevance, validate outcomes, and contextualize findings. This co-creation process enhances the credibility and applicability of organizational knowledge.

2.3 Transparency and Ethical Alignment: Transparency is a prerequisite for trust. This component emphasizes explainability, accountability, and ethical responsibility in AI-supported knowledge processes. When decision-makers understand how and why AI produces certain outputs, trust and acceptance increase, strengthening collaborative decision-making.

2.4 Adaptive Learning: Adaptive learning reflects the system's ability to evolve through feedback mechanisms. AI models learn from user interactions and performance outcomes, while humans refine their judgment based on system insights. This reciprocal learning process ensures continuous improvement and long-term organizational adaptability.

3. Outer Layer: Organizational Outcomes: The outer layer represents the organizational outcomes generated through trust-centered human–AI collaboration. These outcomes include:

- Enhanced decision quality, driven by more accurate, transparent, and context-aware insights;
- Organizational learning, supported by continuous feedback and knowledge refinement;
- Strategic agility, enabling organizations to respond effectively to dynamic environments;
- Sustainable performance, achieved through balanced integration of human expertise and intelligent technologies.

This layer illustrates how trust-centered collaboration transforms knowledge into actionable value, strengthening organizational resilience and long-term competitiveness.

## 4.Conclusion

This study proposed a trust-oriented conceptual framework to explain how human–AI collaboration can enhance knowledge management and decision quality within organizational contexts. In an era characterized by increasing complexity, uncertainty, and data intensity, organizations must go beyond purely technological solutions and adopt socio-technical approaches that integrate human judgment with artificial intelligence. The proposed framework responds to this need by positioning trust as the central mechanism that enables effective interaction between humans and intelligent systems.

The framework emphasizes that artificial intelligence alone is insufficient to ensure high-quality decision making. Instead, decision effectiveness emerges from the dynamic interaction between

147

human cognition and AI capabilities, supported by transparency, ethical alignment, and continuous learning. By conceptualizing trust as a dynamic and evolving construct, this study highlights its role in shaping how knowledge is interpreted, validated, and transformed into actionable insights. In this sense, trust functions not merely as an outcome but as a foundational enabler of sustainable human–AI collaboration.

From a theoretical perspective, this study contributes to the literature by integrating knowledge management, artificial intelligence, and organizational decision-making within a unified trust-centered framework. Unlike technology-centric models, the proposed approach emphasizes relational and cognitive dimensions, offering a more holistic understanding of how AI can be embedded into organizational knowledge processes. This perspective extends existing research by framing trust as an active mechanism that mediates the relationship between AI capabilities and decision quality.

From a practical standpoint, the framework provides actionable guidance for organizations seeking to implement trustworthy AI systems. By emphasizing transparency, human oversight, and adaptive learning, organizations can enhance decision quality while maintaining accountability and ethical responsibility. The model also supports organizational learning and resilience by enabling continuous feedback and knowledge refinement.

Despite its contributions, this study has certain limitations. The proposed framework is conceptual in nature and has not yet been empirically validated. Future research should therefore focus on empirical testing across diverse organizational contexts and industries. Additionally, future studies may explore how emerging technologies—such as generative AI, digital twins, and advanced analytics—interact with trust dynamics in knowledge management processes.

In conclusion, this study underscores the importance of trust as a foundational element in human–AI collaboration. By integrating trust into knowledge management systems, organizations can enhance decision quality, strengthen learning capabilities, and achieve sustainable performance in increasingly complex and dynamic environments.

References

Alavi, M., & Leidner, D. E. (2001). Review: Knowledge management and knowledge management systems: Conceptual foundations and research issues. MIS Quarterly, 25(1), 107–136. https://doi.org/10.2307/3250961

Davenport, T. H., & Prusak, L. (1998). Working knowledge: How organizations manage what they know. Harvard Business School Press.

Duan, Y., Edwards, J. S., & Dwivedi, Y. K. (2019). Artificial intelligence for decision making in the era of big data – Evolution, challenges and research agenda. International Journal of Information Management, 48, 63–71. https://doi.org/10.1016/j.ijinfomgt.2019.01.021

Gunning, D., Stefik, M., Choi, J., Miller, T., Stumpf, S., & Yang, G.-Z. (2019). XAI—Explainable artificial intelligence. Science Robotics, 4(37), eaay7120.https://doi.org/10.1126/scirobotics.aay7120

Nonaka, I., & Takeuchi, H. (1995). The knowledge-creating company: How Japanese companies create the dynamics of innovation. Oxford University Press.

Provost, F., & Fawcett, T. (2013). Data science for business: What you need to know about data mining and data-analytic thinking. O'Reilly Media.

Rai, A., Constantinides, P., & Sarker, S. (2019). Next-generation digital platforms: Toward human–AI hybrid systems. MIS Quarterly, 43(1), iii–ix. https://doi.org/10.25300/MISQ/2019/14575

Russell, S. J., & Norvig, P. (2021). Artificial intelligence: A modern approach (4th ed.). Pearson.

Shrestha, Y. R., Ben-Menahem, S. M., & von Krogh, G. (2021). Organizational decision-making structures in the age of artificial intelligence. California Management Review, 63(1), 66–83. https://doi.org/10.1177/0008125620972149

# Half Value Layer Properties of Cellulose Acetate CdO-ZnO Polymer Composites

## İskender AKKURT

*Suleyman Demirel University, Isparta-Turkey, E Mail: iskenderakkurt@sdu.edu.tr*

## Abstract

This study investigates the radiation shielding properties of cellulose acetate (CA) polymer composites enhanced with cadmium oxide (CdO) and zinc oxide (ZnO). The Half Value Layer (HVL), a key parameter indicating a material's ability to attenuate radiation, is measured for CA-CdO-ZnO composites with various additive concentrations. The HVL values of these composites are evaluated against X-rays and gamma radiation, and the effects of material composition, density, and thickness are discussed.

**Keyword*s :***Cellulose acetate, CdO, ZnO, polymer composites, half value layer, radiation shielding, linear attenuation coefficient.

## 1. Introduction

Radiation shielding is a critical concern in fields such as healthcare, nuclear energy, and space engineering. The **Half Value Layer (HVL)** is an important parameter that quantifies the thickness required for a material to attenuate radiation by 50%. This property is widely used to evaluate the effectiveness of shielding materials.The aim of this study is to explore the radiation shielding capabilities of cellulose acetate (CA) polymer composites with the addition of CdO and ZnO. Cellulose acetate is a versatile polymer known for its flexibility and ease of processing but has limited radiation shielding properties on its own. The inclusion of high atomic number additives such as CdO and ZnO improves the material's ability to absorb and scatter ionizing radiation, particularly gamma rays and X-rays.

## 2. Materials and Methods

- **Cellulose Acetate (CA):** A modified form of cellulose, cellulose acetate is widely used for its transparency, biocompatibility, and flexibility. It is not highly effective for radiation shielding alone due to its low atomic number.
- **CdO (Cadmium Oxide) and ZnO (Zinc Oxide):** Both CdO and ZnO are compounds with higher atomic numbers, which enhance the material's ability to attenuate gamma rays and X-rays.

Cellulose acetate-based composites were prepared by mixing CdO and ZnO at varying concentrations. The mixture was processed using a solvent-casting method to obtain homogenous films, which were then fabricated into thin layers of desired thickness for testing.

The HVL values of the composites were determined by measuring the attenuation of X-rays and gamma rays at different energies (0.1 MeV - 1 MeV). The radiation was passed through the composite samples, and the transmitted intensity was measured using a radiation detector. The linear attenuation coefficient ($\mu$\mu$\mu$) was calculated, and the HVL was derived using the formula:

$$HVL = \frac{\ln(2)}{\mu}$$

Gamma and X-ray sources were used for the radiation attenuation measurements. The transmitted radiation was detected using scintillation detectors or Geiger-Müller tubes, and the data were analyzed to calculate the HVL for each sample.

## 3. Results and Discussion

The measured HVL values showed a clear dependence on the CdO-ZnO content. Composites with higher CdO and ZnO concentrations demonstrated significantly lower HVL values, indicating better shielding efficiency. Specifically, for **gamma radiation**, the composites exhibited a substantial reduction in transmitted radiation, demonstrating their effective shielding properties.

The density of the composites had a direct impact on the attenuation capabilities. As the density of the material increased (with higher concentrations of CdO and ZnO), the linear attenuation coefficient ($\mu$\mu$\mu$) also increased, leading to a decrease in the HVL. This highlights the role of material density in improving radiation shielding by increasing the likelihood of interaction between the radiation and the atoms in the material.

For low-energy X-rays, the composites with CdO-ZnO additives showed significant attenuation, resulting in lower HVL values. However, as the energy of the radiation increased (towards the higher energy gamma rays), thicker composite layers were required to achieve similar attenuation, suggesting that the shielding efficiency decreases with higher radiation energy.

## 4. Conclusion and Future Directions

This study demonstrates that **cellulose acetate CdO-ZnO polymer composites** are effective materials for radiation shielding, particularly against gamma rays and X-rays. The HVL values of these composites can be optimized by adjusting the concentration of CdO and ZnO, as well as their density and thickness. The results suggest that these composites could be used in applications requiring lightweight, efficient radiation protection, such as medical imaging, nuclear reactors, and space exploration.Further research should focus on exploring additional nanomaterials or further optimizing the composite formulations for improved shielding properties and mechanical strength. Additionally, investigating the biocompatibility and practical processing methods of these composites could open up new avenues for their use in radiation protection applications.

## References

[1] Aközcan, S., Külahcı, F., Günay, O., & Özden, S. (2021). Radiological risk from activity concentrations of natural radionuclides: Cumulative Hazard Index. *Journal of Radioanalytical and Nuclear Chemistry*, *327*, 105-122.

[11] Matsunaga, Y., Kawaguchi, A., Kobayashi, M., Suzuki, S., Suzuki, S., & Chida, K. (2017). Radiation doses for pregnant women in the late pregnancy undergoing fetal-computed tomography: a comparison of dosimetry and Monte Carlo simulations. Radiological physics and technology, 10, 148-154.

[3] Albıdhanı, H., Gunoglu, K., & Akkurt, İ. (2019). Natural radiation measurement in some soil samples from basra oil field, Iraq state. International Journal of Computational and Experimental Science and Engineering, 5(1), 48–51. https://doi.org/10.22399/ ijcesen.498695

[4] Boodaghi Malidarre, R., Akkurt, İ., Gunoglu, K., & Akyıldırım, H. (2021a). Fast neutrons shielding properties for HAP-Fe2O3 composite materials. International Journal of Computational and Experimental Science and Engineering, 7(3), 143–145. https://doi. org/10.22399/ijcesen.1012039

[5] Buyuk, B., Tugrul, A. B., Cengiz, M., Yucel, O., Goller, G., & Sahin, F. C. (2015). Radiation shielding properties of spark plasma sintered boron carbide–aluminium composites. Acta Physica Polonica A, 128–2B, 132–134. https://doi.org/10.12693/ APhysPolA.128.B-132

[6] Goodman, T. R., & Amurao, M. (2012). Medical imaging radiation safety for the female patient: rationale and implementation. *Radiographics*, *32*(6), 1829-1837.

[7] Jawad, A. A., Demirkol, N., Gunoglu, ˘ K., & Akkurt, I. (2019). Radiation shielding properties of some ceramic wasted samples. International Journal of Environmental Science and Technology16, 5039–5042. https://doi.org/10.1007/s13762-019-02240-

[8] Karpuz, N. (2023). Radiation shielding properties of glass composition. Journal of Radiation Research and Applied Sciences, 16(4), Article 100689. https://doi.org/ 10.1016/j.jrras.2023.100689

[9] Malidarre, R. B., Akkurt, I., & Kavas, T. (2021). Monte Carlo simulation onshielding properties of neutron-gamma from 252Cf source for Alumino-Boro-Silicate Glasses. Radiation Physics and Chemistry, 186, Article 109540. https://doi.org/10.1016/j. radphyschem.2021.109540

[10] Malidarrea, R. B., Kulali, F., Inal, A., & Ali, O. (2020). Monte Carlo simulation of the Waste Soda-Lime-Silica Glass system contained Sb2O3. Emerging Materials Research, 9–4, 1334–1340. https://doi.org/10.1680/jemmr.20.00202

# Investigation of Effective Electrical Conductivity (Ceff) of $YbMn_{0.8}Fe_{0.2}O_3$ Ceramic Compound

## İskender AKKURT

*Suleyman Demirel University, Isparta-Turkey, E Mail: iskenderakkurt@sdu.edu.tr*

## Abstract

In this study, the effective electrical conductivity (Ceff) of Fe-doped rare-earth manganite $YbMn_{0.8}Fe_{0.2}O_3$ was investigated. The substitution of $Fe^{3+}$ ions at the $Mn^{3+}$ site is expected to significantly influence the electrical transport properties by modifying the charge carrier concentration and hopping mechanisms. The compound was synthesized using a conventional solid-state reaction method, and its electrical behavior was analyzed using impedance spectroscopy over a wide temperature and frequency range. The results indicate semiconducting behavior with thermally activated conduction. The effective conductivity was found to be strongly dependent on temperature, which suggests a dominant small polaron hopping conduction mechanism. Grain and grain boundary contributions to the overall conductivity were analyzed using equivalent circuit modeling.

***Keywords:** $YbMnO_3$, Fe doping, effective conductivity, impedance spectroscopy, small polaron hopping*

## 1. Introduction

Rare-earth manganites with the general formula $RMnO_3$ (R = rare-earth element) have attracted considerable attention due to their multifunctional properties, including multiferroicity, magnetoelectric coupling, and interesting electrical transport behavior. Among them, $YbMnO_3$ exhibits semiconducting properties and strong electron–lattice interactions.Partial substitution of $Mn^{3+}$ ions with transition metal ions such as $Fe^{3+}$ is an effective strategy to tailor the electrical and structural properties of manganites. Fe doping can alter the $Mn^{3+}/Mn^{4+}$ ratio, induce lattice distortion, and introduce localized electronic states, thereby influencing the charge transport mechanism. However, reports on the effective electrical conductivity of $YbMn_{0.8}Fe_{0.2}O_3$ are limited. Therefore, this work focuses on the investigation of the effective conductivity (Ceff) and the underlying conduction mechanism in this compound.

## 2. Experimental Procedure

The $YbMn_{0.8}Fe_{0.2}O_3$ ceramic samples were synthesized using the conventional solid-state reaction method. High-purity $Yb_2O_3$, $MnO_2$, and $Fe_2O_3$ powders were weighed according to stoichiometric ratios and thoroughly mixed using agate mortar grinding. The mixed powders were calcined at elevated temperatures to ensure phase formation, followed by

152

pelletization and sintering to obtain dense ceramic samples.Electrical properties were investigated using impedance spectroscopy in the frequency range of 100 Hz to 1 MHz and over a wide temperature range. Silver paste was applied on both sides of the pellets to ensure good electrical contact.

## 3. Results and Discussion

The complex impedance plots (Nyquist plots) of $YbMn_{0.8}Fe_{0.2}O_3$ exhibit semicircular arcs, indicating contributions from both grain interiors and grain boundaries. The impedance data were successfully fitted using an equivalent circuit consisting of parallel RC elements representing bulk and grain boundary effects.The temperature dependence of Ceff shows an increase in conductivity with rising temperature, confirming the semiconducting nature of the material. The extracted activation energy suggests that the conduction mechanism is dominated by small polaron hopping between localized $Mn^{3+}/Mn^{4+}$ and $Fe^{3+}$ sites.The introduction of $Fe^{3+}$ ions modifies the local electronic environment and affects carrier mobility. Fe doping is found to influence both the bulk and grain boundary conductivity, indicating its strong role in determining the effective electrical transport properties of the compound.
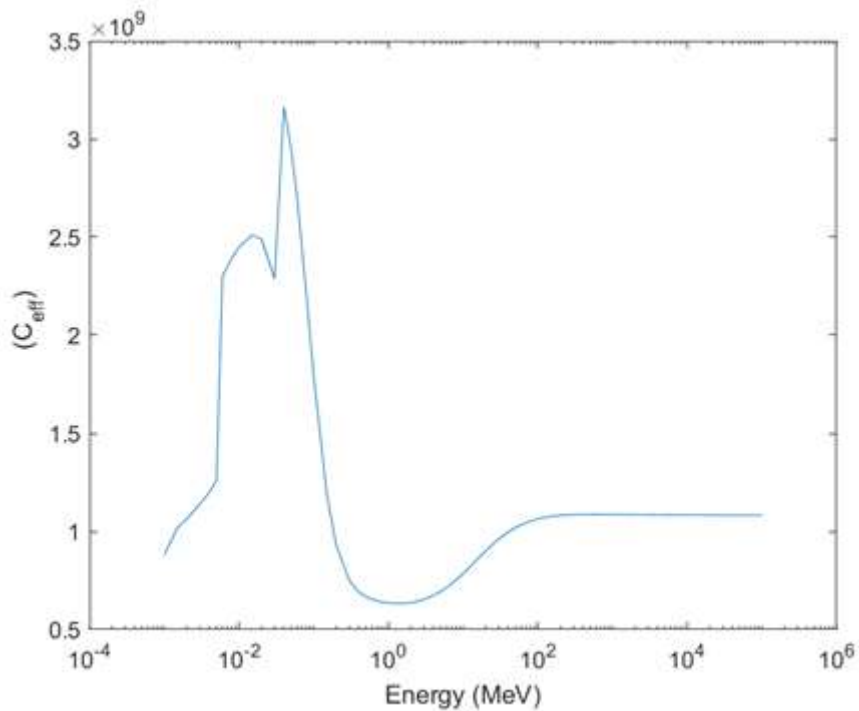


Figure 1. Effective Conductivity

153

## 4. Conclusion

The effective electrical conductivity of $YbMn_{0.8}Fe_{0.2}O_3$ ceramic has been systematically investigated. The compound exhibits semiconducting behavior with thermally activated conduction. Impedance spectroscopy reveals distinct grain and grain boundary contributions to the overall conductivity. The conduction mechanism is well described by a small polaron hopping model, and Fe substitution plays a crucial role in tailoring the effective conductivity. These results suggest that Fe-doped $YbMnO_3$ compounds are promising candidates for functional oxide-based electronic applications.

## References

[1] Henaish AMA, Mostafa M, Salem B, Zakaly HMH, Issa S, Weinstein, I, Hemeda OM (2020) Spectral, Electrical, Magnetic and Radiation Shielding Studies of Mg-doped Ni–Cu–Zn Nanoferrites. Journal of Materials Science: Materials in Electronics. 22:1–13

[2] Şakar, E., Özpolat, Ö. F., Alım, B., Sayyed, M. I., & Kurudirek, M. (2020). Phy-X/PSD: development of a user friendly online software for calculation of parameters relevant to radiation shielding and dosimetry. Radiation Physics and Chemistry, 166, 108496

[3] Sonia M. Reda, Hosam M. Saleh, Calculation of the gamma radiation shielding efficiency of cement-bitumen portable container using MCNPX code, Progress in Nuclear Energy, Volume 142. 104012. ISSN 2021;0149–1970. https://doi.org/ 10.1016/j.pnucene.2021.104012.

[4] Aygun M, Aygün Z (2023) A Comprehensive Analysis on Radiation Shielding Characteristics of Borogypsum (Boron Waster) by Phy-X/PSD code. Rev. Mex. Fis. 69:1-7

[5] Sayyed MI, Kumar A, Tekin HO, Kaur R, Sigh M, Agar O, Khandaker MU (2020) Evaluaiton of Gamma-Ray and Neutron Shielding Features of Heavy Metals Doped $Bi_2O_3$-BaO-$Na_2$-MgO-$B_2O_3$ Glass Systems. Prog. Nucl. Energy 118:103118

[6] Issa SAM, Ali AM, Susoy G, Tekin HO, Saddeek YB, Elsaman R, et al. Mechanical, physical and gamma ray shielding properties of xPbO-(50–x) MoO3–50V2O5 (25 ≤x ≤ 45 mol %) glass system. Ceram Int 2020. https://doi.org/10.1016/j. ceramint.2020.05.107.

[7] "Technical Properties of Radiation Shielding Glasses | SCHOTT." Technical Properties of Radiation Shielding Glasses | SCHOTT, www.schott.com/en-gb/ products/radiation-shielding-glasses-p1000330/technical-details.

# Gamma Ray Shielding Properties of Polymer Composites

## İskender AKKURT

*Suleyman Demirel University, Isparta-Turkey, E Mail: iskenderakkurt@sdu.edu.tr*

**Abstract**

The increasing use of ionizing radiation in medical, industrial, and nuclear applications has intensified the demand for effective and lightweight radiation shielding materials. Traditional shielding materials such as lead and concrete, although effective, suffer from disadvantages including high density, toxicity, and limited mechanical flexibility. In recent years, polymer composites filled with high atomic number (high-Z) materials have emerged as promising alternatives for gamma-ray shielding. This study reviews the gamma-ray shielding properties of polymer-based composites, focusing on attenuation parameters such as linear and mass attenuation coefficients, half-value layer, mean free path, and effective atomic number. The influence of filler type, concentration, and photon energy on shielding performance is discussed. The results indicate that polymer composites containing heavy metal oxides such as $PbO$, $Bi_2O_3$, and $WO_3$ demonstrate significantly improved gamma-ray attenuation compared to pure polymers, making them suitable candidates for advanced radiation protection applications.

***Keywords:*** *Gamma radiation, Polymer composites, Shielding materials, Attenuation coefficient, Heavy metal oxides*

## 1. Introduction

Gamma radiation is widely used in various fields such as nuclear power generation, medical imaging and radiotherapy, industrial radiography, and space technology. However, exposure to gamma radiation poses serious health risks, necessitating effective shielding materials. Conventional gamma-ray shielding materials, including lead and concrete, provide high attenuation efficiency but are associated with drawbacks such as high weight, toxicity, and limited design flexibility.Polymers are attractive materials due to their low cost, ease of fabrication, corrosion resistance, and mechanical flexibility. Nevertheless, their low density and low atomic number make them inefficient against gamma radiation. To overcome this limitation, polymer composites reinforced with high-Z fillers have been developed. These composites combine the mechanical advantages of polymers with the radiation attenuation capability of heavy elements, offering a new generation of shielding materials.

## 2. Gamma-Ray Interaction Mechanisms

Gamma rays interact with matter through three main mechanisms: photoelectric absorption, Compton scattering, and pair production. The dominance of each interaction depends on the photon energy and the atomic number of the material.

155

At low photon energies, the photoelectric effect dominates and is strongly dependent on the atomic number of the absorber. In the intermediate energy range, Compton scattering becomes the primary interaction and shows weak dependence on atomic number. At high energies, pair production occurs, and its probability increases with atomic number. Therefore, incorporating high-Z fillers into polymer matrices significantly enhances gamma-ray attenuation, particularly at low and high energy regions.

## 3. Polymer Composites for Gamma Shielding

Commonly used polymer matrices for gamma-ray shielding composites include epoxy resin, polyethylene, polyvinyl chloride (PVC), polystyrene, and polymethyl methacrylate (PMMA). These polymers offer good mechanical properties, ease of processing, and chemical stability.High-density and high-Z fillers are added to polymers to improve their shielding efficiency. Typical fillers include lead oxide (PbO), bismuth oxide ($Bi_2O_3$), tungsten oxide ($WO_3$), barium sulfate ($BaSO_4$), iron oxide ($Fe_2O_3$), and rare-earth oxides such as gadolinium oxide ($Gd_2O_3$). Among these, $Bi_2O_3$ has gained attention as an environmentally friendly alternative to lead-based fillers.

## 4. Shielding Parameters

The gamma-ray shielding performance of polymer composites is evaluated using several parameters. The linear attenuation coefficient ($\mu$) represents the probability of gamma-ray interaction per unit thickness, while the mass attenuation coefficient ($\mu/\rho$) allows comparison between materials independent of density. The half-value layer (HVL) is defined as the thickness required to reduce the gamma-ray intensity by half, and a lower HVL indicates better shielding efficiency. Additionally, the mean free path (MFP) and effective atomic number ($Z_e$ff) provide further insight into photon interaction behavior within the composite.Experimental and theoretical studies have shown that increasing the filler concentration in polymer composites leads to higher attenuation coefficients and lower HVL values. However, excessive filler loading may negatively affect mechanical properties and processability. Moreover, gamma-ray shielding effectiveness generally decreases with increasing photon energy. Composites containing high-Z fillers exhibit superior performance across a wide energy range compared to pure polymers or low-Z filled composites.Polymer composite gamma-ray shielding materials are increasingly used in medical radiation facilities, nuclear waste storage, portable shielding devices, industrial radiography, and aerospace applications. Their lightweight nature, non-toxicity, and design flexibility make them especially suitable for applications where conventional shielding materials are impractical.

## 7. Conclusion

Polymer composites reinforced with high-Z fillers represent a promising class of materials for gamma-ray shielding applications. By optimizing filler type, concentration, and dispersion, it is possible to achieve significant radiation attenuation while maintaining desirable mechanical and physical properties. Continued research in this field is expected to further enhance the performance of polymer-based shielding materials and expand their practical applications.

## References

[1] Kurtulus, R., Kavas, T., Akkurt, I., Gunoglu, K., Tekin, H.O., Kurtulus, C., 2021. A comprehensive study on novel alumino-borosilicate glass reinforced with Bi2O3 for radiation shielding applications: synthesis, spectrometer, XCOM, and MCNP-X works. J. Mater. Sci. Mater. Electron. 32, 13882–13896.

[2] Malidarre, R.B., Akkurt, I., Kavas, T., 2021. Monte Carlo simulation onshielding properties of neutron-gamma from 252Cf source for Alumino-Boro-Silicate Glasses. Radiat. Phys. Chem. 186, 109540.

[3] Nouf Almousa, Roya Boudaghi Malidarreh, S. A. M. Issa, Hesham M. H. Zakaly,Synergistic effects of Gd2O3 and SiO2 in enhancing the acoustic, mechanical, andshielding qualities of borate glasses, Radiation Physics and Chemistry, 224. 112060, (2024).

[4] Erkan Ilik, Gokhan Kilic, U. Gokhan Issever, Shams A. M. Issa, Hesham M. H.Zakaly, H. O. Tekin, Cerium (IV) oxide reinforced Lithium-Borotellurite glasses: Acharacterization study through physical, optical, structural and radiation shieldingproperties, Ceramics International, 48. 1152-1165, (2022).

[5] Şakar, E., Özpolat, Ö. F., Alım, B., Sayyed, M. I., & Kurudirek, M. (2020). Phy-X/PSD: development of a user friendly online software for calculation of parameters relevant to radiation shielding and dosimetry. Radiation Physics and Chemistry, 166, 108496.